The effects of oncolytic Maraba virus (MG1) in advanced non-small cell lung cancer

Matthew Kin Liang Chiu

The Institute of Cancer Research, University of London

A Thesis Submitted for the Degree of Doctor of Philosophy

January 2021

Declaration

This thesis was completed under the supervision of Dr Fiona McDonald, Professor Alan Melcher and Professor Kevin J. Harrington. The work described here was carried out at The Institute of Cancer Research, Chester Beatty Laboratories, 237 Fulham Road, London, SW3 6JB.

I, Matthew Kin Liang Chiu, confirm that the work presented in this thesis is my own. Where information has been derived from other sources, I confirm that this has been indicated in the thesis.

Date: 12th January 2021

Signature: 

1. Chapter 1: Preface

1.1 Abstract

Lung cancer is responsible for the highest cancer mortality worldwide. The prognosis for patients with advanced disease remains poor with five-year overall survival of <10%, highlighting the urgent unmet need for novel treatments. Oncolytic viruses (OV) are a promising form of IO that has demonstrated selective infection, replication and killing of tumour cells, as well as subsequent activation of anti-tumour immunity. Maraba virus, MG1, is one such OV that is currently being investigated in phase I/II clinical trials as part of a “prime-boost” cancer vaccine.

This thesis explores the anti-cancer effects of clinical-grade Maraba virus (MG1) in a panel of lung cancer cell lines *in vitro* and then also *in vivo* in an immunocompetent murine lung cancer model. The ability of MG1 to reach the tumour, replicate within it and exert anti-tumour benefits with systemic, as opposed to intratumoural, administration *in vivo* was investigated. Moreover, the ability of MG1 infection to induce immunogenic cell death in lung cancer cell lines and the changes in the tumour immune microenvironment *in vivo* was examined. Finally, as the current body of evidence suggests that OVs often have limited efficacy as single agents, the potential synergistic enhancement of MG1 virotherapy in combination with other standard modalities of treatment was investigated.

The results discussed here show that oncolytic Maraba virus was able to selectively infect, replicate inside and kill non-small cell lung cancer cells, both *in vitro* and *in vivo*. Furthermore, *in vivo*, the virus retained its tumour tropism properties even after systemic delivery and replicated to doses that were comparable to intratumoural delivered MG1, despite the development of anti-viral neutralising antibodies rising in parallel with viral replication in treatment-naïve mice. Finally, MG1 was shown to inhibit tumour growth delay in a murine lung cancer model, likely due to stimulation of anti-tumoural innate immune effects.

1.2 Statement of impact

The global impact of COVID-19 has been profound and its effects have not only been devastating for public health but impacted virtually every aspect of work and life. There has been major disruption to research which has also impacted me directly; during the final year of my PhD, the Institute of Cancer Research was completely closed for 3 months. After a phased return to a COVID-secure environment, the services available for wet lab research were very restricted due to social distancing measures. One aspect that affected me the most was the limited access to the animal unit that prohibited me from repeating or initiating new *in vivo* experiments. In this thesis, I have therefore highlighted experiments which, if given more time and in the absence of COVID, would have benefited in strengthening my conclusions. Whilst both myself and my supervisors believe this disruption has not prevented me submitting an acceptable thesis, we thought this was worth highlighting and hope these issues can be taken into consideration when assessing my work.

Student: 

Supervisor: 

1.3 Contents

1.4 List of Tables

1.5 List of Figures

1.6 Acknowledgements

I would like to thank my supervisors, Professor Alan Melcher, Dr Fiona McDonald and Professor Kevin Harrington, for giving me the opportunity to work on such an interesting and varied project, as well as for their guidance throughout my PhD. I would also like to express my gratitude to Victoria Jennings for all her practical advice and support in supervising my lab work and also in writing my thesis. I am also grateful to Shane Foo, who not only introduced me to the lab, but also taught me tissue culture, viral plaque assays, MTT assays and running animal experiments; to Eva Crespo-Rodriguez, for teaching me western blotting, PCR and trouble-shooting crises often associated with flow cytometry; to Emmanuel Patin, for teaching me flow cytometry, especially the difficulties around compensation; to Edward Armstrong, for helping with *in vivo* experiments and being a fellow medic supporting me through my struggles adapting from clinical practice to scientific research; to Gabby Baker, for guiding me through the NK degranulation assay; to Malin Pedersen, Martin Mclaughlin and Dave Mansfield for ensuring the day to day running of the lab was as smooth as possible; to Harriet Whittock and Holly Baldock for animal care and measurements; and the other Harrington-Melcher lab members: Joan Kyula, Vicky Roulstone, Jen Lee, Gabby Bozhanova and Lorna Grove.

I gratefully acknowledge Cancer Research UK for funding me and my PhD project.

I am forever indebted to my parents for their love, care and sacrifice for which I owe them my every success and achievement in life.

I would also like to thank my loving wife, Dede Chan, for her unwavering support and understanding throughout my PhD, especially during writing of this thesis, and for making sure I am watered and fed.

Finally, I would like to dedicate this thesis to my children Hailey and Hugo Chiu, for making everything I do worthwhile.

1.7 Table of abbreviations

Abbreviations

ADV	Adenovirus
AE	Adverse events
ALK	Anaplastic lymphoma kinase
amiRNA	Artificial micro ribonucleic acid
APC	Antigen presenting cells
ARID1A	AT-rich interactive domain-containing protein 1A
ATP	Adenosine triphosphate
AUC	Area under the curve
BRCA	Breast cancer gene
BRAF	V-raf murine sarcoma viral oncogene homologueB1
CARDIF	Caspase activation recruitment domain adaptor inducing interferon-beta
CAV	Coxsackievirus
CCL	Chemokine (C-C motif) ligand
CD	Cluster of differentiation
CDKN2A	Cyclin-dependent kinase inhibitor 2A
CI	Confidence Interval
CRR	Complete response rate
CRT	Calreticulin
CT	Computer tomography
CTL	Cytotoxic T lymphocytes
CTLA-4	Cytotoxic T-lymphocyte-associated protein 4
CUG	Cancer up-regulated gene
CXCL	Chemokine (C-X-C motif) ligand
DAF	Decay accelerating factor
DAMP	Danger-associated molecular patterns
DC	Dendritic cells
DCT	Dopachrome tautomerase
DMSO	Dimethyl sulfoxide
DNA	Deoxyribonucleic acid
DSB	Double-stand breaks
EBRT	External beam radiotherapy
EBUS	Endobronchial ultrasound
ECM	Extracellular matrix
EGFR	Epidermal growth factor receptor
eIF2	Eukaryotic initiation factor 2
ELISA	Enzyme-linked immunosorbent assay
EML4	Echinoderm microtubule-associated protein-like 4
ENI	Elective draining lymph node irradiation
ER	Endoplasmic reticulum

FACS	Fluorescence activated cell sorting
FBS	Foetal bovine serum
FDA	Food and Drug Administration
FLUC	Firefly luciferase
GADD	Growth-arrest-and DNA-damage-induced transcript
GAPDH	Glyceraldehyde 3-phosphate dehydrogenase
GFP	Green Fluorescent protein
GM-CSF	Granulocyte-macrophage colony-stimulating factor
GITRL	Glucocorticoid-Induced tumour necrosis factor receptor ligand
HER	Human epidermal growth factor receptor
HFF	Human foreskin fibroblast
HMGB	High motility group box
HPV	Human papillomavirus
HR	Hazard ratio
HSP	Heat shock protein
HSV	Herpes simplex virus
HVEM	Herpesvirus entry mediator
IASLC	International Association for the Study of Lung Cancer
ICAM	intra cellular adhesion molecule
ICD	Immunogenic cell death
ICI	Immune checkpoint inhibitors
ICP	Infected cell protein
ICV	Infected cell vaccine
IFN	Interferon
IHC	Immunohistochemistry
IL	Interleukin
IM	Intramuscular
IMRT	Intensity modulated radiotherapy
IO	Immune oncology
IP	Intraperitoneal
IPS-1	Interferon-beta promoter stimulator 1
IRF	Interferon regulatory factor
IT	Intratumoural
IV	Intravenous
KEAP	Kelch-like ECH-associated protein
KIT	v-kit Hardy-Zuckerman 4 feline sarcoma viral oncogene homolog
KRAS	Kirsten rat sarcoma
LAG-3	Lymphocyte-activation gene 3
LDLR	Low-density lipoprotein receptor
LLC	Lewis Lung carcinoma (otherwise known as 3LL)
LUAD	Lung adenocarcinoma
LUSC	Lung squamous cell carcinoma
MAGE	Melanoma antigen gene protein
MAPK	Mitogen-activated protein kinase

MAVS	Mitochondrial antiviral signalling protein
MDA-5	Melanoma differentiation associated protein 5
MDSC	Myeloid derived suppressor cells
MEF	Mouse embryonic fibroblast
MET	Mesenchymal-epithelial transition factor
MG1	Maraba virus
MHC	Major histocompatibility complex
MOI	Multiplicity of infection
mRNA	Messenger ribonucleic acid
MV	Measles virus
NAbs	Neutralising antibodies
NDV	Newcastle disease virus
NF1	Neurofibromatosis type 1
NFκB	Nuclear factor kappa-light0cahin-enhancer of activated B cells
NGS	Next generation sequencing
NHEJ	Non-homologous end joining
NK	Natural Killer
NKT	Natural Killer T cells
NLST	National Lung Cancer Screening Trial
NSCLC	Non-small cell lung cancer
NTRK	Neurotrophic tyrosine receptor kinase
ORR	Objective response rate
OS	Overall survival
OV	Oncolytic viruses
OX40L	OX40 ligand
PAMP	Pathogen-associated molecular pattern molecules
PARP	Poly-ADP ribose polymerase
PBMC	Peripheral blood mononuclear cells
PBS	Phosphate-buffered saline
PCR	Polymerase Chain Reaction
PD-1	Programmed cell death protein 1
PD-L1	Programmed death-ligand 1
PET	Positron emission tomography
PFA	Paraformaldehyde
PFS	Progression free survival
pfu	Plaque forming unit
PIK3CA	Phosphatidylinositol-4,5-iphosphate 3-kinase catalytic subunit
PKR	Protein kinase R
PRR	Pattern recognition receptor
RB	Retinoblastoma
RBM10	RNA binding motif 10
RET	Rearranged during transfection
RIG-I	Retinoic acid-inducible gene 1
RLU	Relative light units

RNA	Ribonucleic acid
ROS1	c-ros oncogene 1
RT	Radiotherapy
RT3D	Reovirus type 3 Dearing
SARRP	Small animal radiation research platform
SCC	Squamous cell carcinoma
SD	Standard deviation
SETD2	Suppressor of Variegation, Enhancer of zeste, Trithorax (SET)-domain containing 2
SFV	Semliki forest virus
shRNA	Short hairpin ribonucleic acid
siRNA	Small interfering ribonucleic acid
STAT1	Signal transducer and activator of transcription 1
STEAP	Six transmembrane antigen of the prostate
STK	Serine/threonine kinase
SV	Shuttle vector
TAA	Tumour-associated antigens
TAM	Tumour-associated macrophages
TBK	TANK-binding kinase
TCGA	The Cancer Genome Atlas
TGF	Transforming growth factor
TIGIT	T cell immunoreceptor with Ig and ITIM domains
TIL	Tumour infiltrating lymphocytes
TIM3	T-cell immunoglobulin and mucin-domain containing-3
TKI	Tyrosine kinase inhibitor
TME	Tumour microenvironment
TNBC	Triple negative breast cancer
TNM	Tumour node metastases
TP53	Tumour protein p53
TTF	Tumour-treating fields
T-VEC	Talimogene laherparepvec
U2AF1	U2 small nuclear RNA auxiliary factor 1
UV	Ultraviolet radiation
VISA	Virus induced signalling adaptor
VSV	Vesicular stomatitis virus
VV	Vaccinia virus

Chapter 2:
Introduction

2. Chapter 2: Introduction

2.1 NSCLC:

2.1.1 Background and staging

Lung cancer is the most common cancer in the world with 2.09 million new cases diagnosed in 2018 contributing to 12.3% of total global new cancer cases that year (1). It is also the leading cause of cancer mortality worldwide accounting for 1.76 million deaths in 2018 (1). Most patients (80-85%) presents with non-small cell lung cancer (NSCLC) subtype, of which lung adenocarcinoma (LUAD) and lung squamous cell carcinoma (LUSC) are the most common histological subgroups (2). Tobacco smoking remains to be the most common aetiology for lung malignancies with a stronger association with small cell and squamous cell histology more than LUAD which is the most common subtype in never smokers (3). Other risk factors include, passive smoking, air pollution, exposure to occupational carcinogens (e.g., silica dust and asbestos fibres) and inherited genetic predispositions (e.g., TP53 carriers) (2, 4, 5).

Lung cancers diagnosed at early stages have a favourable prognosis, with a 5-year overall survival (OS) of 70-90% for small, localised tumours (stage I) after surgical resection (6, 7). Unfortunately, most patients with lung cancer (around 75%) present with advanced disease (stage III/IV) at the time of diagnosis with a 5-year survival of <10% (8). Therefore, early detection could have significant improvements on survival, which has been supported by the recent publication of the 10 year results from the NELSON trial (9). This was a population-based randomised controlled trial which randomised individuals with high risk of developing lung cancer to either periodic screening (at baseline, year 1, 3 and 5.5) with low dose computed tomography (CT) or no screening. The investigators found that there was a 24% lung cancer mortality reduction for men and 33% for women in favour of screening compared to no screening. Furthermore, the trial's findings also point to the increased likelihood of early detection and a significant reduction of false positives and

unnecessary procedures due to CT screening (9). This result followed the positive findings from the National Lung Cancer Screening Trial (NLST) conducted in the US, which also found a 20% reduction in lung cancer specific mortality rate and a reduction of 6.7% in overall mortality rate in favour of CT chest screening for patients who were current or ex-smokers with a ≥30 pack year history (10). Both the NELSON and NLST trials could prompt access to lung cancer screening programmes in Europe for high-risk individuals in the future.

As mentioned earlier, the stage of lung cancer has an important impact on treatment options and prognosis for patients. Better access to positron emission tomography with CT (PET-CT) scanning and endobronchial ultrasound (EBUS) for mediastinal lymph node sampling have all increased the accuracy for lung cancer staging (11). The 8th edition of the International Association for the Study of Lung Cancer's (IASLC) (12) staging project is based on tumour, node and metastasis (TNM) classification (summarised in Table 6 and 7 appendix).

For most lung cancer patients who have incurable Stage IV disease, the OS remains poor. This is despite substantial improvements in systemic treatment over the past 20 years, advancing from the empirical use of cytotoxic chemotherapy based on physician's choice to a more patient-tailored approach with subsets of patients who possess oncogenic driver mutated tumours receiving tyrosine kinase inhibitors (TKI) and those with expression of programmed death ligand-1 (PD-L1) benefiting from immune checkpoint inhibitors (ICI). This has only become possible due to a better understanding of lung cancer biology through advances in next-generation sequencing (NGS) and other high-throughput genomic profiling platforms.

2.1.2 Molecular landscape of lung cancer:

Lung cancer is a molecularly heterogenous disease and the genomic landscape is markedly different between never smokers and smokers. Tobacco-smoking related lung cancers are associated with a high tumour mutational burden with a mean somatic mutation rate of 8 to 10 mutations per

megabase (1 million base pairs), regardless of the histological subtype, as revealed by whole exome sequencing of lung malignant tissue (13). In contrast tumours from never smokers have a much lower tumour mutation burden with a rate of 0.1 to 1 mutation per megabase (14-17). LUAD from smokers are characterised predominantly with cytosine to adenine (C>A) nucleotide transversion mutations and non-actionable mutations such as Kirsten rat sarcoma (KRAS) and tumour protein p53 (TP53). Whereas in tumours of never smokers there is a predominant transition of cytosine to thymine (C>T) mutations and a higher prevalence of actionable driving gene alterations including epidermal growth factor receptor (EGFR) activating and ROS1 mutations as well as anaplastic lymphoma kinase (ALK) translocations (15, 18).

Data from The Cancer Genome Atlas (TCGA) showed that the most common mutated oncogenes in LUAD are KRAS (in 33% of tumours), EGFR (in 14%), BRAF (in 10%), PIK3CA (in 7%) and MET (in 7%). Mutations in tumour suppressing genes include, TP53 (in 46%), STK11 (in 17%), KEAP (in 17%), NF1 (in 11%), RB1 (in 4%) and CDKN2A (in 4%). Mutations involving chromatin-modifying genes (SETD2, ARID1A and SMARCA4) and RNA-splicing genes (RBM10 and U2AF1) are found in around 10% of specimens from LUAD (15). KRAS and EGFR mutations are usually mutually exclusive, but when they co-exist, KRAS mutations may confer resistance to EGFR tyrosine kinase inhibitor therapies (19). The frequency of KRAS mutations in LUAD seems equal across tumour grades suggesting a role in tumour initiation and early carcinogenesis whereas mutations in TP53 are more commonly present with advancing grade, suggesting a role during tumour progression (20). Unlike LUAD, actionable mutations are rarely detected in LUSC (21).

Lung cancer, like many other malignancies, is composed of sub-population of cells, or clones, with distinct molecular features resulting in intratumoural heterogeneity. There is increasing evidence from genomic analyses of solid tumours, that the process of branched evolution occurs, whereby multiple sub-clones can share a common ancestor, only to differ in subtle genomic alterations that occur later in the evolution of the tumour (22). A study by Zhang *et al*. applied multi-region, whole-exome sequencing to specimens from 11

patients with early-stage LUAD and found clear evidence of intratumour heterogeneity and branched evolution in every case (23). Furthermore, they gave evidence to suggest that a single-sample approach in early-stage NSCLC may be sufficient to depict the driver of the disease mutational landscape as they found that among 21 mutations known to be related to the cancer, 20 were present in every region. The authors also discovered a larger fraction of subclonal mutations were present in patients who had relapsed within 21 months after surgery compared to those who did not have recurrence. Larger prospective trials such as the Tracking Cancer Evolution through Therapy (Rx) (TRACERx) program (ClinicalTrials.gov number, NCT01888601) in the United Kingdom, will be able to examine this association further. The identification of truncal targetable genetic alterations occurring early during cancer evolution may enhance success of therapy.

2.1.3 NSCLC and Tumour microenvironment

The tumour microenvironment (TME) consists of not only tumour cells but is also comprised of immune cells, mesenchymal cells, endothelial cells, inflammatory mediators and extracellular matrix (ECM) molecules (24, 25). The type, density and location of immune cells within the TME is increasingly recognised to play an important role in the development of the disease and offer clinical prognostic values (26). Genetic events that drive tumour evolution will also shape the TME, for example the inactivation of the tumour suppressor serine/threonine kinase 11 (STK11), which occurs in one-third of KRAS-mutated LUAD, skews the TME towards an immunosuppressive climate with the accumulation of immunosuppressive neutrophils, reduction of tumour-infiltrating lymphocytes and loss of PD-L1 expression (27).

The high tumour mutation burden in tobacco-smoking related lung cancers can result in the production of neoantigens which are recognisable by tumour-infiltrating cytotoxic T cells. A high clonal neoantigen burden in LUAD promotes an inflamed TME that is enriched with activated effector T cells and expresses proteins associated with T cell migration (CXCL-9 and 10), antigen presentation and effector T cell function, as well as negative regulators of T cell activity such as programmed death-1 (PD-1), PD-L1 and lymphocyte

activation gene-3 (LAG-3) (28). The increase in expression of PD1 and PD-L1 confers sensitivity to ICI therapy.

2.1.4 NSCLC treatment and advances

As mentioned previously, the treatment for NSCLC has revolutionised over the past 20 years, moving from generic chemotherapy to more targeted and individually tailored treatments dependant on histological diagnosis, detection of oncogenic driver mutations and PD-L1 status. The first step towards this personalised approach became apparent when patients with LUAD were found to have superior survival with cisplatin/pemetrexed chemotherapy compared to cisplatin/gemcitabine, but vice versa for patients with LUSC (29), highlighting the importance of tumour histology when choosing therapy. Furthermore, maintenance pemetrexed reduces risk of progression and improves OS in patients with LUAD who did not progress after induction (4 to 6 cycles) platinum-pemetrexed chemotherapy (30, 31). The addition of a third chemotherapeutic agent to the standard of care platinum-based doublet (4-6 cycles) seemed to only improve response rates, but not increase in OS, at the expense of increased toxicity (32-34). Second line docetaxel with or without ramucirumab (a monoclonal antibody against vascular endothelial growth factor receptor 2) was the standard of care prior to the immunotherapy era (35).

An improved understanding of the molecular pathways that drive NSCLC subsequently led to the identification of targetable genetic alterations which revolutionised the treatment of lung cancer. One of the first oncogenic driver mutations to be identified in lung cancer was EGFR, a transmembrane surface protein that is activated by the binding of epidermal growth factor (EGF). Once bound, an intracellular tyrosine kinase domain causes a cascade of events leading to DNA synthesis and cellular proliferation (36). Erlotinib and gefitinib were the first-generation EGFR agents to be shown to induce higher objective response rates (ORR) and progression-free survival (PFS) compared to cytotoxic therapy in patients with previously untreated EGFR mutated NSCLC (37-42). In contrast to first-generation EGFR inhibitors, which only reversibly targets EGFR, second-generation agents such as afatanib and dacomitinib

bind EGFR irreversibly as well as targeting HER2 and HER4. Both afatanib and dacomitinib have shown PFS benefit over gefitinib (43, 44), with dacomitinib resulting in improved OS as well (34 vs 27 months; HR 0.76) after longer follow-up (45).

Almost all patients who initially respond to an EGFR TKI subsequently develop disease progression. The most common cause of acquired resistance (which accounts for approximately 50% of cases) is a secondary mutation in EGFR which involves the substitution of methionine for threonine at position 790 (T790M) (46). This mutation causes steric hindrance to prevent the binding of the initial EGFR TKI or increase ATP affinity to the tyrosine kinase binding domain, hence reducing its efficacy. Amplification of the MET oncogene has also been associated with resistance to first-generation EGFR TKIs in 5-20% of cases (47, 48). Third-generation EGFR inhibitors, e.g., Osimertinib, bind covalently to cysteine on codon 797, which can overcome the enhanced ATP affinity from the T790M mutation. Osimertinib was granted accelerated approval by US Food and Drug Administration (FDA) for use in patients with NSCLC harbouring a T790M mutation whose disease progressed on other EGFR-inhibiting agents, based on results of a phase I/II study showing a response rate of 61% and a median PFS of 10 months in the same setting (49). In the subsequent phase III study of patients fulfilling the same criteria as in the phase I/II study, osimertinib demonstrated an improved PFS (10.1 vs. 4.4 months; hazard ratio [HR] for progression or death 0.30) and ORR (71% vs. 31%) compared with platinum- or pemetrexed- based chemotherapy combination (50). The recent results from the FLAURA trial, which randomised patients with previously untreated advanced NSCLC harbouring an EGFR mutation (exon 19 deletion or L858R allele) to osimertinib or one of two first generation EGFR TKIs (erlotinib or gefitinib), showed a median OS improvement in favour of osimertinib (38.6 vs. 31.8 months; HR for death 0.80) hence promoting its earlier role in patients treatment pathway (51).

ALK gene rearrangement on chromosome 2 are found in approximately 5% of NSCLC (52). The most common ALK rearrangement in NSCLC involves the 5’ end of the echinoderm microtubule-associated protein-like (EML4) gene juxtaposed with the 3’ end of the ALK gene, resulting in a novel fusion

oncogene EML4-ALK (53). Advanced NSCLC associated with the ALK fusion oncogene is highly sensitive to ALK TKIs and the first agent to be approved for this purpose was crizotinib, an oral competitive ATP inhibitor of ALK, MET and ROS1 tyrosine kinases. Crizotinib (54) and ceretinib (55) (a second generation ALK TKI) were both shown to prolong PFS and ORR when compared to chemotherapy in previously untreated patients with NSCLC harbouring ALK aberration. Subsequently another two second generation ALK TKIs, alectinib (56-58) and brigatinib (59), have both shown improved PFS, ORR and higher intracranial response rates when compared to crizotinib hence superseding crizotinib as standard first line treatment for patients with ALK translocated NSCLC.

Resistance to ALK TKIs may occur due to upregulation of bypass signalling pathways involving EGFR and mitogen-activated protein kinase (MAPK), but the most common resistance mechanism is secondary ALK mutations such as I1171 and G1202R (60). A potent third generation ALK TKI, lorlatinib has shown activity against all known ALK inhibitor resistance mutations and is the preferred agent of choice on progression of up to three previous lines of ALK inhibitors (61).

ROS1 gene encodes for the receptor tyrosine kinase and chromosomal rearrangements can lead to the formation of oncogenic fusion proteins with constitutive kinase activity (62). ROS1 rearrangements are identified in approximately 1-2% of patients with NSCLC and due to amino acid similarities between the kinase domains of ROS1 and ALK, some ALK TKIs are also active against ROS1 including crizotinib, ceretinib and lorlatinib (61, 63-66). Resistance mechanisms to crizotinib usually involves secondary mutations within the ROS1 kinase domain, most commonly G2032R (67), or KRAS and KIT mutations (68).

Other genetic alterations have been investigated as potential targets in NSCLC, including BRAF, HER2, RET, MET and fusions of the neurotrophic tyrosine receptor kinase (NTRK) genes. Inhibitors to all these targets have shown modest activity in early phase clinical trials and further promotes development in histology-agnostic therapies (69).

2.1.5 NSCLC and immune surveillance

Lung cancer initiation and progression does not only depend on the evolving genomics and molecular properties of cancer cells but also on their interaction with the TME especially with the immune system (70). The concept that the immune system can recognise and eliminate nascent malignant cells was first proposed by Paul Ehrlich in 1909 and was later formulated into the cancer immunosurveillance theory by Burnet and Thomas in 1950s (71, 72). The theory was initially supported by the immune-mediated rejection of transplanted tumours induced by chemical carcinogens or viruses in syngeneic mice (73, 74). Despite this, the concept of cancer immunosurveillance was largely abandoned by 1978 mainly due to the observation that athymic nude mice did not show an increased incidence of spontaneous or chemically induced tumours compared to wild-type animals (75, 76). However, since the 1990s the role of the immune system in cancer immunosurveillance was reinvigorated with key experiments using knock-out mice which highlighted the importance of different immune components including, interferon (IFN) γ, perforin, interleukin (IL)-12, T cells, natural killer T (NKT) and natural killer (NK) cells (reviewed by Dunn *et al*. (77)).

The immune system is now recognised to inhibit tumour growth and destroy cancer cells through its innate and adaptive responses (78). Innate immune responses are antigen nonspecific, develop rapidly and are mediated by various effector cells such as NK cells, polymorphonuclear leukocytes, mast cells and dendritic cells. NK cells have an important role in recognising and destroying malignant and virally infected cells. NK cells monitor cells for expression of major histocompatibility complex class (MHC)-I molecules and cell stress markers, detecting changes in self-molecules rather than identifying foreign antigens. NK cells release IFN-γ and perforin as well as inflammatory cytokines that induces tumour apoptotic cell death (79). Conversely, adaptive immune responses are antigen specific, develop more slowly, offer immune memory and comprise both humoral and cellular immunity mediated by B and T cells, respectively (78, 80). In this respect, adaptive rather than innate

immunity offers the greatest potential for durable, robust anti-tumoural immune responses.

In the adaptive immune response, cancer cells release antigens which can engage antigen presenting cells (APC), such as immature DCs, and in the correct context leads to maturation (activation). DCs then present these tumour-associated antigens (TAA) within major histocompatibility complex (MHC) molecules to naïve T cells in the tumour-draining lymph nodes which triggers specific CD4+ helper T cells and CD8+ cytotoxic T cells activation. Effective T cell priming relies on an array of co-stimulatory molecules including CD80/86 on DCs, which are upregulated on the cell surface following maturation, and the CD28 receptor on T cells. After recruiting effector CD8+ T cells to the tumour, these cells can directly destroy cancer cells in an MHC-restricted fashion. However, as tumours can arise in the presence of an intact innate and adaptive immune system, the hypothesis of immunoediting was proposed by Dunn *et al*. (81). This theory explains the effects the immune system has on cancer progression through three dynamic processes called the three E's: elimination, equilibrium and escape.

In the first phase of elimination, the immune system recognises tumour cells as abnormal, leading to their destruction. If all the nascent transforming cells are successfully destroyed at this stage, then then whole cancer editing process is complete. However, if not then phase two (equilibrium) would ensue. At this stage, some malignant cell variants would have survived the elimination process and enter into a dynamic equilibrium, whereby lymphocytes and IFN-γ exert potent and relentless selection pressure on the tumour cells that is enough to contract, but not fully eradicate it. Although many of the original tumour cell escape variants are destroyed, new variants arise carrying different mutations that provide them with increased immune resistance. The end result is a new population of tumour clones with reduced immunogenicity which developed due to the sculpting forces of the immune system. This equilibrium phase can last over many years and may account for the clinical observations where patients undergo prolonged periods of remission before cancer relapse.

Finally, the escape phase follows, whereby the tumour cell variants in the equilibrium phase can now grow in an immunologically intact environment. This is most likely due to the genetic and epigenetic changes in the tumour cells to confer resistance to immune detection and/or elimination by both the innate and adaptive immune responses. It is now recognised that tumours can either directly or indirectly impede the development of anti-tumour immune responses either through the elaboration of immunosuppressive cytokines (e.g., transforming growth factor-β (TGF-β) and interleukin-10 (IL-10)) or via mechanisms involving T cell immunosuppression (e.g., regulatory T cells (Tregs) and myeloid-derived suppressor cells MDSCs). Tumour escape can also result from protein expression level in the tumour, such as loss of tumour associated antigen expression (82), loss of MHC components (83), shedding of NKG2D ligands (84), development of IFN-γ insensitivity (85) and upregulation of immune checkpoints e.g. PD-L1 (86). All these immune escape mechanisms allow the tumour to grow and metastasise.

Like other tumour types, NSCLC can establish an immunosuppressive TME that is permissive for tumour growth (86). For example, NSCLC tumours have been shown to contain large numbers of Tregs that constitutively express high levels of CTLA-4 on their surface and directly inhibit T cell proliferation (87). In addition, there is a reduction of tumour-infiltrating CD8+ T cells (88), which also possesses increased PD-1 expression (89). Furthermore, NSCLC tumour cells have been found to up-regulate PD-L1 expression (90) and down-regulate surface expression of MHC class I/tumour antigen expression, thereby helping these cells to evade the immune system (91). Finally lung cancer cells may also release immunosuppressive cytokines, including IL-10 and TGF-β (92).

2.1.6 NSCLC and Immunotherapy

Immune checkpoint molecules produced upon T-cell activation, regulate the immunological synapse between T cells and DCs in lymph nodes (CTLA-4-B7.1) and between T cells and tumour cells (PD-1 and PD-L1), all of which acts as a negative feedback to suppress T-cell activation. Blocking the CTLA4, PD-L1 and PD-1 axis with monoclonal antibodies restores T-cell mediated

anti-tumour immunity and these have emerged as a revolutionising treatment for many tumour types including advanced NSCLC (Table 1).

ICI have been approved as a standard of care for patients with NSCLC whose tumours have progressed after first-line cytotoxic therapy. Two trials compared nivolumab (a humanised IgG4 anti-PD-1 antibody) to docetaxel in patients with NSCLC who progressed on platinum-based chemotherapy, in squamous cell carcinoma (SCC) subset (CheckMate 017 trial) (93) and non-SCC histology (CheckMate 057 trial) (94). In patients with SCC NSCLC, nivolumab resulted in an improved mOS (9.2 months vs. 6.0 months, HR 0.59; p<0.001), PFS (3.5 months vs 2.8 months, HR 0.62; p<0.001) and response rate (20% vs. 9%, p<0.008) over docetaxel. These benefits were largely independent of clinical and tumour characteristics including PD-L1 expression (93). In the non-SCC NSCLC trials, nivolumab improved mOS (12.2 months vs. 9.4 months, HR 0.73) and response rate (19% vs. 12%, P=0.02), but not PFS (94). Nivolumab therefore obtained regulatory approval in the USA and Europe for treatment of advanced NSCLC in patients who progressed on first-line chemotherapy. Pembrolizumab (another humanized IgG4 anti-PD-1 antibody) was also tested against docetaxel in a randomised phase III trial in patients with NSCLC who progressed on first-line chemotherapy. The results this time showed that the magnitude of OS benefit was related to PD-L1 expression with HR of 0.53 if tumours had a PD-L1 expression of >50% and HR of 0.76 if PD-L1 expression was between 1-49% (95). The authors concluded that PD-L1 testing may allow selection of patients who would better respond to pembrolizumab. Finally, a humanised IgG1 anti-PD-L1 antibody, atezolizumab, has also shown survival advantage over docetaxel in patients with NSCLC in a similar setting (mOS 13.8 vs. 9.6 months) (96). ICI have therefore become the preferred therapy over standard chemotherapy in patients with NSCLC who have progressed on first-line cytotoxic treatment.

In untreated patients with NSCLC, pembrolizumab has also proven OS benefit when combined with chemotherapy over placebo/chemotherapy combination in two randomised phase III clinical trials. For patients with squamous NSCLC, the KEYNOTE-407 trial showed the mOS was 15.9 months (95% CI, 13.2 to not reached) in pembrolizumab-carboplatin/paclitaxel or nab-paclitaxel group,

and 11.3 months (95% CI, 9.5-14.8) in the placebo-combination group (HR for death, 0.64; 95% CI, 0.49-0.85; p<0.001) (97). The OS benefit seen in this trial was consistent regardless of the level of PD-L1 expression. Similarly in patients with non-squamous NSCLC, the KEYNOTE-189 showed the 12 months OS rate was 69.2% (95% CI, 64.1-73.8) in the pembrolizumab-platinum/pemetrexed group vs. 49.4% (95% CI, 42.1-56.2) in the placebo-combination group (HR 0.49; CI, 0.38-0.64; p<0.001) (98). Again, the improvement in OS was seen irrespective of PD-L1 expression. Therefore, ICI in combination with chemotherapy has now become the preferred treatment in untreated patients with NSCLC.

Despite the success of these monoclonal antibodies directed to PD-1 or its ligand PD-L1 against NSCLC, durable responses only occur in about 14-20% of pre-treated patients (69) and even amongst responders, resistance can ensue. These issues highlight an unmet need for exploring new therapeutic approaches for patients with advanced NSCLC.

Table 1: Pivotal studies of ICI in advanced NSCLC

Study name	**Phase**	**Histology, PD-L1**	**Line of treatment**	**Study design**	**Control arm outcome (months)**	**Experimental arm outcome (months)**	**Hazard ratio (95% CI, p-value)**
First line ICI only							
KEYNOTE-024	III	NSCLC, PD-L1 TPS≥50%	Treatment-naive	Pembrolizumab (Pem) vs. chemotherapy (chemo)	mOS 14.2	mOS 30.0	0.63 (0.47-0.86), P=0.002
KEYNOTE-042	III	NSCLC, PD-L1 TPS≥1%	Treatment-naive	Pem vs. chemo	mOS 12.1	mOS 16.7	0.85 (0.71-0.93), p=0.0018
CheckMate-026	III	NSCLC, PD-L1 TPS≥1%	Treatment-naive	Nivolumab (Nivo) vs. chemo	mOS 13.2	mOS 14.4	1.02 (0.80-1.30), p=NS
CheckMate-227	III	NSCLC	Treatment-naive	PD-L1 ≥1% Nivo vs. Nivo+Ipilimumab (Ipi) vs. chemo	mOS 14.9	mOS 17.1 (Nivo+Ipi)	0.79 (97.72% CI: 0.65-0.96)
				PD-L1 <1% Nivo vs. Nivo+chemo vs. chemo	mOS 12.2	mOS 17.2 (Nivo+Ipi)	0.62 (0.48-0.78)
MYSTIC	III	NSCLC	Treatment-naive	Durvalumab (D) vs. durvaluman+tremelimumab (D+Tr) vs. chemo(chemo)	mOS 12.9	mOS 16.3 (D)	0.76 (0.56-1.02), p=NS (D vs. chemo)

						mOS 11.9 (D+Tr)	0.85 (0.61-1.17), p=NS (D+Tr) vs. chemo
First-line ICI + Chemotherapy combination							
KEYNOTE-189	III	Non-squamous	Treatment-naive	Pembro+chemo vs. placebo+chemo	12-month OS 49.4%	12-month OS 69.2%	0.49 (0.38-0.64), p<0.001
KEYNOTE-407	III	Squamous	Treatment-naive	Pembro+/-carboplatin/paclitaxel or nab-paclitaxel	mOS 11.3	mOS 15.9	0.64 (0.49-0.85), p<0.001
IMpower-150	III	Non-squamous including EGFR/ALK+	Treatment-naive	Atezolizumab (Atezo)+/-bevacizumab/paclitaxel/carboplatin	mOS 14.7	mOS 19.2	0.78 (0.64-0.96), p=0.02
IMpower-132	III	Non-squamous	Treatment-naive	Atezo+/-platinum/pemetrexed	mPFS 5.2	mPFS 7.6	0.60 (0.49-0.73), p<0.0001
IMpower-131	III	Squamous	Treatment-naive	Atezo+chemo	mPFS 5.6	mPFS 6.3	0.715 (0.603-0.848), p=0.0001
Later-line ICI							
CheckMate-017	III	Squamous	Second or later	Nivo vs. docetaxel	mOS 6.0	mOS 9.2	0.62 (0.47-0.80)

CheckMate-057	III	Non-squamous	Second or later	Nivo vs. docetaxel	mOS 12.2	mOS 9.5	0.75 (0.63-0.91)
KEYNOTE-010	II/III	NSCLC, PD-L1 TPS≥1%	Second or later	Pembro 2mg/kg or 10mg/kg vs. docetaxel	mOS 8.5	2mg/kg: mOS 10.4	2mg/kg: 0.71, p-0.0008
						10mg/kg: mOS 12.7	10mg/kg: 0.61, p<0.0001
OAK	III	NSCLC	Second or later	Atezo vs. docetaxel	mOS 9.6	mOS 13.8	0.73 (0.62-0.87), p=0.0003

2.2 Oncolytic viruses

Oncolytic viruses (OVs) are a promising class of immunotherapy, which can be naturally occurring or genetically modified and can be RNA or DNA based (Figure 1). Since Dock *et al*. (1904) first reported a female patient with myelogenous leukaemia who underwent tumour regression after an influenza infection, attempts to harness viruses for anti-neoplastic effects have never stopped. OVs possess a dual mechanism of action; firstly, they were originally developed to selectively infect, replicate and cause direct lysis of tumour cells, but they are now also recognised to promote anti-tumour immune responses via multiple mechanisms including induction of immunogenic cell death (99) (discussed in more detail in section 2.2.2).

There are more than 3,000 species of viruses but not all are suitable as oncolytic agents. The key desirable characteristics for OVs include the intrinsic cancer-selectivity and potency to kill infected cells; ability to activate innate immune cells such as NK cells; the ability to generate adaptive anti-tumour immunity; and the versatility to be engineered to express attenuating genes or arming genes (100).

2.2.1 Tumour-selectivity

Cancer cells possess alterations in cell physiology that distinguishes them from normal counterparts such as limitless replication potential, insensitivity to growth inhibition signals, evasion of apoptosis, self-sufficiency in growth signals, sustained angiogenesis and tissue invasion and metastasis. OVs can naturally or be genetically modified to exploit these differences to achieve tumour tropism. Some mechanisms of tumour specificity are described below.

2.2.1.1 Transductional targeting

OVs can exploit tumour specific receptors that are displayed at high levels by tumour cells; for example, intracellular adhesion molecule-1 (ICAM-1) and decay accelerating factor (DAF) are overexpressed on many cancer cells and acts as entry receptors for coxsackievirus A21 (CAV21) (101). Another enterovirus, echovirus type 1, targets overexpression of integrin α2β1 on

ovarian cancer cells (102) and poliovirus infects cells expressing CD155 receptor which is abundant on many cancer cell types (103). Talimogene laherparepvec (T-VEC), which is the only FDA approved OV for clinical use in melanoma, is a based on herpes simplex virus type I (HSV-1) and binds to herpesvirus entry mediator (HVEM) receptors on melanoma cells (104).

2.2.1.2 Translational targeting

Upon viral infection of normal cells, type I interferon (IFN) is produced which leads to the shutdown of protein synthesis in neighbouring cells, prohibiting viral replication. However, cancer cells generally have a defective IFN signalling pathway and therefore are more susceptible to OV replication compared to their normal counterparts. Naturally occurring vesicular stomatitis virus (VSV) (105) and Newcastle disease virus (NDV) (106) are restricted to tumour cells with defective IFN responses.

2.2.1.3 Transcriptional targeting

OV can be engineered to be tumour selective by placing essential viral genes under the regulation of tumour specific promoters thus restricting viral replication only within cancer cells. For example, adenovirus can be modified so that the essential viral gene (E1) is under the control of human E2F-1 promotor (107) which is selectively activated in tumour cells with a defect in Rb pathway. Also HSV replication can be limited within liver and hepatocellular carcinoma due to placing the immediate-early ICP4 gene under the control of the albumin-enhancer-promoter (108).

2.2.1.4 Pro-apoptotic targeting

Delayed apoptosis of infected cells can assist viral replication and therefore some viruses alter the activity of regulators of programmed cell death such as p53 and pRb. Adenovirus protein E1A and E1B can render p53 inactive during natural infection, therefore a deletion in E1 proteins within the virus results in an adenovirus that specifically replicates in tumour cells which have a p53 mutation, while sparing normal cells. One example of this is ONYX-15 which has deletions in two viral genes E1B and E3 (109) and is clinically approved for treatment in head and neck cancers in China.

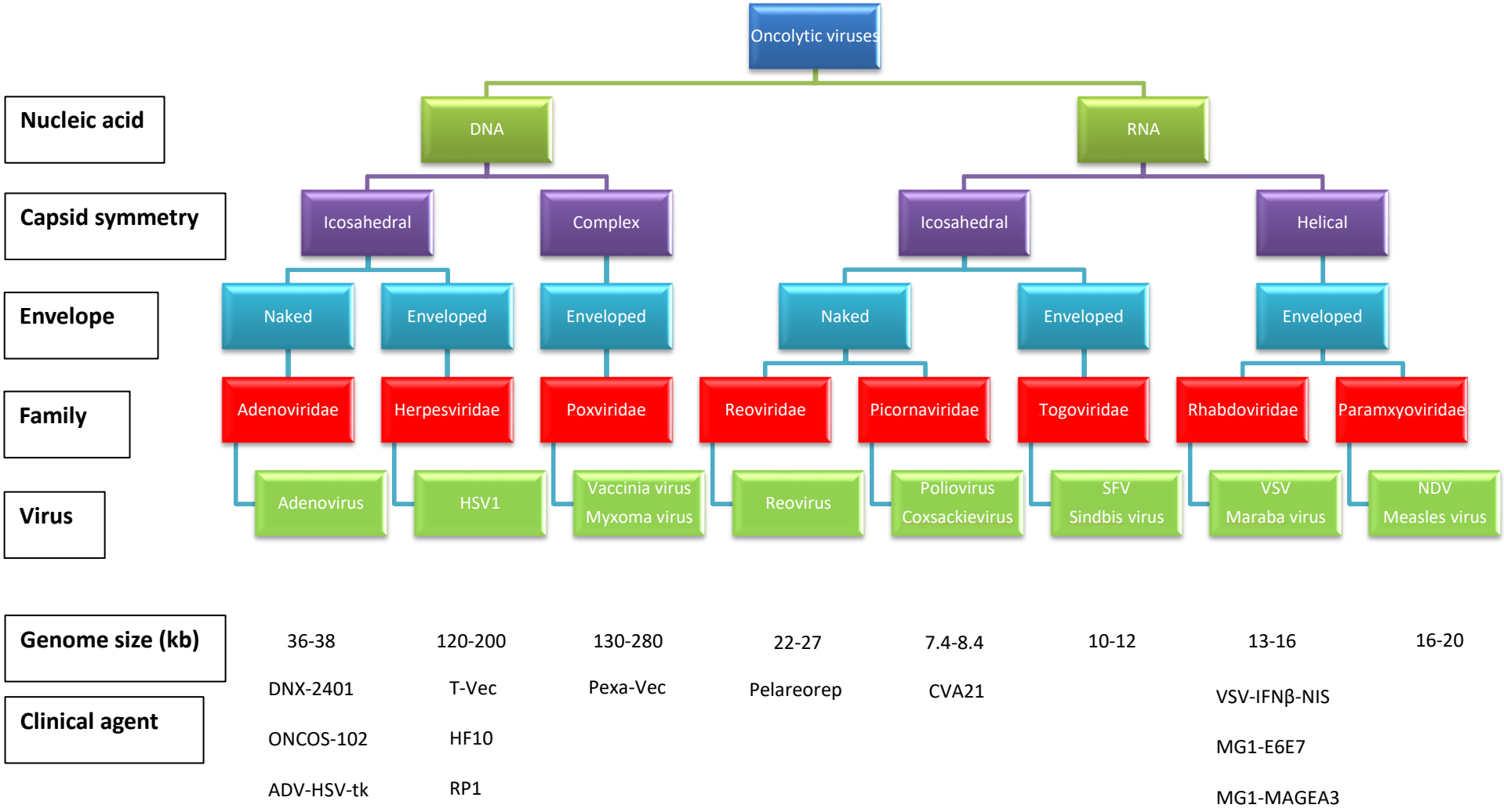

Figure 1: OV classification and viruses.

HSV1: Herpes simplex virus type 1; SFV: Semliki forest virus; VSV: Vesicular stomatitis virus; NDV: Newcastle disease virus

2.2.2 Oncolytic virus and immune effects

As mentioned previously, OVs were initially developed for their direct oncolytic properties, however it is increasingly recognised that OVs can also induce beneficial changes in the tumour immune microenvironment (110). Tumours generally secrete soluble immunosuppressive mediators, such as nitric oxide and cytokines including IL-10 and TGF-β (111). In addition tumours may lack tumour-infiltrating lymphocytes (TILs) and instead recruit immune suppressive cell subsets (such as macrophages, regulatory T cells, MDSC or neutrophils), all of which can hinder the capacity of the acquired immune system to clear the cancer (112). Virotherapy can revert this immunosuppressive ("cold") TME to a "hotter" immunostimulatory one by inducing pro-inflammatory cytokines (113) pathogen-associated molecular pattern molecules (PAMPs), danger-associated molecular patterns (DAMPS), which in turn leads to APCs maturation, as well as, releasing tumour-associated antigens (TAA) that can be processed and presented by APCs to effector T-cells to initiate an adaptive anti-cancer immune response.

The importance of an intact immune system for the efficacy of oncolytic virotherapy has been shown in studies comparing OVs in immunodeficient and immunocompetent mouse models. One example of such a study is by Toda *et al*. (114) who showed that HSV type 1 (HSV-1) was effective in immunocompetent mice but the anti-tumour effect was lost in athymic mice, highlighting the role of endogenous CD8+ cytotoxic T lymphocyte (CTL). This finding was consistent in VSV therapy where anti-cancer effects were dependant on CD8+ T cells and NK cells (115). Other OVs have also shown dependence on the immune system for its anti-tumour properties such as maraba virus (MG1) (116), Newcastle disease virus (NDV) (117), reovirus (118) and sendai virus (119). Furthermore, OVs have also been shown to initiate an innate and adaptive immune response in the clinical setting; in a phase Ib clinical trial with T-VEC, Ribas *et al*. showed changes in immune infiltration in the on-treatment biopsies from some patients including influx of CD4+ and CD8+ T cells as well as CD56+ cells and CD20+ B cells (120). In these biopsies, although there was also an influx of immunosuppressive

Tregs, the magnitude of effector T cell (Teff) increase was much larger, hence the Treg to Teff ratio was overall decreased with intratumoural T-VEC injection. Similar changes have been observed clinically with reovirus (Pelarorep, previously known as Reolysin) (121) and adenovirus-CD40L (122).

2.2.3 Oncolytic virus and clinical use

There are numerous OVs that have been investigated for clinical use, including reovirus, VV, HSV, coxsackie virus, measles virus, retrovirus and adenovirus (123). To date, only T-VEC is FDA-approved for clinical use in malignant melanoma. T-VEC is a modified oHSV1 with deletions in the ICP34.5 and ICP47 genes resulting in enhanced tumour tropism and decreased neurovirulence (124). The addition of a GM-CSF transgene also improves the immune modulatory effects of the virus (104). T-VEC was FDA-approved for clinical use based on results of the phase III OPTiM (Oncovex [GM-CSF] Pivotal Trial in Melanoma) trial (125). In this study, intralesional injection of T-VEC led to a statistically significant improvement in durable ORR when compared to GM-CSF alone (16.2% vs 2.1%, $p<0.001$), in patients with unresectable stage IIIB or IV melanoma. Importantly, an anenestic response was also noted, as 15% of measurable visceral (non-injected) lesions reduced in size by ≥50% following T-VEC treatment. The final analyses revealed a mOS benefit of 23.3 months vs. 18.9 months in the T-VEC and GM-CSF arms, respectively, while also exhibiting a tolerable safety profile with low rates of grade 3/4 adverse events (AEs) (126). T-VEC was also found to alter the tumour immune microenvironment by reducing the number of CD4+ Tregs, CD8+ T suppressor cells and MDSC (127).

Tasadenoturev (DNX-2401) is another OV which has shown promising responses clinically. It is a tumour selective, replication-competent oADV that has been modified with a deletion in the E1A gene, which allows it to replicate only in cells defective in the retinoblastoma (RB) pathway. A dose-escalation phase I study showed that DNX-2401 was safe and capable of robust viral replication and tumour control in recurrent high-grade glioma patients. 72% of

patients (18 out of 25) had tumour reduction and remarkably 20% (5 patients) survived for more than 3 years (128).

Other OVs have also been investigated in clinical trials with positive results, such as pelareorep (a reovirus) (121) researched in advanced pancreatic cancer and oncorine (H101) which is an attenuated oADV used to treat head and neck squamous cell carcinoma (129).

Therefore, OV therapy can be safe and efficacious to use clinically to treat different cancers and have the potential to be a promising addition to conventional anti-tumour treatments such as chemotherapy, radiotherapy and ICI.

2.3 Maraba virus (MG1)

2.3.1 Background

Maraba virus belongs to the *vesiculovirus* genus of the *Rhabdoviridae* family and was first isolated from Amazonian phlebotomine sand flies in Brazil, thereby avoiding the risk of livestock infection associated with VSV. A lack of pre-existing antibodies in the human population gives further advantage to its therapeutic potential. The virion consists of a bullet-shaped enveloped particle (Ø: 70nm, L: 170nm) harbouring an 11-kb single-stranded negative sense RNA genome (NCBI reference: NC_025255). Its genome consists of a 3' leader sequence and a 5' trailer sequence separated by five open reading frames, each encoding one viral protein: nucleocapsid (N), phosphoprotein (P), matrix (M), glycoprotein (G) and polymerase (L) (Figure 2).

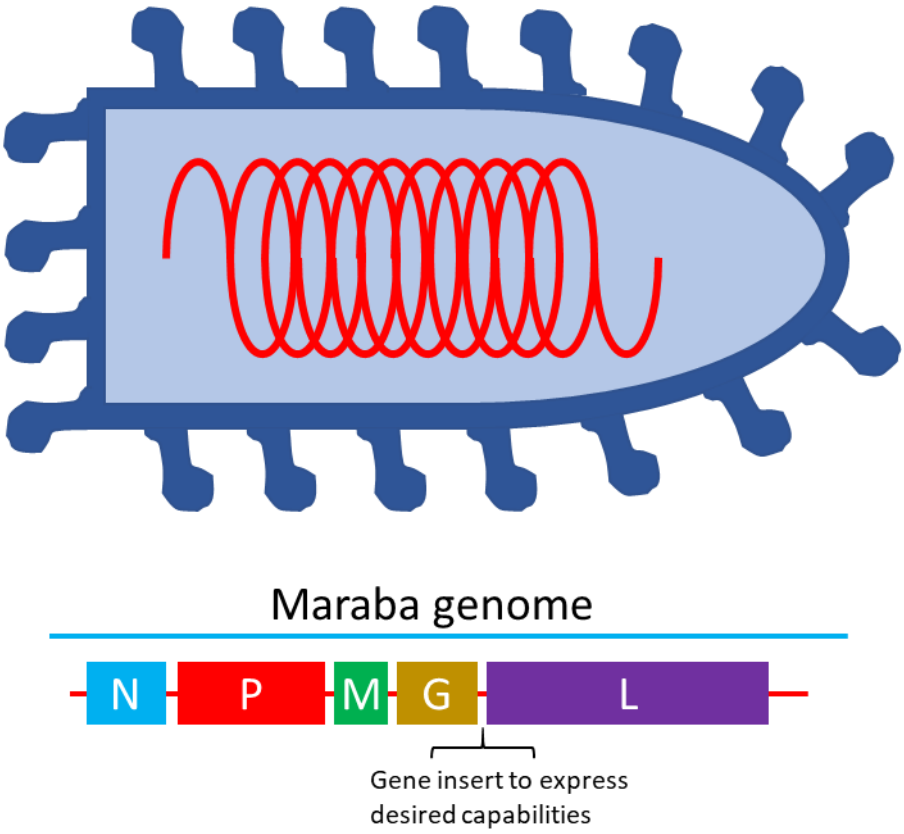

Figure 2: Maraba virus structure

There has been no reported maraba-related pathogenicity in humans and only one case of seroconversion against viral antigens documented in the literature (130) and therefore maraba possesses good OV characteristics. The life cycle of maraba virus (Figure 3) occurs exclusively in the cytoplasm and so there is no risk of genotoxicity. Maraba virus exploits the ubiquitous low-density lipoprotein receptor (LDLR) to attach (1) and enters into host cells via endocytosis (2). After receptor-mediated endocytosis, the cellular endosome undergoes acidification and the drop in endosomal pH triggers a conformational change in the glycoprotein that mediates fusion between the viral envelope and the endosomal membrane (3). The viral nucleocapsid is then able to escape into the cytoplasm and initiate viral replication. The viral polymerase first transcribes the individual mRNAs for each viral gene (4) which are then translated via host ribosomes to yield viral proteins (5). At the later stages of infection, the viral polymerase switches from transcription to replication and synthesises copies of the negative-sense maraba genome through positive-strand intermediates (6). Finally, the viral proteins and genomic RNA are assembled into complete virus particles and the virus exits the cell by budding through the plasma membrane (7).

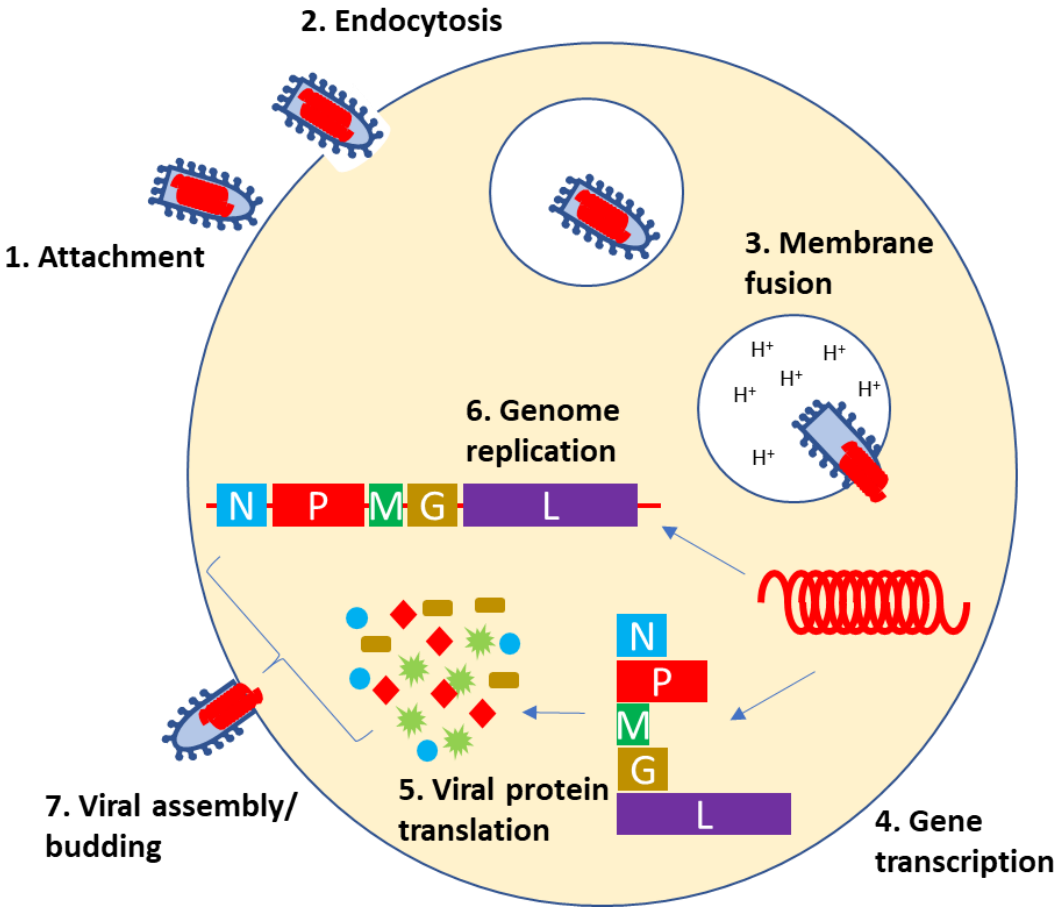

Figure 3: Lifecycle of maraba virus

Figure adapted from:

Lichty, B.D. et al., Vesicular stomatitis virus: re-inventing the bullet. Trends in Molecular Medicine, 2004. ***10****(5): p. 210-216.*

Maraba virus has been genetically modified with two mutations which translates into the L123W and Q242R substitutions in the sequence of the M and G proteins, respectively. This novel strain, named MG1, demonstrated faster replication, larger burst size and increased killing potency in a panel of human tumour cells (ES 2 ovarian cancer, A549 lung cancer and SW620 colorectal cell lines) compared to wild type maraba virus (131). Conversely MG1 was also strongly attenuated in normal primary cells validating its oncotropism. The abortive replication of MG1 in normal cells is mostly due to the inability of MG1 to block type I IFN-mediated antiviral immunity whereas this IFN pathway is often defective/deficient in malignant cells (131).

2.3.2 MG1 Cytotoxicity

In vitro, MG1 has shown oncolytic activity against multiple adherent cancer cell lines of human, canine and murine origins (Table 2). In addition, Tong *et al.* also found that MG1 was able to induce cell death in ovarian cancer cells whether the cells were adherent, in suspension or in three-dimensional spheroid form (which can be found in the peritoneal cavity of ovarian cancer patients) (132). MG1 cytopathic effect was also superior when evaluated across a panel of sarcoma cell lines *in vitro*, when compared to VSVΔ51, HSV N212, VVdd and Pelareorep (reovirus) (133).

Ex vivo primary human cancer biopsies were also shown to be amenable to MG1 infection and replication resulting in significant cytopathic effects across a range of tumour tissues including prostate cancer, head and neck squamous cell carcinoma and sarcoma (133, 140, 146). The latter two of these tumour sites tend to possess very poor prognosis in the advanced setting and so MG1 is an enticing therapeutic prospect for these cancers.

The efficacy of OV therapy, as with other treatments, depends heavily on the successful delivery of the anti-tumour agent to the malignant mass. Many OVs have demonstrated that the most efficient and safest way to administer the viral vector is via direct intratumoural injection, however this limits the applicability of OVs to cancers that are accessible and localised. Conversely, MG1 has shown successful systemic delivery in mice harbouring syngeneic

subcutaneous CT26 colorectal carcinoma. Repeated systemic administration of MG1 was shown to reach the tumour bed and replicated in situ, leading to complete tumour regression and durable cures resistant to tumour rechallenge (131). In addition, there was also impressive efficacy in clearing CT26 lung metastases. Since this initial study, there have been multiple publications to show MG1 efficacy in other syngeneic or xenograft models, including breast, ovarian, leukaemia, mammary gland, prostate, sarcoma and skin cancers (147).

MG1 has also shown versatility to be combined effectively with other treatments such as chemotherapy. Bourgeois-Daigneault *et al*. demonstrated that combination MG1 and paclitaxel provided synergistic benefit in mice bearing subcutaneous breast tumours (134). Mechanistically, paclitaxel was shown to impair IFN-β production hence allowing MG1 replication and oncolysis in the breast cancers.

Table 2: Cell lines in which MG1 oncolytic activity has been investigated

Origin	Cancer type	Cell line	References
Canis familiaris	Sarcoma	D17	(133)
Homo Sapiens	Breast cancer	BT549 HS587T MCF7 MDA-MB-231 MBA-MB-435 NCI/ADR-RES T47D	(131, 134, 135)
	Central nervous system cancer	SF268 SF295 SF539 SNB19 SNB75 U118 U243 U273	(131, 136)
	Colon cancer	COLO205 HCT116 HCT15 HT29 SW620	(131, 137)
	Leukaemia, lymphoma	A301 Jurkat OCI-Ly18	(138)
	Lung cancer	A549 HOP62 HOP92 NCI-H226 NCI-H23	(131, 136)
	Ovarian Cancer	ES2 HEYA8 iOvCa105 iOvCa131 iOvCa142 iOvCa147 OVCAR3 OVCAR4 OVCAR8 SKOV3	(131, 132, 136, 139)
	Pancreatic cancer	PANC-1	(131)
	Prostatic cancer	DU145 LNCaP PC3	(131, 140)
	Renal Cancer	786-O ACHN SN12C	(131)

		TK10	
	Sarcoma	143B RD-ES SW982 U2OS	(131, 133, 141)
	Skin Cancer	A431 M14 MALME3M SKMEL28 UACC257 UACC62	(131)
Mus musculus	Central nervous system cancer	GL261	(131)
	Colon cancer	CT26 CT26lacZ	(131, 137)
	Leukaemia, lymphoma	EL4 L1210	(138)
	Lung cancer	TC1	(142)
	Mammary gland cancer	E0771 EMT6 4T1	(131, 134, 143)
	Ovarian cancer	ID8	(144)
	Prostate cancer	TRAMP-C1 TRAMP-C2	(140)
	Skin cancer	B16 B16F10 B16lacZ	(116, 137, 145)

Table adapted from:

Pol, J.G. *et al*. *Development and applications of oncolytic Maraba virus vaccines.* Oncolytic Virother, 2018. **7**: p. 117-128.

2.3.3 MG1 and the immune system

The therapeutic effects of MG1 are not only dependent on its potent oncolytic properties but also its ability to stimulate an anti-tumoural immune response. Zhang *et al*. demonstrated that an UV inactivated MG1 (MG1-UV^{2min}) was as effective in reducing lung metastases in a syngeneic B16lacZ melanoma lung murine model as live MG1 (116). There was no detection of MG1 protein or genome in the lungs of MG1-treated mice, further indicating that the *in vivo* efficacy of MG1 in the B16lacZ model is attributed to immune-mediated cytolysis rather than viral oncolysis (116). In this same model, they observed splenomegaly 5 days post-MG1 systemic delivery caused by an expansion in innate immune cells (NK cells and DCs) compared to other immune populations. This was accompanied by a remarkable enhancement of effector NKs secreting IFN-γ or granzyme B which was dependent on the virus interaction with DCs. NK cell activation appeared critical for the therapeutic efficacy as selective depletion of NKs abolished tumour growth control.

The stimulation of anti-tumoural immune response by MG1 seems to be of particular interest in the neoadjuvant setting (116, 135). Surgical stress seems to be associated with immunosuppression and cancer progression (146). However, perioperative live or attenuated MG1 was able to decrease tumour metastases post-surgery in B16lacZ melanoma and 4T1 breast murine models compared to surgery alone, which also led to improved overall survival in the B16lacZ lung metastasis model (116). Neoadjuvant MG1 also demonstrated benefit in murine triple-negative breast cancer (TNBC) models (135). Intratumoural injection of MG1 to the primary tumour, which was subsequently surgically resected provided protection against secondary cancer rechallenge in at least 20% of mice across all three TNBC models tested. This effect was shown to be dependent on viral replication as UV-inactivated MG1 negated the benefit in this rechallenge murine model. Intravenous MG1 was found to be more efficient than local administration with 40% of mice remaining disease-free in this rechallenge setting. Furthermore, 90% of cured mice from the post-operative rechallenge completely rejected a second one afterwards, suggesting that anti-neoplastic T cell memory had been stimulated.

Transcriptomic analysis demonstrated that pathways linked to immune response were enriched during MG1 infection such as increased expression of chemokines (CCL5 and CXCL11), as well as activation of STAT1, NFκB subunit p65 and IRF3 (135). *In vivo*, there was greater T-cell infiltration in MG1-injected than untreated tumours at the time of surgery, whereby the migration was dependent on CXCR3, CXCL-9, -10 and -11. *Ex vivo*, there was production of IFN-γ in restimulated splenocytes to tumour in MG1-treated mice that was reliant on receptor IFN-αR1. Finally, MG1 treatment of TNBC cell lines resulted in increased PD-L1 protein *in vitro*, while *in vivo* combination of intratumourally-delivered MG1 and immune checkpoint blockade slowed down tumour growth in the 4T1 murine model compared to untreated or animals receiving either ICIs or MG1 alone. Furthermore, neoadjuvant MG1 coupled with primary tumour resection responded well to ICI as 60-90% of animals experienced complete response after tumour rechallenge, which was completely ineffective in mice who did not receive neoadjuvant MG1 (135). Therefore, MG1 is proving to be a very promising neoadjuvant treatment immunotherapy candidate.

The immunogenic properties of MG1-infected tumour cells are also being investigated as potential cancer vaccines against leukaemia (138) and metastatic solid tumours (137). Infusion of MG1-infected γ-irradiated leukaemia cells (iLOV) to leukemic mice resulted in 60% of the animals having complete responses. Furthermore, if iLOV treatment was delivered prophylactically to mice, there was complete protection against leukaemia challenge (138). Similarly, in B16 melanoma and CT26 colon carcinoma murine models, MG1 expressing IL-12 infected cell vaccine (MG1-IL12-ICV) resulted in reduction of pulmonary lesions and increase in activated/cytotoxic NK cells in the lungs (137). The efficacy of this vaccine was dependent on both NK cells and CD8+ T cells as their selective depletion abolished anti-tumour effects.

Finally, MG1 can be utilised as a potent oncolytic vaccine vector (142, 145). This was initially shown by Pol *et al*. whereby a melanoma-associated tumour antigen (dopachrome tautomerase [DCT]) was inserted into the MG1 genome forming MG1-DCT. Although MG1-DCT alone did not prime detectable

adaptive T-cell response against melanoma antigen in a syngeneic murine melanoma model, the use in a prime-boost strategy with a replication-defective (E1/E3 deleted) adenovirus expressing the same DCT antigen (Ad-DCT) did. Out of total circulating CD8+ T-lymphocytes, 30% demonstrated reactivity against the DCT epitope following MG1-DCT infusion which was preceded by intramuscular delivery of Ad-DCT (this is in comparison to 6% with Ad-DCT alone and 20% with Ad-DCT/VSV-DCT prime boost). The Ad-DCT/MG1-DCT prime-boost not only extended median survivals in B16-F10 melanoma harbouring mice compared to Ad-DCT monotherapy but also cured 20% and 30% of the animals bearing brain and lung metastases, respectively (145). The Ad:MG1 prime-boost also incurred long-term anti-tumour memory and protected cured mice from tumour rechallenge. These anti-neoplastic effects are largely mediated by CD8+ T effectors as selective depletion of this immune subset abolished these beneficial results. The prime-boost vaccination strategy has since been demonstrated in HPV-positive tumours and prostate cancer (140, 142). MG1 virus encoding E6 and E7 antigens of the HPV serotypes 16 and 18 (MG1-E6E7) was able to clear tumours in 60% of mice harbouring HPV-positive TC1 lung tumours and these cured mice were completely protected against a long-term aggressive tumour re-challenge. Twenty-four hours after intravenous delivery of MG1-E6E7 infection was associated with a local increase in the expression of genes involved in antigen presentation (e.g. H2-K1, Tap1, Tapbp), antiviral innate immunity (e.g. Ddx28, Irf7, Stat1) or T-cell activation (e.g. Cd28, Il2ra), in comparison to untreated tumours (142). Similarly, MG1 expressing the human six-transmembrane antigen of the prostate (STEAP) protein (MG1-STEAP) generated specific CD8+ T-cell responses against STEAP epitopes and *in vivo* delayed tumour progression in mice with bulky TRAMP-C2 tumours (140).

2.3.4 MG1 clinical trials

Following the promising results with the prime-boost strategy in preclinical studies, subsequent non-human primate trials with Ad:MG1 oncolytic vaccination in cats (147) and macaque monkeys (148) revealed Ad and MG1

vaccination to be tolerable, non-pathogenic and able to initiate humoral and cellular immunities to the epitopes of the tumour associated antigens incorporated in both viruses.

These results led to three human clinical trials to be initiated; the first phase I/II trial evaluates Ad:MG1-MAGEA3 in human patients with MAGE-A3-positive solid tumours (commonly NSCLC, melanoma and certain haematological malignancies) [clinicaltrials.gov reference NCT02285816]. Patient received either 2 infusions (3 days apart) of MG1-MAGEA3 at a dose of $1x10^{10}$ pfu (arm A), or intramuscular Ad-MAGEA3 at a dose of $1x10^{10}$ pfu (arm B) or IM Ad-MAGEA3 followed 2 weeks later with systemic MG1-MAGEA3 (arm C). In this trial, MG1-MAGEA3 genomes were detected in blood samples of patients 2 weeks post-treatment, hence confirming the ability of the virus to replicate in humans. Importantly, anti-tumour immunity was evident in 3 out of 6 patients evaluated, with over 1% of total circulating CD8+ T cells reacting against MAGE-A3 in one participant (149). A second phase I/II clinical trial will evaluate Ad-MAGEA3:MG1-MAGEA3 in combination with pembrolizumab in previously treated metastatic NSCLC (clinicaltrials.gov reference NCT02879760). The third clinical trial again investigates the prime-boost strategy, but this time the viruses incorporates the HPV E6 and E7 proteins. Ad-E6E7:MG1-E6E7 in combination with atezolizumab is being evaluated in advanced or recurrent HPV associated tumours (clinicaltrials.gov reference NCT03618953).

2.4 Enhancing oncolytic virus therapy

The self-amplifying, immunogenic and oncolytic properties of OVs makes them promising anti-cancer agents to investigate and develop. However, it is perhaps unsurprising, as with many other cancer therapeutics, that there is unfortunately limited single agent activity of OVs in the majority of patients and that the greatest therapeutic gains are likely to be harboured through combination strategies built upon understanding of cancer biology. There are many factors to consider in selecting both a virus and a combination partner, such as viral genome (DNA vs. RNA and transgene capacity), ability of virus

to engage immune system, route of viral delivery (IT vs. IV), non-overlapping toxicity profiles and sequencing of treatments are just to name a few. There have been recent reviews (112, 150) written on this topic and here I discuss just a couple of the most promising OVs combination strategies.

2.4.1 OVs and Radiotherapy

Radiotherapy (RT) is an essential treatment modality in cancer with around 60% of patients with malignancy receiving RT in their treatment lifetime. Many viruses develop strategies to inhibit cellular DNA repair pathways which can prove to be a fatal synergistic combination for tumour cells when concurrently treated with RT, that also induces double strand DNA breaks (151). Adenoviruses have been shown in particular to target non-homologous end joining (NHEJ) DNA repair pathway (152). This hypothesis was tested with the oncolytic adenovirus CG7870 with RT in LNCaP xenograft (human prostate adenocarcinoma) model, which resulted in a synergistic increase in cell killing, both *in vitro* and *in vivo* compared to either single agent alone (153). This synergistic finding with RT were also true with other adenoviruses in A549 lung cancer (154), ovarian cancer cell lines (155) and glioma xenografts (156).

Another potential mechanism for RT and OV combination is where RT can induce increased viral replication, which was demonstrated with reovirus type 3 Dearing (RT3D) when combined with EBRT showed significant enhancement of cytotoxicity relative to either single agent alone both *in vitro* and *in vivo* in melanoma cell lines (157). This increased replication was mediated by RT-induced cancer up-regulated gene 2 (CUG2) up-regulation and subsequent down-regulation of pPKR and p-elF2α which led to mitochondrial apoptotic signalling and increased cell death. HSV replication has also been shown to increase with radiation exposure, resulting in significant reduction of tumour volume compared to single treatment alone for NSCLC (158) and malignant mesothelioma (159). The underlying mechanism of increased replication with RT is hypothesized due to RT-mediated increase in cellular GADD34 expression (158), which is a DNA damage- and growth arrest-inducible gene that helps to protect cells against genetic insults. A region of GADD34 shows significant homology to HSV-1 γ34.5 protein (160),

which is often deleted in oncolytic HSV to reduce viral induced neurotoxicity. However, the deletion of γ34.5 protein reduces viral replication and cytotoxicity in tumour cells. Therefore, RT-mediated upregulation of cellular GADD34 can functionally replace γ34.5 resulting in increased viral replication and improved tumour-cytotoxicity without the risk of neurovirulence.

Another example for OV and RT synergistic combination is demonstrated with oVV, GLV-1h68) and RT which led to increased cytotoxicity in sarcoma cell lines. This time, the effect was mediated through the induction of intrinsic apoptosis (161). The differences in mechanisms of synergy between EBRT and OV combinations are most likely due to the inherent differences in characteristics between different OVs.

OV could also be engineered to induce selective radiosensitivity in tumour cells with many viruses being modified to include promoters that are activated by RT exposure or genes that sensitize cells to RT-induced cell death. An example of this strategy was in oncolytic adenovirus, AdΔ24 (E1A-deleted) (162) which was modified to express the tumour suppressor gene p53. Introduction of functional p53 into p53-negative cells results in increased sensitivity to RT-induced cell death (163). *In vitro*, AdΔ24-p53 and RT resulted in synergistic cytotoxicity in human glioma cell lines than single treatments alone and this combination resulted in 50% long-term survival in immunocompromised s.c. glioma models *in vivo* (164).

To date, clinical experience with OV and RT combinations have been mainly limited to local administration (mostly intratumoural (IT)). One example of such trials is the randomised phase II trial of intra-prostatic injection of an oncolytic adenovirus in combination with radical dose of intensity modulated radiotherapy (IMRT) (165). The results confirmed safety as well as efficacy showing 42% relative reduction in biopsy positivity at 2 years in the investigational arm versus IMRT alone. Another phase I/II trial investigated IT delivered oncolytic HSV GM-CSF in combination with radical chemo-radiotherapy in squamous cell head and neck cancers followed by neck dissection 6 to 10 weeks later (166). The results again showed safety of the combination treatment as well as impressive efficacy data whereby not only

was the disease-specific survival 82.4%, but 94% of patients had complete pathologic responses. There were also no locoregional relapses at 29 months of follow-up (historic control series indicate two-year locoregional relapse rate of 30-50%).

The pre-clinical and clinical data supports the safety and scientific rationale for OV and RT combination. However, clinical investigation of this strategy has mainly been limited by the need to access the tumour directly for OV delivery.

2.4.2 OVs and immune checkpoint inhibitors

Immune checkpoint inhibitors have been the most clinically impactful step forward in cancer treatment over the last decade. These agents block the negative regulators of T cell function, leading to T cell activation. Amongst these agents, PD-1/ PD-L1 and CTLA-4 inhibitors have been the most successful to date, resulting in clear clinical benefit in multiple tumour sites (167-170). Currently, the FDA has approved 6 ICIs for clinical use: ipilimumab, nivolumab, pembrolizumab, atezolizumab, avelumab and durvalumab. The effectiveness of anti-PD1/PD-L1 therapy is related to the immune TME, with tumours lacking lymphocyte infiltration and an IFN-γ gene signature being less responsive to ICIs (171). Therefore, the ability of OVs to convert the tumour to a more immune cell-rich environment should result in better therapeutic responses to ICIs (Figure 4). This paradigm has stimulated active, ongoing research combining OVs and ICI treatments in cancer therapy which we have recently reviewed (172).

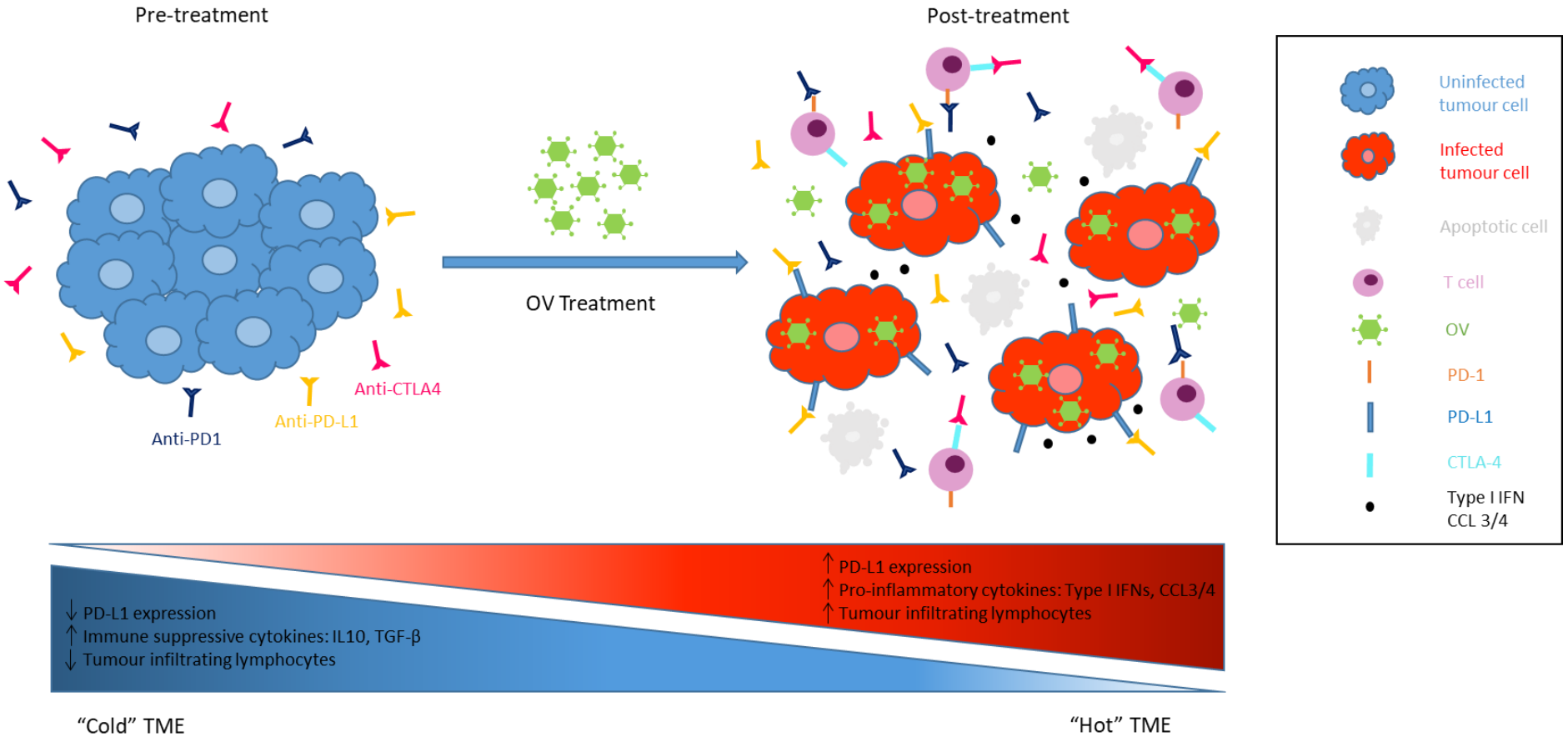
Pre-treatment
Post-treatment
OV Treatment
Anti-PD1
Anti-PD-L1
Anti-CTLA4
Uninfected tumour cell
Infected tumour cell
Apoptotic cell
T cell
OV
PD-1
PD-L1
CTLA-4
Type I IFN
CCL 3/4
↓ PD-L1 expression
↑ Immune suppressive cytokines: IL10, TGF-β
↓ Tumour infiltrating lymphocytes
↑ PD-L1 expression
↑ Pro-inflammatory cytokines: Type I IFNs, CCL3/4
↑ Tumour infiltrating lymphocytes
"Cold" TME
"Hot" TME

Figure 4: OV have the ability to turn the TME from "cold" to "hot".

Prior to OV treatment, checkpoint inhibition is therapeutically inefficient as the tumour expresses low levels of PD-L1 (therefore no target for anti-PD-L1 antibodies) and is poorly infiltrated with immune cells (therefore no target for anti-PD1 and anti-CTLA4 antibodies). After OV infection, the tumour increases expression of PD-L1 and releases pro-inflammatory cytokines e.g., type I IFNs and CCL3/4, which attract immune cell infiltration, thereby increasing the efficacy of immune checkpoint blockade. OV: oncolytic virus; PD-1: Programmed death-1; PD-L1: Programmed death ligand-1; CTLA-4: Cytotoxic T-lymphocyte-associated protein 4; IFN: Interferon; CCL3/4: Chemokine (C-C motif) ligand 3 or 4

Many DNA and RNA viruses have been shown to stimulate a “hotter” immune TME when combined with ICI, for example Chen *et al*. showed that HSV1716 and anti-PD-1 antibody led to increased infiltration of effector CD4+ and CD8+ T cells, but no similar increase in FoxP3 Treg cells resulting in extended survival in murine models of rhabdomyosarcoma (173). Similar synergistic effects were observed when ICIs were combined with vaccinia virus (174), reovirus (175), rotavirus (176) and measles virus (177), all resulting from beneficial changes in the tumour immune microenvironment. Many other viruses have also been deliberately engineered to be armed with anti-PD1 or anti-CTLA4 antibodies to deliver this lethal combination to tumour cells. For example, Kleinpeter *et al*. inserted three forms of murine PD-1 (mPD-1) binders into Western Reserve strain of oncolytic vaccinia virus (oVV). The authors then assessed the expression of the resulting anti-PD-1 antibodies and their anti-tumour efficacy *in vitro* and *in vivo* in multiple tumour models. They showed the resulting viruses were indeed produced, assembled and able to block murine PD-1 ligand binding after virus infection, which subsequently led to improved survival in mice harbouring subcutaneous fibrosarcoma (178). Engeland *et al*. also engineered attenuated measles virus by encoding antibodies against CTLA-4 and PD-L1 (MV-aCTLA-4 and MV-aPD-L1). Using an immunocompetent murine model of malignant melanoma, treatment with MV-aPD-L1 mediated checkpoint modulation demonstrated an increase in CD8+ T cell tumour infiltration, increase in IFN γ-expressing CD8+ T cell production and a decrease in Tregs cells. Delayed tumour progression and improved mOS were observed for animals treated with measles virus encoding anti-CTLA-4 and anti-PD-L1 when compared to controls (179).

Clinically T-VEC is the only FDA-approved OV for the treatment of metastatic melanoma. With the success of T-VEC monotherapy and its ability to modulate the immune response to tumours, it was postulated that there would be a greater therapeutic benefit in combination with ICIs. A Phase Ib/II trial of T-VEC in combination with ipilimumab (an anti-CTLA-4 antibody) for patients with previously untreated unresectable stage IIIB-IV melanoma. The first part of the study recruited nineteen patients in total and resulted in an ORR of 50%; 44% of patients had a durable response lasting ≥6months and there were no

documented dose-limiting toxicities (180). The subsequent phase II part of the trial randomised patients with advanced melanoma to either ipilimumab alone or in combination with T-VEC. The outcome demonstrated an ORR in 39% of patients receiving T-VEC and ipilimumab compared to 18% in patients receiving ipilimumab monotherapy. Importantly distant non-injected sites also showed anenestic responses with visceral lesions reducing in size in 52% of patients with combination treatment, compared to 23% of patients in the ipilimumab alone arm (181) (ClinicalTrials.gov: NCT01740297).

T-VEC has also been tested in combination with an anti-PD-1 antibody (pembrolizumab) for patients with advanced melanoma in the Masterkey-265 trial (ClinicalTrials.gov: NCT02263508). This is a phase Ib/III trial that has revealed promising results so far. The phase I component demonstrated an ORR of 62%, with a complete response rate (CRR) of 33% in patients receiving T-VEC + pembrolizumab combination therapy. The treatment was well tolerated with no dose-limiting toxicities occurring. Patients who responded to combination treatment had increased CD8+ T cells, elevated PD-L1 expression as well as IFN-γ gene expression on several cell subsets in tumours after induction T-VEC alone treatment (120). These data support the theory that oncolytic virotherapy can enhance the efficacy of ICI by altering the TME, making cold tumours hotter, and priming for more effective checkpoint blockade. The subsequent phase III trial has now completed recruitment and outcome data are eagerly awaited.

Therefore, there is vast amount of pre-clinical and clinical data to support the promise of OV and ICI combination as novel strategy to add to the artillery of anti-cancer treatments.

2.5 Conclusion:

Although there has been drastic improvement in the treatment of advanced NSCLC over the past decade, mainly resulting from the application of ICI, the 5-year OS in the metastatic setting is still poor (~6%) and the response rates to ICIs is low (10-20%). Therefore, there is still an unmet need to find novel

treatments or combination therapies with better response rates to improve the survival in these groups of patients.

OVs represent a promising therapeutic platform with their self-amplifying, tumour-tropic, oncolytic and immune stimulatory properties. These viruses can also be genetically manipulated to include inserts that can boost its anti-tumour effects either as monotherapy or to enhance combination potential with other therapeutic agents. Furthermore, OVs have shown to be effective partners when deployed with ICI as they can promote recruitment of effector lymphocytes as well as inducing the expression of PD-1/PD-L1 to increase the response and reverse resistant to ICI. RT has also been shown to improve OVs effects by enhancing viral replication and inducing cellular apoptotic pathways. OVs can also be genetically engineered to contain RT-induced transgenes that can lead to selective radiosensitisation of cancer cells to improve anti-tumour effects. OVs therefore represents an attractive, potent and versatile weapon to add to the armoury of cancer treatment. However, to date, established clinical use of OVs has been limited to local delivery for accessible tumours as systemic delivery of viruses often does not reach the tumour in the presence of neutralising antibodies (NAbs), which can impede oncolytic therapy, both direct cytotoxicity and induction of anti-tumour immunity.

Maraba virus is a relatively novel OVs that appears to be a powerful multifunctional tool in the fight against cancer, with very little pre-existing immunity in the general population. Firstly, many tumours are susceptible to MG1-mediated oncolysis. Furthermore, MG1 oncotoxicity has been shown to stimulate both the innate and adaptive anti-tumour immune response. Clinical application of MG1 virus, to date, has been focused on the prime-boost strategy for vaccination against tumour associated antigens which has led to remarkable extension of the survival in several pre-clinical murine models. MG1 has also demonstrated efficacy when delivered systemically in murine melanoma models which can slow down subcutaneous tumour growth as well as distant metastases, giving promise to widespread clinical use in metastatic malignancies. In conclusion, MG1-maraba virus represents an encouraging

OVs to investigate for anti-cancer effects either as monotherapy or in novel therapeutic combinations.

2.6 Aims

The aims of this study were to examine MG1-maraba virus as a potential anti-cancer agent for the treatment of NSCLC, by investigating both direct cytotoxicity and generation of anti-tumour immunity. In addition, to determine whether MG1 efficacy can be enhanced by combining with other standard of care cancer treatments such as RT or ICI.

Specific aims of the project are:

1. Investigate the cytotoxicity of MG1-maraba virus against murine and human NSCLC cell lines and primary human cell line.
2. Test the efficacy of intratumoural and systemic delivery of MG1-maraba virus in murine NSCLC *in vivo* model.
3. Characterise the immune effects of MG1-maraba virus in NSCLC in terms of identifying DAMPS, type I IFN production and changes in the tumour immune microenvironment *in vivo*.
4. Determine whether oncolytic MG1-maraba virus can be effectively enhanced with RT and ICI

Chapter 3:
Material and Methods

3. Chapter 3: Material and Methods

3.1 Cell Culture

Human non-small cell lung cancer cell lines: NCI-H1792, NCI- H1437, NCI-H1573, NCI-H1975 (all adenocarcinomas) and NCI-H1299 (large cell carcinoma) were purchased from ATCC in 2017. 3LL (Lewis lung carcinoma) cell line was obtained from Professor Julian Downward (The Francis Crick Institute, London, 2017). Sum149 Parental and Revertant cell lines were provided by Dr Rachel Brough (ICR, London, 2019). Primary human foreskin fibroblast (HFF), B16-F1 and vero cell line were obtained from existing ICR laboratory stocks. Sum149 Parental and Revertant cell lines were grown in F-12 Hams supplemented with 5% heat-inactivated foetal bovine serum (FBS), 1 ug/ml hydrocortisone (H4001, Sigma), 2.5mM L-glutamine and 5 ug/ml insulin (I9278, Sigma). Vero and HFF cells were cultured in Dulbecco's Modified Eagle's Medium (DMEM) supplemented with 5% FBS, 2.5 mM L-glutamine and penicillin-streptomycin (60 mg/L and 100 mg/L respectively). All other cell lines were cultured in Roswell Park Memorial Institute (RPMI) media with the same supplementations as DMEM. All media and reagents were supplied by Laboratory Support Services, ICR, London unless stated otherwise. Cells were cultured at 37^{o}C in a humidified atmosphere of 5% CO_2. Cell lines were routinely tested for *mycoplasma* using the e-Myco PCR kit (Intron Biotechnology, South Korea) and experiments carried out within 3 months of resuscitation.

3.1.1 Cryopreservation

Cells were harvested and pelleted by centrifugation; cell pellets were re-suspended in freezing medium (90% (v/v) FBS; 10% (v/v) dimethyl sulfoxide (DMSO)) and stored in 1 ml cryovials (Nunc®). Cryovials were immediately placed at –80˚C. Cells were thawed in a 37˚C water bath, washed in a large volume of RPMI or DMEM to remove DMSO, re-suspended in growth medium and placed into a culture flask.

3.1.2 Isolation of human PBMC

Fresh blood from healthy volunteers were collected in 10 ml K2EDTA BD Vacutainer™ tubes (Fisher Scientific 10331254) and diluted 1:1 with Hanks' Balanced Salt Solution (HBSS) at room temperature. 30 ml aliquots were then layered on top of 15 ml Lymphoprep© (Alere Ltd.) before being centrifuged in a Heraeus Megafuge 2.0R centrifuge at 800g for 25 mins with no brake. Plasma was removed and the white cell layer isolated using a wide-tipped Pasteur pipette (Alpha laboratories Ltd.). Cells were washed with 50 ml HBSS and centrifuged at 400g for 10 mins. Cells were washed again with 50 ml HBSS and centrifuged at 300g for 5 mins. Freshly isolated PBMCs were used immediately for human NK cell degranulation assay.

3.2 Maraba (MG1) virus

MG1-green fluorescent protein (MG1-GFP) and MG1-firefly luciferase (MG1-FLUC) were originally produced and provided by Ottawa Hospital Research Institute (Ottawa, Canada) (131) in PBS. Each virus was amplified (2.4.1) and aliquoted into 200 µl eppendorfs to be stored long term at -80˚C. Virus titre was determined by plaque assay using vero cells (3.4.2).

3.2.1 MG1 viral amplification

T175 flasks which were 100% confluent with vero cells were infected with 0.01 MOI MG1-GFP/FLUC virus and left at 37ºC in a humidified atmosphere of 5% CO_2 for 24 hrs. The supernatant in these flasks were harvested and centrifuged in a Heraeus Megafuge 2.0R centrifuge at 400g for 10 mins to pellet the cellular debris for disposal. The residual supernatant was then filtered through 0.2 µm filters (Sartorius™ Minisart™ High Flow (HF) syringe filters, Fisher Scientific, 10686521) and centrifuged again at 14000rpm (Beckman Coulter Optima XPN ultracentrifuge) for 1 hr. The final pellet was then resuspended in 1 ml of PBS prior to aliquoting for storage as described above.

3.2.2 Plaque assay

Vero cells were seeded at $1.5x10^5$ cells/well in 24-well plates and incubated at 37˚C for 24 hrs. Serial dilutions between $2x10^{-4}$ and $2x10^{-9}$ of MG1 infected lysates and stock MG1 were prepared in virus serum-free dilution medium (DMEM, 2mM L-glutamine). Medium was removed from the vero cells and replaced with 200µl virus serum-free dilution medium followed by 100 µl of diluted viral samples, in duplicates. After 1 hr incubation at 37ºC, the supernatant medium was removed, and the cells overlaid with a 1:1 solution of 3% (w/v) CMC (sodium carboxymethyl cellulose; Sigma) and 10% DMEM. After 72 hrs incubation at 37ºC, plates were fixed with 0.1% (v/v) glutaraldehyde in PBS for 10 mins. The fixative was removed, and cells stained with crystal violet (0.05% (w/v) in 80% ddH2O; 20% ethanol) for 5 mins. Plates containing plaques were scanned and counted manually. The average of duplicate wells was used to calculate viral titre, using the following calculation:

$$\text{pfu/ml} = \frac{\text{Average number of plaques}}{\text{Dilution}}$$

3.2.3 MG1 infection of NSCLC cells

Cells were harvested and seeded into 6-well plates with $4.5x10^5$ cells per well in 4 mls growth medium. MG1-GFP was diluted in PBS and added at various concentrations 0, 0.01, 0.1 and 1 multiplicity of infection (MOI). Images were taken using an EVOS Fl cell imaging system (ThermoFisher Scientific) microscope at 24 and 48 hrs. In a separate experiment, cells were infected in a similar fashion, this time with MG1-FLUC virus prior to harvesting at 24 and 48 hrs. $1x10^5$ cells were added per FACS tube (BD Falcon) and cells were washed with 2 mls of FACS buffer (PBS; 1% (v/v) FCS; 0.1% (w/v) sodium azide) and centrifuged in a Heraeus Megafuge 2.0R centrifuge at 400g for 5 mins at 4ºC. Cells were re-suspended in 100 µl FACS buffer before the

addition of viability dye (eBiosceience fixable viability dye eFluor 780 (65-0865-15). Cells were incubated for 30 mins at 4^{o}C in the dark and then washed with 4 mls FACs buffer, cells were fixed with 1% PFA (1% (w/v) paraformaldehyde in PBS) and stored at 4^{o}C prior to acquisition on a BD LSRII flow cytometer.

3.2.4 MG1 replication in NSCLC cells

Cells were harvested and seeded into 6-well plates with 4.5x10^{5} cells per well in 4 mls growth medium and infected with MG1-GFP at 0.1 MOI dose. Cells and supernatants were collected using a wide-tipped Pasteur pipette at 24, 48 and 72 hrs. Lysates were generated by 3 cycles of freeze-thaw (10 mins dry ice, then in a water bath at 37^{o}C and MG1 virus titre determined by plaque assay (see section 3.2.2).

3.2.5 MTT assay in MG1-infected NSCLC cells

MTT is a colorimetric test which relies on NAD(P)H-dependent oxidoreductase enzymes within viable cells to reduce a yellow tetrazolium salt (3-(4,5-dimethylthiazol-2-yl)-2,5-diphenyltetrazolium bromide or MTT) to formazan. The insoluble formazan crystals are dissolved with dimethyl sulfoxide (DMSO) and the resulting purple coloured solution is quantified by measuring absorbance at 550nm using a multi-well spectrophotometer.

Cells were seeded into 96-well plates with 1x10^{4} cells per well in 200 µl growth media and infected the following day with various concentrations of MG1-GFP at 0, 0.0001, 0.001. 0.01 and 0.1 MOI. Cell viability was determined at 48 hrs. 20µl of 12mM MTT was added for the final 4 hrs, then the medium was aspirated, and crystals dissolved in 200 µl DMSO before absorbance at 550 nm was measured and normalised to DMSO-treated cells.

MTT assays were also performed to assess cell viability after combination RT and MG1 therapy. In these experiments, the process was identical to the description above, except RT was administered (as described in section 3.3 below) 24 hrs prior to MG1-GFP exposure and cell viability was assessed at 72 hrs after RT.

3.2.6 IFN-beta protection against MG1 infection

B16-F1 melanoma cells were seeded into 6-well plates with $4.5x10^5$ cells per well in 4 mls growth medium. Exogenous recombinant murine IFN-beta (R&D systems catalogue ref: 8234-MB) was added at concentrations of 0 (control), 20, 200 and 2000 pg/ml and incubated for 24 hours prior to MG1-GFP viral infection at 0.1 MOI. Cell viability was then assessed using MTT assay (described in section 3.2.5).

3.3 External beam radiotherapy (EBRT)

All irradiation was performed using an Orthovoltage X-ray source (320/250kV; serial no:20090606) (AGO X-Ray Ltd, Reading, UK) at 250kVp and at a dose rate of approximately 0.6 Gy/min, as measured directly by a UNIDOS©E Universal Dosimeter (PTW, Grantham, UK). Cells were irradiated in 6-, 24- or 96-well plates (Nunc. Denmark) in single fractions up to 8 Gy. Eppendorf tubes containing MG1-GFP at $3x10^7$pfu (plaque forming units)/ml were irradiated at 0, 2, 4, 8, 16 and 32 Gy.

3.4 Enzyme-linked immunosorbent assay (ELISA)

HMGB1 was assessed using Tecan HMGB1 ELISA kit (catalogue ref: ST51011), while IFN-β was determined via mouse IFN-beta ELISA kit; R&D systems (catalogue ref: 42400-1). Samples were collected as described in 3.5 and 3.11. For both ELISA assays, standard curves were prepared as follows:

HMGB1 ELISA:

Concentration (ng/ml)	Dilution method	Standard
80	Add 100 µl of standard solution (320 ng/ml) to 300 µl of Diluent buffer and mix.	7
40	Add 100 µl of **Standard 7** to 100 µl of Diluent buffer and mix.	6

20	Add 100 µl of **Standard 6** to 100 µl of Diluent buffer and mix.	5
10	Add 100 µl of **Standard 5** to 100 µl of Diluent buffer and mix.	4
5	Add 100 µl of **Standard 4** to 100 µl of Diluent buffer and mix.	3
2.5	Add 100 µl of **Standard 3** to 100 µl of Diluent buffer and mix.	2
0	Diluent buffer only.	1

IFN-beta ELISA:

Concentration (pg/ml)	Dilution method	Standard
500	Add 500 µl of standard solution (1000 pg/ml) to 500 µl of Diluent buffer and mix.	7
250	Add 500 µl of **Standard 7** to 500 µl of Diluent buffer and mix.	6
125	Add 500 µl of **Standard 6** to 500 µl of Diluent buffer and mix.	5
62.5	Add 500 µl of **Standard 5** to 500 µl of Diluent buffer and mix.	4
31.3	Add 500 µl of **Standard 4** to 500 µl of Diluent buffer and mix.	3
15.6	Add 500 µl of **Standard 3** to 100 µl of Diluent buffer and mix.	2

7.81	Add 500 µl of **Standard 2** to 100 µl of Diluent buffer and mix.	1

Test procedure for each ELISA assay were as follows:

HMGB1 ELISA:

1) 100 µl of Diluent buffer was added into respective wells of the microtiter plate.
2) 10 µl of Diluent buffer was added into the blank-well of the microtiter plate.
3) 10 µl of standard, positive control and of each cell sample was added into respective wells of the microtiter plate and the plate was shaken briefly for 30 seconds.
4) The plate was covered with adhesive foil and incubated for 24 hours at 37^{o}C.
5) The adhesive foil was removed and the incubation solution was discarded. The plate was washed 5 x with 400 µl diluted Wash buffer. Excess solution was removed by tapping the inverted plate on a paper towel.
6) 100 µl of Enzyme conjugate was added into each well.
7) The plate was covered with adhesive foil and incubated for 2 hours at 25^{o}C.
8) The adhesive foil was removed and the incubation solution was discarded. The plate was washed 5 x with 400 µl of diluted Wash buffer. Excess solution was removed by tapping the inverted plate on a paper towel.
9) 100 µl Colour solution was added into each well and incubated for 30 minutes at room temperature (18-25^{o}C).
10) 100 µl of Stop solution was added into each well and briefly mixed by gently shaking the plate.
11) The plate was read on a SpectraMax 384 plate reader (Molecular Devices) at 450 nm wavelength.

IFN-beta ELISA:

1) The 96-well microplate was coated with 100 µl per well of diluted Capture Antibody. The plate was sealed and incubated overnight at room temperature.
2) Each well was aspirated and washed with 400 µl of Wash Buffer per well three times. Excess solution was removed by tapping the inverted plate on a paper towel.
3) The plates were then blocked by adding 300 µl of Reagent Diluent to each well and incubated at room temperature for 1-2 hours.
4) Step 2 aspiration/wash was repeated and the plates were then ready for sample addition.
5) 100 µl of sample or standards were added per well. The plate was covered and incubated for 2 hours at room temperature.
6) Step 2 aspiration/wash was repeated.
7) 100 µl of Detection Antibody was added to each well. The plate was covered and incubated for 2 hours at room temperature.
8) Step 2 aspiration/wash was repeated.
9) 100 µl of Substrate Solution was added to each well and incubated for 20 minutes at room temperature.
10) 50 µl of Stop Solution was added to each well and briefly mixed by gently shaking the plate.
11) The plate was read on a SpectraMax 384 plate reader (Molecular Devices) at 450 nm wavelength.

3.5 Immunogenic cell death assays

For ATP release, cells were seeded into 6-well plates with $4.5x10^5$ cells per well in 2 mls growth medium and incubated overnight. The following day, the medium was aspirated and replaced with 2 mls of fresh growth medium before adding various concentrations of MG1-GFP virus; 0, 0.0001, 0.001, 0.01, 0.1 and 1 MOI. The supernatants were then collected with a wide-tipped Pasteur pipette at 24 and 48 hrs and centrifuged at 400g in a Heraeus Megafuge 2.0R

centrifuge for 4 mins to remove cell debris. 100 µl of each supernatant was distributed into a Corning™ 96-well solid white polystyrene microplate (Fisher scientific) and 25 µl of CellTiter-Glo® Luminescent assay (Promega) was then added to each well. After the plate was incubated for 10 mins at 37ºC, the luminescent signal was read on a SpectraMax 384 plate reader (Molecular Devices).

For HMGB1 secretion, cells were plated and treated in a similar fashion as described above for ATP release assay. Culture supernatants were collected after 24 and 48 hrs and secreted HMGB1 was quantified by ELISA (method described in 3.4).

For cell surface calreticulin (CRT) expression, cells were plated in 12-well pates with $1x10^5$ cells/well, incubated overnight and treated with different concentrations of MG1-FLUC; 0, 0.01, 0.1 and 1 MOI. After 48 hrs, cells were collected and stained with recombinant anti-CRT (Alexa Fluor 647; Abcam; catalogue re: ab196159) and fixable viability dye-eFluor 780 (Thermo Fisher Scientific; catalogue ref: 65-0865-15). CRT expression was then analysed with flow cytometry. Gating was performed using “fluorescence minus one” controls and an isotype control (recombinant rabbit IgG antibody; alexa fluor 647; Abcam; catalogue ref: ab199093) was used.

3.6 Western blotting

3.6.1 Buffers

2x Loading buffer	100 mM Tris HCl pH 6-8. 4% (w/v) SDS; 0.2% (w/v) bromophenol blue; 20% (v/v) glycerol; 200 mM dithiothreitol (DTT) in ddH_20
Running buffer	25 mM Tris base; 250 mM glycine; 0.1% (w/v) SDS in ddH_20

3.6.2 Method

For western blotting, lysates were obtained directly on the culture surface with RIPA buffer (Thermo Fisher) containing protease (Complete, Roche) and

phosphatase inhibitors (phophoSTOP, Roche) and subjected to protein quantification (BCA; Thermo Scientific) prior to western blotting. Samples were mixed with an equal volume of 2x loading buffer and heated at 95^{o}C for 5 mins. 30 µl of each sample and 2 µl of Odyssey® Protein Molecular Weight Marker (LI-COR® Biosciences), to verify protein size, was loaded on to 10% Criterion^{TM} TGX^{TM} Precast Midi Protein Gel (Bio-Rad; catalogue ref: 5671034). Gels were run in Bio-Rad Mini Trans-Blot® cell containing running buffer at 100 V/gel for approximately 90 mins until the loading dye had run to the bottom of the gel. The gels were then removed from the cassettes and briefly washed with running buffer. Protein transfer was completed in a Trans-Blot Turbo Transfer System (Bio-Rad) and transferred to Trans-Blot Turbo Midi 0.2 µm nitrocellulose transfer membranes. These membranes were then briefly washed in PBS and then blocked in a 1:1 mixture of Odyssey blocking buffer (LI-COR® Biosciences) and TBST (0.05% Tween 20 in tris buffered saline) for 1 hr. Primary antibodies were added in a 1:1 mixture of blocking buffer and TBST and incubated for 24 hrs (Table 3). Primary antibodies were removed by 4 washes of 15 mins TBST. Secondary antibodies were added in blocking buffer and TBST as above and incubated for 1 hr at room temperature (Table 3). Secondary antibodies were removed by 4 washes of 15 mins in TBST. Nitrocellulose membranes were read on a LI-COR® Odyssey infrared imager and analysed using LI-COR Image Studio software.

Table 3: Antibodies used in western blotting

Antibody	Primary/Secondary	Species of origin	Dilution	Supplier	Catalogue ref
RIG-I (D14G6)	Primary	Rabbit	1:1000	Cell signalling	#3743
pTBK1 (ser172)	Primary	Rabbit	1:1000	Cell signalling	#5483
pIRF3 (Ser396)	Primary	Rabbit	1:1000	Cell signalling	#3743
BRCA1	Primary	Mouse	1ug/ml	RnD Systems	MAB22101
Tubulin	Primary	Mouse	1:1000	Sigma	T5168
GAPDH	Primary	Rabbit	1:1000	Cell signalling	#2118
Goat anti-mouse IgG, Alexa Fluor 680	Secondary	Goat	1:10000	Invitrogen	A-21058
IRDye® 800CW Goat anti-Rabbit IgG	Secondary	Goat	1:10000	LI-COR	926-32211

3.7 Polymerase chain reaction

RNA was isolated from cells using the RNeasy mini kit (Qiagen; catalogue ref: 74106) and then converted into cDNA using Biolabs ProtoScript® II reverse transcriptase (catalogue ref: M0368L), the procedures were as follows:

RNA extraction:

1. Cells were seeded in 6-well plates at $4.5x10^5$ cells per well. The medium was discarded and the cells were washed with PBS before adding 2mls of 0.25% trypsin to detach cells. Medium was added to inactivate the trypsin and the cells were isolated after centrifuging at 1400 rpm for 5 minutes.
2. 350 µl of Buffer RLT solution was added to the cell pellet and mixed using a pipet.
3. The lysate was passed at least 5 times through a blunt 20-gauge needle fitted to an RNAse-free syringe.
4. 1 volume of 70% ethanol was added to the homogenised lysate and mixed well by pipetting.
5. 700 µl of the samples were added into an RNeasy spin column and placed in a 2 ml collection tube. The lid was closed gently and centrifuged for 15 seconds at >10,000 rpm. The flow-through was discarded.
6. 700 µl of Buffer RW1 was added to the RNeasy spin column and the lid was closed gently, again centrifuged for 15 seconds at >10,000 rpm. The flow-through was discarded.
7. 500 µl Buffer RPE was added to the RNeasy spin column. The lid was closed gently and centrifuged for 15 seconds at >10,000 rpm. The flow-through was discarded. The flow-through was discarded.
8. Step 7 repeated.
9. The RNeasy spin column was placed in a new 1.5ml collection tube and 50 µl RNAse-free water was directly added to the spin column membrane. The lid was closed gently and centrifuged for 1 minute at >10,000 rpm to elute the RNA.

10. The concentration of RNA was determined by measuring the absorbance at 260 nm using the NanoDrop.

cDNA conversion:

1. 1-6 µl (up to 1 µg) of total RNA was mixed with 2 µl of $d(t)_{23}VN$ and nuclease-free water to a total volume of 8 µl.
2. The sample was heated at 65^{o}C for 5 minutes, spun briefly and put promptly on ice.
3. 10 µl of ProtoScript II Reaction mix (2X) and 2 µl of ProtoScript II Enzyme Mix (10X) was added to the samples.
4. The 20 µl of cDNA synthesis reaction was incubated at 42^{o}C for one hour.
5. The enzyme was inactivated at 80^{o}C for 5 minutes.

cDNA concentration was determined by NanoDrop and each sample was diluted to a concentration of 100 ng with nucleotide-free water to a volume of 30 µl. Primers used for human BRCA1 was 5'-GCGTCCCCTCACAAATAAAT-3' (forward) and 5'-CTTGACCATTCTGCTCCGTT-3' and mouse BRCA1 was 5'-AGGGCCATGATTGTCAGTTC-3' (forward) and 5'-GATGGAAGCTCCTTCACCAC-3' (reverse). PCR was performed using MyTaq^{TM} Mix (Bioline; catalogue ref: BIO-25041) according to manufacturer's instructions and the resulting PCR product was ran on a 2% agarose gel.

3.8 Flow cytometry- fluorescence activated cell sorting (FACS)

Viability dye: eBioscience fixable viability dye eFluor 780 (catalogue ref: 65-0865-14). Antibodies: conjugated antibodies were obtained from BioLegend (san Diego, USA) unless otherwise stated. All FACs acquisition and analysis was carried out using LSR II flow cytometer and FlowJo Software (BD Biosciences, Oxford, UK and Ashland, USA respectively). Photomultiplier tube voltages were set using fully stained samples and compensation was performed using single-stained UltraComp eBeads (eBioscience). Gating was

performed using “fluorescence minus one” controls and a limited number of isotype controls were used (Table 4).

3.8.1 Immunophenotyping in 3LL tumours

Tumours were harvested and kept on ice, then blotted dry and weighed before mechanical dissociation with scissors and enzymatic digestion for 30 mins at 37^{o}C with (per sample) 40 µl 0.25% trypsin, 20 µl collagenase (Sigma C1639 25mg/ml in PBS), 2 µl dispase (200 mg/ml) and 10 µl DNAse (20 mg/ml), before passing through a 70 µm cell strainer and rinsing with RPMI supplemented with 10% FCS and 5mM EDTA. Samples were resuspended in PBS with 5% FCS, blocked with anti-CD16/32 antibody (Biolegend 101319) for 10 mins on ice then stained immediately on ice in a staining volume of 40 µl, diluting antibodies at the dilutions given in Table 4 in PBS with 5% FCS for 30 mins before washing twice. For intracellular epitopes, samples were fixed and permeabilized after staining for extracellular epitopes, using the FoxP3/Transcription factor fixation/permeabilization kit (eBioscience 00-5521-00, Thermo Fisher, Waltham, USA) in accordance with the manufacturer protocol; subsequent staining was performed using the permeabilization buffer from this kit. After fixation, samples were washed twice and fixed using 1% formaldehyde in PBS before acquisition on a BD LSRII flow cytometer. The sample was divided equally into staining panels and each sample was acquired entirely. Counts were normalised to tumour weight and corrected for the number of panels into which the sample was divided.

Harvested spleens were crushed through a 70 µm cell strainers using the stoppers from a 2.5 ml syringes into 50 ml falcon tubes containing 5 mls of RPMI medium. After centrifugation at 400g for 5 mins, the medium was discarded, and the cell pellet resuspended in 5 mls of ACK lysing buffer (Thermo Fisher; catalogue ref: A1049201) for 2 mins. 15 mls RPMI medium was then added to the falcon tubes, before filtering through a second 70 µm cell strainer. After centrifuging at 400g for 5 mins, the cell pellet was resuspended in 1 ml of FACs buffer and stained/fixed in a similar process as described above prior to acquisition.

Table 4: Antibodies used in flow cytometry for immunophenotyping

Target	Clone	Conjugate	Cat. Number	Dilution
CD4	RM4.4	V500	560783 (BD bioscience)	1:300
CD8	53-6.7	Pe-Cy7	100722	1:300
CD8	RPA-T8	PE-CF594	562282 (BD bioscience)	1:300
CD3	17A2	PerCp Cy5.5	100218	1:100
CD3	17A2	BV650	100229	1:100
CD45	30-F11	AF700	103128	1:300
CD25	PC62	BV650	102037	1:100
NK1.1	PK136	PE-Dazzle 594	108748	1:100
NK1.1	PK136	BV421	108731	1:100
CD69	H1.2F3	FITC	104506	1:100
FoxP3	FJK-16s	eFluor 450	48-5773-82 (Invitrogen)	1:100
Ki67	16A8	PE	652404	1:100
Grzmb	GB11	AF647	515406	1:100
CTLA4	UC10-489	PE	106306	1:100
PD1	29F.1A12	Pe-Cy7	135216	1:100
TIGIT	A15153G	PerCp Cy5.5	372718	1:100
LAG3	C9B7W	BB515	564672 (BD Bioscience)	1:100
TIM3	B8 2C12	APC	134008	1:100
Hamster IgG	HTK888	PE	400907	As antibody of interest
Rat IgG2a κ	RTK2758	PE	400507	As antibody of interest
Rat IgG2a κ	RTK2758	PE-Cy7	400521	As antibody of interest
Rat IgG2a κ	eBR2a	Pacific Blue	48-4321-80 (Invitrogen)	As antibody of interest
Rat IgG2a κ	MOPC-21	APC	400135	
Biotin Rat anti-mouse CD16/CD32	2.4G2	FITC	553143 (BD biosciences)	1:100

3.8.2 PD-L1 in 3LL cells

Cells were seeded in 12-well plates with $1x10^5$ cells/well and incubated overnight at 37^{o}C. The following day, the cells were treated with either PBS or 0.1 MOI of MG1-FLUC. The cells were harvested 24 hrs later with trypsin and then washed twice with PBS prior to centrifugation at 400g for 5 mins to obtain a cell pellet. The cells were stained with fixable viability dye eFluor 780 (eBioscience; catalogue ref: 65-0865-14) at a dilution of 1:10000 and PE anti-mouse PD-L1 antibody (Biolegend; catalogue ref: 1243307) at a dilution of 1:100, all in FACs buffer for 30 mins. After washing twice with PBS, the cells were fixed with 1% PFA for 20 mins before acquisition.

3.8.3 CD107 degranulation assay

NK cell degranulation was determined by cell surface expression of CD107. PBMC were isolated as described in 3.1.2. PBMC were counted and seeded at $1x10^8$ cells per T25 flask in RPMI growth medium and either treated with PBS or 0.1 MOI MG1-GFP. After 24 hrs incubation at 37^{o}C, the PBMCs were again incubated alone or against irradiated (8Gy) and non-irradiated target NSCLC cells at a 5:1 (PBMC:target cells) ratio in FACs tubes containing 400 µl of RPMI growth medium at 37^{o}C. After 1 hr, antibodies against CD3, CD56, CD107a and CD107b (see table 5) were added to each tube along with 10 µg/ml Brefeldin A (Biolegend; catalogue ref: 420601). Cells were then incubated for a further 4 hrs at 37^{o}C, washed with 4 mls FACs buffer, fixed in 200 µl 1% PFA and stored at 4^{o}C prior to acquisition.

Table 5: Antibodies used in flow cytometry for immunophenotyping

Target	Clone	Conjugate	Cat. Number	Dilution
CD3	UCHT1	FITC	300406	1:100
CD56	MEM-188	APC	304610	1:100
CD107a	H4A3	PE	328608	1:100
CD107b	H4B4	PE	354304	1:100

3.9 siRNA knockdown of BRCA1

H1299 cells were cultured and trypsinised to be resuspended at a concentration of 200,000 cells per ml of antibiotic free media. 2mls of cell suspension was transfected with a 1:1 (v:v i.e. 250ul:250ul) mixture of 20 µM siGENOME human BRCA1 siRNA Smartpool (Horizon inspired cell solutions; catalogue ref: M-003461-02-0010) and lipofectamine RNAiMax reagent (Thermo Fisher; catalogue ref: 13778100), both diluted in Opti-MEM medium (Thermo Fisher; catalogue ref: 31985062). After a minimum of 4 hrs, the medium was aspirated and replaced with fresh RPMI growth medium. Cells were harvested 72 hrs after transfection to be assessed for BRCA1 knockdown via western blot.

3.10 *In vivo* experiments

3LL (Lewis lung carcinoma) cells were obtained from Julian Downward, Francis Crick Institute, London, UK. $5x10^5$ cells were injected subcutaneously in the right flank of c57bl/6 mice that were 5-6 weeks old (Charles River, UK); treatments were started 10-11 days later, generally tumours were 50-100 mm^3 at this point. For systemic treatments, a total volume of 100 µl was injected via tail vein with a 27-gauge needle. In contrast, a total volume of 50 µl was used for intratumoural administration via insulin needles with a 28-gauge diameter. Tumours were measured twice weekly and tumour volume were calculated using the formula: length x width x height (mm) x 0.5236. Two-way analysis of variance (*ANOVA*) on area under curve (AUC) was performed using Prism Software (GraphPad) to compare tumour growth curves. For survival experiments, tumours were allowed to reach 15 mm in any dimension and then sacrificed. The Kaplan-Meier survival curves were compared using log-rank (Mantel-Cox) test using Prism Software (GraphPad).

3.10.1 Radiation in C57bl/6 mice

5-6-week-old female C57bl/6 mice were obtained from Charles River (UK). $5x10^5$ 3LL cells were implanted on the right flank subcutaneously as described

above. Once the tumours reached 50-100 mm volume, animals were irradiated under light anaesthetic using 120 µl of a 1:1:10 solution of hypnorm (Janssen Pharmaceutical Ltd), hypnovel (Roche) and sterile water, via intraperitoneal (IP) injection. The resulting mixture contains 0.315 mg of fentanyl citrate, 10 mg fluanisone, 1.8 mg methyl paradroxybenzoate, 0.2 mg proxyl paradroxybenzoate and 5 mg midazolam. Animals were then positioned with tumours exposed under an aperture in 3 mm lead shielding and irradiated to required doses for each experiment. Treatments, measurements and endpoints were as above.

3.10.2 Detection of NAbs

Tumour-naïve C57bl/6 mice were systemically administered with MG1-FLUC at a dose of $1x10^6$ pfu. Mice were sacrificed and blood were harvested via intra-cardiac puncture at 48 hrs, 72 hrs, 7 and 14 days. Whole blood was placed into 1.5ml plasma collection tubes (Thermo Fisher) and spun at 2000g in a Heraeus Megafuge 2.0R centrifuge to separate the plasma which was then transferred to sterile Eppendorf tubes and heated at 56^o for 30 mins to inactivate complement proteins. 0.1 MOI of MG1-FLUC was then added to each plasma sample and incubated at 37^oC for 4 hrs. The presence of replication active MG1 within each plasma/MG1-FLUC mix was then assessed via plaque assay (section 3.2.2).

Mice harbouring subcutaneous 3LL tumours were also systemically injected initially with either PBS or $1x10^6$ pfu of MG1-GFP virus. 5 days later all mice were challenged intravenously with $1x10^6$ pfu MG1-FLUC and the tumours and organs were harvested for IVIS imaging 48 hrs later.

3.10.3 MG1 and anti-PD1 therapy

5-6-week-old female c57bl/6 mice were subcutaneously implanted with $5x10^5$ 3LL cells on the right flank. Treatment commenced on day 11 when the tumours were between 50-100 mm^3 in volume. 6 mice per group was treated with either IT PBS+IP isotype (InVivoMab mouse IgG2b isotype control, clone MPC-11; 2bscientific; catalogue ref: BE0056), IT MG1 FLUC ($1x10^7$pfu)+IP Isotype, IP anti-PD1 (InVivoMab rat anti-mouse PD-1 (CD279), clone- RMP1-

14 monoclonal antibody, IgG2a κ; 2bscientific; catalogue ref: BE0146) or IT MG1-FLUC+IP anti-PD1. Isotype control and anti-PD1 therapy was administered three times a week (alternate days apart) until mice were sacrificed. Measurements and endpoints were as above.

3.10.4 MG1-shBRCA1 and Radiotherapy

To construct and rescue the amiRNA-expressing MG1 viruses, plasmids containing the siBRCA sequence (5'-CACAAAGTGTGACCACATA-3') (182)) and non-targeting control (NTC; sequence targeting the Firefly luciferase mRNA 5'- GTTGGCCACCGAAGCAGCGCAC-3') encoded in the pre-miR30 based short hairpin cassette flanked by MLU1 restriction sites were purchased from GenScript. Plasmids were digested by MLU1 and amiRNA inserts were ligated with MG-1 shuttle vector (MG-1 SV) using T4 ligase enzyme. Positive colonies were selected by PCR screening and verified by sequencing. MG-1 SV containing the amiRNA sequences were then PCR amplified using specific primers (Forward 5'-AAC ACT CTT GAT CGA GGT ACC CAG TTA TAT TTG TTA-3' and Reverse 5'- TGA TTG TCA CCT TGA GCT AGC ACT TTC ACG GCG GTG-3'). PCR products were then used in an in-fusion reaction along with MG1 backbone plasmid. Viruses were rescued using an infection-transfection method as previously described (section 3.2.1).

Mice harbouring 3LL tumours (as described above) were treated on day 11, when tumour volume was between 50-100mm^3, with IT MG1-shBRCA1 (dose 1x10^{7}pfu) or IT MG1-NTC (non-targeting control). On day 14, the mice then received 8 Gy RT (as described in section 3.10.1). Measurements and endpoints were as described above.

3.11 *Ex vivo* tumour processing

3LL cells were implanted subcutaneously into c57bl/6 mice and received planned treatments within each experiment. At the desired time points, the mice were sacrificed, and the tumours were harvested. The whole tumours were homogenised in lysis buffer (cOmplete™ Protease inhibitor cocktail (Merck; catalogue ref: 11697498001) in PBS) using Precelly's 24 homogeniser

(Bertin Technologies). The resulting supernatant was then assessed with plaque assay to determine MG1 viral titre and also tested for IFN-β via ELISA.

3.12 Statistics

P values were calculated using a paired Student's T test with two-tailed distribution. When comparing untreated vs. treated controls. When comparing 3 or more groups, a one-way *ANOVA* was performed, comparing all groups to each other and corrected for multiple comparison using Dunnett's or Sidak's test. If comparing 3 or more groups and there is more than one variable to consider (e.g., different RT doses), a two-way *ANOVA* was performed, comparing all groups to each other and again correcting for multiple comparison using Tukey's or Sidak's test. Statistical analysis of survival in the *in vivo* experiments were performed using a Log rank (Mantel Cox) test. Statistical significance was determined as follows: *ns p>0.1234, *p<0.0332, **p<0.0021, ***p<0.0002 and ****p<0.0001.* All statistical analysis was performed using Prism Software (GraphPad).

Chapter 4:

Investigating the *in vitro* and *in vivo* cytotoxic effects of Maraba virus in lung cancer models

4. Chapter 4: Investigating the *in vitro* and *in vivo* cytotoxic effects of Maraba virus in lung cancer models

4.1 Introduction

OVs selectively infects and self-replicates within tumour cells, eventually destroying them through lysis. By hijacking the cell's protein synthesis, the virus prevents the cell from producing host products and diverts resources to produce viral ones. After the infected host cells lyse, they release many viral progenies that have the ability of infecting other cells. This chapter aims to investigate the direct cytotoxic effects of oncolytic MG1-maraba virus using murine and human NSCLC malignant cell lines. The ability of MG1 virus to reach the tumour, and replicate within it, after systemic delivery is also explored in 3LL (NSCLC) murine model.

MG1-maraba virus has been shown to exhibit potent cytotoxicity across many different murine and human cancer cell lines. Two previous studies by Brun *et al*. (131) and Mahoney *et al*. (136) have examined MG1-oncolysis in lung cancer cell lines, confirming five human lung malignant cells lines (A549, HOP62, HOP92, NCI-H226 and NCI-H23) are susceptible to MG1-cytotoxicity, whereas the virulence was attenuated in human GM38 primary fibroblasts. Previous studies also showed that systemic delivery of MG1 was able to reach the tumour bed and replicate within subcutaneous CT26 colorectal and TC1 lung tumours by utilising MG1 strains expressing GFP or firefly luciferase (131, 183). Expanding on this work, our aim was to investigate MG1 oncolysis in a wider panel of human and murine NSCLC cell lines, as well as exploring whether MG1 virus was able to reach and replicate within a syngeneic 3LL murine lung cancer model after both intratumoural and systemic delivery. Intravenous virotherapy is not only important because of the ability to deliver treatment to tumours or metastases that are inaccessible via intratumoural injections, but also systemic virus delivery has the potential to enhance the

generation of a wider anti-tumour immune responses compared to its intratumoural counterpart. Therefore, the potential of MG1 reaching malignant sites via intravenous delivery would be of major benefit and warrants exploration. The ability of MG1 virus to be tumour selective is important to avoid unnecessary toxicity from normal tissue damage and therefore we set out to examine tumour tropism *in vivo* after systemic delivery of MG1, which has not been previously explored. One of the barriers to systemic delivery of OVs is the production of NAbs which can prevent viruses reaching their malignant target, however whether NAbs are produced after MG1 challenge *in vivo* remains unknown. Therefore, in this chapter we also explore whether NAbs are produced after systemic delivery of MG1 in our immunocompetent NSCLC murine model, which again has not been previously investigated.

4.2 Susceptibility of NSCLC cell lines to MG1 infection

4.2.1 MG1-GFP infection

As previous mentioned in section 2.3.1 Maraba virus binds LDLR and has the capacity to infect a broad range of cancer cells (131, 184). To enhance tumour specificity, two specific point mutations were introduced: L123W and Q242R in M and G proteins respectively which enhances replication efficacy in cancer cells (131). To date there are only five human lung cancer cell lines in the literature that have been reported to be susceptible to MG1 oncolysis (184). Therefore, to build on this knowledge and determine whether MG1-GFP was able to infect a further panel of human (H1299, H1573, H1792, H1975 and H1437) and murine NSCLC cell lines (3LL), as well as normal human foreskin fibroblast (HFF), fluoresce microscopy imaging was performed at 24 and 48 hrs after GFP-expressing virus infection at concentration doses of 0.01, 0.1 and 1 MOI. Figure 5 A-F are representative brightfield and GFP images of NSCLC cells lines exposed to either PBS or 0.1 MOI MG1-GFP after 48 hrs from virus exposure. All NSCLC cell lines tested were found to be sensitive to MG1-GFP infection as evidenced by GFP expression after virus exposure. MG1 was found to be tumour tropic as GFP expression was not detected in

primary HFF, even at the highest concentration tested of 1 MOI after 48 hrs (Figure 5G).

To quantify differences in the susceptibility of infection across the cell lines, flow cytometry analysis was performed. All cell lines were exposed to either PBS or MG1-GFP at concentrations of 0.01, 0.1 and 1 MOI for 24 and 48 hrs at which point cells were harvested and stained with a viability dye to distinguish between viable and dead cells. Figure 6A. shows a two-colour fluorescence dot plot of H1299 cells, 24hrs after 1 MOI MG1-GFP infection, demonstrating viability stain versus GFP expression as an example of how each cell line was gated for analysis. Figure 6B shows the mean percentage of GFP expression from viable cells from two independent experiments plotted for all NSCLC cell lines after indicated concentrations of MG1-GFP exposure at 24 and 48 hr time points. Once more, all NSCLC cell lines were shown to be vulnerable to MG1-GFP infection, while HFF remains unaffected. Figure 6C shows a two-colour fluorescence dot plot of HFF cells, 24hrs after 1 MOI MG1-GFP infection confirming tumour tropism. There was generally a dose-dependent increase in GFP expression across all human lung cancer cell lines, but not with 3LL murine cell line; GFP expression was highest with 0.01 MOI infection compared to 0.1 or 1 MOI (mean % GFP expression was 76.8%, vs. 68.2% and 42% respectively). This correlates with the later finding that 3LLs were the most sensitive cell line to MG1-cytotoxicity (shown in Figure 8F), with 3LL cell viability being affected even at low concentrations of MG1-GFP (i.e., 0.0001 MOI), hence at the higher viral concentrations of 0.1 and 1 MOI, the number of live cells susceptible to infection, and leading to GFP expression, in 3LLs would have been reduced. With the same rationale, % GFP expression was greatest after 24 hrs and reduced after 48 hrs in all cell lines. The susceptibility to MG1-infection across the human NSCLC cell lines varied, with H1437 being most sensitive, followed by H1975, H1299, H1573 and then H1792 (highest % GFP expression reached at 24 hr post-infection was 58.8% in H1437 vs. 58.6%, 49.9%, 45.6% and 31.9% or the other cell lines, respectively). 3LL murine cell line was more sensitive than the human NSCLC cell lines to MG1-GFP infection, with 76.8% GFP expression at 0.01 MOI at the 24hr timepoint.

From both the fluorescence microscopy and flow cytometry analysis, it can be seen that all five human- (H1299, H1573, H1792, H1975 and H1437) and 3LL murine-lung cancer cell lines used in this study were sensitive to MG1 infection and the virus demonstrated tumour selectivity *in vitro*. These results are consistent to what has been demonstrated in previous MG1 studies as discussed earlier (131, 184).

(A)

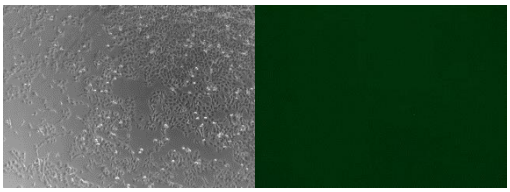

PBS

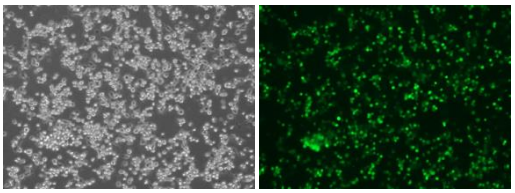

0.1MOI

H1299

(B)

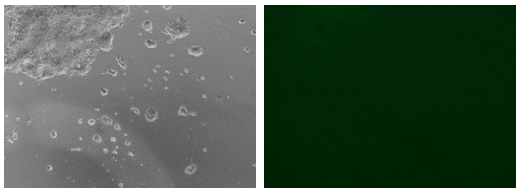

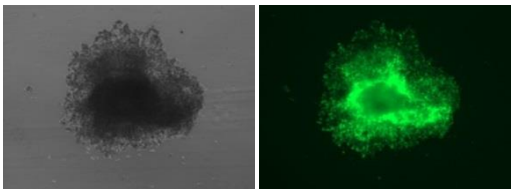

H1573

(C)

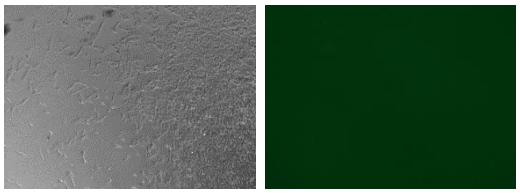

PBS

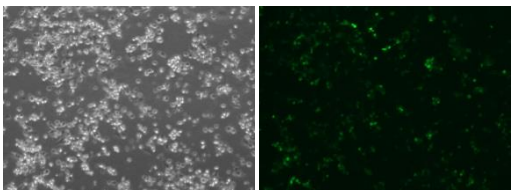

0.1 MOI

H1792

(D)

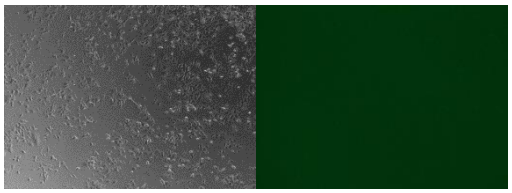

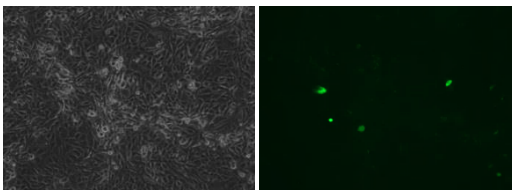

H1975

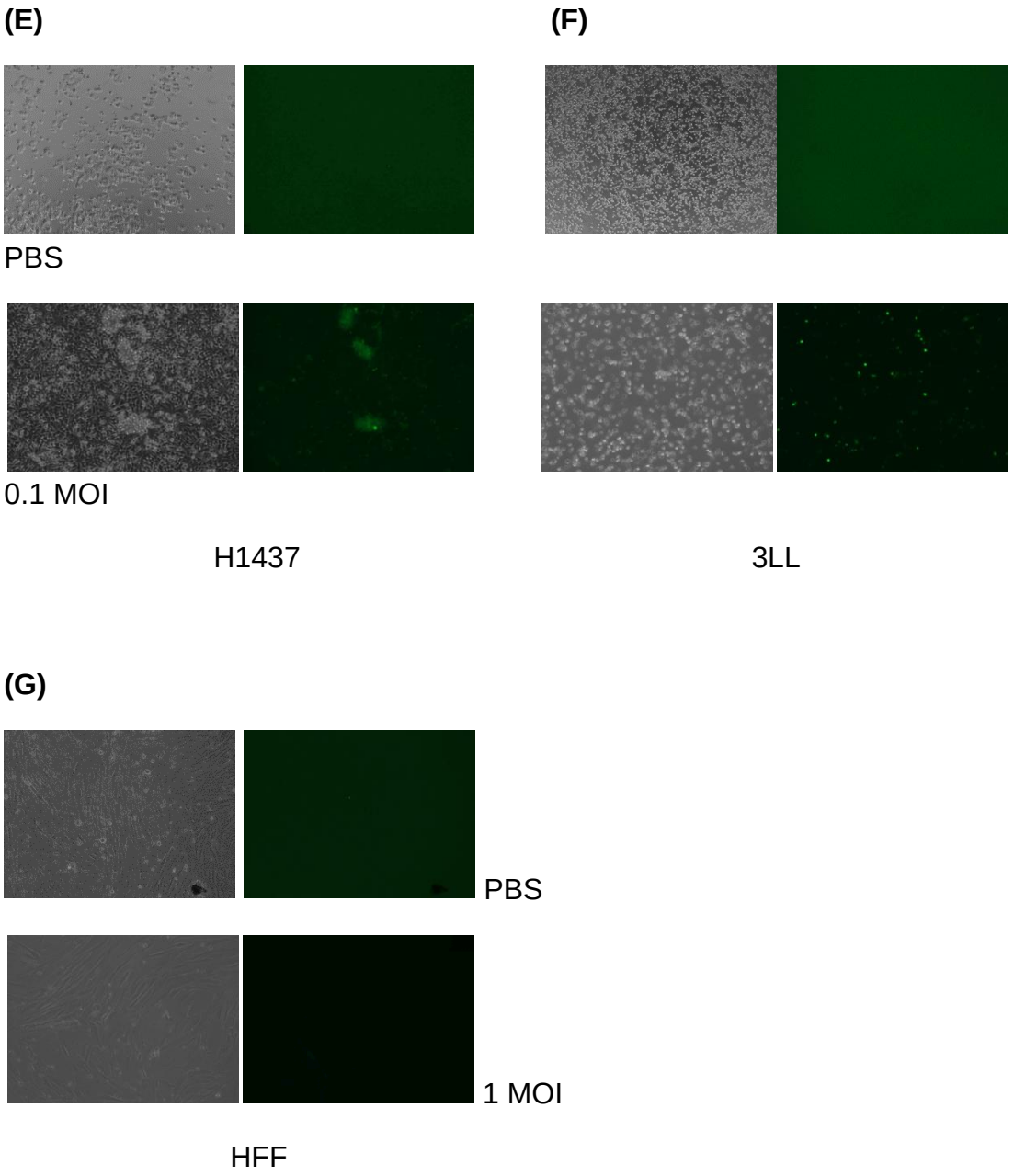

Figure 5: Human and murine NSCLC cell lines are susceptible to MG1-GFP infection, but primary HFF is uninfected.

Fluorescence microscopy was performed using EVOS cell imaging systems after cell lines were exposed to either PBS or MG1-GFP at 48hrs (A)-(F) GFP expression detected after 0.1 MOI MG1-GFP in all human and murine NSCLC cell lines. (G) There was no evident GFP expression in HFF even after 48 hrs of infection at 1 MOI MG1-GFP.

(A) H1299- 24hrs post-infection with 1MOI MG1-GFP

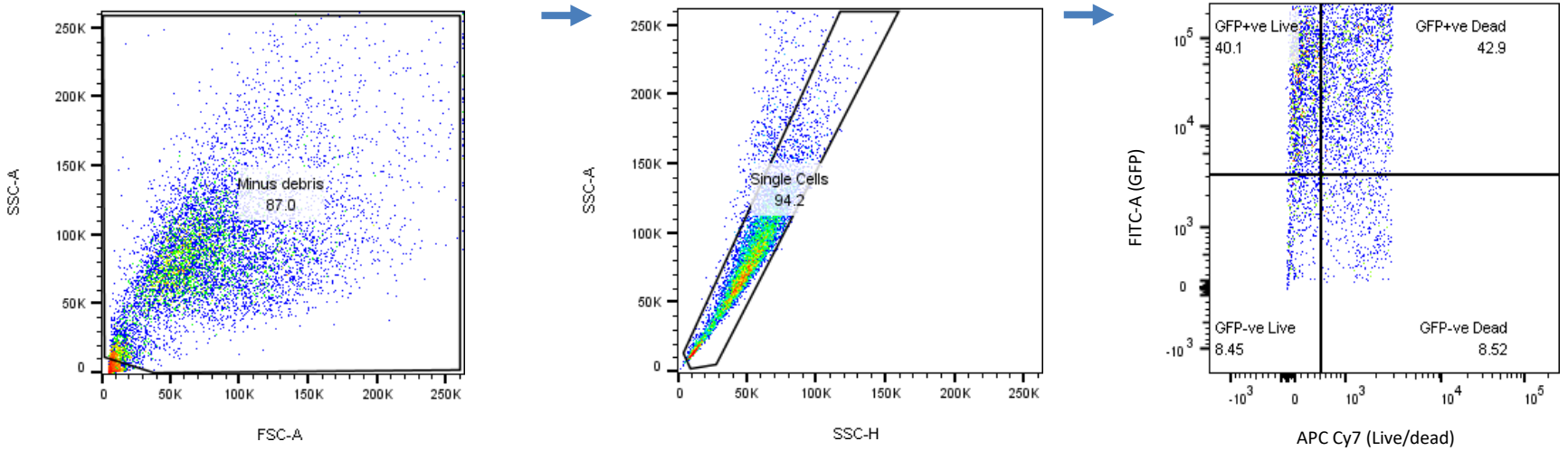

(B)

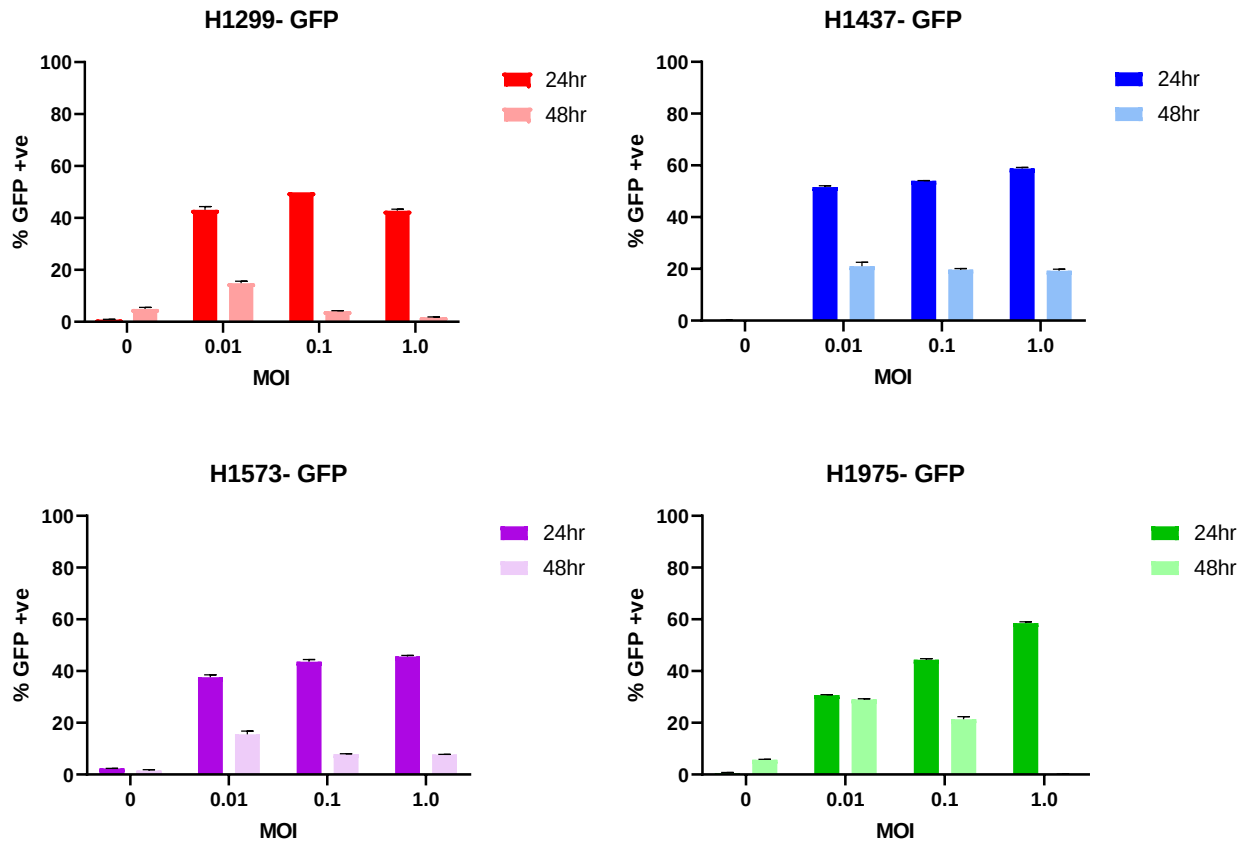
H1299- GFP
% GFP +ve
100
80
60
40
20
0
0
0.01
0.1
1.0
MOI
24hr
48hr
H1437- GFP
% GFP +ve
100
80
60
40
20
0
0
0.01
0.1
1.0
MOI
24hr
48hr
H1573- GFP
% GFP +ve
100
80
60
40
20
0
0
0.01
0.1
1.0
MOI
24hr
48hr
H1975- GFP
% GFP +ve
100
80
60
40
20
0
0
0.01
0.1
1.0
MOI
24hr
48hr

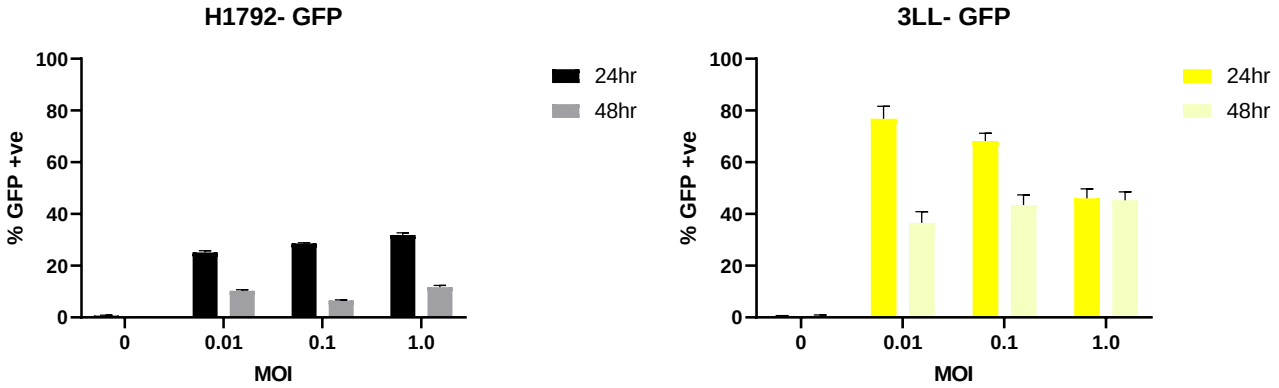
H1792- GFP
% GFP +ve
100
80
60
40
20
0
0
0.01
0.1
1.0
MOI
24hr
48hr
3LL- GFP
% GFP +ve
100
80
60
40
20
0
0
0.01
0.1
1.0
MOI
24hr
48hr

(C) HFF- 24hrs post-infection with 1MOI MG1-GFP

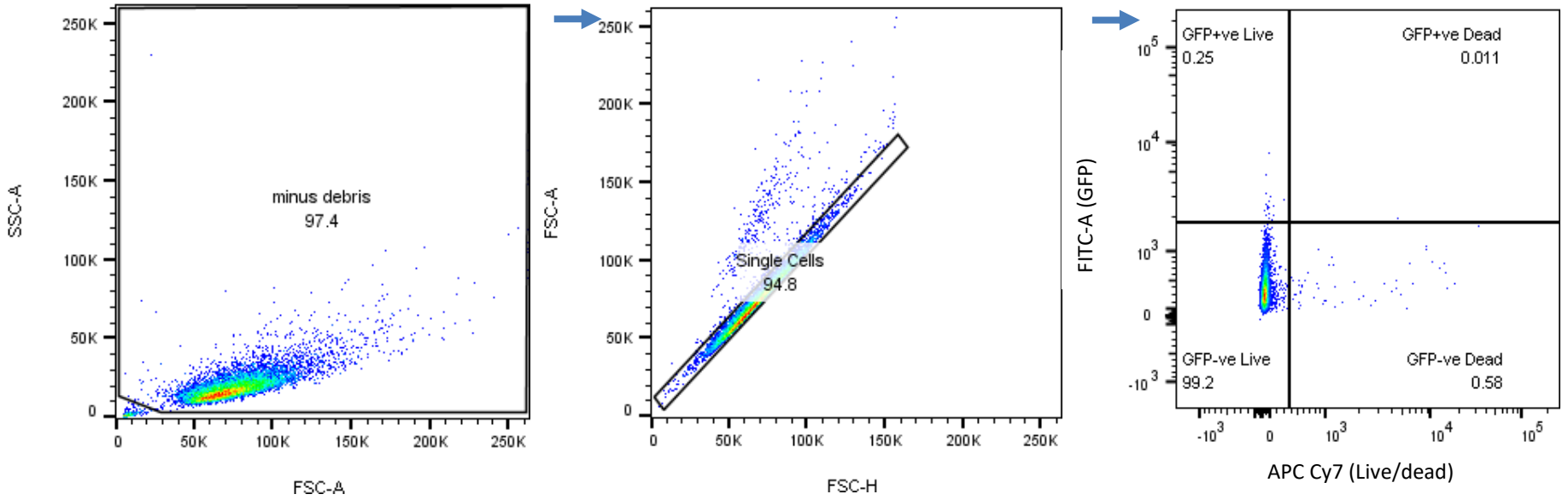

Figure 6: Degree of susceptibility of MG1-GFP infection is different in each cell line.

Tumour tropism is again observed as primary HFF is uninfected. Flow cytometry analysis of all cell lines infected with PBS or MG1-GFP. (A) Representative fluorescence dot plots, with gating strategy, showing viability dye (APC-Cy 7) and GFP expression (FITC) on H1299 cells, 24 hrs after 1 MOI MG1-GFP infection; quadrants with percentage of total cells that are GFP+/-ve live and GFP+/-ve dead shown. All other cell lines had similar light scatter and fluorescence dot plots created (data not shown) (B) Bar charts showing percentage of total GFP+ve live cells within whole population within each respective cell line after 24 or 48 hrs exposure to MG1-GFP at concentrations of 0, 0.01, 0.1 and 1.0 MOI. Graphs show the mean +SD of two independent experiments. (C) Representative fluorescence dot plots, with gating strategy, showing viability dye (APC-Cy 7) and GFP expression (FITC) on HFF cells, 24 hrs after 1MOI MG1-GFP infection; quadrants with percentage of total cells that are GFP+/-ve live and GFP+/-ve dead shown.

4.2.2 MG1 replication

Having established that NSCLC cell lines were indeed susceptible to MG1 infection, the ability of MG1 to replicate within the cells was investigated. H1299, H1437 and H1573 cell lines were chosen to be infected with 0.1 MOI MG1-GFP. Cells and supernatant were harvested at 24, 48 and 72 hrs post infection and lysates were generated by freeze-thaw cycles, thus releasing MG1-GFP from the cells. Viral titre was determined using vero cells which are highly susceptible to MG1 infection. Viral titre was calculated for each time point and fold increase was determined from input MG1-GFP titre. Figure 7A-C shows replication of MG1-GFP in the three NSCLC cell lines tested; the mean of three independent experiments is plotted. All NSCLC cell lines show time-dependent replication of MG1-GFP. In contrast to MG1-infection where H1437 was the most sensitive, followed by H1299 and then H1573 (shown in the previous section), H1299 generated the greatest level of MG1-GFP replication across all time points (160, 3000 and 22000 mean fold increase at 24, 48 and 72 hrs respectively) compared to H1437 (0.15, 63.3 and 4133.3 mean fold increase) and H1573 (13.3, 110 and 95.33 mean fold increase). Interestingly, H1437 required longer than 24hrs before producing viral progeny (even if the cells were highly infected by this timepoint as shown in Figure 6), however once replication started it produced 4133.3 mean fold increase by 72 hrs which was more than in H1573 (95.33 mean fold increase) at the same time point.

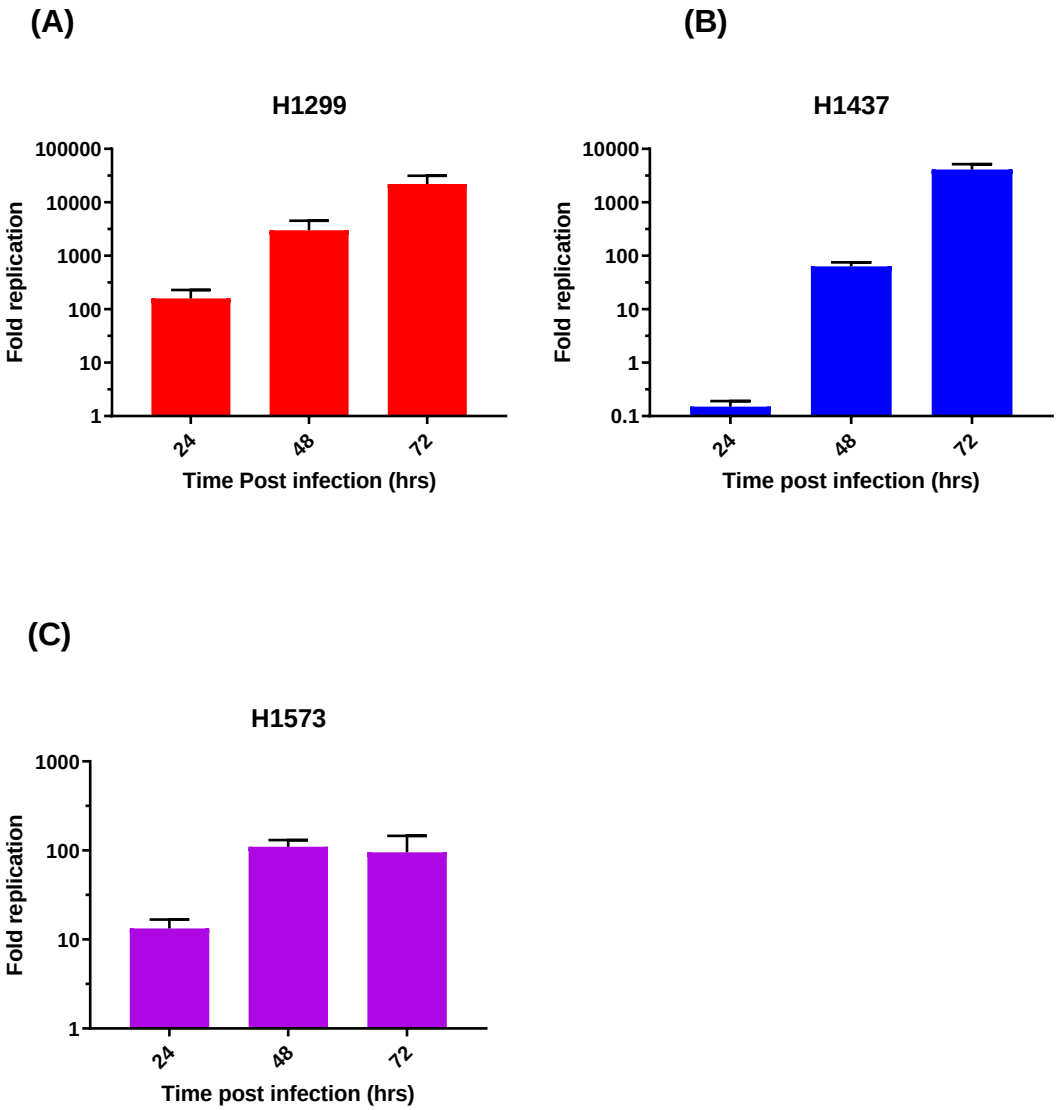

Figure 7: NSCLC cell lines are permissive to MG1-GFP replication.

*NSCLC cell lines were infected with MG1-GFP at 0.1 MOI for 24, 48 and 72 hrs. Cells and supernatants were harvested, and lysates prepared by three cycles of freeze-thaw. MG1-GFP concentration was subsequently determined by plaque assay using vero cells and fold increase was calculated from initial input MG1-GFP virus in **A)** H1299 cells, **B)** H1437 cells and **C)** H1573 cells. Graphs show the mean +SD of three independent experiments.*

4.2.3 MG1-induced cytotoxicity

After establishing that MG1-GFP was able to infect and replicate within NSCLC cell lines tested in this study, their susceptibility to MG1-induced cell death was investigated. Lung cancer cells and primary HFF were treated with PBS or MG1-GFP at MOIs ranging from 0.0001 to 0.1 and cell viability was assessed via MTT assay after 48 hrs incubation. The mean percentage of viable cells from three independent experiments is shown in Figure 8A-G and demonstrates that MG1-GFP had a cytotoxic effect on all lung cancer cell lines tested in a dose-dependent fashion. Furthermore, the virus is again shown to be tumour tropic as there was no detrimental effect on primary HFF even at the highest dose of MG1-GFP (0.1 MOI) tested. H1975 cell line appeared to be the most resistant to MG1-induced cell toxicity with only 39.6% cells death after 0.1 MOI MG1-GFP infection, followed by H1437, H1573, H1299, H1792 and 3LL, with 49.3%, 56.5%, 72%, 76.6% and 88.6% cell death respectively, at the same dose of virus tested. This seems to be in contrast to previous data shown where H1975 and H1437 cell lines were the most sensitive to MG1-infection, whereas H1792 and H1573 were the most resistant (as shown in section 4.2.1). This raises the possibility that with H1792 and H1573 cell lines, there could be an element of bystander cytotoxicity where the death of one cell propagates to other cells even if they are uninfected (as previously described with HSV (185, 186)). 3LL cells were the most sensitive to MG1-induced oncolysis, as demonstrated in Figure 8F, with significant reduction in viable cells (31%, $p=0.01$) even at a low concentration of MG1-GFP (0.0001MOI) after 48 hrs exposure to the virus. This death correlates with 3LLs being the most sensitive cell line to MG1 infection as described in section 4.2.1.2.

(A)

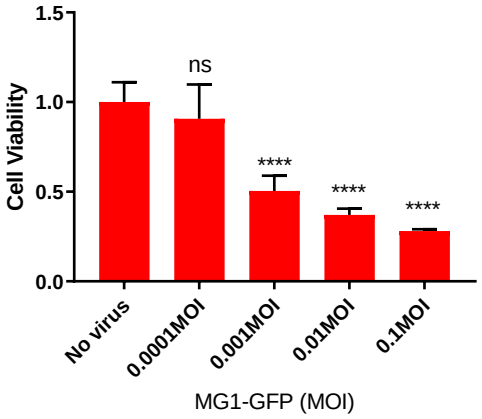
MG1-GFP on H1299 cells at 48hrs
Cell Viability
1.5
1.0
0.5
0.0
ns
****
****
****
No virus
0.0001MOI
0.001MOI
0.01MOI
0.1MOI
MG1-GFP (MOI)

(B)

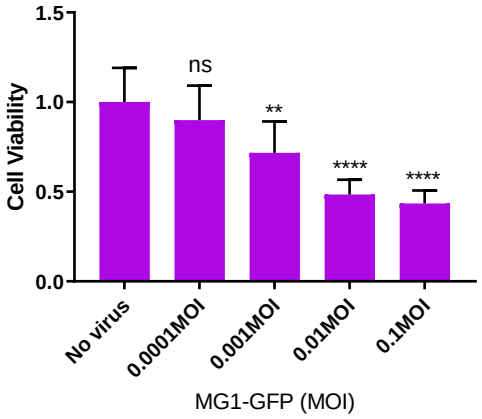
MG1-GFP on H1573 cells at 48hrs
Cell Viability
1.5
1.0
0.5
0.0
ns
**
****
****
No virus
0.0001MOI
0.001MOI
0.01MOI
0.1MOI
MG1-GFP (MOI)

(C)

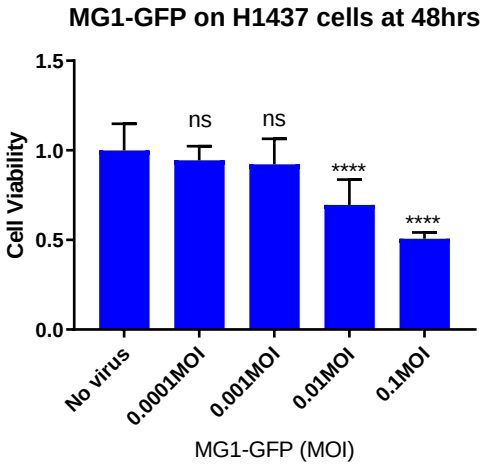
MG1-GFP on H1437 cells at 48hrs
Cell Viability
1.5
1.0
0.5
0.0
ns
ns
****
****
No virus
0.0001MOI
0.001MOI
0.01MOI
0.1MOI
MG1-GFP (MOI)

(D)

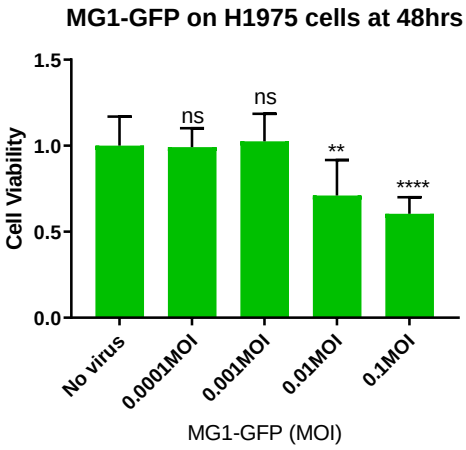
MG1-GFP on H1975 cells at 48hrs
Cell Viability
1.5
1.0
0.5
0.0
ns
ns
**
****
No virus
0.0001MOI
0.001MOI
0.01MOI
0.1MOI
MG1-GFP (MOI)

(E)

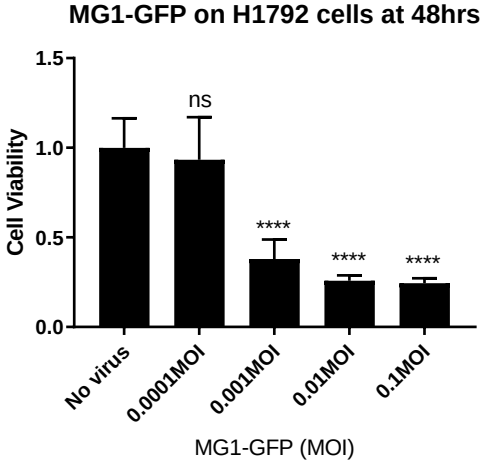
MG1-GFP on H1792 cells at 48hrs
Cell Viability
1.5
1.0
0.5
0.0
ns
****
****
****
No virus
0.0001MOI
0.001MOI
0.01MOI
0.1MOI
MG1-GFP (MOI)

(F)

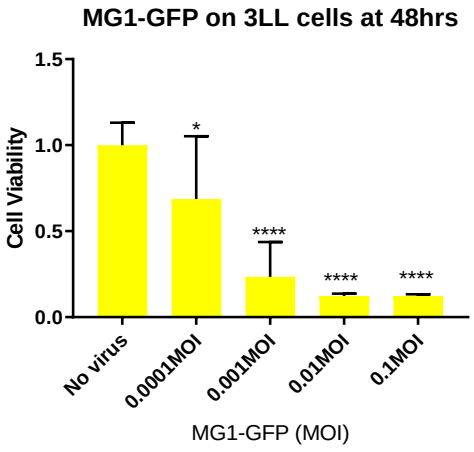
MG1-GFP on 3LL cells at 48hrs
Cell Viability
1.5
1.0
0.5
0.0
*
****
****
****
No virus
0.0001MOI
0.001MOI
0.01MOI
0.1MOI
MG1-GFP (MOI)

(G)

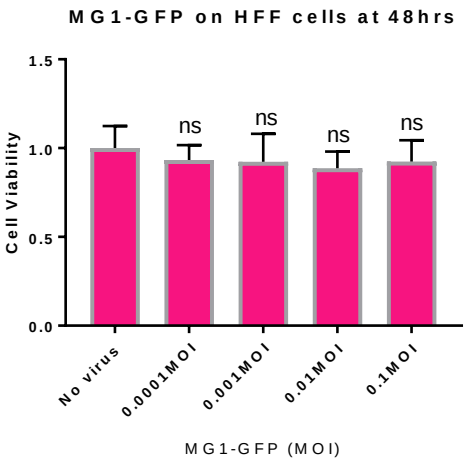

Figure 8: NSCLC cells lines are susceptible to MG1-induced death, but primary HFF is spared.

*NSCLC cell lines were infected with MG1-GFP at concentrations of 0, 0.001, 0.001, 0.01 and 0.1 MOI for 48 hrs. MTT assay was used to determine cell viability. Graphs show the mean +SD of three independent experiments (*p<0.033, **P<0.0021, ***p<0.0002 and ****p<0.0001; MG1-GFP treated vs. uninfected control; Ordinary one-way ANOVA statistical analysis corrected for multi-comparison using Dunnett test). Dose dependent cytotoxicity was demonstrated in all lung cancer cell lines (A-F) with MG1-GFP infection. Cell viability was not affected in HFF (G) with MG1-GFP infection indicating MG1 is tumour tropic.*

4.2.4 MG1-induced cytotoxicity prevented by IFN-beta

A common mechanism for tumour tropism for many OVs, in particular viruses from the rhabdovirus family, is mediated by the exquisite sensitivity of the virus to type I IFN and the parallel loss of IFN responsiveness within tumour cells (as described in section 2.2.1.2). Pol et al. reported that MG1's onco-selective properties was also Type I IFN-dependent (184).

To ascertain whether IFN-beta was protective against MG1 infection, B16-F1 cells were pre-exposed to three different concentrations of exogenous IFN-beta (20, 200 and 2000 pg/mL) for 24 hours prior to MG1-GFP viral infection at 0.1 MOI. After a further 24 hours, an MTT assay was performed. Figure 4.2.4 illustrates the protective effect of IFN-beta by demonstrating that MG1-GFP was unable to kill B16-F1 cells that have been pre-exposed to all three concentrations of IFN-beta (survival fraction was 0.78, 0.78 and 0.80 for 2000, 200 and 20 pg/ml respectively in both presence and absence of MG1-virus, whereas without IFN-beta pre-exposure, the survival fraction was 1.0 without MG1-GFP infection compared to 0.35 after viral exposure.

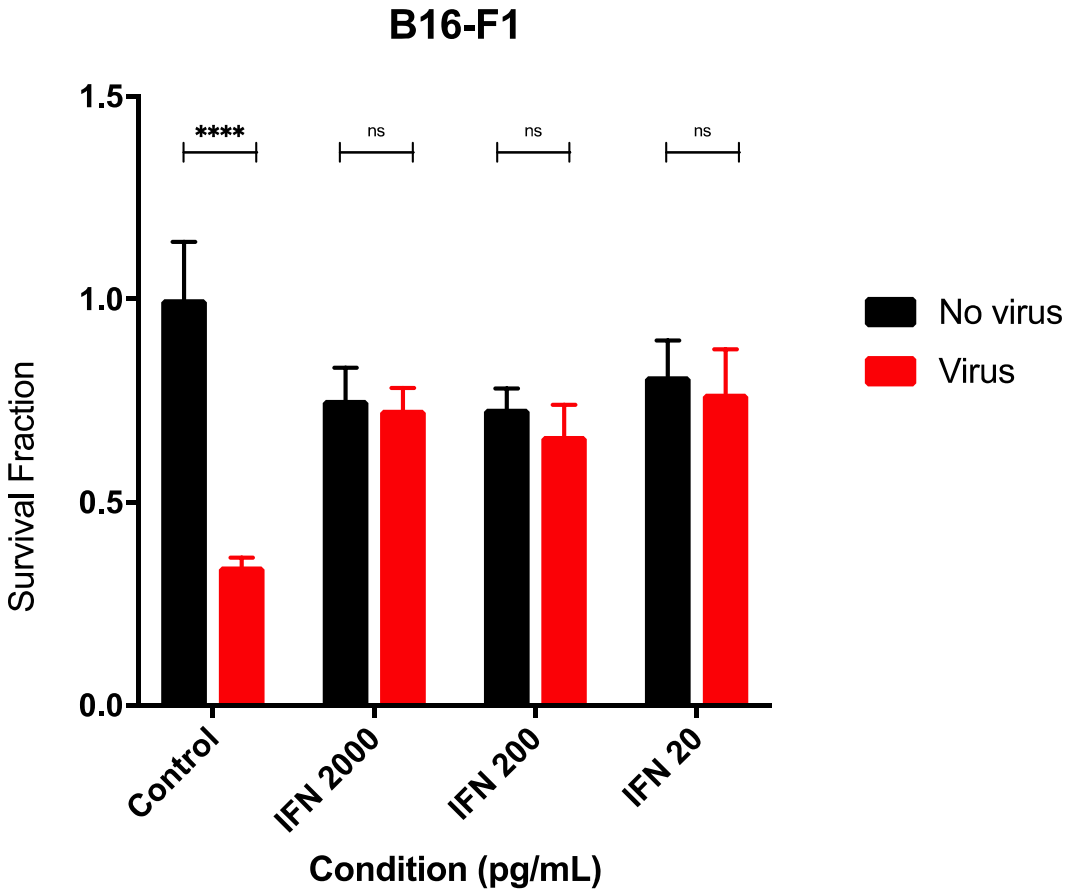

Figure 9: MG1-induced cytotoxicity prevented by IFN-beta.

*B16-F1 murine melanoma cells were either pre-exposed to three different concentrations of IFN-beta (20, 200 or 2000 pg/ml) or not, 24 hrs prior to MG1-GFP addition at 0.1 MOI. MTT assay was used to determine cell viability after a further 24 hrs. Graph show the mean +SD of three independent experiments ((*p<0.033, **P<0.0021, ***p<0.0002 and ****p<0.0001; MG1-GFP treated vs. untreated; Ordinary one-way ANOVA statistical analysis corrected for multi-comparison using Dunnett test). IFN-beta pre-exposure protected B16-F1 cells from MG1-induced cytotoxicity at all three concentrations tested.*

4.3 MG1 effects in 3LL murine model

4.3.1 Intravenous vs. Intratumoural delivery of MG1 *in vivo*

In vitro experiments have shown that MG1 is able to infect, replicate and kill the panel of human and murine lung cancer cell lines used in this study, while sparing normal primary HFF. Furthermore, 3LL murine lung cancer cells seem to be the most susceptible to infection and virus-induced oncolysis compared to the human counterpart cells tested in this report. Subsequently, the effects of MG1 in 3LL murine lung cancer model *in vivo* was explored. Brun *et al*. have shown that MG1 is able to reach the tumour bed and replicate inside subcutaneous CT26 colorectal tumour after systemic delivery (131). With regards to lung cancer, only one study has investigated MG1's effectiveness *in vivo*; in this analysis Atherton *et al*. engineered MG1 virus to overexpress HPV proteins E6 and E7 and showed that this virus was effective as a prime-boost vaccine in combination with adenovirus incorporating the same transgenes in the HPV-positive TC1 lung murine model (183). In this study, MG1-GFP was also shown to be recoverable in the TC1 subcutaneous tumour after tail vein administration. To expand on this data in another syngeneic murine lung cancer model, MG1 virus expressing firefly luciferase (MG1-FLUC) was administered at a dose of $1x10^6$ pfu either systemically or intratumourally into mice harbouring subcutaneous 3LL tumours (three mice per group). D-luciferin (substrate to luciferase enzyme) was then given intraperitoneally at 48 hrs prior to imaging the anaesthetised mice using the IVIS imaging system. The mice were then sacrificed, and the organs were harvested for further IVIS imaging and to perform *ex vivo* plaque assays. Figure 9 illustrates that MG1 virus can be detected whether the virus is delivered (A) intratumourally or (B) systemically in the 3LL murine subcutaneous tumours. Furthermore, the virus appears tumour tropic *in vivo* as there was no presence of detectable luminescence in other organs of any mice, as shown in Figure 9C. It was noted that the strength of the luminescence signal within the tumour was not a good indicator of the concentration of virus within the sample; for example although IT1's tumour

had a higher luminescence signal over 3000 counts, while IV1's tumour was over 80 counts (Figure 10C), the subsequent plaque assays revealed the concentration of replication competent virus within IT1s' tumour was lower than in IV1s' ($2x10^8$ vs. $6x10^9$ pfu/ml respectively as shown in Figure 10D and 10E). This discrepancy could have been due to the inaccuracy of the IVIS imaging system to quantify luminescence according to different densities of sample. However as the aim of this study was to detect the presence or absence of MG1 virus after different routes of delivery *in vivo* within the tumour and other organs, rather than quantification of the virus present, the endpoint was still achieved with this methodology. Of note, the scales of luminescence in Figure 10C varied between each dissected mice, as the setting was set to optimal reading for each individual plate, with the aim to improve detection of virus present. As each plate was analysed independently rather than as a comparison between the different mice, the scales were not modified to be equivocal. Finally, *ex vivo* plaque assays of homogenised tumours and organs confirmed that only tumours possessed recoverable live, replication competent MG1 virus, which was not detected in any normal tissues, examples are shown in Figure 10D and 10E. The viral replication following IV and IT delivery was investigated in more detail and will be discussed in section 4.3.3.

(A) Intratumoural MG1-FLUC

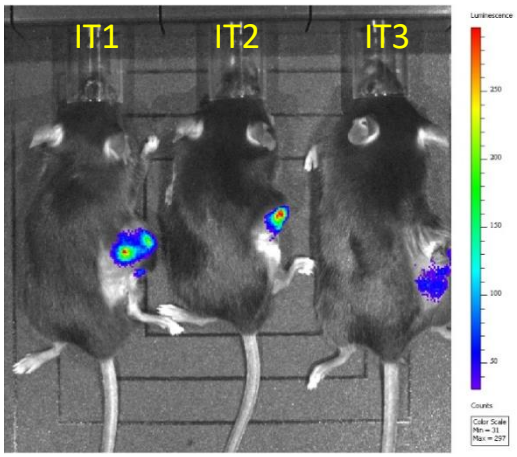

(B) Intravenous MG1-FLUC

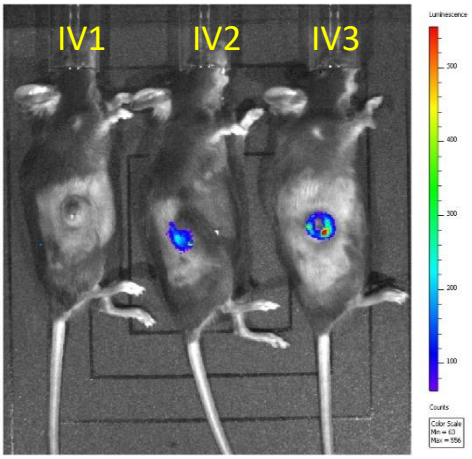

(C) IVIS imaging of tumours and organs

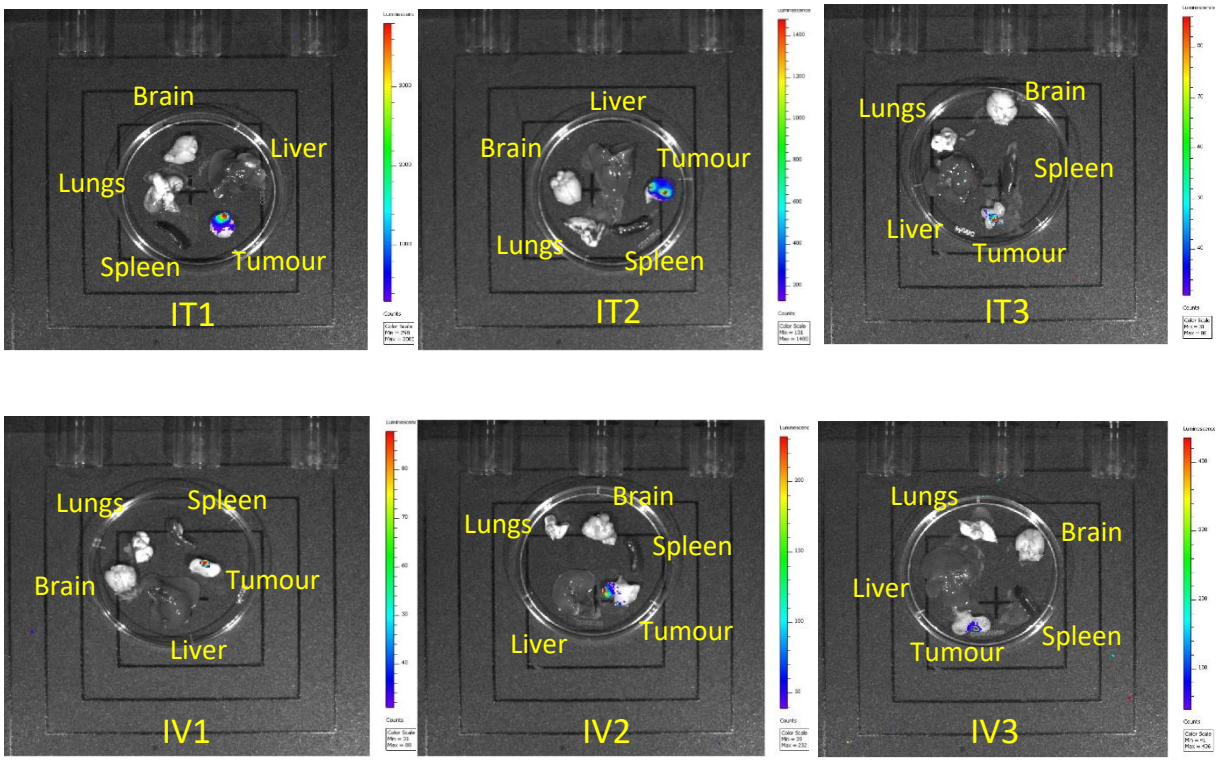

(D) Representative *ex vivo* plaque assays for IV1

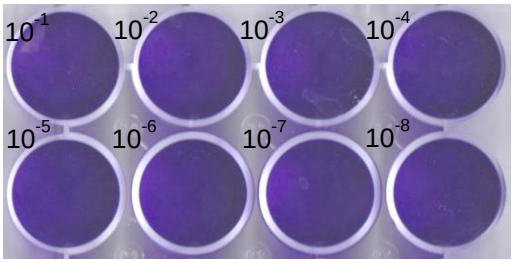

Lungs

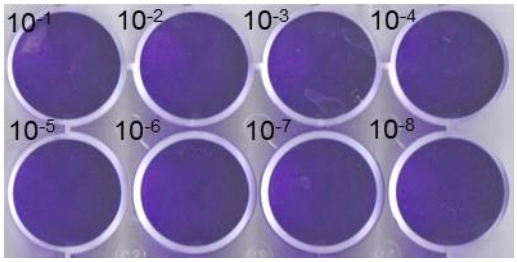

Brain

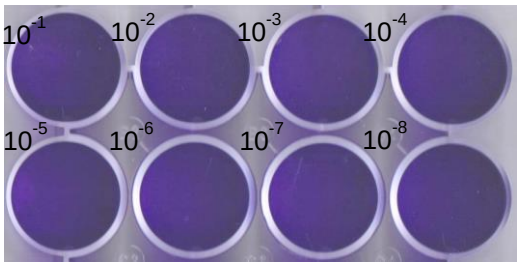

Spleen

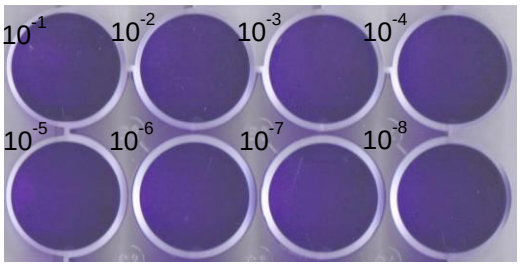

Liver

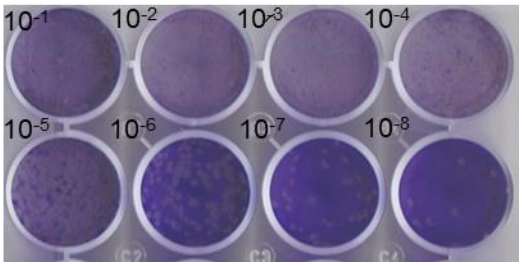

Tumour

(E) Representative *ex vivo* plaque assays for IT1

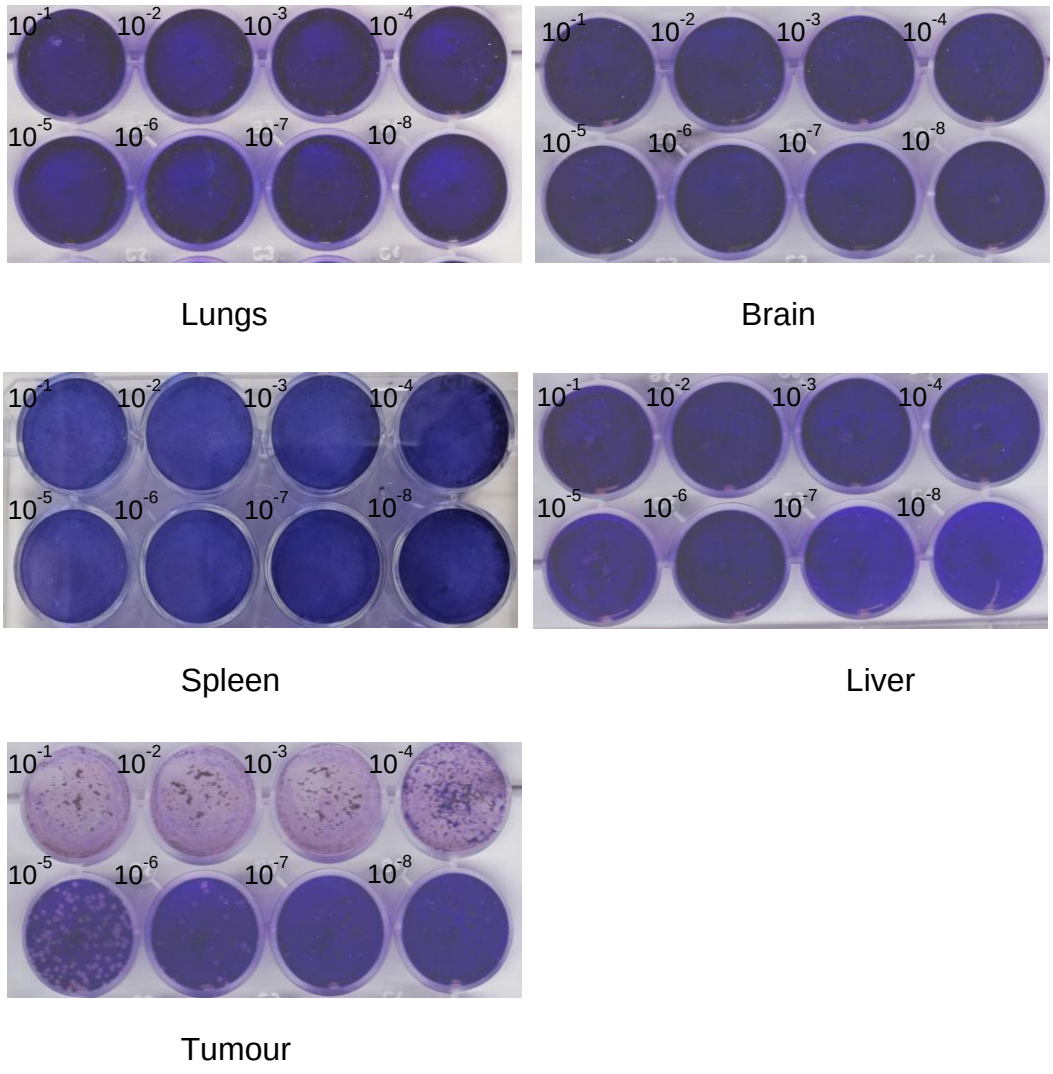

Figure 10: Replication competent MG1 was retrieved from subcutaneous 3LL tumours whether virus was delivered intratumourally or systemically

IVIS imaging of mice harbouring syngeneic 3LL subcutaneous tumours after MG1-FLUC virus at a dose of 1x10^6 pfu was delivered either (A) intratumourally or (B) intravenously via tail vein at 48 hrs post virus injection. (C) IVIS imaging of tumour and organs of each corresponding mouse. (D) Representative example of ex vivo plaque assay for IV1 mouse (IV2 and IV3 demonstrated same results). (E) Representative example of ex vivo plaque assay for IT1 mouse (IT2 and IT3 demonstrated same results). Each well in the plaque assay represents 10-fold dilution of homogenised sample tested. Plaques form only when virus is present and is replicating.

To further interrogate the systemic delivery of MG1 and determine whether the virus can reach lung tumours in an orthotopic site, 3LL cells expressing FLUC (3LL-FLUC) were injected into three C57bl/6 mice via tail vein at a quantity of $2x10^5$ cells. Only one mouse subsequently developed a 3LL tumour in the lungs, which was evident by the luminescent signal seen in the chest via IVIS imaging (Figure 11A). MG1 virus expressing GFP (MG1-GFP) was then administered systemically at a dose of $1x10^6$pfu to the mouse with established 3LL lung tumour and after 48 hrs was sacrificed. The organs were harvested to be IVIS imaged and for *ex vivo* plaque assay analysis. Figure 11B demonstrates that the harvested organs revealed a 3LL tumour in the murine left lower lung, which was evident as a luminescent signal from the IVIS image (left panel) and a tumour mass seen in the photographs (right panels). Figure 11C illustrates that replication competent MG1 virus was retrieved from the left lung tumour only in the *ex vivo* plaque assay. The viral dose recovered from the tumour was $1.6x10^6$pfu, which was similar to the administration dose given 48 hrs before (which correlates to the doses recovered from subcutaneous 3LL tumours described in section 4.3.3 also at 48 hrs post-infection). This not only further consolidates that MG1 is tumour selective and can reach lung tumours at its orthotopic site but also importantly that the viral dose achieved in the tumour after systemic delivery is similar to administration dose, although this finding is limited to a single mouse and further repeat experiments with greater samples would be required add robustness to this conclusion.

(A)

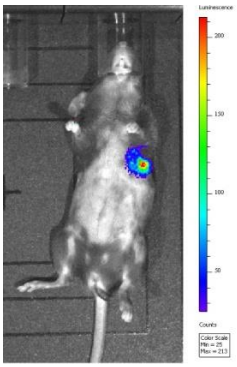

(B)

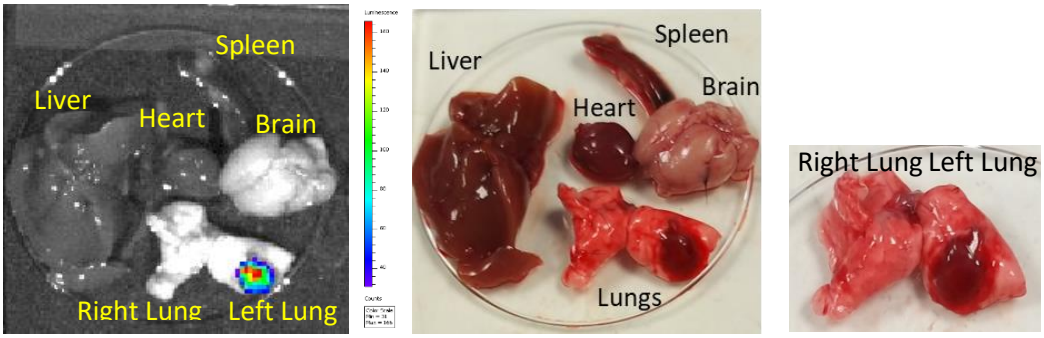

(C)

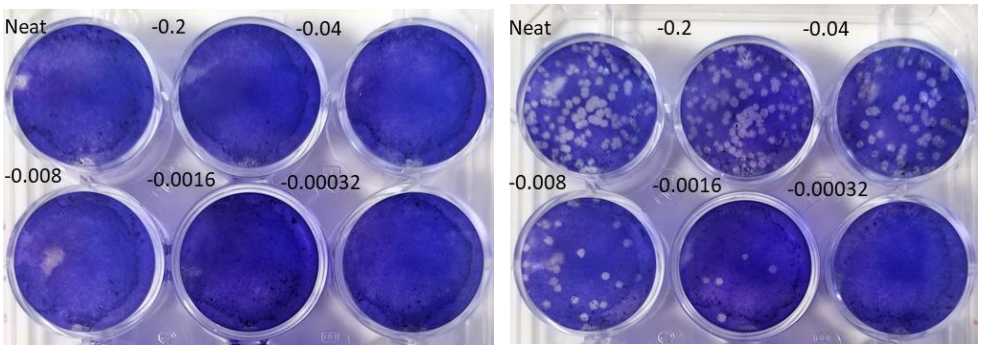

Right lung Left Lung

Figure 11: Replication competent MG1 virus was retrieved from 3LL tumour at orthotopic site after systemic delivery.

(A) IVIS imaging of mouse with established syngeneic 3LL lung tumour after 3LL-FLUC (2x10^5 cells) was delivered intravenously via tail vein after 14 days. (B) IVIS imaging and photographs of 3LL tumour identified in the left lung and organs of each corresponding mouse. (C) Ex vivo plaque assay of right and left lungs demonstrating retrieved replication competent MG1 virus only present in the tumour (after MG1-GFP virus was given systemically 48 hrs prior to organ harvesting). Ex vivo plaque assays of all other organs were void of virus (data not shown). Each well in the plaque assay represents 5-fold dilution of homogenised sample tested. Plaques form only when virus is present and is replicating.

4.3.2 Neutralising antibodies to MG1

Having established that intravenous delivery of MG1 does indeed reach both subcutaneous and orthotopic 3LL tumours, the ideal treatment regimen was investigated. One of the major limitations to systemic OV therapy is the development of treatment-induced NAbs which can reduce the effective virus titre and hinder any repetitive OV systemic delivery schedule and contribute to anti-viral immunity (112). Previous studies have reported NAbs arising after exposure to a range of OVs including vaccinia virus, measles virus, adenovirus and reovirus, all of which showed the presence of NAbs decreases anti-tumour activity (187, 188).

To date there has been no reports investigating whether NAbs against MG1 virus are produced *in vivo*. Therefore, to fill this gap in the literature as well as determining the optimal treatment regimen for use in 3LL murine model, C57bl/6 mice were injected with MG1-GFP virus systemically at $1x10^6$ pfu and cardiac puncture was performed at 2, 3, 7 and 14 days to obtain blood for the detection of NAbs. The harvested blood was centrifuged, plasma collected, and heat inactivated prior to serial dilutions by a factor of 10 resulting in four concentrations of diluted plasma for each time point; neat, 10^{-1}, 10^{-2} and 10^{-3}. Each plasma dilution was incubated with 0.1 MOI of MG1-GFP virus (a concentration identified to be cytotoxic to vero cells as determined by MTT assay and results shown in Figure 12A) for 4 hrs at 37^{o}C, prior to detection of virus-neutralisation using plaque assay methodology, MG1-GFP not incubated with plasma was used as a positive control. Figure 12B shows plaque assays of the positive control and the diluted mice serum at different time points. The positive control (top panel) shows the number of plaques observed under non-neutralised conditions, plaques can be seen in each dilution indicating replication effective virus, a similar number of plaques can be seen in the day 2 plasma samples indicating at this timepoint there was no NAbs present in the plasma. However, at the day 3 samples no plaques were seen in the neat plasma well and a reduced number of plaques was evident in the 10^{-1} and 10^{-2} compared to positive control and day 2 samples, signifying the presence of NAbs in the plasma to neutralise MG1. By Day 7 there were no plaques

detected in the neat or 10-1 sample and the number of plaques seen in the 10-2 and 10-3 samples were reduced compare to day 2 and 3 samples, indicating the number of NAbs within the plasma had substantially increased at this time point. Finally, at day 14, there were no plaques seen in the neat, 10^{-1} and 10^{-2} samples and only two plaques detected in the 10^{-3} sample which was considerably less than the day 7 sample. Results in Figure 12B show that NAbs appear in the plasma for virus treated mice at day 3 and the quantity of NAbs increases over time as demonstrated by the fact that greater dilutions of the plasma was required at later time points before replication competent virus was detectable again.

After determining that MG1-induced NAbs are produced from day 3 onwards and increase with time in C57bl/6 mice, it was important to determine whether the presence of NAbs affects systemic delivery of MG1 in 3LL murine model. Ilett *et al*. showed that, in the case of reovirus, virus-antibody complexes carried by human monocytes can still deliver functional replicative virus to tumour cells resulting in tumour cell infection and lysis (189). Therefore, an anti-viral immunological response may not be detrimental to OV delivery. To assess the effect of MG1-induced NAbs, mice harbouring subcutaneous 3LL tumours were systemically challenged with either PBS or MG1-GFP virus. After 5 days, which allows enough time for NAbs to be produced, the mice were all intravenously injected with MG1-FLUC and the tumours and organs were harvested for IVIS imaging 48 hrs later (Figure 12C shows schematic of experiment). Figure 12D shows the IVIS images of the tumours and organs from mice that either had systemic PBS followed by intravenous MG1-FLUC or systemic MG1-GFP followed by intravenous MG1-FLUC. The results demonstrate that luminescence signal was detected in mice receiving PBS followed by MG1-FLUC, however no luminescence signal was detected in mice receiving an initial dose of MG1-GFP followed by MG1-FLUC.

These results suggest that MG1-induced NAbs which arise by day 3 after systemic viral injections, were able to neutralise further intravenously delivered MG1 doses and prevent them from reaching and replicating in the tumour. This implies that the optimal MG1 treatment regimen for future *in vivo* experiments would be either single dose or to deliver multiple doses of virus within a short

timeframe (I.e., prior to day 3) to mitigate any negative impact from NAbs on viral delivery to target.

(A)

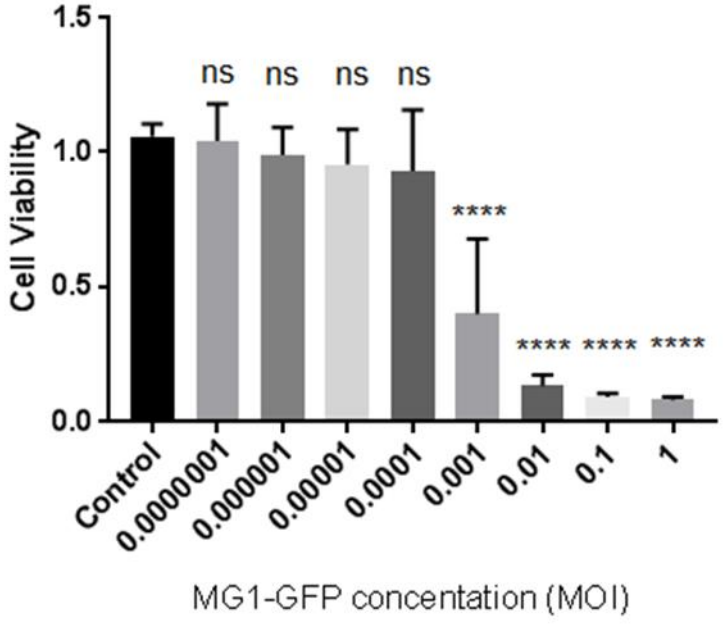

(B)

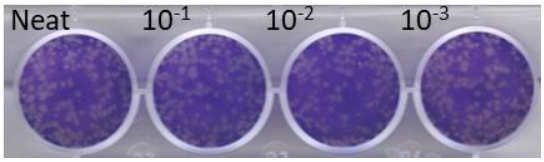

0.1MOI MG1-GFP alone (+ve control)

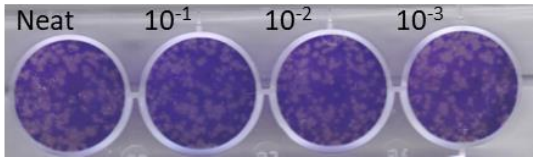

2 days

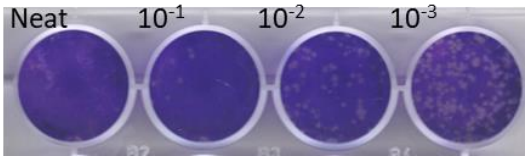

3 days

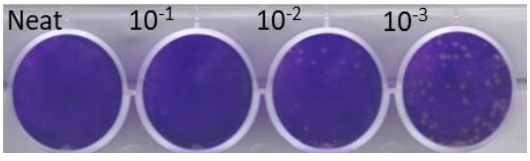

7 days

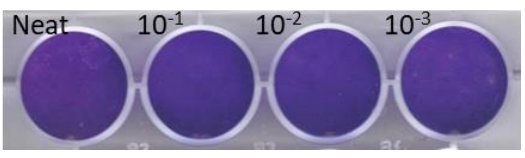

14 days

(C)

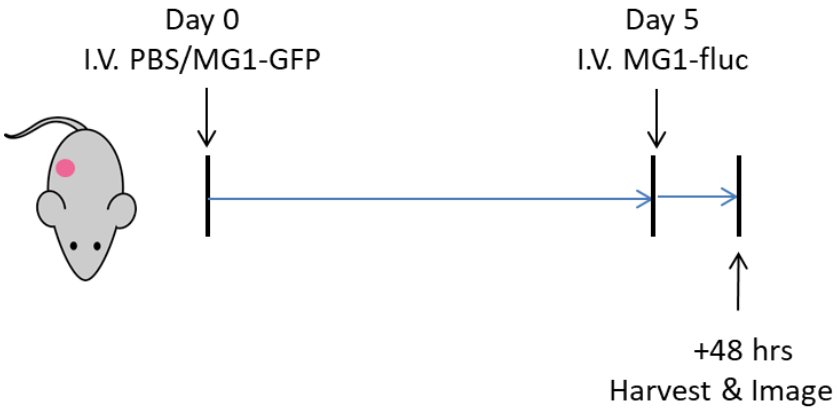

(D)

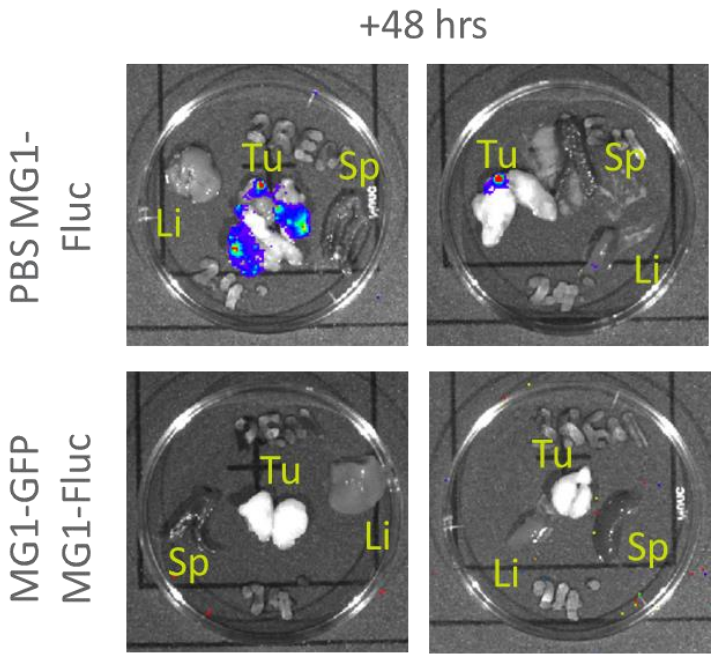

Figure 12: Intravenously delivered MG1 induces NAbs which neutralises and prevents further MG1 doses from reaching 3LL tumours.

*(A) Graph shows mean cell viability of vero cells +SD from three independent experiments with increasing concentrations of MG1 (*p<0.033, **P<0.0021, ***p<0.0002 and ****p<0.0001; MG1-GFP treated vs. uninfected control; Ordinary one-way ANOVA statistical analysis corrected for multi-comparison using Dunnett test). (B) Plaque assay of 0.1 MOI MG1-GFP as positive control and heat inactivated plasma-MG1-GFP samples at different timepoints. (C) Schematic of assessing systemic MG1 rechallenge in 3LL murine model. (D) IVIS images of harvested tumours and organs at 48 hrs after intravenous MG1-FLUC challenge, post PBS or MG1-GFP initial treatments (2 mice per group). Tu= tumour, Sp=spleen and Li=liver*

4.3.3 MG1 replication within 3LL tumours after IT and IV delivery

Having established that MG1 is able to reach 3LL tumours after systemic delivery, it was important to determine whether the dose of MG1 delivered was at an adequate level to maintain replication that was comparable to intratumoural delivery, as subtherapeutic doses of OV can lead to treatment failure. To date, there has only been one clinical study reporting IV delivery of OVs with an IT injection comparator arm. In this trial, there was a cohort of patients with colorectal cancer who were treated with either IT or IV enadenotucirev (an oncolytic A11/Ad3 chimeric group B adenovirus) and the tumour was resected 8-15 days later. Enadenotucirev activity was then measured using immunohistochemical staining of nuclear viral hexon and quantitative PCR for viral genomic DNA. The investigators detected virus in tumour tissues following both injection methods, but while virus was more commonly confirmed in IV-treated tumours, intense hexon IHC staining (>8%) was more common in IT-treated lesions. The authors, however, did not report viral titres from the tumour sites (190).

To compare the MG1 doses within *ex vivo* tumours following IT vs. IV delivery, mice with established 3LL subcutaneous tumours were administered with $1x10^7$pfu MG1-FLUC either intratumourally or intravenously. Three mice per treatment cohort were then sacrificed and tumours harvested at 6, 24, 48 and 72 hrs. The *ex vivo* tumours were then homogenised and the viral tire within each sample were determined by plaque assays. Figure 13 shows the graph of mean viral titre within the tumours in the IT and IV cohorts at different time-points. The results show that at 6 hrs after administration, MG1 viral titre is unsurprisingly greater with IT delivery compared to IV delivery ($4.97x10^6$pfu/gram of tumour vs. $3.74x10^5$pfu/gram of tumour respectively; p=0.026, multiple t tests statistical analysis with correction for multiple comparison using the Holm-Sidak method). However, there was no significant difference in viral titre between the two routes of administration at the 24, 48 and 72 hr timepoints. This result suggests that although IT delivery is more efficient in delivering MG1 virus to the tumour in the early stages, the dose of

MG1 reaching the tumour via IV administration is still sufficient to allow for infection and replication to the extent that catches up with its IT delivered counterparts after 24 hr.

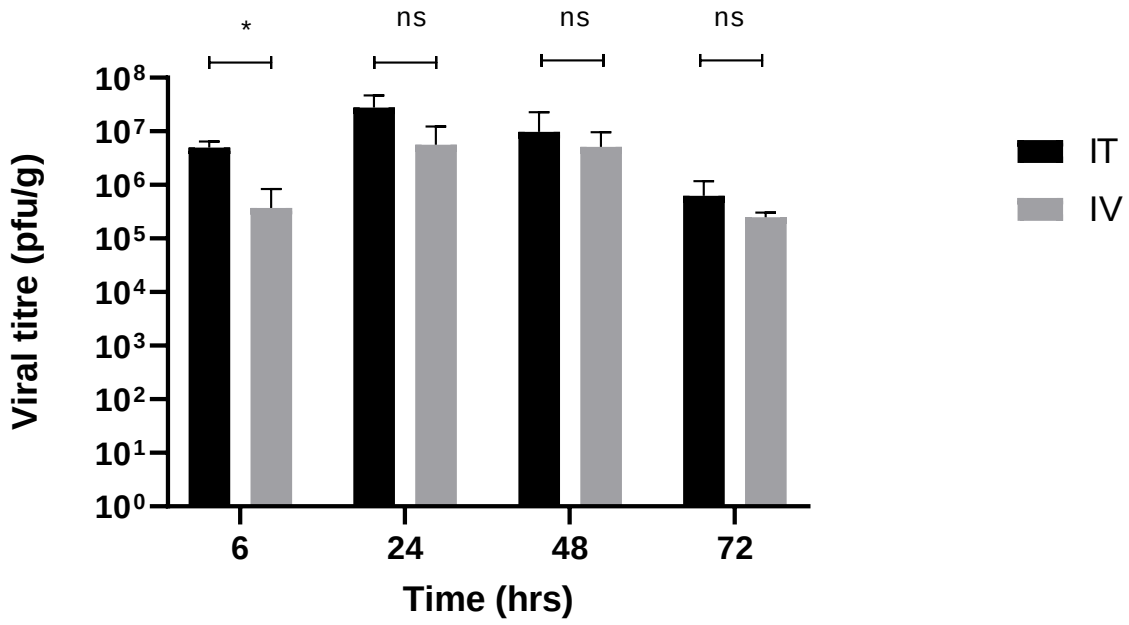

Figure 13: MG1-FLUC viral titre in *ex vivo* 3LL tumours is greater with IT delivery compared to IV delivery at the 6hr timepoint, but after 24hrs there is no significant difference in viral dose between the two routes of administration.

Graph shows mean viral titre (pfu/gram of tumour) +SD within *ex vivo* 3LL tumours from three individual mice per group at each timepoint *(*p<0.05; IT treated vs. IV treated; multiple t test statistical analysis corrected for multi-comparison using Holme-Sidak method).*

4.3.4 MG1 efficacy *in vivo* 3LL murine model

Having determined that MG1 can infect, replicate and kill lung cancer cells *in vitro*, as well as its ability to reach 3LL murine subcutaneous or orthotopic tumours after systemic delivery, the next aim of the project was to explore the efficacy of MG1 on tumour control *in vivo*. MG1 therapy has been shown to possess potent oncolytic activity in xenograft models using human cancer cell lines or patient-derived tumours implanted in immunodeficient mice (133-135). Brun *et al*. also showed that MG1 virus led to complete tumour regression and durable cures in rodents bearing syngeneic subcutaneous CT26 colorectal carcinoma (131). With regards to a murine lung cancer model, MG1-GFP exerted antineoplastic activity, with 50% of mice bearing TC1 flank tumours exhibiting reduction in tumour volume. Expanding on these previous studies, the efficacy of MG virotherapy to treat 3LL subcutaneous tumours was investigated. Tumour bearing mice were challenged with either 1 or 3 doses of MG1-FLUC virus systemically or intratumourally. Consideration was given to limit the number of MG1 doses within a short time frame, as we had shown that NAbs are produced from 72 hrs onwards which can prevent further systemically delivered virus from reaching the tumour. Figure 14A illustrates the schematic of the *in vivo* experiment, which included a control group which received one dose of intravenous PBS. Figure 14B shows graphs of tumour growth for individual mice in each treatment cohort and it can be seen that mice receiving systemic MG1-FLUC ($1x10^7$pfu), irrespective of one or three doses, led to tumour growth delay compared to mice receiving IV PBS (control group). However, in this experiment, mice receiving IT MG1-FLUC ($1x10^7$pfu) did not experience any benefits in tumour control. Figure 14C, which shows the mean tumour growth for each treatment cohort, confirms significant growth retardation in mice receiving IV MG1-FLUC (p value<0.001 for 1 and 3 doses) but not in the IT MG1-FLUC groups, when compared to the control cohort. Finally, Figure 14D illustrates the overall survival graphs for each treatment cohort and despite the tumour growth retardation in the systemically treated mice, none of the groups revealed any significant survival advantage when compared to control mice.

(A)

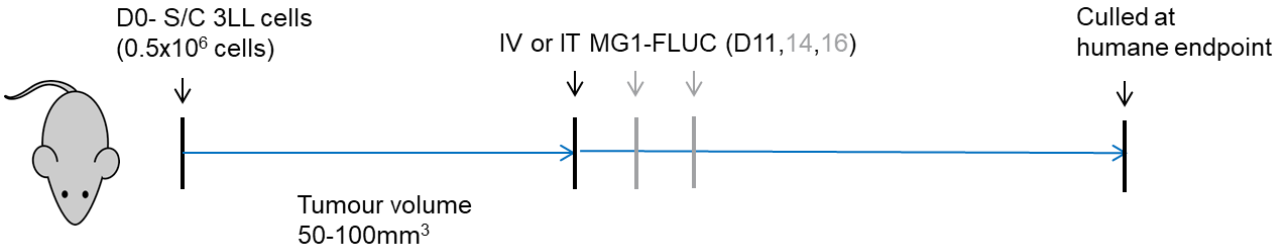
D0- S/C 3LL cells
(0.5x10^6 cells)
IV or IT MG1-FLUC (D11,14,16)
Culled at
humane endpoint
Tumour volume
50-100mm^3

(B)

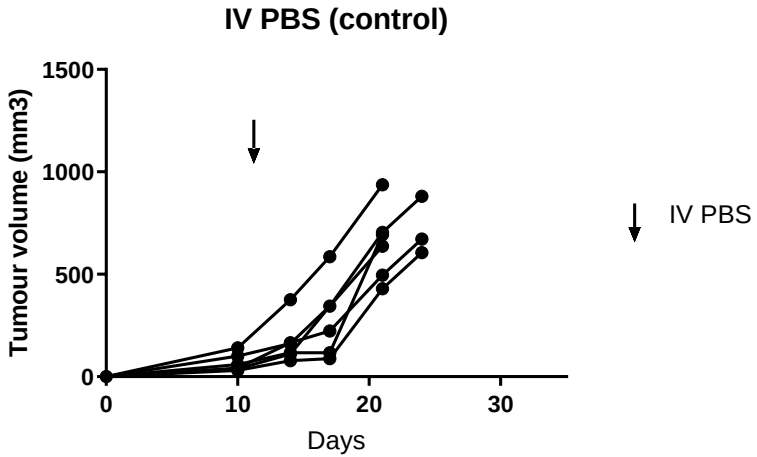
IV PBS (control)
Tumour volume (mm3)
1500
1000
500
0
0
10
20
30
Days
IV PBS

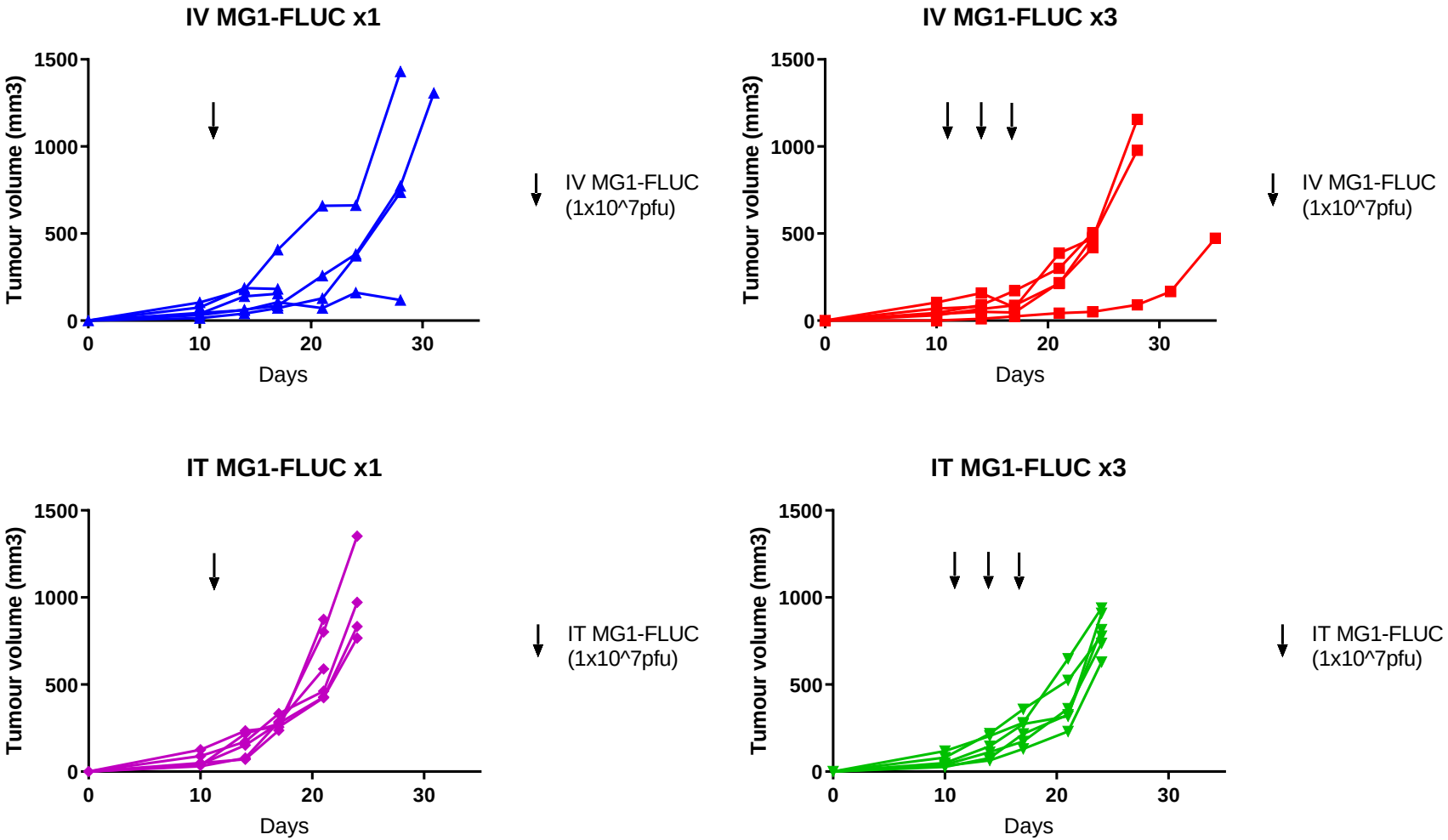
IV MG1-FLUC x1
Tumour volume (mm3)
1500
1000
500
0
0
10
20
30
Days
IV MG1-FLUC
(1x10^7pfu)
IV MG1-FLUC x3
Tumour volume (mm3)
1500
1000
500
0
0
10
20
30
Days
IV MG1-FLUC
(1x10^7pfu)
IT MG1-FLUC x1
Tumour volume (mm3)
1500
1000
500
0
0
10
20
30
Days
IT MG1-FLUC
(1x10^7pfu)
IT MG1-FLUC x3
Tumour volume (mm3)
1500
1000
500
0
0
10
20
30
Days
IT MG1-FLUC
(1x10^7pfu)

(C)

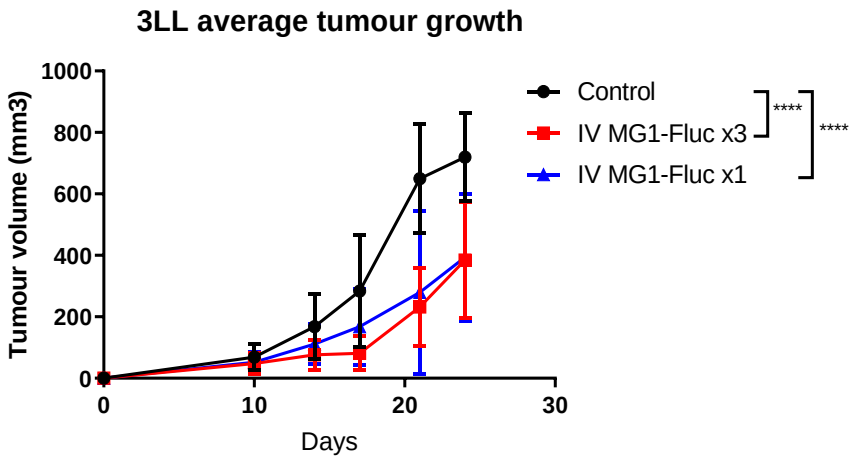
3LL average tumour growth
Tumour volume (mm3)
1000
800
600
400
200
0
0
10
20
30
Days
Control
IV MG1-Fluc x3
IV MG1-Fluc x1
****
****

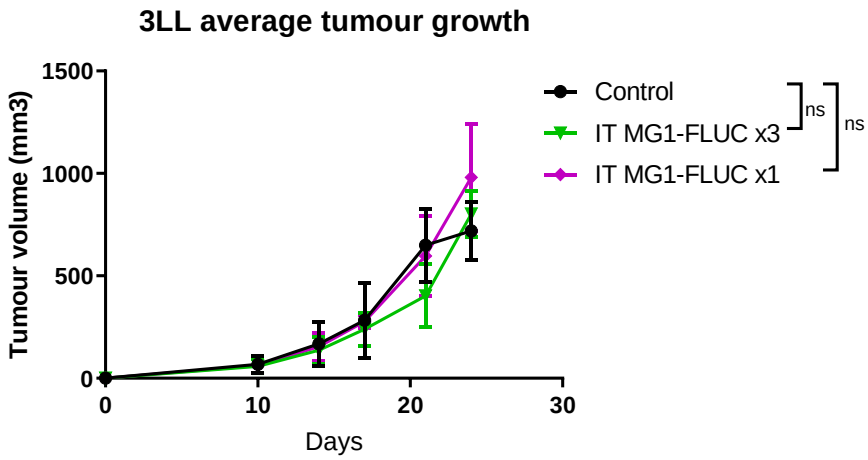
3LL average tumour growth
Tumour volume (mm3)
1500
1000
500
0
0
10
20
30
Days
Control
IT MG1-FLUC x3
IT MG1-FLUC x1
ns
ns

(D)

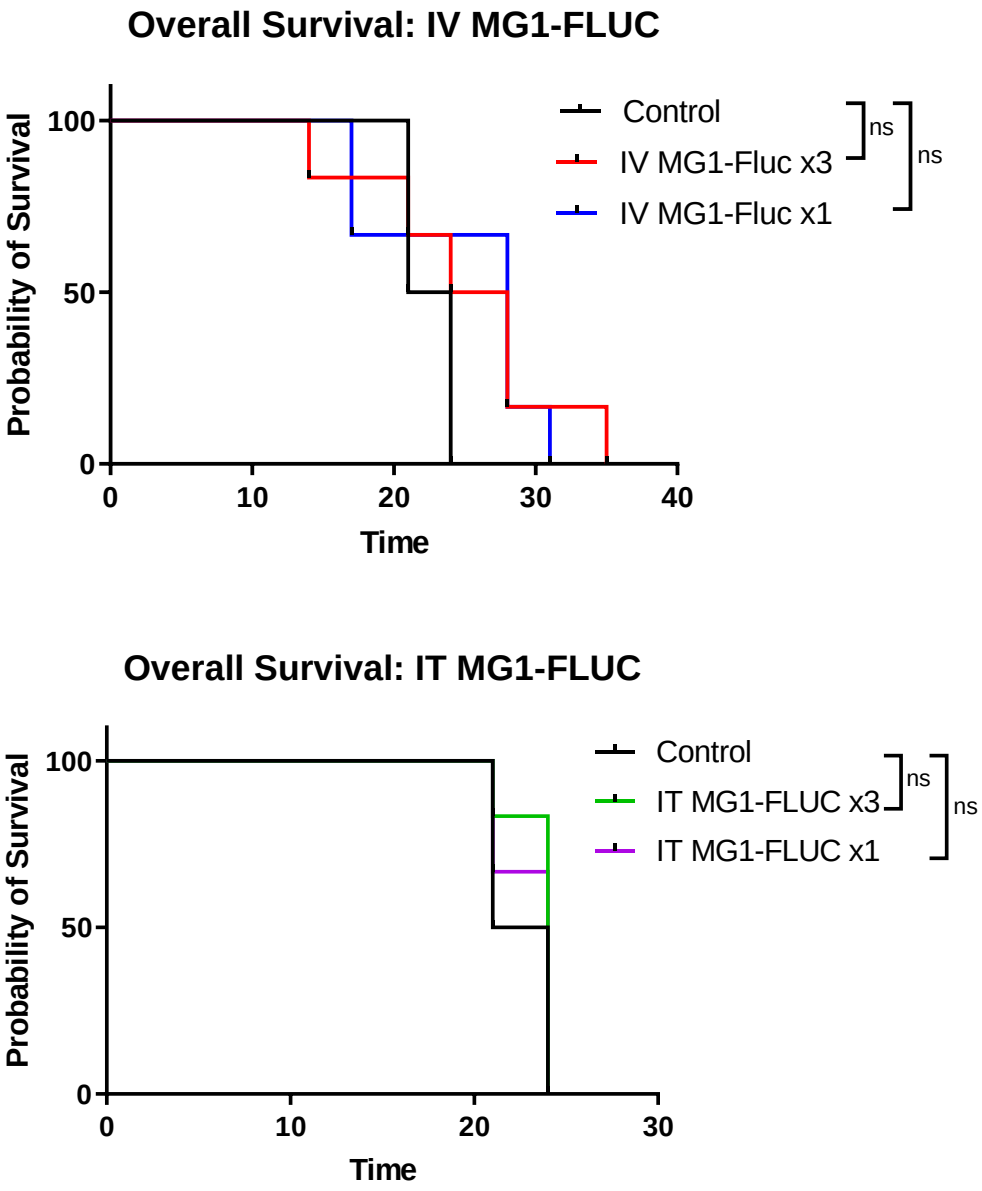

Figure 14: Intravenously delivered MG1 leads to tumour growth retardation in syngeneic 3LL subcutaneous murine model but does not result in overall survival benefit. Intratumourally injected MG1 had no impact on 3LL tumour growth or survival.

*(A) Schematic of in vivo experiment. (B) Graphs showing 3LL tumour growth of individual mice in each treatment cohort. (C) Graphs representing the average 3LL tumour growth in intravenous and intratumoural MG1-FLUC groups. (****p<0.0001; MG1-FLUC treated vs. control; Two-way ANOVA statistical analysis corrected for multi-comparison using Tukey's test). (D) Survival curves for mice treated with intravenous and intratumoural MG1-FLUC. (MG1-FLUC treated vs. control; Mantel-Cox log-rank statistical analysis)*

4.4 Discussion

Maraba is a single-stranded, negative-sense enveloped RNA virus that has demonstrated broad oncotropism and cytotoxic activity across a wide range of human and murine cancer cell lines (131, 184). Genetically engineered maraba virus, MG1, has faster replication and enhanced tumour killing potency and has clinically been developed as a vector for oncolytic vaccination which is being currently investigated in phase I/II clinical trials (section 2.3.4).

In this chapter, the direct effect of maraba virus, MG1, was investigated in a panel of human lung cancer cell lines, as well as in a syngeneic 3LL lung cancer murine model.

The panel of human lung cancer cell lines H1792, H1299, H1573, H1437, H1975 and murine 3LL cell line were all susceptible to MG1 infection and subsequent cell death. MG1 was able to infect all cell lines tested (Figure 5 and 6) and replicate in the 3 human lung cancer cell lines that were investigated, H1299, H1437 and H1573 to varying degrees, with H1299 cells producing greater fold increase in MG1 progeny than H1437 and H1573 (Figure 7). The level of MG1 replication correlated with cell sensitivity to maraba virus-induced cytotoxicity; H1299 had a reduction of 50% (95% CI 0.35-0.65, $p<0.0001$) cell viability after 0.001 MOI MG1-GFP exposure by 48 hrs, while H1573 decreased by 28% (95% CI 0.08-0.48, $p=0.0035$) and H1437 had no significant effect on cell viability at the same viral dose concentration and at the same timepoint. Murine 3LL cells were the most sensitive to MG1-induced cell death with 77% (95% CI 0.52-1.0, $p<0.0001$) reduction in cell viability by 48 hrs after 0.001 MOI MG1 exposure (Figure 9). MG1 also demonstrated tumour selectivity as there was no significant impact to cell viability in primary HFF even at the higher doses of virus tested (0.01 and 0.1 MOI), which was consistent with data from the initial study by Brun *et al*. (131).

Suboptimal delivery of OVs is a potential cause of treatment failure, therefore intratumoural delivery has become the most common route of OV administration. The 2 OVs which have been approved for clinic use: H101 (an E1B-deleted serotype 5 adenovirus, approved in China for treatment of head

and neck cancer) and TVEC (a modified HSV that is FDA-approved for treatment of malignant melanoma) are both intratumourally delivered. Although IT administration allows maximal delivery of high viral titres to tumours, bypassing systemic neutralisation and preventing premature clearance, it has limited use in disseminated metastatic cancer where sites may not be easily accessible. Intravenous delivery of OVs therefore is arguably the more attractive route of administration for clinical applications, precluding the need for additional training and interventional procedures associated with IT delivery with the potential of reaching all diseased sites. MG1 virus is one of few OVs that is able to reach tumours after systemic delivery in murine models and demonstrate potent oncolytic activity (131, 142). Our data supports this finding as intravenously delivered MG1 was able to reach 3LL syngeneic tumours whether it was subcutaneous or at the orthotopic site and furthermore, MG1 was tumour tropic as the virus was not detectable in any other organs via IVIS imaging or *ex vivo* plaque assays (Figure 9 and 10).

However, one of the major challenges of delivering the virus via the bloodstream is the rapid clearance through induced antibody titres, which can prevent the virus reaching the tumour. Even if the virus manages to reach the malignant site, it then needs to have maintained a sufficient level of replication and activity to be able to infect and kill cancer cells. Therefore, in this chapter we set out to determine firstly whether NAbs are induced after systemic delivery of MG1 virus *in vivo* and if so whether the viral titre within the tumours is significantly different between the 2 routes of administration. The results showed that MG1-induced NAbs were detectable within the serum of mice which received IV injection of the virus from day 3 onwards. The quantity of NAbs seems to increase with time as evidenced by the greater number of dilutions required to dilute out the antibodies in the plasma taken at later timepoints (7 and 14 days) before neutralisation becomes ineffective compared with plasma at day 3 (Figure 12B). Furthermore, it was shown that a second dose of MG1 virus given systemically after an initial dose administered 5 days earlier in immunocompetent mice bearing 3LL subcutaneous tumours, was prevented from reaching the malignant site

(Figure 12D). This is likely due to the anti-viral immune response which has been primed by the initial exposure to the virus and hence the subsequent dose of virus is neutralised and cleared before it can reach the tumour. This has implications when designing the optimal regimen for MG1-therapy as multiple doses may reveal limiting returns in efficacy.

As stated previously, another concern with IV delivery of OV is whether the dose of virus that eventually reaches the tumour is sufficient to maintain replication and efficacy. Le Boeuf *et al*. observed that IV injection of MG1 at a dose of $1x10^8$ pfu did not lead to productive viral replication in tumours of mice bearing S180 sarcomas, whereas IT administration of the same dose did (133). Contrary to this publication, we found that both IT and IV delivery of MG1 (given even at a lower dose of $1x10^7$pfu compared to the previous authors) led to replication competent virus within the 3LL subcutaneous tumours as evidenced by *ex vivo* plaque assays (Figure 9). The ability of MG1 to reach and replicate within tumours after systemic delivery seems therefore to be tumour-type specific. Furthermore the viral titre, although unsurprisingly at 6 hrs after administration was greater with IT delivery compared to IV, at 24, 48 and 72 hrs was not significantly different between the 2 groups (Figure 13). This gave rationale for both routes of administration to be tested in an efficacy experiment with MG1 virus in the 3LL murine model.

From this experiment we observed that intravenously delivered MG1 led to significant tumour growth retardation in immunocompetent mice harbouring subcutaneous 3LL tumours, whereas there was no significant effect with intratumoural administration of the virus. However, disappointingly the tumour growth delay did not translate to overall survival benefit with IV MG1 treatment. In support of the previous data which showed that NAbs were induced by systemic MG1 from 72 hrs onwards, there was also no significant difference observed in tumour growth retardation or survival between single dose or 3 doses of intravenously delivered MG1. Therefore, the presence of MG1-induced NAbs could have neutralised and cleared the virus from additional intravenous doses, rendering them ineffective. However, one of the limitations to this experiment is the presence of only one control group (mice bearing 3LL tumours treated with one dose of IV PBS) and ideally there would have been

4 control groups; mice treated with either one dose of IV or IT PBS and mice treated with either three doses of IV or IT PBS. One may argue that the mice treated with IT MG1 is not a fair comparison to mice receiving IV PBS as the routes of administration could itself lead to discrepancy in the results. However, our data in fact showed that IT delivery of MG1 was equally as ineffective as IV PBS and only IV MG1 treatment displayed any tumour control efficacy. Therefore, we still believe the conclusions from this experiment holds true although, if time had allowed, we would repeat this experiment with all necessary controls.

As we have shown that the viral titres within the tumours are equivalent after IT and IV delivery from 24 hrs onwards, the difference in tumour growth control between the 2 routes of administration is unlikely due to direct oncolytic effect. MG1, as with other OVs, have a second mode of action, which is its intrinsic ability to induce anti-tumour immunity. For example, murine B16 melanoma responded to MG1 independently of its replication cycle (116). Also, IV injection has been shown to enhance the generation of anti-tumour immune responses compared to intralesional delivery (135) which could explain the benefit in tumour control with systemic MG1 compared to IT delivery. In the next chapter, we will therefore explore the immunogenic properties of MG1 virus.

Chapter 5:

Immunological effects of MG1 virus

5. Chapter 5: Immunological effects of MG1 virus

5.1 Introduction

OVs have a dual mechanism of action; aside from direct oncolytic activity, OVs can also induce both innate and adaptive anti-tumour immune responses. Gujar *et al*. (111) in fact stated that many of the "undesirable" anti-viral immune responses actually resulted in activation of the immune system against the tumour, transforming them from immune "cold" to immune "hot". MG1 has also been shown to induce these beneficial anti-tumour immune sequalae as both parental and replication-incompetent minimally UV-inactivated MG1 was able to clear lung metastases in murine B16 melanoma murine model (116). In this study, the authors reported local increase of DCs and NKs following systemic delivery of MG1. Tumour growth control was dependent on NK cell activity as selective depletion of this immune subset abolished any therapeutic efficacy. MG1 can also initiate an adaptive anti-tumour immune response as demonstrated in murine triple-negative breast tumour model (135); the authors reported neoadjuvant MG1 was able to protect animals against distant postoperative tumour rechallenge whether the virus was administered intratumourally or systemically. Moreover, systemic delivery appeared more efficient than intralesional injection leading to 40% disease-free mice compared to 20% following tumour rechallenge. In this chapter we aim to explore the immunogenic properties of MG1 virus in NSCLC, which might explain the difference in tumour growth control seen in 3LL murine model between IT and IV delivery seen in the previous chapter.

5.2 MG1 induces immunogenic cell death

OVs have the potential to induce "immunogenic cell death" (ICD) that is sufficient to induce an adaptive immune response. ICD is also somtimes

defined as a type of apoptotic cell death that is characterised by the release of danger signals such as DAMPs, which in turn activate the innate immune system by interacting with pattern recognition receptors (PRRs) (191). The main hallmarks of ICD that can be measured in culture and have been more described so far include ATP release, ecto-expression of calreticulin (CRT), which is an “eat-me” signal, and late apoptotic release of high mobility group box 1 protein (HMGB1), which is an activation signal for immune cells. Collectively these act as strong immune stimulants and ICD is regarded as a keystone of anti-tumour immune stimulation (99, 192). Therefore, we set out to identify the main hallmarks of ICD induced after MG1 infection in NSCLC cell lines.

Firstly, the panel of human NSCLC cell lines (H1792, H1299, H1975, H1437 and H1573) and 3LL murine cell line was infected with a range of MG1-GFP doses (between 0-1 MOI) or PBS (control). At the 24 and 48 hr timepoint after infection, the supernatants from these cells were collected and spun to remove debris prior to being analysed for presence of ATP via CellTiter-Glo® Luminescent assay. The luminescent signal is proportional to the amount of ATP present. Figure 15 shows the luminescent signal increases in a dose dependant fashion after MG1 infection at the 24 hr timepoint for both human (A) and murine (B) cell lines. By the 48 hr timepoint, the luminescent signal decreases with increasing doses of MG1 virus across most cell lines (except in H1573 and H1437), likely due to the fact that by this later time the number of viable cells, not killed by the virus, and able to release ATP would be markedly reduced. These results demonstrate that MG1 infection induces ATP release in the NSCLC cell lines tested and to different quantities; highest peak luminescent signal detected with H1792 cells after 0.0001 MOI at 48 hrs (mean=303217 RLU) and lowest peak luminescent signal with H1975 after 1 MOI at 24 hrs (mean=8445 RLU).

(A)

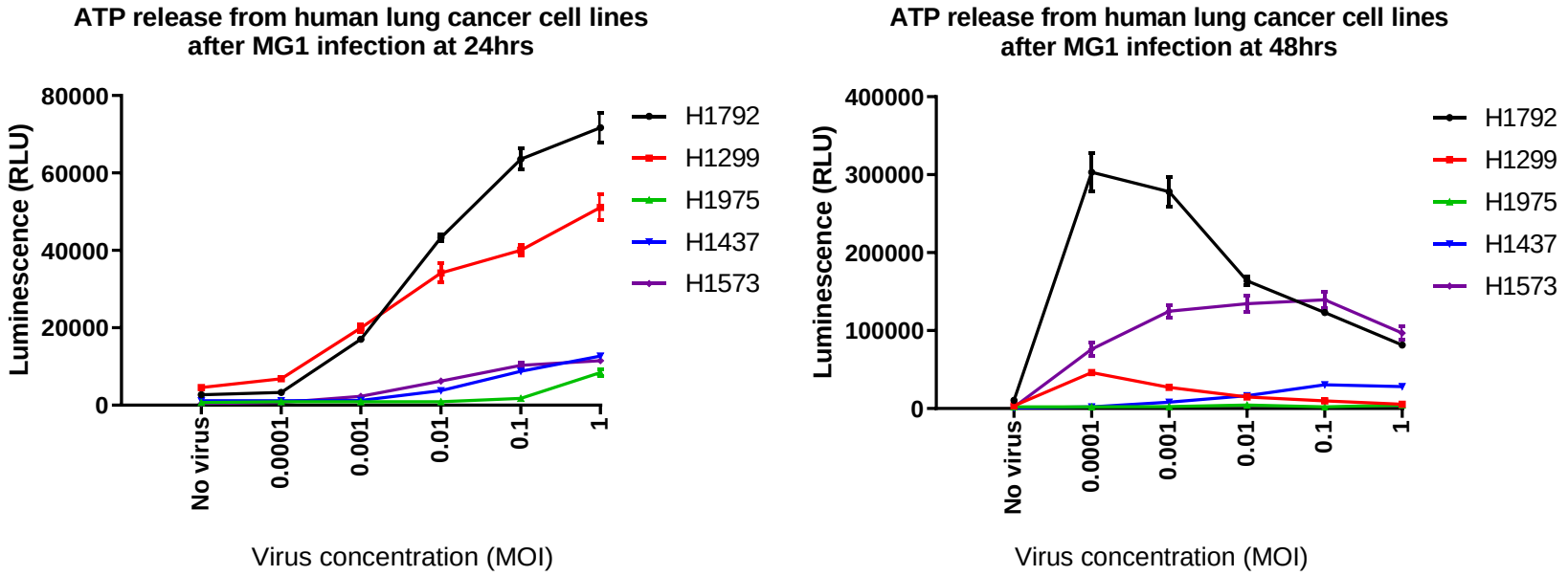
ATP release from human lung cancer cell lines after MG1 infection at 24hrs
Luminescence (RLU)
80000
60000
40000
20000
0
No virus
0.0001
0.001
0.01
0.1
1
Virus concentration (MOI)
H1792
H1299
H1975
H1437
H1573
ATP release from human lung cancer cell lines after MG1 infection at 48hrs
Luminescence (RLU)
400000
300000
200000
100000
0
No virus
0.0001
0.001
0.01
0.1
1
Virus concentration (MOI)
H1792
H1299
H1975
H1437
H1573

(B)

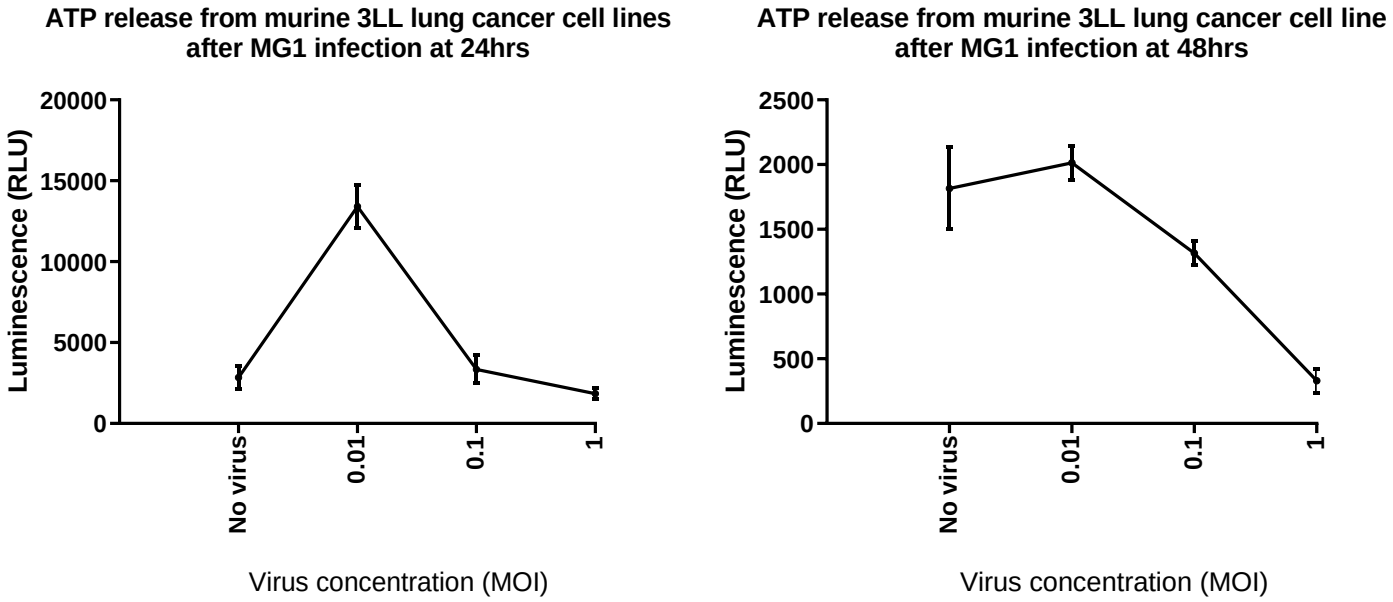

Figure 15: MG1 infection induces ATP release from human and murine NSCLC cell lines.

Graphs to show luminescence (RLU), which correlates with ATP quantity, after different doses of MG1 exposure or PBS (no virus) in (A) human- and (B) 3LL murine- lung cancer cell lines at 24 and 48 hrs. Mean +SD of three independent experiments plotted.

Next, to assess for release of HMGB1, three human lung cancer cell lines (H1299, H1792 and H1975) and 3LL were infected with 0.1 MOI MG1-GFP or PBS (control). The supernatants were then collected after 24 and 48 hrs and spun to remove debris before analysing for the presence of HMGB1 via ELISA. Graphs shown in Figure 16, demonstrate that MG1 infection leads to statistically significant release of HMGB1 for all cell lines after 48 hrs. At the 24 hr timepoint, increased concentrations of HMGB1 were detected for 3LL and H1299, but not for H1792 or H1975 cells. 3LL and H1299 cell lines also produced the highest concentration of HMGB1 after 48 hrs exposure to the virus (mean concentration= 28.9ng/ml and 19.1ng/ml respectively), while H1975 and H1792 cells released the least (mean concentration= 10.4ng/ml and 12.2ng/ml) at the same timepoint. These data are consistent with 3LL and H1299 cell lines being more sensitive to MG1 infection and MG1-induced cytotoxicity, whereas both H1975 and H1792 are less sensitive (see Figure 6 and Figure 9).

Finally, to assess for ecto-expression of calreticulin in human NSCLC cells, H1299 and H1975 cells were selected to be infected with MG1-FLUC at concentrations 0.01, 0.1 and 1 MOI or with PBS (control). The cells were then collected after 48 hrs of infection, not permeabilized and stained with CRT-specific antibody for flow cytometry analysis. There were no differences seen in surface CRT when gating on live cells (data not shown), but as it is not known at what point during the live-to-dead transition surface CRT really matters the level of CRT was also measured on the gated dead cells by flow cytometry. As CRT is an “eat-me” signal harboured by dying cells participating in their recognition by phagocytes, it would have been ideal to repeat this experiment with an apoptotic marker such as Annexin V which would identify dying cells for analysis. The results on gated dead cells however are shown in Figure 17 illustrating a dose dependent increase in CRT after MG1 infection in both cell lines. Unsurprisingly the more MG1-infection sensitive H1299 cell line expressed CRT even with the lowest virus concentration tested (0.01 MOI) whereas the more MG1-infection resistant H1975 only had CRT detectable with higher doses of 0.1 and 1 MOI.

Collectively these results demonstrate that MG1 can induce the hallmarks of ICD in human and murine lung cancer cells.

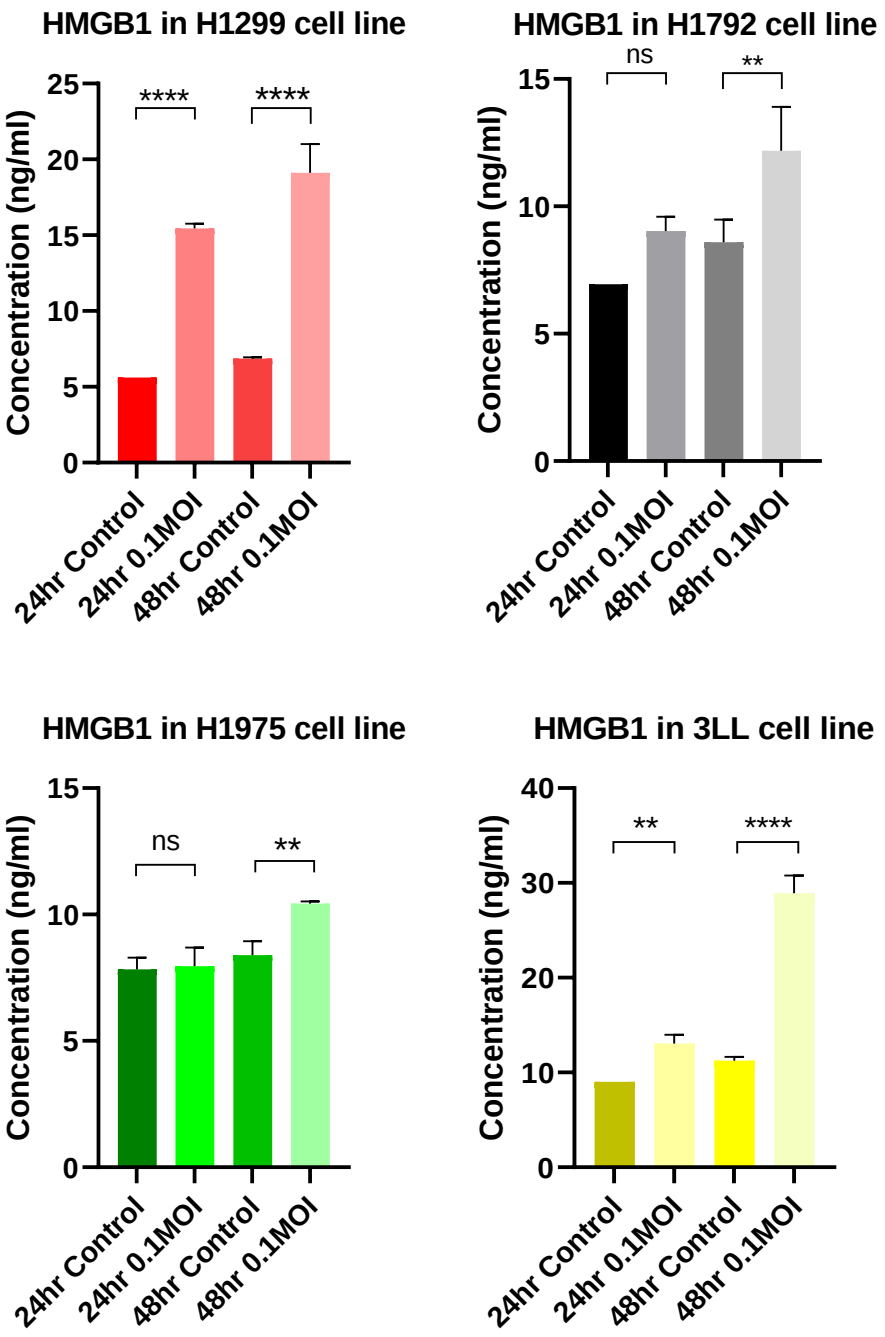

Figure 16: MG1 infection induces HMGB1 release from human and murine NSCLC cell lines.

*Graphs showing concentration of HMGB1 within supernatants after exposure to 0.1 MOI of MG1-GFP or PBS (control) in H1299, H1792, H1975 and 3LL cells at 24 and 48 hr timepoints, measured using HMGB1 ELISA. Mean +SD of three independent experiments plotted. (*p<0.0332, **p<0.0021, ***p<0.0002 and ****p<0.0001; 0.1 MOI MG1-treated vs. control for each timepoint; ordinary one-way ANOVA statistical analysis with Sidak's multiple comparison test.*

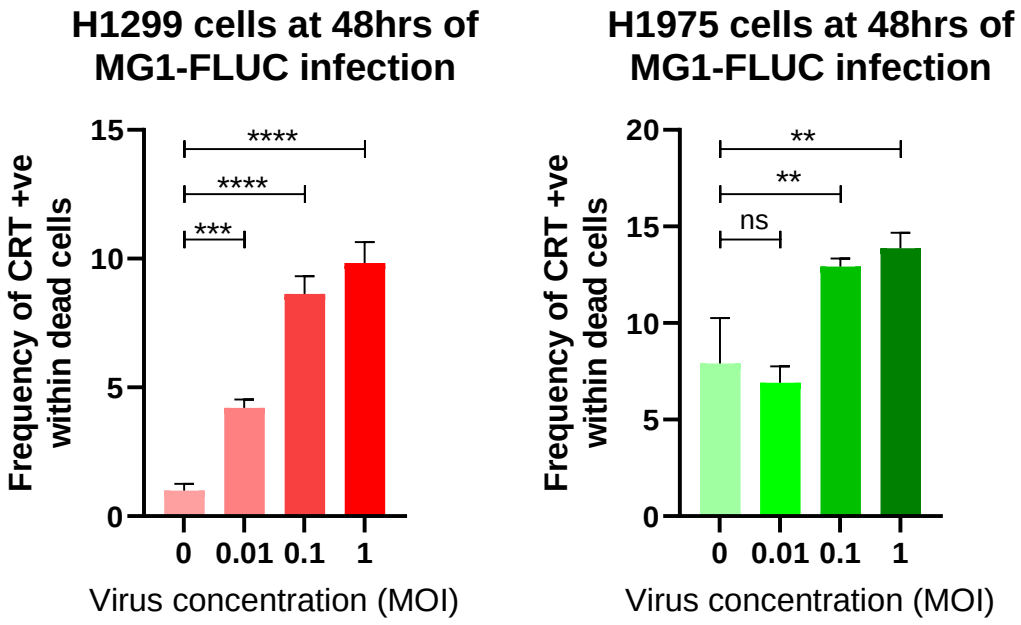

Figure 17: MG1 infection results in expression of calreticulin in H1299 and H1975 human lung cancer cell lines.

*Graphs showing frequency of calreticulin expression within gated dead cell populations of H1299 and H1975 after infection with different concentrations of MG1-FLUC or PBS (control) at 48 hrs. Mean +SD of three independent experiments plotted. (*p<0.0332, **p<0.0021, ***p<0.0002 and ****p<0.0001; MG1-treated vs. control for each dose of virus; ordinary one-way ANOVA statistical analysis with Dunnett multiple comparison test.*

5.3 MG1 induces Type I IFN production

Having shown that MG1 can induce the main hallmarks of ICD, there are other indicators of ICD that have been recently described, such as activation of annexin I, type I IFN, IL-1β, exposure of F-actin and heat shock proteins (HSP70, HSP90) (193, 194). Of these, type I IFN is one of the main players on the dynamic crosstalk between OV therapy and the immune system; on the one hand the virus relies on frequent dysfunctional IFN signalling in cancer cells to make them more susceptible to OV infection, replication and oncolysis. However, on the other hand, type I IFN (IFN-α and IFN-β) also have an important role in the anti-tumour response by stimulating immune cells within the TME, such as DC, NK and CD8+ T cells (195). In turn activated NK and other immune cells produce type II IFN (IFN-γ), which inhibits angiogenesis, induces apoptosis and acts as an immune stimulant by activating MHC class II in DCs, as well as promoting the phagocytic activity of macrophages and CD8 T cell responses (196). Importantly the ability to induce type I IFN in tumours and the intensity to which this signalling pathway is activated, varies dramatically among OVs (110). The fine balance between OVs being able to induce type I IFNs which could lead to beneficial anti-tumour immune response, but not allowing this anti-viral signal to limit replication and oncolysis has been demonstrated with NDV by Elankumaran *et al*. The authors in this study showed that the virus was able to progress and replicate in tumour cells defective in IFN-α expression, however infected tumour cells were still able to secrete IFN-β. Furthermore some tumour cells were also capable of responding with IFN-α expression after NDV infection and maintain permissiveness for viral replication as there were defects in downstream signalling of antiviral effectors (197).

MG1 has been shown to target type I IFN defective tumours (131), but whether the virus is capable of inducing IFN-β, as in the case of NDV, for potentially beneficial anti-tumour response has not been previously explored. To investigate this question, 2 human (H1792 and H1299) and 3LL murine lung cancer cells were infected with 0.1 MOI MG1-GFP for western blot analysis after 24 hrs of virus exposure. A reovirus infected 4434 melanoma cell line,

known to stimulate the IFN signalling pathway, was used as a positive control. Figure 18A illustrates how RNA viruses are detected through RNA sensing proteins, such as RIG-I and MDA-5. Upon recognition of viral RNA, they are recruited by the adaptor IPS-1 (also known as MAVS, CARDIF or VISA) to the outer membrane of the mitochondria leading to the activation of several transcription factors including IRF3, IRF7 and NFκB (198). IRF3 and IRF7 leads to the expression of type I IFNs, while NFκB regulates the production of inflammatory cytokines.

The western blots shown in Figure 18B reveal that after MG1-infection, there was indeed an increase in expression of pTBK1 and pIRF3, the upstream proteins leading to type I IFN response, which is more evident in H1792 and H1299 cell lines compared to 3LL. Despite equal loading of protein in the 3LL western blot, the MG1-treated cells always resulted in a narrower tubulin band in comparison to untreated samples. This may be due to the inherent high sensitivity of 3LL cells to MG1-cytotoxicity (as shown in section 4.2.3) causing tubulin degradation in these samples. Reovirus infected 4434 melanoma cells, known to stimulate type I IFN signalling through RIG-I, were used as positive control. Using densitometry (graphs shown in Figure 18C) to normalise the intensity of the bands to tubulin, reveals that in all three cell lines there were an increase in expression of pTBK1 and pIRF3 after viral infection. Furthermore, the relative fold increase in pTBK1 and pIRF3 was greatest in MG1-infected 3LL compared with H1792 and H1299 cells; for pTBK1, there was a 150.6-fold increase in 3LL after viral infection compared to 34.5 and 13.5-fold increase in H1792 and H1299 respectively. As for pIRF3, there was a 1173-fold increase in expression in MG1-infected 3LL compared to 66-fold in both other cell lines. This was again consistent with 3LL being the most sensitive cell line in terms of MG1-infection and oncolysis (section 4.2). In all 3 cell lines, there was no RIG-I detected with or without MG1 virus, suggesting that another RNA sensing protein could be involved in this signalling cascade, e.g., MDA-5.

To further determine whether MG1 induces type I IFN expression, which can lead to a beneficial anti-tumour immune response, the supernatants from 3LL cells infected with 0.1 MOI MG1-GFP were collected after 24 hrs of viral

exposure. The samples were then spun and the presence of murine IFN-β was assessed via ELISA. Figure 18D shows that significant quantities of IFN- β was released after MG1 infection compared to uninfected samples (70.97 pg/ml vs. 0 pg/ml respectively).

Collectively these results show that MG1 leads to stimulation of the type I signalling pathway in the selected lung cancer cell lines tested and IFN-β was released to significant levels from 3LL after virus infection.

(A)

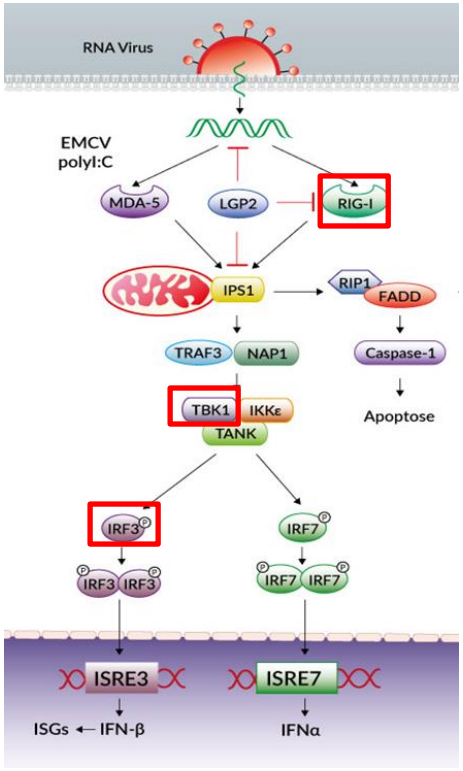
RNA Virus
EMCV
polyI:C
MDA-5
LGP2
RIG-I
IPS1
RIP1
FADD
TRAF3
NAP1
Caspase-1
TBK1
IKKε
TANK
Apoptose
IRF3
IRF7
IRF3
IRF3
IRF7
IRF7
ISRE3
ISRE7
ISGs ← IFN-β
IFNα

(B)

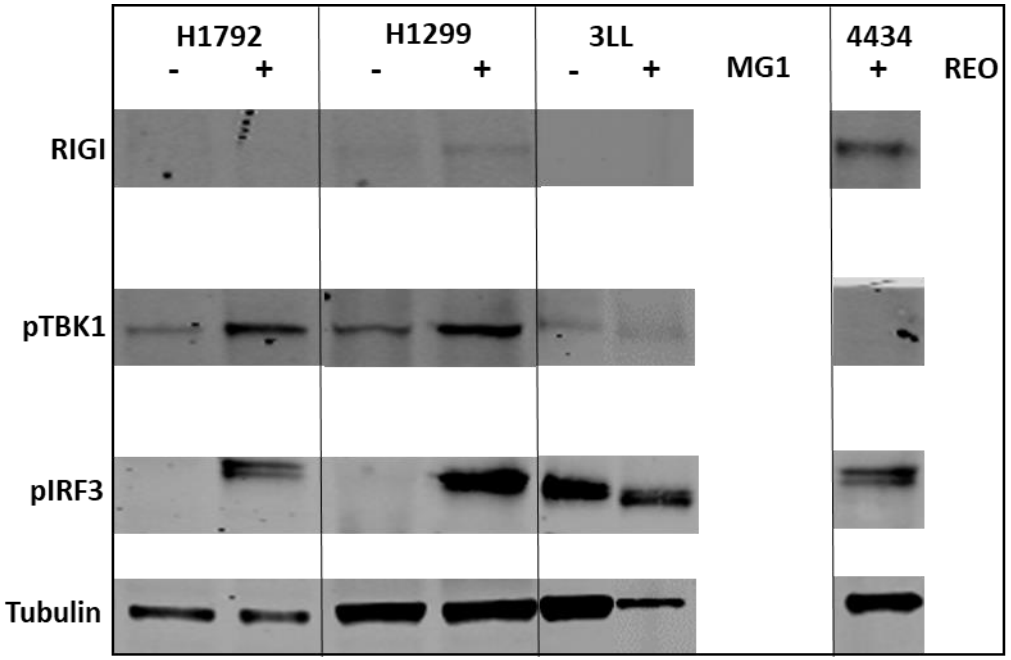
H1792
- +
H1299
- +
3LL
- +
MG1
4434
+
REO
RIGI
pTBK1
pIRF3
Tubulin

(C)

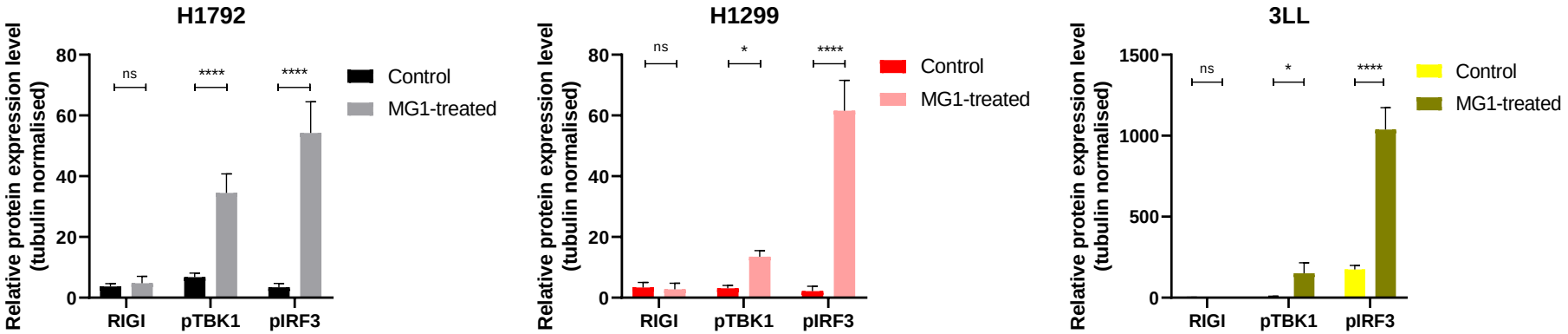
H1792
Relative protein expression level (tubulin normalised)
80
60
40
20
0
ns
****
****
RIGI
pTBK1
pIRF3
Control
MG1-treated
H1299
Relative protein expression level (tubulin normalised)
80
60
40
20
0
ns
*
****
RIGI
pTBK1
pIRF3
Control
MG1-treated
3LL
Relative protein expression level (tubulin normalised)
1500
1000
500
0
ns
*
****
RIGI
pTBK1
pIRF3
Control
MG1-treated

(D)

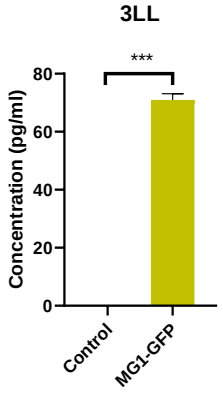
3LL
Concentration (pg/ml)
80
60
40
20
0
***
Control
MG1-GFP

Figure 18: MG1 stimulates expression of pTBK1 and pIRF3 in human and murine NSCLC cell lines and leads to secretion of IFN-β in 3LL murine cells

*(A) Type I IFN signalling pathway for RNA viruses. Red boxes highlight the proteins of interest tested for in subsequent western blots. (B) Western blot analysis of upstream proteins involved in Type I IFN signalling after 0.1 MOI MG1-GFP infection in H1792, H1299 and 3LL cells; RIG-I, pTBK1 and pIRF3. Reovirus infected 4434 melanoma cells used as positive control for western blot antibodies (C) Densitometric presentation of western blots. Data are mean +SD of three independent experiments. (*p<0.0332, **p<0.0021, ***p<0.0002 and ****p<0.0001; MG1-treated vs. control; Two-way ANOVA statistical analysis with Sidak's multiple comparison test. (D) Graph showing concentration of IFN-β detected via ELISA after 0.1 MOI MG1-GFP exposure in 3LL cells at 24 hrs. Data are mean +SD of three independent experiments. (***p=0.0003 two-tailed P-value; MG1-treated vs. control; Paired Student T-test statistical analysis)*

5.4 MG1 effects on tumour immune microenvironment in 3LL tumours

Having established that MG1 infection causes ICD and stimulates the type I IFN signalling pathway in human and murine NSCLC cell lines, with IFN-β release detected in 3LL cells, the resulting immunological changes were explored in the 3LL murine lung cancer model. As previously described in section 2.3.3, systemic MG1 led to increase in splenic population of DC and NK cells in mice harbouring B16 tumours within 24 hrs following injection (116). These effector NKs were also more activated with secretion of IFN-γ and granzyme B. Furthermore, selective depletion of NKs abolished the beneficial tumour growth control in this melanoma model. MG1-induced immunological changes have been explored as part of a prime-boost strategy with Ad-E6E7 in lung TC1 tumours, showing MG1-E6E7 significantly boosted specific immune responses against multiple epitopes encompassing all 4 antigens of the tetravalent transgene (16E6, 16E7, 18E6 and 18E7). There have not, to our knowledge, been any other studies investigating immune changes in murine lung cancer models resulting from MG1 infection alone and neither has the comparison between systemic or intratumoural delivery to TME been explored. To answer these questions, mice bearing 3LL syngeneic subcutaneous flank tumours were either treated with PBS or MG1-FLUC ($1x10^7$pfu), either with intravenous or intratumoural administration. 3 mice per group were sacrificed and their tumours and spleens were processed for flow cytometry analysis at day 3 and day 10 post treatment (Figure 19A shows schematic of experiment). Cells were stained and phenotyped into live CD45+/CD3+/CD4+ T cells, live CD45+/CD3+/CD8+ T cells and live CD45+/CD3-/NK1.1+ NK cells. The CD3+/CD4+ T cells were further characterised into CD3+/CD4+/CD25+/FoxP3+ T regulatory cells and CD3+CD4+/FoxP3- T effector cells (Figure 19B shows the gating strategy for flow cytometry analysis). These subsets of immune cells were further stained with antibodies against: Granzyme B (GrzmB), CD69 and Ki67 as activation markers, as well as PD1, T cell immunoreceptor with IG and ITIM domains

(TIGIT), LAG3 and T-cell immunoglobulin and mucin-domain containing-3 (TIM3) for monitoring changes in expression of checkpoint proteins.

5.4.1 MG1 infection induces early immune changes within spleen

Figure 19C shows that both IV and IT delivery of MG1 led to an increasing trend in the percentage of NK cells (out of the total CD45+ cell population) within the spleen at the 3 days timepoint compared to PBS controls, although this was not statistically significant (6.1% vs. 4.7% for MG1-treated vs. PBS for IV delivery and 5.7% vs. 4.3% for IT delivery). Although the increase was not statistically significant, the splenic NKs were more stimulated with enhanced activity as shown by an increase in Ki67 and GrzmB markers (for Ki67 there was a 48.0%, $p<0.0001$, increase on NK cells after IV MG1 vs. IV PBS and 32.7%, $p<0.0001$, increase for IT MG1 vs. IT PBS; as for GrzmB there was an increase of 40.1%, $p<0.0001$, after IV MG1 vs. IV PBS and 24.6%, $p=0.0005$, increase for IT MG1 vs. IT PBS). The early activation marker CD69 was also increased after IV MG1 (by 4.2%, $p=0.0139$) compared to IV PBS, but this was not statistically raised after IT MG1 (increase by 1.7%, $p=0.2746$). With all activation markers on splenic NK cells, the rise was significantly greater with IV administration of MG1 compared to the IT route. Interestingly TIGIT, which is an immune receptor present on T and NK cells for negative regulation, was also increased on the splenic NK population after IV and IT MG1 challenge (19.0%, $p=0.0056$, and 14.3%, $p=0.0236$, respectively compared to PBS controls).

MG1 did not change the percentage of CD8+ T cells within the splenic environment (~9-10% of live CD45+ cell population) at the 3 days timepoint, as shown in Figure 19D. However, the splenic T cells were again more activated especially after systemic delivery of MG1 compared with PBS controls (increases of 10.4%, $p=0.0068$, 5.6%, $p<0.0001$, and 0.9%, $p=0.0280$, in Ki67, GrzmB and CD69 markers respectively). There was an increasing trend in activation markers on CD8 T cells after IT delivery, although these were not statistically significant (increase of 4.8%, 1.3% and 0.1% in Ki67, GrzmB and CD69 respectively). There was also a non-statistically significant

increasing trend in PD1 on CD8+ T cells after MG1 infection compared to PBS controls (2.7% and 2.5% for IV and IT delivery respectively).

(A)

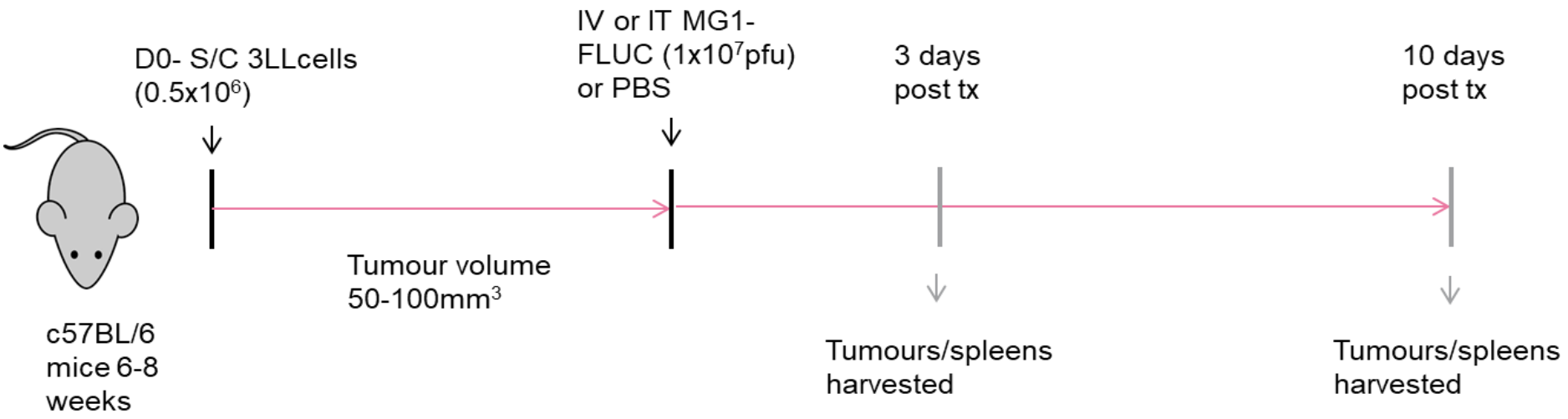
D0- S/C 3LLcells
(0.5x10^6)
IV or IT MG1-
FLUC (1x10^7pfu)
or PBS
3 days
post tx
10 days
post tx
Tumour volume
50-100mm^3
c57BL/6
mice 6-8
weeks
Tumours/spleens
harvested
Tumours/spleens
harvested

(B)

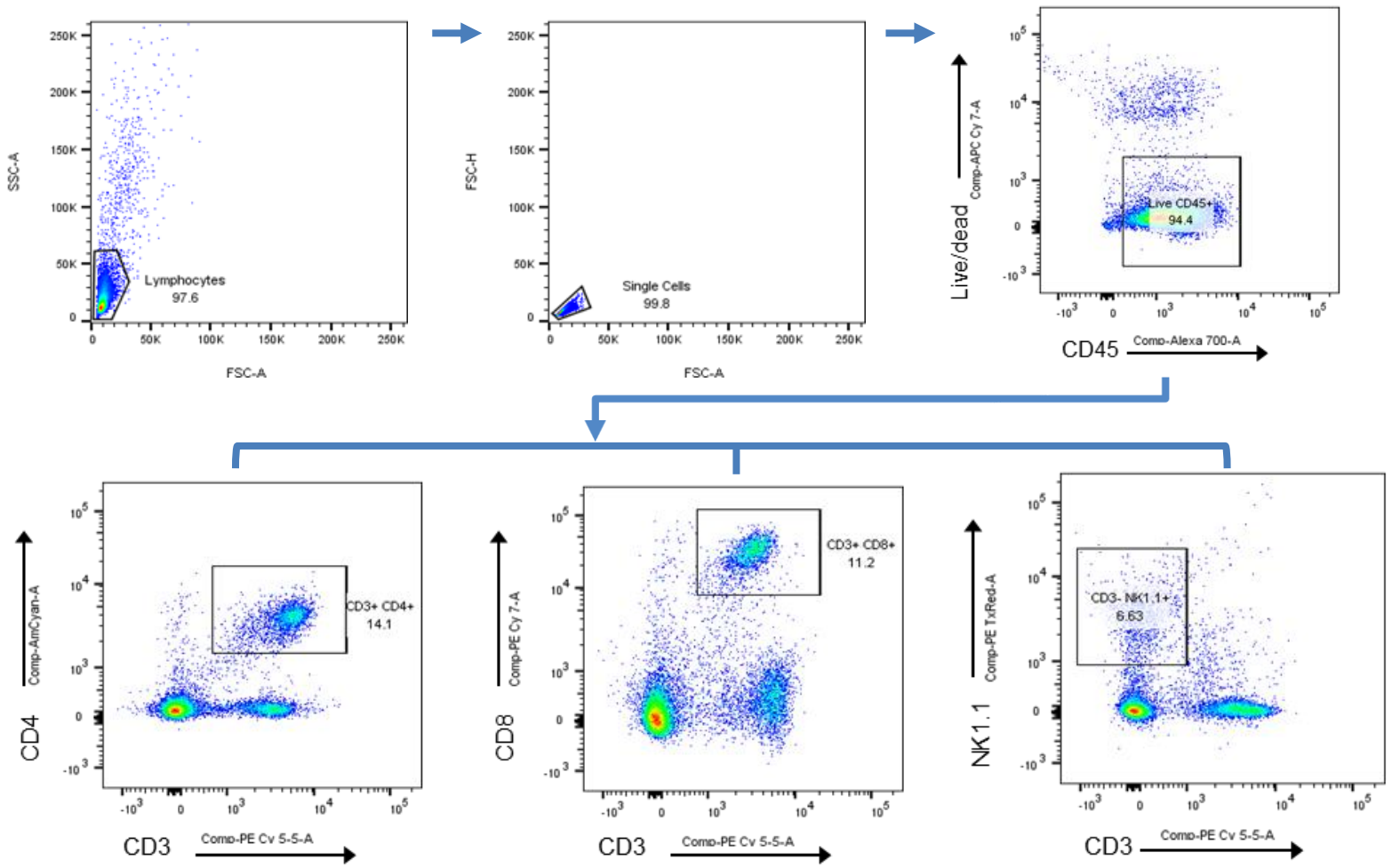
SSC-A
FSC-A
Lymphocytes
97.6
FSC-H
FSC-A
Single Cells
99.8
Live/dead
Comp-APC Cy 7-A
Live CD45+
94.4
CD45
Comp-Alexa 700-A
CD4
Comp-AmCyan-A
CD3+ CD4+
14.1
CD3
Comp-PE Cy 5-5-A
CD8
Comp-PE Cy 7-A
CD3+ CD8+
11.2
CD3
Comp-PE Cy 5-5-A
NK1.1
Comp-PE TxRed-A
CD3- NK1.1+
6.63
CD3
Comp-PE Cy 5-5-A

From CD3+CD4+ cells (see previous page)

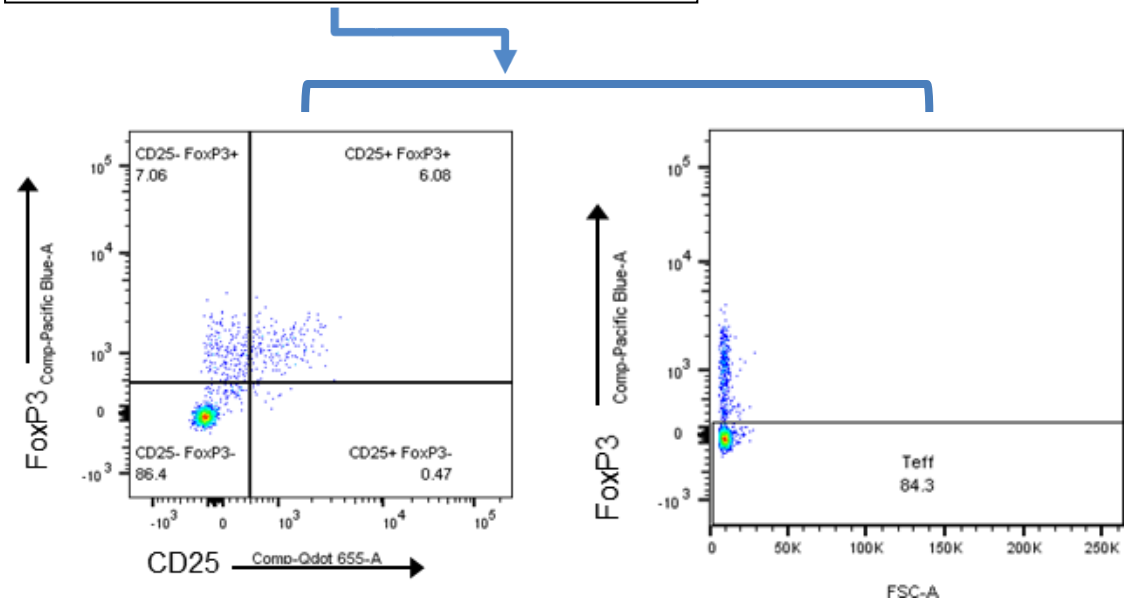

(C)

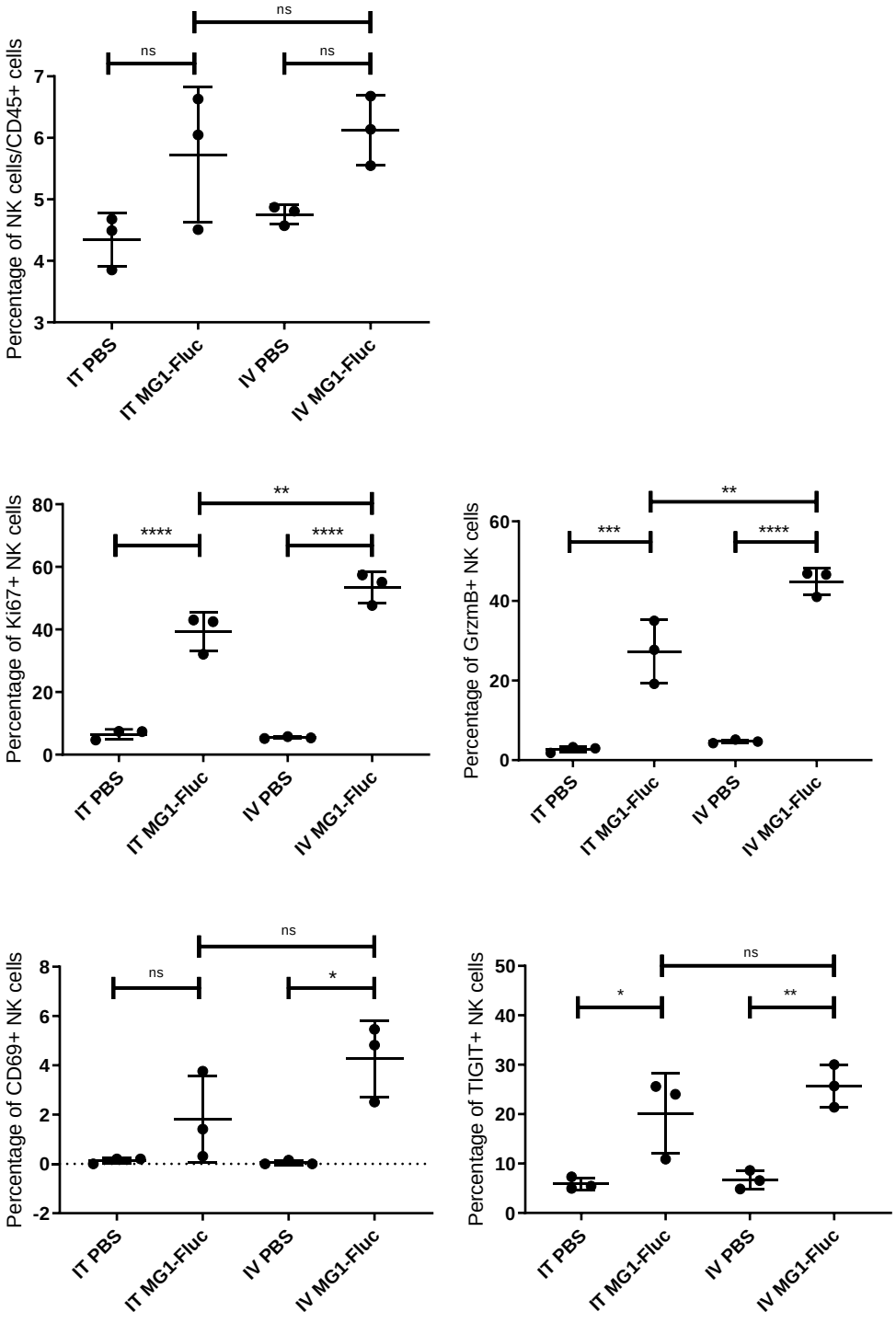
Percentage of NK cells/CD45+ cells
ns
ns
ns
IT PBS
IT MG1-Fluc
IV PBS
IV MG1-Fluc
Percentage of Ki67+ NK cells
**
****
****
Percentage of GrzmB+ NK cells
**
***
****
Percentage of CD69+ NK cells
ns
ns
*
Percentage of TIGIT+ NK cells
ns
*
**

(D)

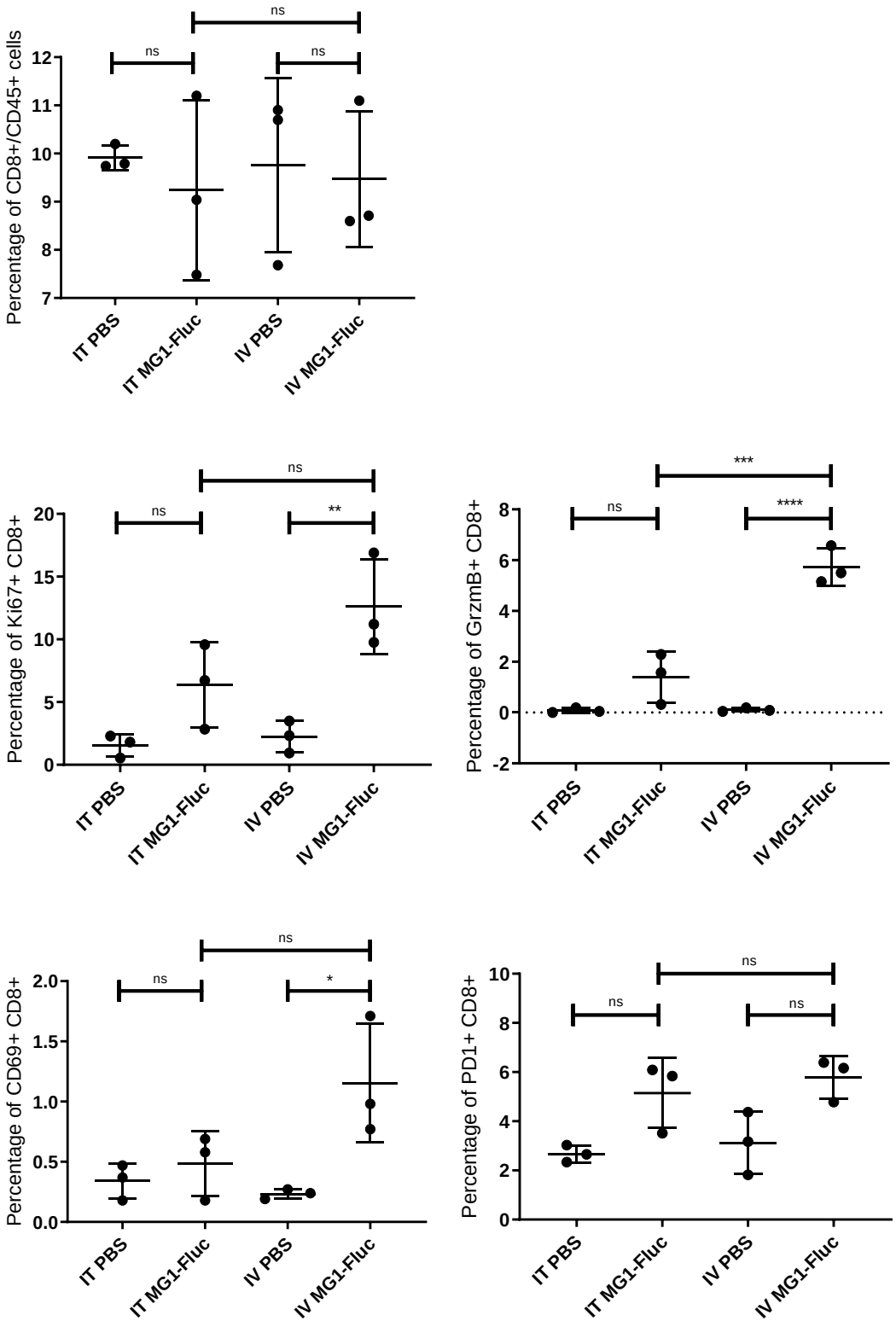
Percentage of CD8+/CD45+ cells
ns
ns
ns
IT PBS
IT MG1-Fluc
IV PBS
IV MG1-Fluc
Percentage of Ki67+ CD8+
ns
**
ns
Percentage of GrzmB+ CD8+
***
****
ns
Percentage of CD69+ CD8+
*
ns
Percentage of PD1+ CD8+
ns
ns

Figure 19: MG1 induces early immune changes within the spleens of mice bearing 3LL syngeneic subcutaneous tumours

*(A) Schematic of in vivo experiment analysing MG1-induced immune consequences in 3LL murine model. (B) Gating strategy shown by representative two-colour fluorescence dot plots identifying initially live CD45+ cells before differentiating cells into CD3+CD4+, CD3+CD8+ and CD3-NK1.1+ cells. CD3+CD4+ T cells further differentiated into CD25+FoxP3+ T regulatory cells and FoxP3- T effector cells. (C) Graphs showing percentage of NK cells out of total live CD45+ cells within the spleen as well as percentage expression of Ki67, GrzmB, CD69 and TIGIT on splenic NK cells at 3 days timepoint. (D) Graphs showing percentage of CD8+ T cells out of total live CD45+ cells within the spleen as well as percentage expression of Ki67, GrzmB, CD69 and PD1 on splenic CD8+ T cells at 3 days timepoint. Mean +SD of three mice within each group. (*p<0.0332, **p<0.0021, ***p<0.0002 and ****p<0.0001; One-way ANOVA statistical analysis with Holm-Sidak multiple comparison test.*

5.4.2 MG1 infection induces early immune changes within tumour

Figure 20A shows there were small increases in the NK cell population within the 3LL tumours after IT and IV delivery of MG1 at the 3 days timepoint (0.8%; p=0.02 for IT delivery and 0.3%; p=0.35 for IV delivery). Although the change in proportion of NK cells were small, the activation markers were again enhanced compared to PBS controls; Ki67 significantly increased by 36.1% (p<0.0001) and 31.8% (p=0.0001); while GrzmB increased by 39.9% (p=0.0352) and 34.0% (p=0.0582) with IV MG1 vs. IT MG1 respectively.

MG1 treatment via both routes of administration failed to initiate any significant CD8 T cell infiltration into the 3LL tumours; (mean percentage of CD8+ T cells of total CD45+ population was 8% vs. 6.1% with IV MG1 vs. IV PBS and was 5.1% vs. 3.7% with IT MG1 vs. IT PBS), as shown in Figure 20B. There were also no significant changes in the activation status of these CD8+ T cells, although there seemed to be an increasing trend with MG1 treatment, whether IV or IT; mean increase in Ki67 on CD8+ T cells was 24.0% with IV and 12% with IT MG1, compared to PBS controls; GrzmB was increased by 4.5% with IV and 16.7% with IT MG1 again compared to PBS controls.

(A)

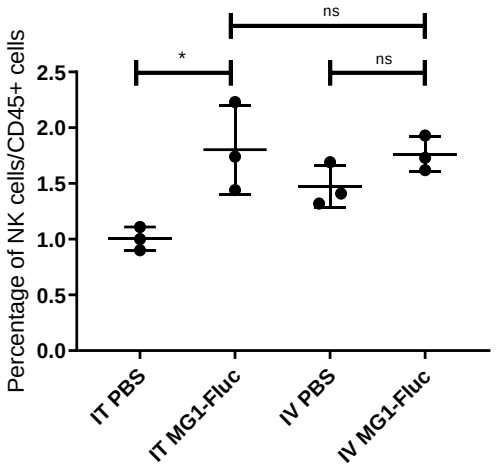
Percentage of NK cells/CD45+ cells
2.5
2.0
1.5
1.0
0.5
0.0
*
ns
ns
IT PBS
IT MG1-Fluc
IV PBS
IV MG1-Fluc

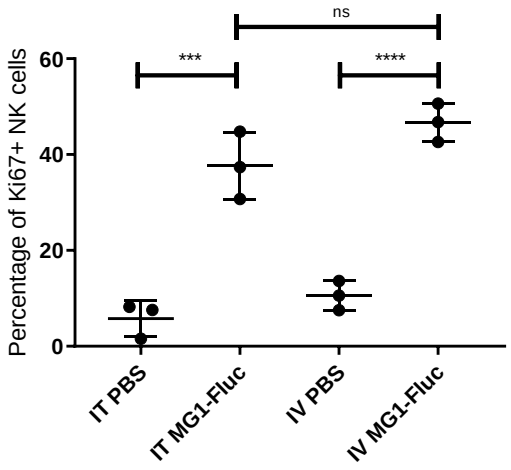
Percentage of Ki67+ NK cells
60
40
20
0
***
****
ns
IT PBS
IT MG1-Fluc
IV PBS
IV MG1-Fluc

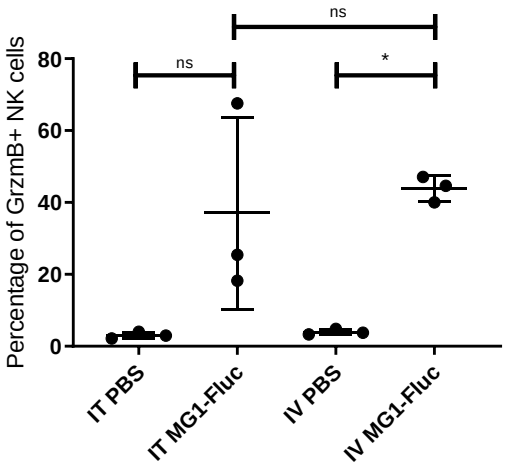
Percentage of GrzmB+ NK cells
80
60
40
20
0
ns
*
ns
IT PBS
IT MG1-Fluc
IV PBS
IV MG1-Fluc

(B)

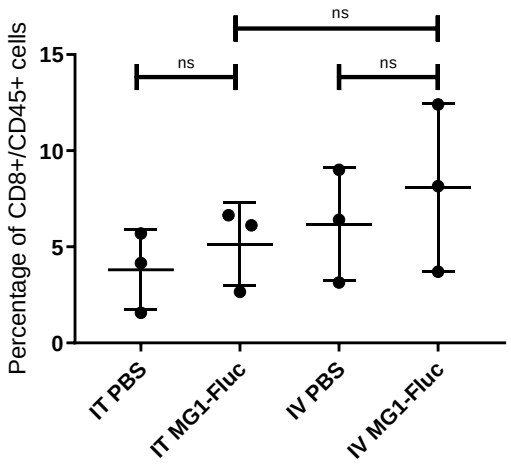
Percentage of CD8+/CD45+ cells
15
10
5
0
ns
ns
ns
IT PBS
IT MG1-Fluc
IV PBS
IV MG1-Fluc

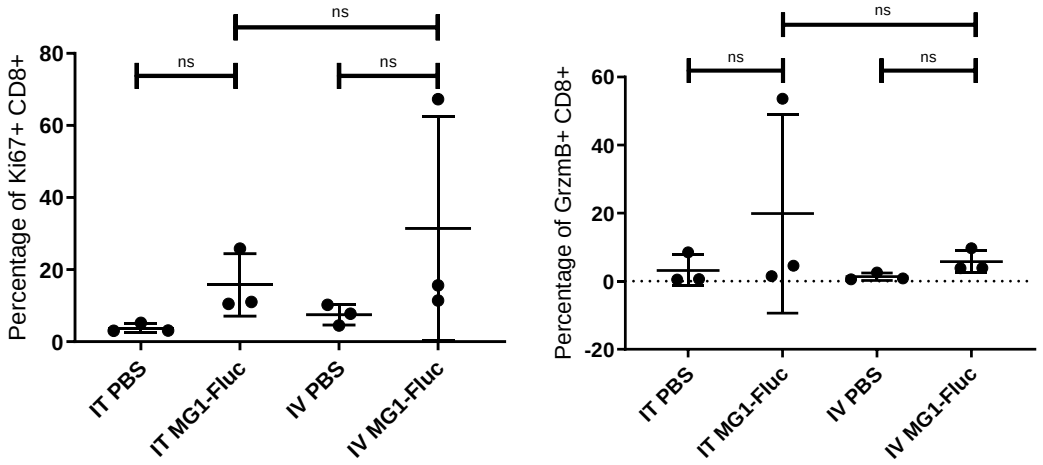

Figure 20: MG1 induces early NK cells infiltration and activation within the 3LL tumours, there were no effect on tumoural CD8+ T cells

*(A) Graphs showing percentage of NK cells out of total live CD45+ cells within the tumours as well as percentage expression of Ki67 and GrzmB on tumoural NK cells at 3 days timepoint. (D) Graphs showing percentage of CD8+ T cells out of total live CD45+ cells within the tumours as well as percentage expression of Ki67 and GrzmB on tumoural CD8+ T cells at 3 days timepoint. Mean +SD of three mice within each group. (*p<0.0332, **p<0.0021, ***p<0.0002 and ****p<0.0001; One-way ANOVA statistical analysis with Holm-Sidak multiple comparison test.*

5.4.3 MG1 does not engage an adaptive response in 3LL murine model

The initial immune changes seen after 3 days from MG1 administration, whether IV or IT, with NK cell infiltration and activation within the spleen and tumours in 3LL murine model (as described in the previous sections) seems to disappear by day 10 as shown in Figure 21. Graphs showing the percentage splenic NK cells and CD8+ T cells (out of total CD45+ population) and their activation markers shows no significant changes after exposure to MG1 (whether via IV or IT route) compared to their counterpart PBS controls (Figure 21A); percentage of splenic NK cells was 5.4% after IT or IV MG1 and 5.9% with IT or IV PBS; GrzmB expression was also not significantly changed on these NKs with 0.2% and 0.5% decreases after IT and IV MG1 respectively compared to their counterpart PBS controls; similarly with percentage of CD8+ T cells the difference was not significant with 5% and 0.5% increases after IT and IV MG1 respectively compared to their PBS controls; as for GrzmB marker on CD8+ T cells, the increase was by 0.01% after IT and IV MG1 compared to IV and IV PBS.

Figure 21B shows graphs of percentage NK cells and CD8+ T cells out of total CD45+ cells and their GrzmB activation markers within 3LL tumours at the 10 days timepoint after IV and IT MG1, and again there were no significant differences compared to their PBS controls; the difference in percentage of NK cell after IT MG1 was +1.4% and after IV MG1 was -1.2% compared to IT and IV PBS; GrzmB activation marker had a difference of -0.7% after IV or IT MG1 compared to PBS controls; difference in percentage of CD8+ T cells within tumours were -4.0% and +6.5% after IT and IV MG1 respectively; finally GrzmB on CD8 T cells altered by +17.4% and -3.7% after IT and IV viral administration respectively compared to IT and IV PBS.

In summary, MG1 infection initiates an early innate immune response within the spleen and tumours at the early timepoint of 3 days (as evidenced by the increase in NK cell infiltration and activation). These changes seem to be greater with systemic compared to intratumoural delivery of the virus. There is also a suggestion that an adaptive immune response is forming with CD8+ T

cells being more activated within the splenic environment but not in the tumours at this early timepoint after MG1 infection. However, these immune changes do not last and there is no significant change in the immune landscape within the spleen and tumours by day 10 after viral exposure when compared to PBS controls.

(A)

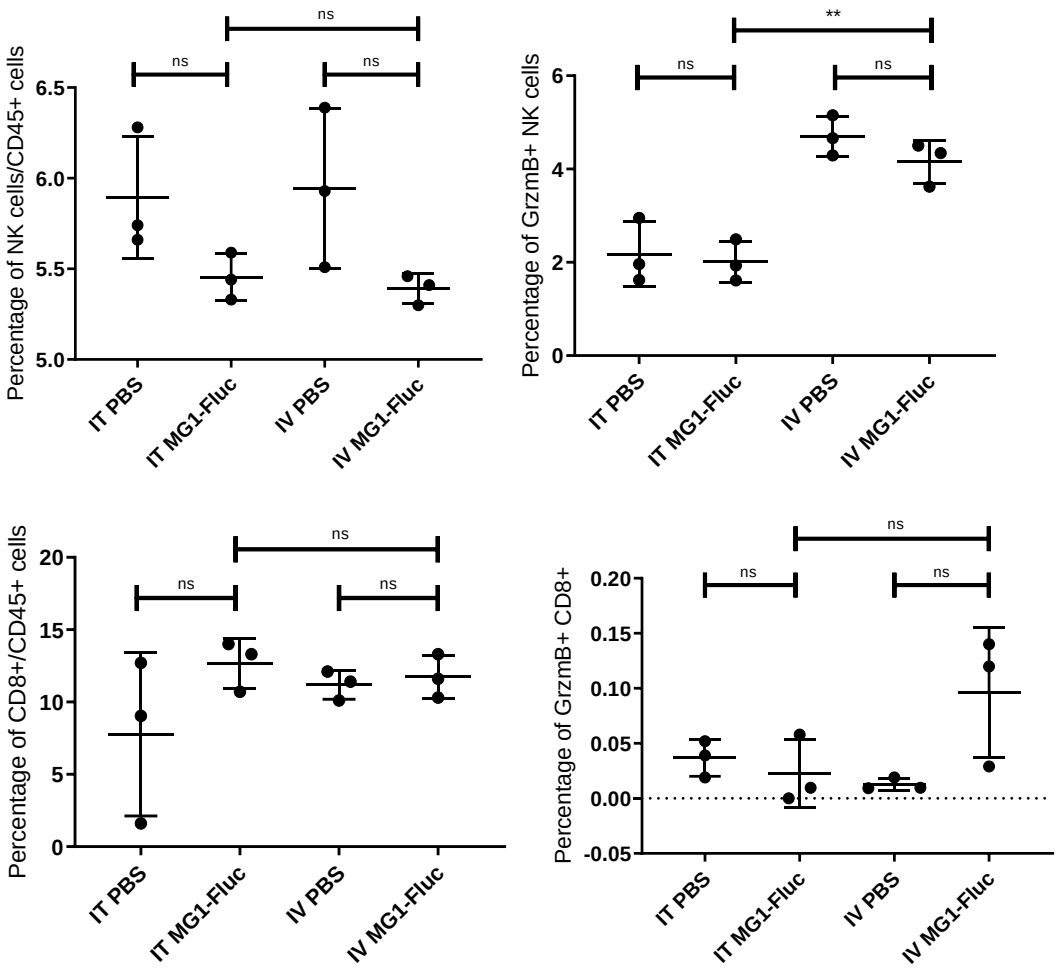
Percentage of NK cells/CD45+ cells
6.5
6.0
5.5
5.0
ns
ns
ns
IT PBS
IT MG1-Fluc
IV PBS
IV MG1-Fluc
Percentage of GrzmB+ NK cells
6
4
2
0
**
ns
ns
Percentage of CD8+/CD45+ cells
20
15
10
5
0
Percentage of GrzmB+ CD8+
0.20
0.15
0.10
0.05
0.00
-0.05

(B)

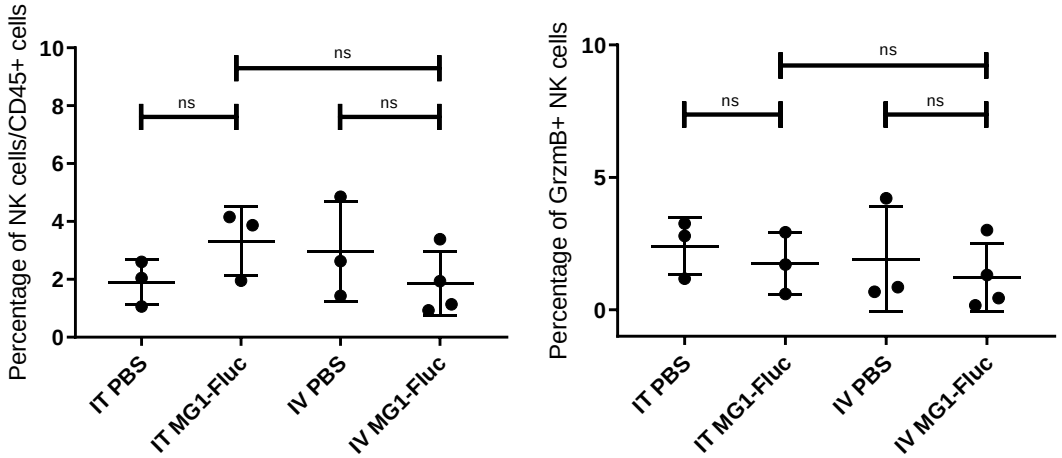
Percentage of NK cells/CD45+ cells
10
8
6
4
2
0
ns
ns
ns
IT PBS
IT MG1-Fluc
IV PBS
IV MG1-Fluc
Percentage of GrzmB+ NK cells
10
5
0

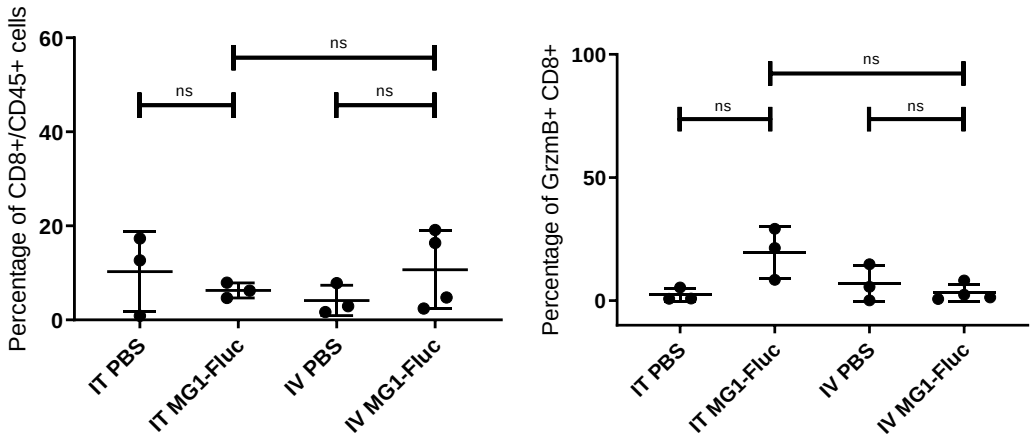

Figure 21: MG1 does not induce adaptive immune response within the 3LL murine model

(A) Graphs showing percentage of NK- and CD8+ T- cells out of total live CD45+ cells within the spleen as well as percentage expression of GrzmB on these cells. (D) Graphs showing percentage of NK- and CD8+ T- cells out of total live CD45+ cells within the tumours as well as percentage expression of GrzmB on these cells. Mean +SD of three mice within each group. (ns, p=0.1234; One-way ANOVA statistical analysis with Holm-Sidak multiple comparison test.

5.5 Human NK cell degranulation against NSCLC cells after MG1 infection

Having observed that MG1 infection led to an innate immune response (with NK cell infiltration and activation) within the spleen and tumours of 3LL bearing mice, we set out to determine whether MG1 would lead to a similar response in a human model. Studies have shown that preoperative oncolytic reovirus and vaccinia virus led to markedly increased NK cell activity in patients with metastatic colorectal cancer undergoing liver metastases resection (199, 200). However, clinical trials of MG1 are still ongoing so there has been no data to date exploring the human immune response to MG1 virus. Jennings *et al*. used a novel *in vitro* pre-clinical assay to show that $HSV^{GM\text{-}CSF}$ induced NK cell degranulation in blood samples, donated by both healthy donors and from patients with melanoma, upon co-culturing with melanoma cell targets (201). Therefore, this technique was adopted to investigate the activation of human innate anti-tumour immunity after MG1 infection against NSCLC.

PBMCs taken from healthy donors were either pulsed with 0.1 MOI MG1-FLUC or PBS overnight and examined for NK cell activation via flow cytometry after co-culturing with H1299, H1792 and H1975 NSCLC cells. Figure 22 shows the pooled fold changes in %CD107 degranulation on NK cells compared to MG1-pulsed PBMCs alone with no NSCLC target from 4 donors. NK cells degranulate against all 3 co-cultured NSCLC cell lines; for H1299, H1792 and H1975 there is a 3.5-, 3.2- and 1.4-fold increase, respectively, in %CD107 degranulation compared to PBMCs with no target. However, after pulsing the PBMCs with 0.1 MOI of MG1-FLUC, NK cell degranulation is enhanced against all 3 lung cancer targets; 8.5-, 5.3- and 3.8- fold increase in %CD107 degranulation compared to PBMCs with no target, when co-cultured with H1299, H1792 and H1975 cells respectively.

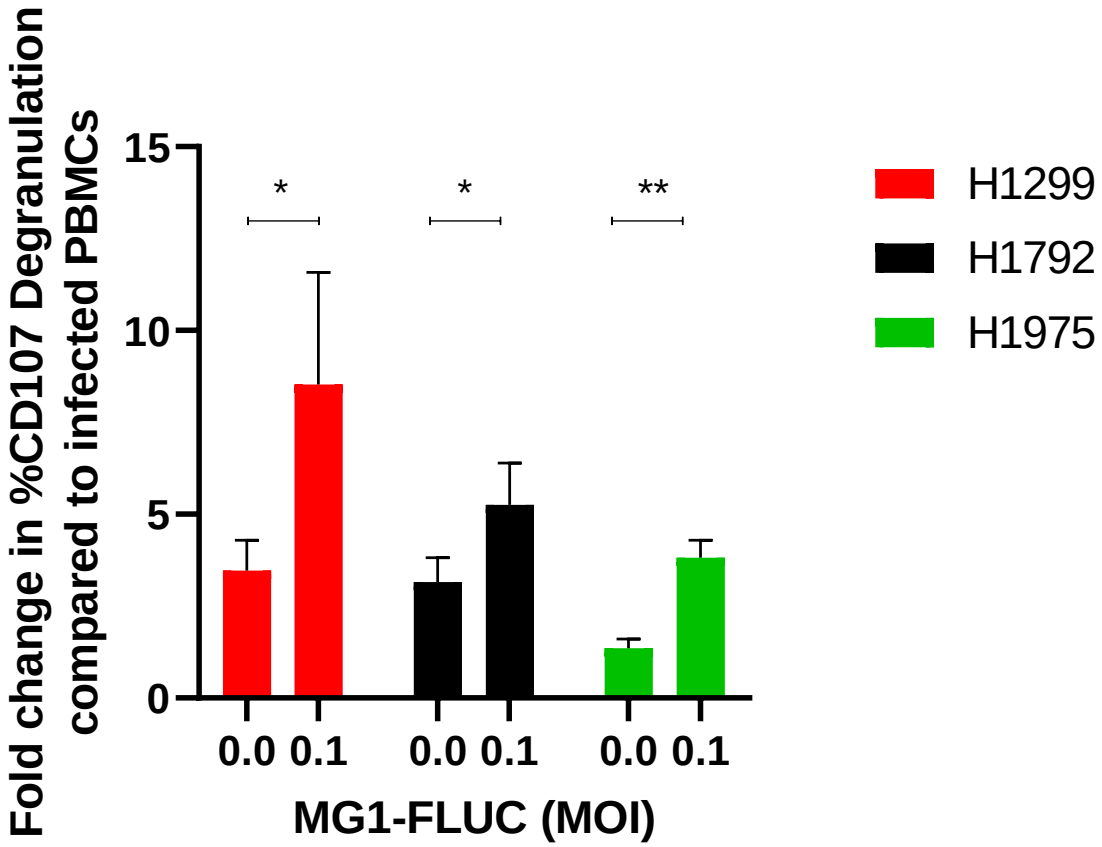

Figure 22: MG1 induces greater NK cell degranulation against NSCLC targets

*Healthy donor PBMC (pulsed with PBS or MG1-FLUC) were cultured with H1299, H1792 and H1975 NSCLC targets, and CD107 degranulation was determined by flow cytometry. Mean fold change in %CD107 degranulation compared to infected PBMCs without NSCLC targets +SD were plotted (n=4 donors) (*p<0.0332, **p<0.0021; Paired Student T-test statistical analysis.*

5.6 Discussion

OVs represent a promising class of novel cytotoxic and immunogenic cancer therapy. Oncolytic MG1 virus has proven efficacy in numerous preclinical cancer models including NSCLC as shown in this thesis thus far. In addition to its potent oncolytic activity, MG1 therapeutic efficacy also relies on its intrinsic ability to induce anti-tumour immunity as evidenced by replication-incompetent minimally UV-inactivated MG1's ability to clear lung metastases in a murine B16 melanoma model (116). In this chapter, the virus's ability to infect NSCLC cells and induce immunostimulatory consequences was explored.

ICD plays a major role in inciting anti-tumour immunity by releasing DAMP signals such as increased surface expression of calreticulin, release of ATP and HMGB1, which can all promote DC maturation and IL-1β production. The ability to induce ICD has been shown in OVs such as adenovirus, semliki forest virus, coxsackie virus, measles virus and vaccinia virus (202-204); however ICD markers ascribed to treatment with oncolytic rhabdoviruses like MG1 have not been reported (184). In this chapter, we were able to show that MG1-infected human NSCLC and 3LL cell lines were able to induce hallmarks of ICD (section 5.2). Furthermore, the more sensitive cell lines to MG1 infection and cytotoxicity (such as H1299 and 3LL), had greater releases of ATP and HMGB1.

Type I IFN is another key player in promoting anti-tumour immunity as it can stimulate DC maturation, enrich granzyme and perforin expression in cytotoxic T-lymphocytes and enhance memory T-cell survival, all of which are essential in cancer immunosurveillance (205). OV therapy has an interesting dilemma with type I IFN, because on the one hand the success of this treatment strongly depends on the presence of a dysfunctional IFN signalling, often present in cancer cells, for susceptibility to viral infection and replication. However, on the other hand, the OV-induced type I IFN response can stimulate beneficial anti-tumour immunity. NDV has been shown to infect IFN-α deficient tumour cells, but still have the ability to promote IFN-β secretion (197). Furthermore,

even in tumour cells capable of responding with IFN-α expression after NDV infection, the virus still maintained permissiveness for replication as there were defects in downstream signalling of antiviral effectors. In this chapter, we showed that MG1 was also able to infect NSCLC cell lines and stimulate the type I IFN signalling pathway, via western blotting; pIRF3 and pTBK1, the upstream proteins to type I IFN, were increased in expression after virus infection. In addition, IFN-β was detected in significant concentrations in MG1-infected 3LL cells, but none in uninfected controls. Future experiments would also include examining the IFN-β production from human NSCLC cell lines to ascertain if MG1 infection induces the production of type I IFN and establishing if IFN-β plays a role in MG1 sensitivity in cell lines. One limitation of the western blotting experiments was the inability to detect any upregulation of RIG-I, a box helicase that detects viral RNA to signal IFN-α/β production in infected cells, although RIG-I could still be activated without upregulation of the protein. The sister rhabdovirus VSV has been demonstrated to trigger RIG-I specific innate immune signalling during infection (206, 207), therefore it was postulated MG1 would also follow a similar detection mechanism. One explanation for this could be that MG1 is recognised by other RNA sensing proteins such as melanoma differentiation-associated gene 5 (MDA5), toll-like receptor 7 or 8, which can also stimulate the type I IFN pathway. Further experiments will be required to characterise the mechanism of MG1 detection definitively.

MG1's ability to induce ICD and IFN-β production in infected NSCLC cells seems to be consistent with the changes in the spleen and tumours of mice bearing 3LL subcutaneous malignancies after infection with MG1 either systemically or intratumourally (section 5.4). Viral infection resulted in an increase in percentage of NK cell population in the spleens and tumours after 72 hrs of administration. Furthermore, these NKs were proliferating and more activated, as indicated by increases in the Ki67 and GrzmB markers. These findings were consistent with a publication by Zhang et al. exploring MG1's activity in murine B16 model (116); the authors observed that within 24 hrs following systemic delivery of MG1, mice showed splenomegaly which resulted from a local increase in dendritic cells and NK cells, although in our

experiment we did not observe splenomegaly despite the increase in NK cell population, albeit examined at a later timepoint of 72hrs compared to Zhang el al's experiments. The level of splenic NK cell activation seems similar between the two systems, as Zhang et al. observed around a 20-fold increase in percentage of CD69+ expression, compared to PBS treatment, after 3 days post MG1 systemic administration, as opposed to 32-fold increase in our experiment. We also noted a much higher level of GrzmB expression in these splenic NK cells, 3 days after intravenous MG1 treatment, of 17-fold increase compared to PBS therapy, as opposed to the 3-fold increase in Zhang et als' publication at the same time point. These innate changes in our experiment were obtained with one lower dose of MG1 IV injection ($1x10^7$ pfu) compared to 3 doses of $1x10^8$ pfu used in the murine B16 model, which suggests that multi-dosing is not necessarily required to achieve similar immunological consequences with oncolytic viruses, which has been a hotly contested subject. Zhang et al. also observed that the NK cell activation lasted up to 5 days post-MG1 administration and, to add to this finding, in our experiment we noted that the MG1-induced NK cell infiltration and activation was lost by day 10 post viral administration, and these effects were completely lost in the *ex vivo* spleen and tumour samples by this time point. The NKs were critical for reducing the number of lung metastases in the B16 murine model, although the authors did not show survival benefit, as selective depletion of this immune subset abolished any beneficial tumour growth control. Further experiments with NK cell ablation would be required to determine whether NKs are similarly critical in the anti-tumour effects in our 3LL murine model.

MG1 infection in 3LL murine model had less impact on the adaptive immune system with only splenic CD8+ T cells showing increase in activity on day 3 post viral administration which was not present in tumoural CD8+ T cells, or at either site in day 10 specimens. The initial MG1-induced innate immune response might explain the findings observed in section 4.3.4, whereby systemic MG1 therapy led to significant tumour growth retardation but no cures in mice bearing 3LL syngeneic tumours, as there was a failure to stimulate an adaptive immune effect. To validate this theory, a further experiment, as mentioned above, with NK cell depletion would be needed to assess whether

the therapeutic tumour control is lost after intravenous MG1 delivery. Also, future work would be required to analysis the dendritic cell population and its phenotype within the 3LL murine model to determine whether MG1 has failed to stimulate maturation of DCs which may account for the lack of engagement of the adaptive immune system. Unsurprisingly, the level of splenic NK cell activation at the 72 hr timepoint is greater with systemic rather than intratumoural MG1 delivery, which is in keeping with the observation that tumour growth retardation was seen with systemic virus therapy but not IT (section 4.3.4).

Finally, this chapter also showed that MG1 infected PBMCs from healthy donors stimulated NK cell activation to NSCLC targets, suggesting that the viral effect on initiating an innate anti-tumour immune effect was also present in a human *in vitro* system. To further investigate this finding, isolation of NK cells from PBMCs could be performed, in order to determine if Type I IFN from APCs play a role in NK cell activation as seen with reovirus (208). Furthermore, NSCLC cell lysis could be measured to determine whether NSCLC are susceptible to NK killing following degranulation.

Despite the oncolytic and immune stimulatory effects of MG1 described in this thesis so far, the therapeutic effect in 3LL murine lung cancer model is still limited to tumour growth control without long term cure. Hence in the next chapter, the possibility of improved outcomes with rationale combination strategies involving MG1 will be explored.

Chapter 6:
MG1 combination strategies

6. Chapter 6: MG1 combination strategies

6.1 Introduction

OVs, in theory, are the ultimate cancer-targeted agent because they can selectively infect and amplify themselves within the tumour milieu increasing therapeutic dose over time. In addition, aside from direct tumour lysis, they can be used to modulate the TME with TIL recruitment, priming of immune responses mediated by CD8+ T cells and innate immune cells, as well as promoting immunogenic cell death which releases PAMPs/DAMPs that attract immune cells to the tumour. Most of these attributes have also been observed with MG1 virus as shown in this thesis so far. Moreover, OVs can also be genetically manipulated to express transgene payloads to expand the immune-inflammatory and priming capabilities of virus infection. However, despite these tumour-selective mechanisms of action, their efficacy has been limited when administered as monotherapies (209) and, like with many other oncology treatments, the greatest therapeutic gains are likely to be harboured through combination strategies (112). Oncolytic MG1 virus is no exception and is being tested in clinical trials as part of a combinatory prime-boost vaccination with adenovirus incorporating specific tumour associated antigens (184).

Having established that MG1 has some tumour growth control in the 3LL murine lung cancer model, this chapter will focus on novel approaches to attempt to enhance the therapeutic capabilities of MG1 virus.

6.2 MG1 virus and anti-PD1 immunotherapy

ICIs have revolutionised cancer treatment in the last decade and have now been incorporated into standard of care in the first and second line setting for patients with metastatic NSCLC. ICIs block the negative regulators of T-cell function leading to T-cell activation and currently the US FDA has approved 6

ICIs for clinical use: ipilimumab, nivolumab, pembrolizumab, atezolizumab, avelumab and durvalumab. However, despite their inarguable success, the percentage of patients with cancer estimated to respond to ICIs is still relatively low (~12.5%) (210). The ability of OVs to convert immune “cold” tumours, which lack lymphocyte infiltration and are less responsive to ICIs, into a more immune cell-rich environment, has resulted in promoting active research into combining OVs and ICIs treatments in cancer therapy. We have recently published a review article on this topic (172).

As previously discussed, Bourgeois-Daigneault *et al*. demonstrated, in a triple negative breast cancer murine model, that neo-adjuvant treatment with MG1 led to reduction in size and number of subsequent lung metastases and improved survival. In addition, MG1 infection led to tumour cell PD-L1 levels increasing. Furthermore, subsequent postoperative combination anti-CTLA-4 and anti-PD1 immune checkpoint blockade (after neoadjuvant MG1) resulted in significantly improved survival compared to both untreated mice and those undergoing either immune checkpoint or MG1 single arm therapy (135). This led to the rational exploration to determine whether a similar synergistic combination effect would be seen in therapy of the 3LL murine lung cancer model.

Figure 23A shows that, in contrast to the previously described triple negative breast cancer model, there was in fact an overall decrease in PD-L1 expression on live 3LL cells observed after 24 hrs of 0.01 MOI MG1-FLUC exposure *in vitro*, detected using flow cytometry (mean PD-L1 expression was 7.29% with PBS and 2.23% with MG1-FLUC, p=0.0009). Consistent with this *in vitro* finding, there was no overall survival advantage seen with combination intratumoural MG1-FLUC and intraperitoneal anti-PD1 therapy compared to either single treatments alone or IT PBS as shown in Figure 23C and 23D; mean OS was 28 days for IT PBS and IT MG1-FLUC, 26.5 days for IP anti-PD1 and 25 days for combination therapy. This lack of therapy seen with IT MG1-FLUC is again consistent with previous experiment shown in Figure 15.

(A)

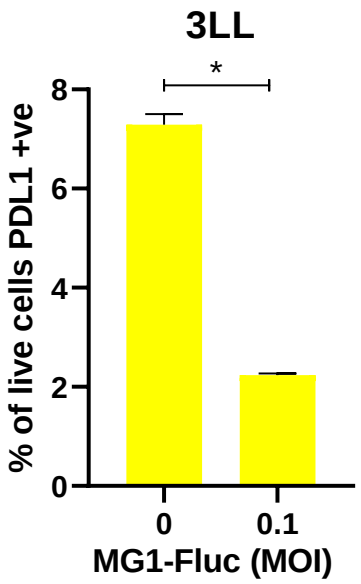
3LL
*
% of live cells PDL1 +ve
8
6
4
2
0
0
0.1
MG1-Fluc (MOI)

(B)

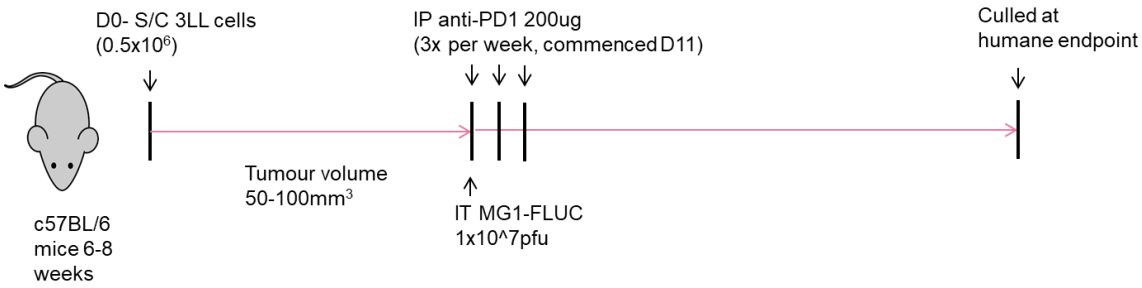
D0- S/C 3LL cells
(0.5x10^6)
IP anti-PD1 200ug
(3x per week, commenced D11)
Culled at
humane endpoint
Tumour volume
50-100mm^3
IT MG1-FLUC
1x10^7pfu
c57BL/6
mice 6-8
weeks

(C)

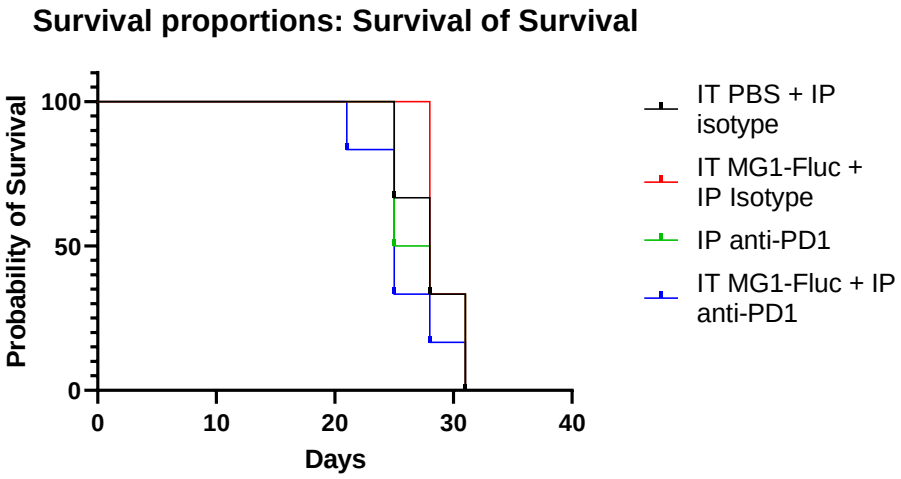
Survival proportions: Survival of Survival
Probability of Survival
100
50
0
0
10
20
30
40
Days
IT PBS + IP isotype
IT MG1-Fluc + IP Isotype
IP anti-PD1
IT MG1-Fluc + IP anti-PD1

(D)

	IT PBS+IP Isotype	IT MG1-Fluc+IP Isotype	IP anti-PD1	IT MG1-Fluc+IP anti-PD1
Median OS (days)	28	28	26.5	25
P-value: Log-rank	-	0.5663 (NS)	0.8501 (NS)	0.2986 (NS)

Figure 23: MG1 infection does not sensitize 3LL tumours to immune checkpoint blockade

*(A) Cell surface programmed death ligand 1 (PD-L1) expression on 3LL cells after 24 hrs of incubation with 0.1 MOI MG1-FLUC. Mean PD-L1 expression + SD (n=3) (*p<0.0332; Paired Student T-test statistical analysis). (B) Schematic of in vivo experiment exploring combination MG1-FLUC and anti-PD1 therapy. (C) Kaplan-Meier survival analysis of 3LL tumour bearing mice after IT PBS, IT MG1-FLUC, IP anti-PD1 or combination therapy (D) Graph to show median OS (days) from each treatment group.*

6.3 MG1 and external beam radiotherapy

Having established that MG1 infection stimulates type I IFN signalling in NSCLC cells (section 5.3) which may be contributing to the anti-tumour immune response observed in 3LL murine lung model (as described in section 5.4), it seemed reasonable to investigate a combination strategy that attempts to boost this immunogenic effect. RT has and remains an important component of cancer treatment with approximately 50% of all cancer patients receiving radiation therapy during their course of illness (211). The efficacy of ionizing radiation is not only based on direct cytotoxicity to cancer cells through the induction of lethal DNA damage, but there is now increasing recognition that RT can also enhance T cell priming and T cell dependent tumour regression through the stimulation of type I IFN production (212, 213). Therefore, the potential synergistic effect of MG1 and RT to boost type I IFN signalling and thereby enhancing anti-tumour immune response was investigated.

6.3.1 Viability of MG1 with RT combination

Successful combination therapies often incorporate treatments with non-overlapping toxicities and where each component does not compromise the efficacy of the other. Therefore first, the direct effect of RT on the viability and replication competency of MG1-GFP virus was assessed *in vitro*. MG1-GFP was treated with increasing doses of RT (0-32 Gy in single fractions) prior to assessing the viral titre with plaque assays.

Figure 24B shows that the mean virus concentration for the unirradiated MG1-GFP was $3.1x10^7$ pfu/ml (95% CI 2.1-4.1 $x10^7$pfu/ml) compared to $3x10^7$pfu/ml (95% CI 2.1-3.9 $x10^7$pfu/ml) after 32 Gy of radiation (the highest dose tested). Furthermore, there was no significant difference in the macroscopic appearance of the plaques between the non-irradiated virus and any of the escalating radiation doses (Figure 24A). Therefore, the results suggest that RT does not negatively impact MG1's replicative ability if used in combination.

(A)

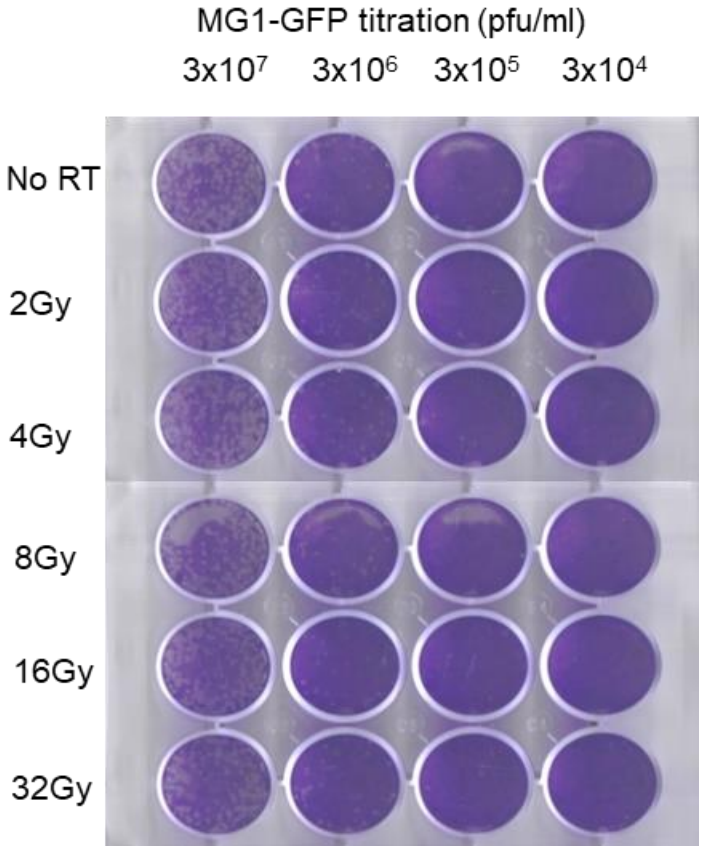

(B)

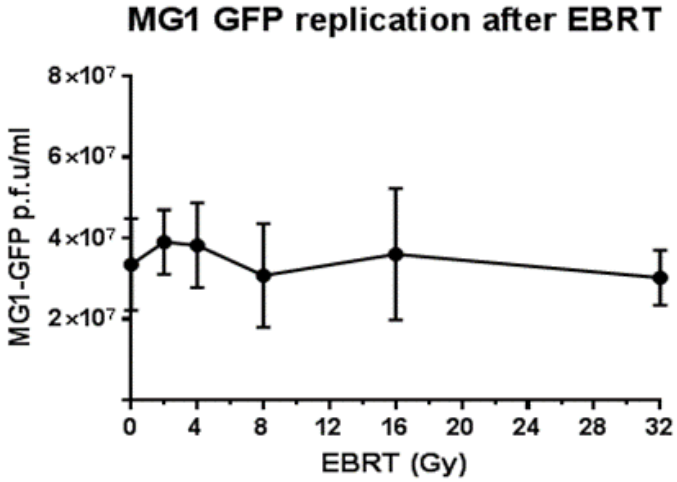

Figure 24: MG1-GFP is not affected by clinically relevant doses of EBRT.

(A) Photographs of viral plaque assays showing MG1-GFP titration post-treatment with increasing doses of irradiation; (B) Line graph showing quantification of viral titres (n=3; mean viral concentration + 95% CI plotted.

6.3.2 MG1 and RT combination cytotoxic effects

Having confirmed that RT does not negatively impact the replication competency of MG1, the cell viability of human and murine NSCLC cells was assessed using MTT assays, after either single treatments alone or in combination. Figure 25 demonstrates that NSCLC cells treated with either (A) 4 Gy or (B) 8 Gy RT followed by 0.1 MOI MG1-GFP 24 hrs later, did not result in any additional cytotoxic effect compared with either of the monotherapies alone at the 72 hr timepoint; for H1299 the mean cell viability after combination treatment with 0.1 MOI MG1-GFP and 4 Gy or 8 Gy RT was 28% and 29% respectively, and 30% with virus alone; for H1573 it was 49% for combination virus and both 4 Gy or 8 Gy RT treatment and 40% with virus alone; for H1473 it was 53% and 47% for combination virus and 4 Gy or 8 Gy RT respectively and 45% for virus alone; for H1975 it was 63% and 56% with combination virus and 4 Gy or 8 Gy RT respectively and 65% with virus alone; for H1792 it was 24% for combination virus and both 4 Gy or 8 Gy RT and 26% with virus alone; and finally for 3LL it was 14% and 15% with combination virus and 4 Gy and 8 Gy RT respectively and 14% with virus alone.

In all these NSCLC cell lines therefore, the combination of 0.1 MOI MG1-GFP with 4 Gy or 8 Gy RT was not significantly different (p value >0.1234) compared to the cytotoxic effect of virus alone.

(A)

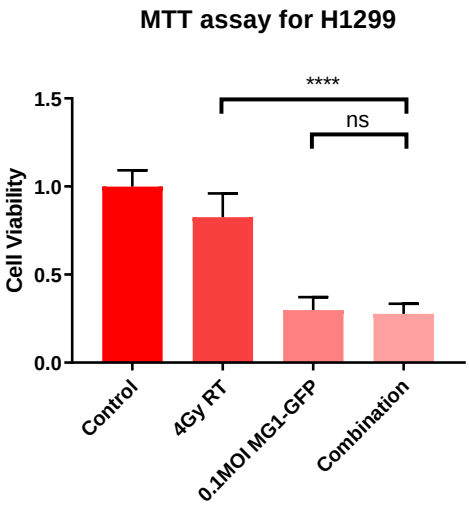
MTT assay for H1299
Cell Viability
1.5
1.0
0.5
0.0
****
ns
Control
4Gy RT
0.1MOI MG1-GFP
Combination

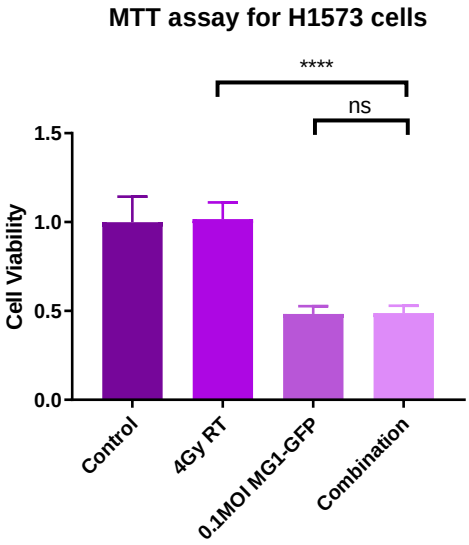
MTT assay for H1573 cells
Cell Viability
1.5
1.0
0.5
0.0
****
ns
Control
4Gy RT
0.1MOI MG1-GFP
Combination

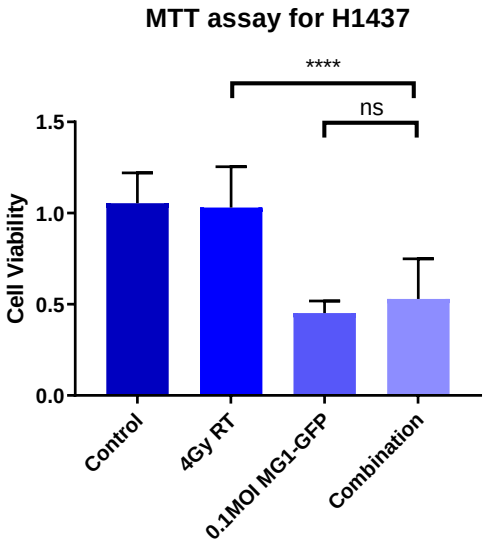
MTT assay for H1437
Cell Viability
1.5
1.0
0.5
0.0
****
ns
Control
4Gy RT
0.1MOI MG1-GFP
Combination

(B)

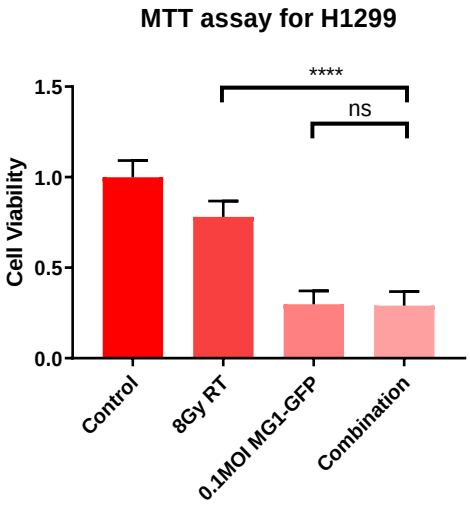
MTT assay for H1299
Cell Viability
1.5
1.0
0.5
0.0
****
ns
Control
8Gy RT
0.1MOI MG1-GFP
Combination

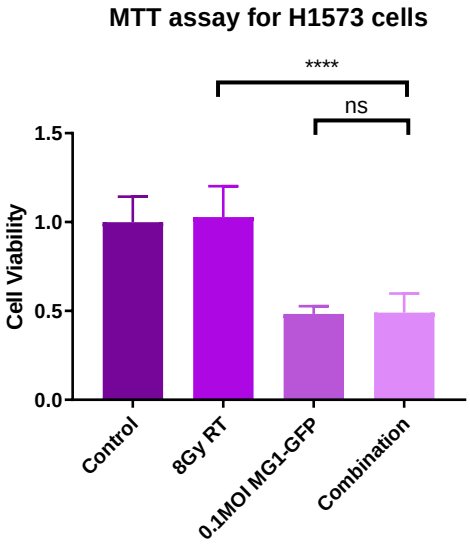
MTT assay for H1573 cells
Cell Viability
1.5
1.0
0.5
0.0
****
ns
Control
8Gy RT
0.1MOI MG1-GFP
Combination

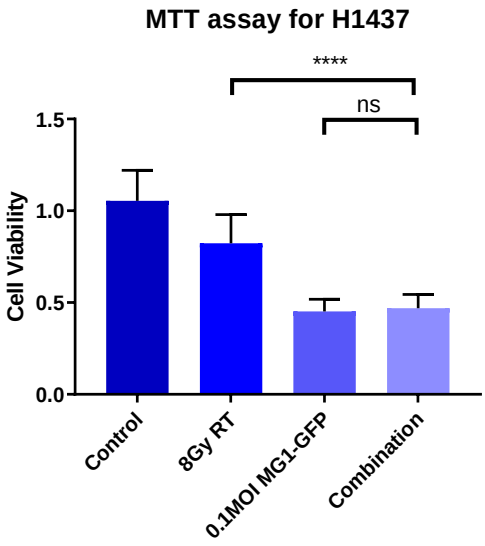
MTT assay for H1437
Cell Viability
1.5
1.0
0.5
0.0
****
ns
Control
8Gy RT
0.1MOI MG1-GFP
Combination

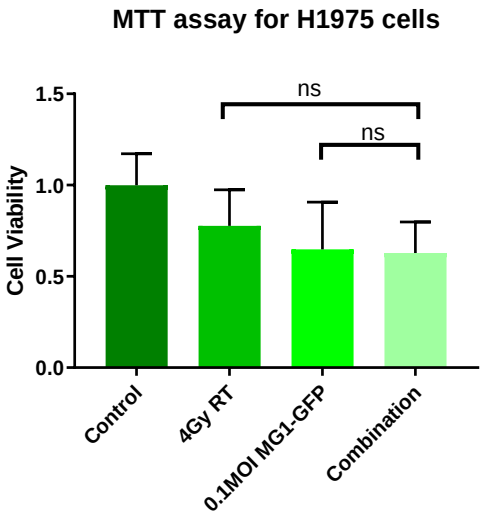
MTT assay for H1975 cells
Cell Viability
1.5
1.0
0.5
0.0
ns
ns
Control
4Gy RT
0.1MOI MG1-GFP
Combination

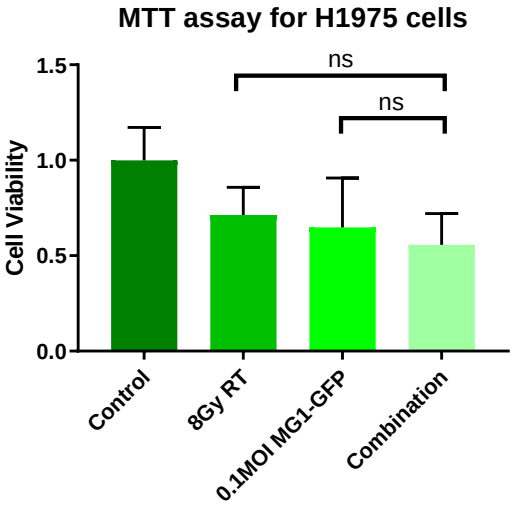
MTT assay for H1975 cells
Cell Viability
1.5
1.0
0.5
0.0
ns
ns
Control
8Gy RT
0.1MOI MG1-GFP
Combination

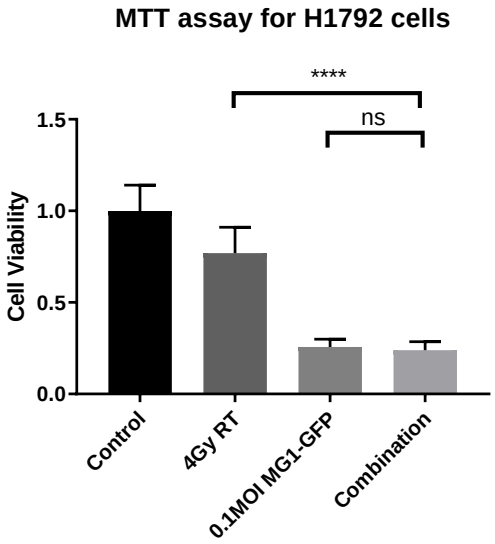
MTT assay for H1792 cells
Cell Viability
1.5
1.0
0.5
0.0
****
ns
Control
4Gy RT
0.1MOI MG1-GFP
Combination

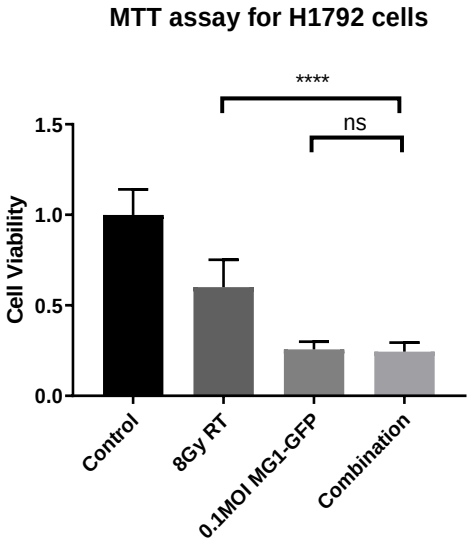
MTT assay for H1792 cells
Cell Viability
1.5
1.0
0.5
0.0
****
ns
Control
8Gy RT
0.1MOI MG1-GFP
Combination

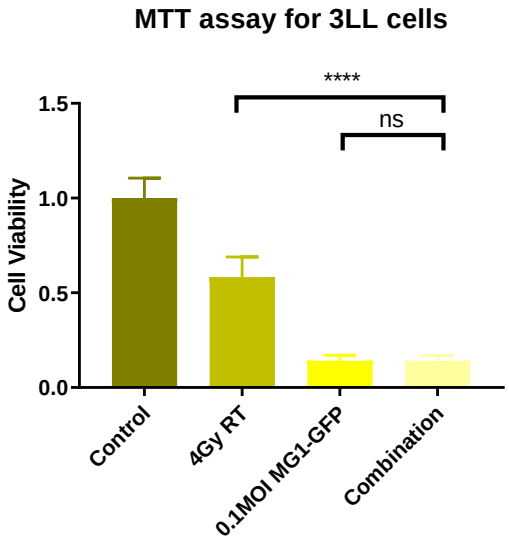
MTT assay for 3LL cells
Cell Viability
1.5
1.0
0.5
0.0
****
ns
Control
4Gy RT
0.1MOI MG1-GFP
Combination

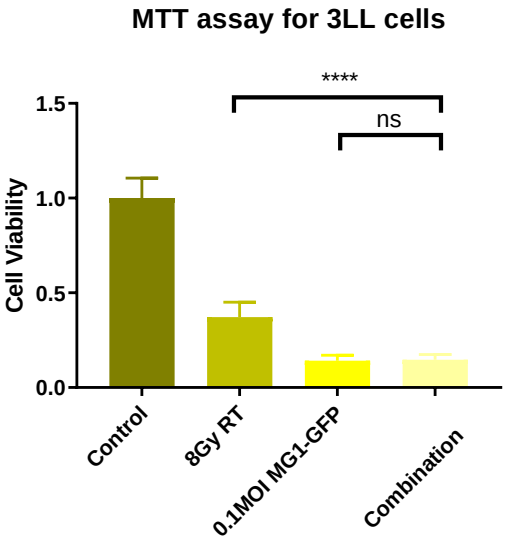
MTT assay for 3LL cells
Cell Viability
1.5
1.0
0.5
0.0
****
ns
Control
8Gy RT
0.1MOI MG1-GFP
Combination

Figure 25: Combination MG1-GFP at concentration of 0.1 MOI with 4 or 8 Gy RT does not result in increased cytotoxicity in NSCLC cell lines compared to virus alone.

*Graphs showing cell viability after combination of 0.1 MOI MG1-GFP infection given 24 hrs after either (A) 4 Gy or (B) 8 Gy RT or after each monotherapy alone. Mean cell viability across three independent experiments (n=4 in each experiment) + SD plotted (ns p>0.1234, *p<0.0332, **p<0.0021, ***p<0.0002 and ****p<0.0001; One-way ANOVA statistical analysis with Tukey multiple comparison test.*

6.3.3 IFN-β production after MG1 and RT combination in 3LL

Although MG1 and RT combination, at the doses tested, failed to enhance cytotoxic effect in NSCLC cells *in vitro* compared to single treatments alone (section 6.3.2), the result may not be translated when tested *in vivo;* the hypothesis for synergism of these two agents relies on boosting of type I IFN signalling in the TME leading to stimulation of anti-tumour immune responses, and hence a combination benefit may only be revealed in immune-competent models tested *in vivo*. The success of this concept has been shown with other OVs that have been engineered to express IFNs; for example, Li *et al*. showed that an oncolytic measles virus encoding IFN-β was more efficient at controlling tumour growth compared to the parental virus in mesothelioma tumour models (214). Willmon *et al*. also tested an IFN-β-engineered VSV variant in mesothelioma and found the virus controlled tumour growth and better induced anti-tumour immunity compared to wild-type VSV (215). A later study by Patel *et al*. demonstrated that the virus improved anti-tumour immunity by decreasing tumour-infiltrating Tregs while increasing CTLs (216). Notably, VSV-IFNβ is currently undergoing clinical testing for solid tumours (ClinicalTrials.gov ID: NCT02923466). As stated previously, RT also enhances anti-tumour immunity by augmenting the innate immune sensing of tumours in a type I IFN-dependent manner, hence providing a rationale for combination with MG1 therapy.

To explore this hypothesis, IFN-β production by 3LL murine cells *in vitro* was determined via ELISA after exposure to MG1-GFP infection, RT or both treatments. Figure 26A shows that combination therapy of 0.1 MOI MG1-GFP and 8 Gy RT resulted in significantly greater release of IFN-β, detected 24 hrs after treatments, compared to either exposure to PBS or monotherapies alone in 3LL cells; mean concentration of IFN-β after combination treatment was 90.2pg/ml vs. 0pg/ml ($p<0.0001$), 80.0pg/ml ($p=0.033$) and 0pg/ml ($p<0.0001$), for PBS, 0.1 MOI MG1-GFP and 8Gy RT treated respectively.

To address this increase in IFN-β production with RT-MG1 combination *in vivo*, 3LL tumours were treated with either IV PBS, IV MG1-GFP (dose of $1x10^7$pfu),

8 Gy RT or combination MG1-GFP and RT (3 mice per group). Tumours were harvested, homogenised and IFN- β production was determined by ELISA. Figure 26B shows the mean concentration of IFN-β per gram of tumour detected 72 hrs. Although combination virus and RT released greater amounts of IFN-β (2890.2pg/ml/g) compared to either MG1-GFP (759.2pg/ml/g) or 8Gy RT (1932.7pg/ml/g) or PBS (914.5pg/ml/g), this was not statistically significant (p value=0.316, 0.840 and 0.374 respectively), potentially due to the high variability within the treatment groups resulting from the small sample size (n=3). A further experiment with greater number of tumours would be required to elucidate a more robust conclusion.

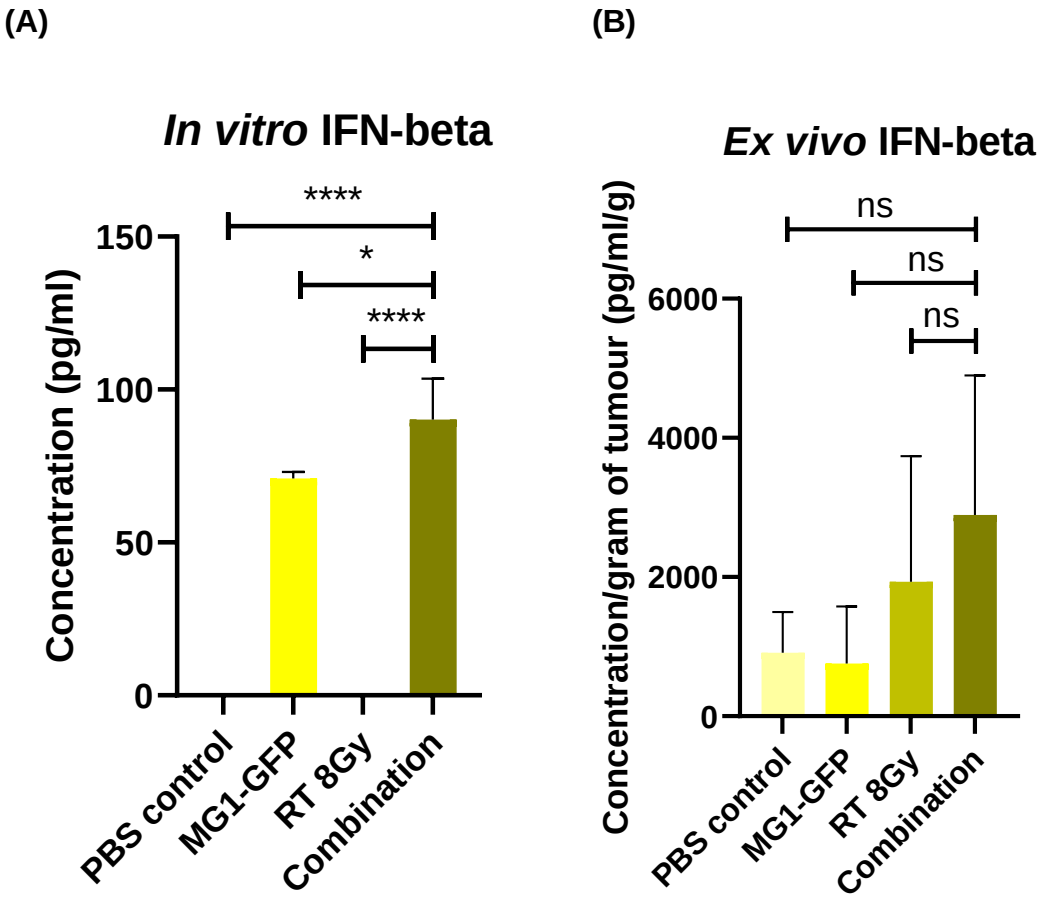

Figure 26: Combination of MG1 and RT resulted in increased IFN-β production in 3LL cells *in vitro* but not *ex vivo* compared to PBS treated or either monotherapies alone.

*(A) Graph showing mean concentration of IFN-β release in 3LL cells in vitro after treatment with PBS (control), 0.1MOI MG1-GFP, 8Gy RT or combination of virus and RT, as detected by ELISA after 24 hrs. Mean + SD across three independent experiments plotted; *p=0.033 and ****p<0.0001; One-way ANOVA statistical analysis with Tukey multiple comparison test. (B) Graph showing mean concentration of IFN-β release from process 3LL tumours ex vivo after treatment with IV PBS (control), 1x10^{7}pfu MG1-GFP, 8 Gy RT or combination of virus and RT, as detected by ELISA after 72 hrs. Mean + SD (n=3); ns p>0.1234; One-way ANOVA statistical analysis with Tukey multiple comparison test.*

6.3.4 Immune response after MG1 and RT

Having previously observed that MG1 can stimulate NK cell degranulation against human NSCLC targets *in vitro* (section 5.5) and furthermore shown that systemically delivered MG1 initiated an innate, but not an adaptive immune response in the spleens and tumours of mice bearing 3LL subcutaneous malignancies (section 5.4), we set out to determine whether the addition of RT to virus could enhance anti-tumour immune reaction.

The appeal of combining OVs with RT continues to grow as the relationship between these two therapies is better understood. Others have shown successful synergistic anti-tumour effects in numerous preclinical models with combination of these two therapies, through either radiation-mediated enhancement of viral oncolysis or virus-mediated sensitisation of cells to radiation therapy. For example, oHSV (NV1066) combined with irradiation significantly reduced tumour volume compared to either treatment alone for non-small cell lung cancer (158) and malignant mesothelioma (159); radiation exposure was found to increase cellular expression of GADD34 (a DNA-damage- and growth arrest- inducible gene that helps protect cells against radiation insults), which is structurally homologous to the HSV-1 γ34.5 protein. This radiation-induced enhancement of GADD34 aided HSV replication and oncolysis. Another example is oncolytic vaccinia virus (GLV-1h68) which again showed synergistic cytotoxic effects in sarcoma cells when combined with RT, this time mediated through induction of intrinsic apoptosis (161). However, the potential benefit of enhancing anti-tumour immune response with RT and OV combination via stimulation of type I IFN signalling has not been explored.

The effect on human NK cell degranulation after irradiated NSCLC targets in addition to pulsing PBMCs with MG1 virus were explored *in vitro.* Isolated PBMCs from 4 healthy donors were treated with 0.1 MOI MG1-FLUC for 24hrs, prior to co-culturing with H1299, H1792 and H1975 cells that had either been untreated or treated with 8 Gy RT. Figure 27A shows that the addition of RT did not result in any significant increase in NK cell degranulation across the 3 human lung cancer targets; for H1299, H1792 and H1975 the mean fold increase in CD107 degranulation compared to PBMCs with no NSCLC target

was 8.5, 5.3 and 3.8 for unirradiated cells and 7.6, 4.7 and 4.0 for irradiated cells, respectively. Therefore, the addition of RT to MG1 infection did not seem to enhance NK cell degranulation to human NSCLC targets.

The effect on the TME with combination virus and radiation therapy was also investigated in mice bearing 3LL subcutaneous tumours. These malignant lesions were harvested 10 days after either systemic MG1-FLUC ($1x10^7$pfu), 8 Gy RT or both treatments were given and processed for flow cytometry analysis. Consistent with the finding that *ex vivo* IFN-β from 3LL tumours was not significantly increased after combination therapy (section 6.3.3) compared to either monotherapies alone, Figure 27 shows that there was also no significant differences in (B) tumoural NK- and (C) CD8+ T- cell numbers or activation status between any of the treatment arms; the percentage of tumoural NK cells within the total live CD45+ population was 2.8%, 1.9%, 2.1% and 2.3% for IV PBS, IV MG1-FLUC, RT and combination therapy respectively. Unsurprisingly, at the day 10 time point, the activation status of these NK cells, as represented by percentage GrzmB expression, also revealed no difference between the different arms: 1.7%, 1.2%, 1.8% and 1.7% for IV PBS, IV MG1-FLUC, RT and combination therapy respectively. These findings are consistent with the results shown in section 5.4, where MG1-induced NK cell infiltration and activation within the spleens and tumours were observed at the early time point of day 3 and these changes were essentially absent by day 10. Therefore, ideally in future work to assess the dynamics of NK cells after combination RT and MG1, tumours would be analysed between day 1-3 after treatments. Similar findings were seen with tumoral CD8+ T cells; percentage of CD8+/live CD45+ cells were 4.5%, 10.7%, 4.3% and 9.3% and GrzmB expression were 6.2%, 3.1%, 16.2% and 11.3% for IV PBS, IV MG1-FLUC, RT and combination therapy respectively. All differences were not statistically significant ($p>0.1234$).

(A)

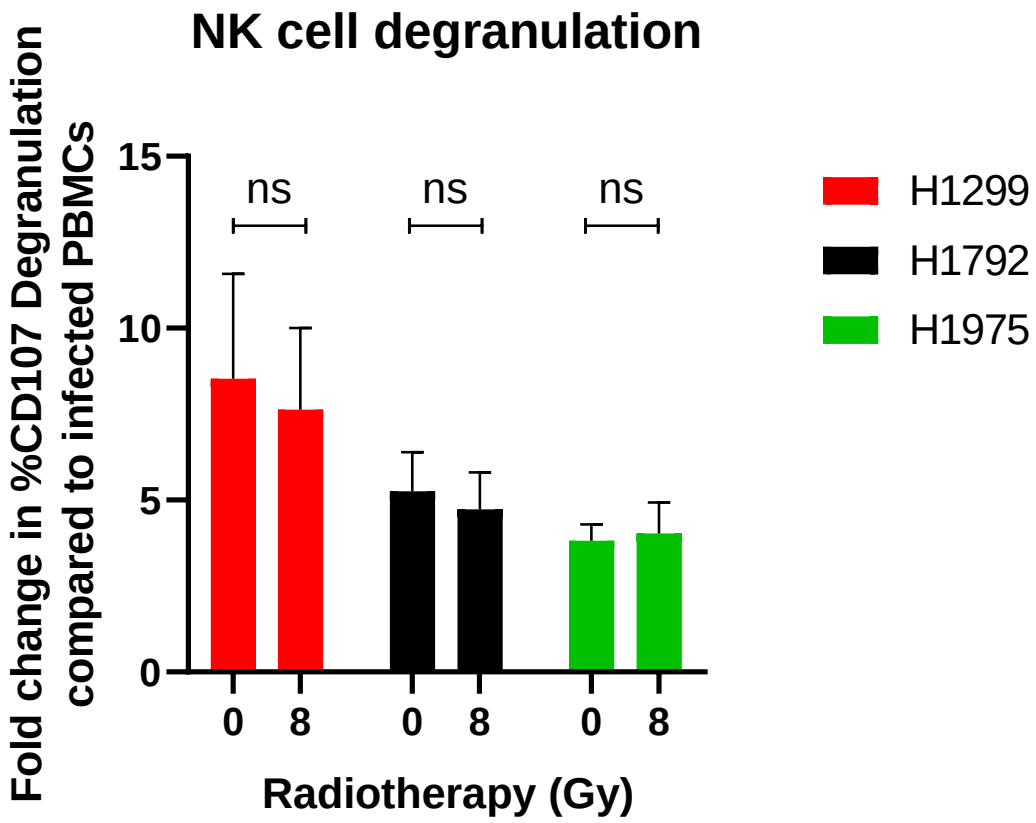
NK cell degranulation
Fold change in %CD107 Degranulation compared to infected PBMCs
15
10
5
0
ns
ns
ns
H1299
H1792
H1975
0
8
0
8
0
8
Radiotherapy (Gy)

(B)

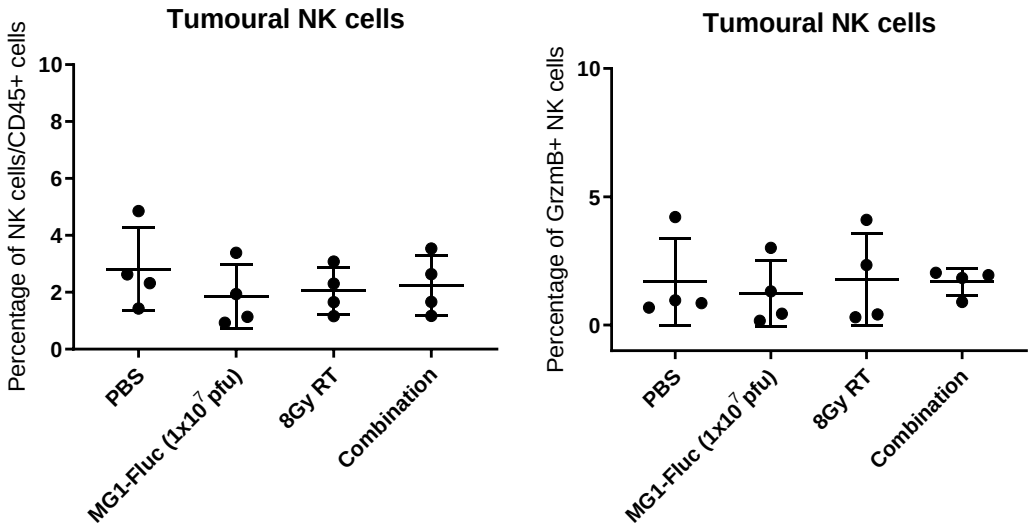
Tumoural NK cells
Percentage of NK cells/CD45+ cells
10
8
6
4
2
0
PBS
MG1-Fluc (1x10^7 pfu)
8Gy RT
Combination
Tumoural NK cells
Percentage of GrzmB+ NK cells
10
5
0
PBS
MG1-Fluc (1x10^7 pfu)
8Gy RT
Combination

(C)

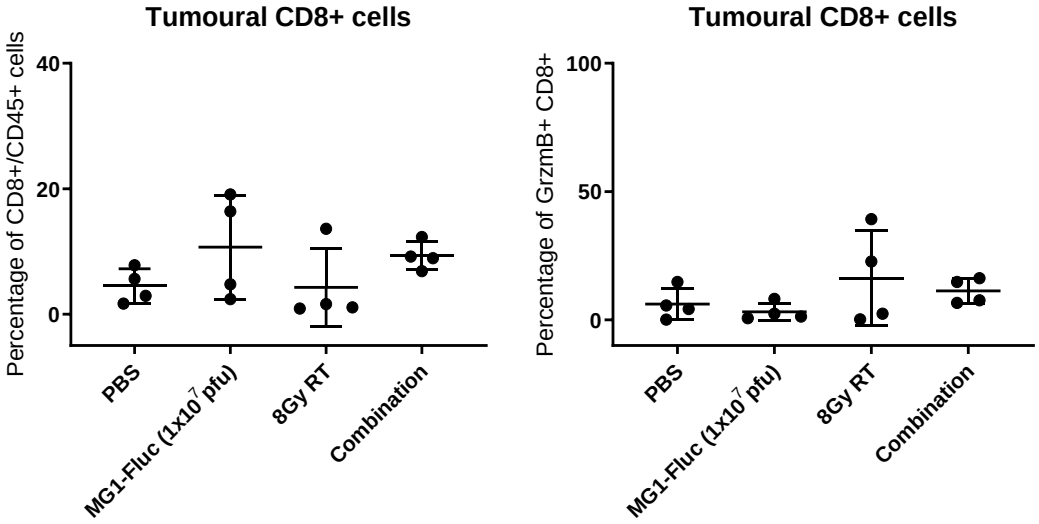

Figure 27: Combination RT and MG1 does not enhance NK cell degranulation against human NSCLC targets *in vitro* or stimulate an adaptive immune response against 3LL tumours *ex vivo*

(A) Healthy donor PBMC (pulsed with 0.1 MOI MG1-FLUC) were cultured with unirradiated or 8 Gy irradiated H1299, H1792 and H1975 NSCLC targets, and CD107 degranulation was determined by flow cytometry. Mean fold change in %CD107 degranulation compared to infected PBMCs without NSCLC targets +SD were plotted (n=4 donors) (ns p>0.1234); Paired student T-test statistical analysis. (B)Tumoural NK- (C) CD8+T-cell percentage within CD45+ population and GrzmB expression in ex vivo 3LL tumours which were treated 10 days prior with either IV PBS, IV MG1-FLUC (1x10^{7}pfu), 8 Gy RT or combination therapy. Mean + SD plotted (n=4 mice) (ns p>0.1234); Two-way ANOVA statistical analysis with Tukey multiple comparison test.

6.3.5 MG1 and RT combination therapy in 3LL tumours *in vivo*

In this chapter so far, we have shown that the addition of RT to MG1 virus led to an enhancement of IFN-β production by 3LL cells *in vitro*, which did not translate in harvested tumours *ex vivo* and there was no significant combination benefit in the stimulation of anti-tumour innate (shown with human NK cell degranulation assay) or adaptive (as shown from *ex vivo* harvested 3LL tumours) immune responses compared with single agents alone. However, especially with *in vivo* TME analysis experiments where the timepoints chosen may have been incorrect, to conclude these findings, the survival advantage of RT in combination with systemic MG1 virus was investigated in the 3LL murine syngeneic murine model. Figure 28 shows the Kaplan Meier survival curves for mice bearing 3LL tumours treated with either (A) 8 Gy in a single fraction or (B) 24 Gy in 3 fractions (given on alternate days) RT, in addition to systemic MG1-FLUC ($1x10^7$pfu) or either treatment alone or IV PBS (control group). Consistent with previous data shown in section 4.3.4, there was no significant survival advantage with systemic MG1 virus alone compared to IV PBS (mOS was 28 and 33 days for IV MG1 in experiments shown in 6.3.5 (A) and (B) respectively and mOS was 29.5 days with IV PBS in both experiments). However, it was observed that irradiation alone, whether given at 8 Gy or 24 Gy, significantly improved median OS in mice bearing 3LL tumours compared to the control arms (mOS was 42 and 48.5 days for 8 and 24 Gy RT respectively and 29.5 days for control groups in both experiments, p= 0.009 and p= 0.004 respectively). However, combination MG1 to RT did not improve survival outcome when compared to RT alone (mOS was 28 and 42 days for 8Gy and 24Gy RT-virus combination respectively, compared to mOS of 42 and 48.5 days for 8Gy and 24 Gy RT monotherapy as described previously). One explanation for not observing any advantage with combination therapy is due to toxicity, as 3 out of 12 mice in the RT-MG1 group across the 2 experiments had to be sacrificed early due to excessive weight loss hence affecting mean overall survival for that cohort.

(A)

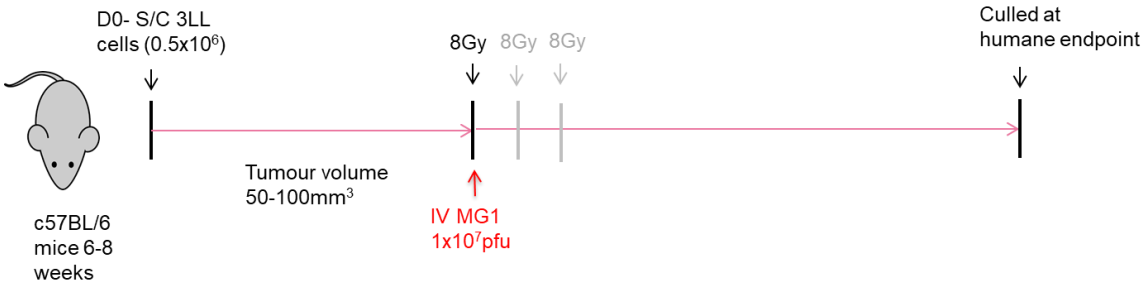

(B)

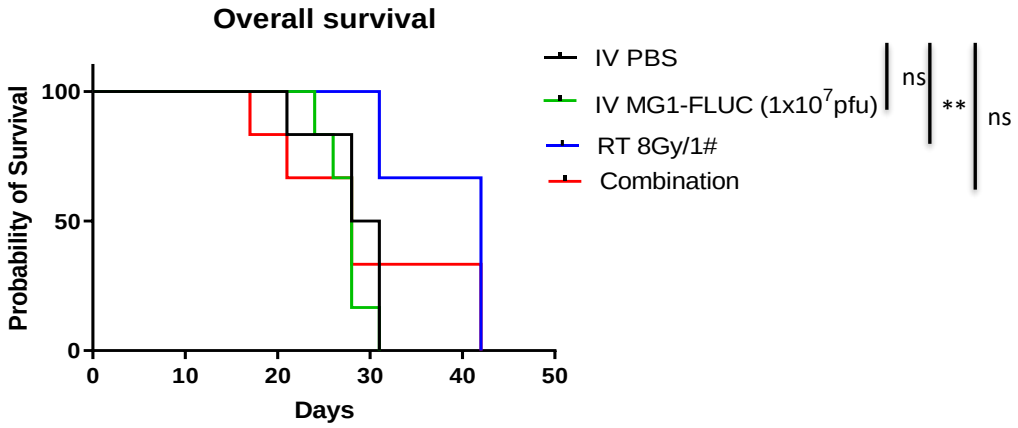

(C)

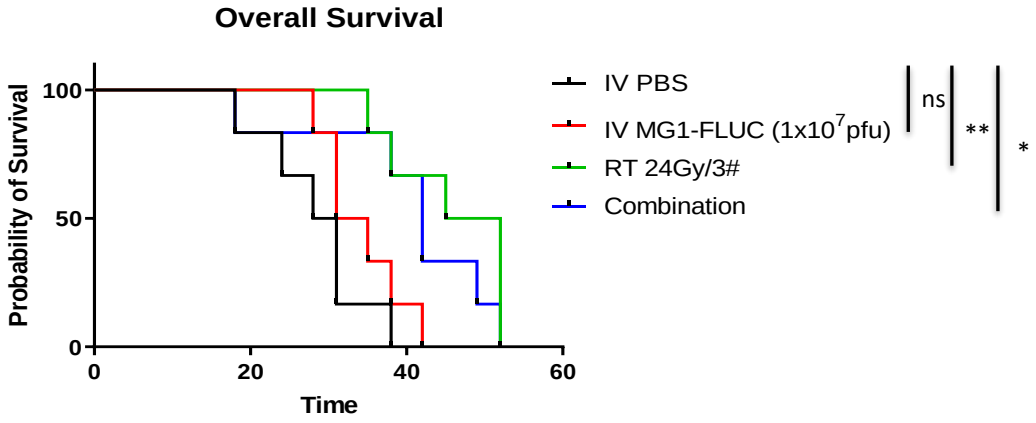

Figure 28: Combination RT and MG1 does not improve survival in mice bearing 3LL subcutaneous tumours compared to monotherapies alone

*(A) Schematic of in vivo experiments with systemically delivery MG1 in combination with either 8Gy single fraction or 24Gy over 3 fractions of RT. Kaplan Meier survival curves for exploring (B) 8 Gy in single fraction and (C) 24 Gy in three fractions of RT with or without combination systemic MG1-FLUC (1x10⁷pfu), IV MG1-FLUC alone and IV PBS in mice bearing 3LL subcutaneous tumours. (ns p>0.1234, *p<0.0332, **p<0.0021); Log-rank (Mantel-Cox) statistical analysis for significance.*

6.4 Modified MG1 virus and external beam radiotherapy

Although MG1-FLUC/GFP and RT did not prove to be a fruitful combination treatment in NSCLC thus far, an attractive feature of maraba virus is the relative ease with which it can be genetically modified to express transgenes, which can substantially increase its functionality. For example, maraba virus has been altered to encode TAA transgenes such as ovalbumin protein (OVA) (144) and the human form of the melanoma-associated antigen dopachrome tautomerase (hDCT) (145) which can successfully induce anti-tumour immunity and lead to therapeutic benefit in preclinical ovarian and melanoma murine models, respectively, as part of a heterologous prime-boost system. Furthermore, MG1-expressing tumour antigen MAGEA3 is currently being used clinically in a heterologous prime-boost regimen with a MAGEA3-expressing adenovirus vector in combination with the anti-PD1 antibodies pembrolizumab (149) and atezolizumab (NCT03618953) and without ICI (NCT02285816).

In order to increase the combinatorial effects of oncolytic virotherapy and radiotherapy, other OVs have been modified to include promoters that are activated by exposure to radiation or genes that sensitize cells to radiation-induced cell death. For example, survivin mRNA markedly increases in response to RT and when this promoter was used to drive adenovirus E1 expression, combination with RT *in vivo* significantly delayed glioma tumour growth at 6 days post-infection compared to either single treatments alone or a combination of RT and wild-type adenovirus (217). Another attempt to improve radiosensitivity of infected cells is with the tumour-specific adenovirus, AdΔ24 (E1A-deleted), expressing the p53 tumour suppressor gene. The lack of p53 expression is common in malignancies and studies have shown that by re-introducing functional p53 into p53-negative cells, it not only increases the effectiveness of adenovirus-mediated cell lysis (218), but also increases sensitivity to radiation-induced cell death (163). Therefore, AdΔ24-p53 led to synergistic cytotoxicity when combined with RT in human glioma

cell lines *in vitro* and in immunocompromised subcutaneous glioma models *in vivo* compared to either single treatments alone (164),

Another potential strategy for enhancing radiosensitivity of tumour cells is to target cellular DNA double-strand break (DSBs) repair, as DSBs represent the most biologically significant lesions induced by ionizing radiation; therefore it can be expected that impaired DSBs repair would lead to radiation sensitivity. The main pathways that are predominantly involved in DSBs repair are homologous recombination and classical nonhomologous end-joining (cNHEJ). The protein BRCA1 encoded by the tumour suppressor gene *BRCA1* regulates all DSBs repair pathways and hence would be a good target for disruption to induce radiosensitisation. And indeed, the radiation sensitivity of cells with BRCA1 mutation has been tested in a variety of experimental models; for example, *BRCA1*-/- mouse embryonic fibroblasts (MEFs) are highly sensitive to RT (219, 220) and radiation sensitivity was also observed in human breast cancer cell line, HCC1937, which has truncated BRCA1 expression. Furthermore, retrovirally expressed wild-type BRCA1 decreased the RT sensitivity and increased the efficiency of DSBs repair of the *BRCA1*-/- HCC1937 cell line and reduced its susceptibility to DSB generation (221). In another interesting study by Karanam *et al*. the authors found that tumour-treating fields (TTFields), an FDA-approved treatment for recurrent and newly diagnosed glioblastomas, which utilises low-intensity, intermediate frequency, alternating electric fields to disrupt mitosis and kill tumour cells, also downregulates many of the BRCA1 pathway genes in NSCLC cell lines. Furthermore, the authors observed that the reduction in BRCA1 expression led to a decrease in DNA DSB repair capacity and, when TTFields was administered following ionising radiation, all of the NSCLC cell lines displayed synergistic enhancement in sensitivity to RT (222). Therefore, in summary the evidence from cell and animal models provide strong evidence supporting a role of BRCA1 mutation in radiosensitivity.

Therefore, in this section the potential combination effect of modified MG1 expressing shBRCA1, to reduce DSB repair capacity, followed by RT in NSCLC cell lines will be explored.

6.4.1 BRCA1 status in NSCLC cell lines

Prior to exploring the combination effect of MG1-shBRCA1 and RT combination, the baseline BRCA1 status was determined in the panel of human NSCLC and 3LL cell lines. Figure 29 shows (A) western blot to assess presence of BRCA1 protein and (B) densitometry graphs normalising the intensity of the bands against tubulin, in these lung cancer cell lines. BRCA1 status was also assessed in SUM149 parental and SUM149 revertant cells, which are human triple negative breast cancer cells, in which the parental line possesses an exon-11 skipping hypomorphic *BRCA1* mutation, that leads to lower expression of functional BRCA1 protein compared to the revertant line, which has a secondary mutation that restores the open reading frame in the parental *BRCA1* gene (223). SUM149 revertant and parental cells were used as positive and negative controls respectively for BRCA1 protein in the western blots. It is observed in Figure 29A that SUM149 Revertant, H1792, H1299, H1975 and 3LL cell lines all express higher quantities of BRCA1 protein, which is confirmed in the densitometry graphs shown in Figure 29B, compared to SUM149 Parental, H1437 and H1573 cell lines. Figure 29C illustrates the presence of *BRCA1* DNA, detected via PCR, in SUM149 revertant, H1792, H1299 and H1975 cell lines but not in SUM149 parental cells.

(A)

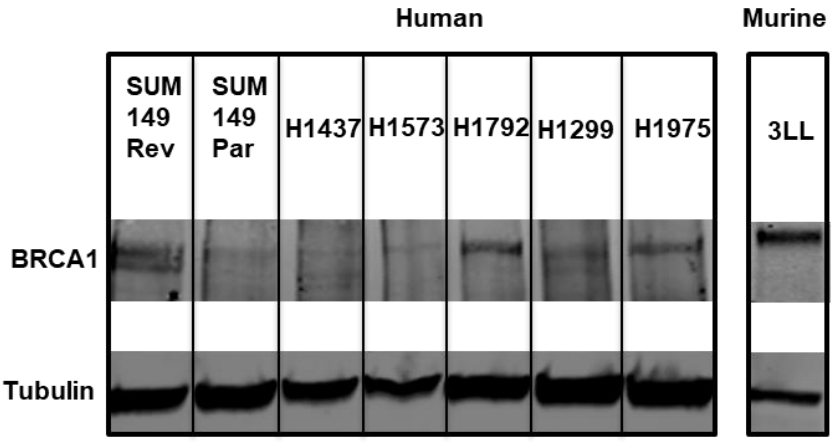
Human
Murine
SUM 149 Rev
SUM 149 Par
H1437
H1573
H1792
H1299
H1975
3LL
BRCA1
Tubulin

(B)

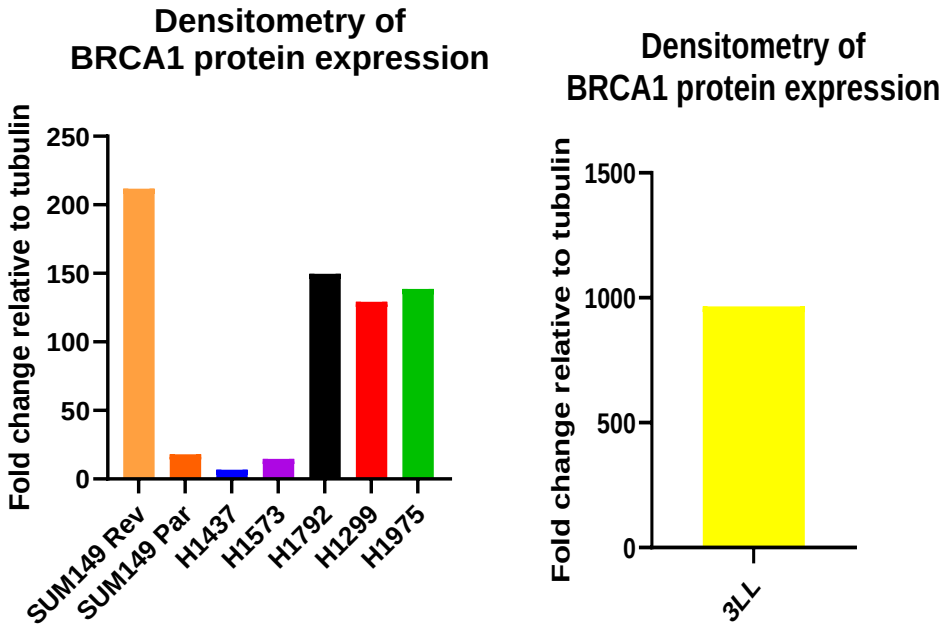
Densitometry of BRCA1 protein expression
Fold change relative to tubulin
250
200
150
100
50
0
SUM149 Rev
SUM149 Par
H1437
H1573
H1792
H1299
H1975
Densitometry of BRCA1 protein expression
Fold change relative to tubulin
1500
1000
500
0
3LL

(C)

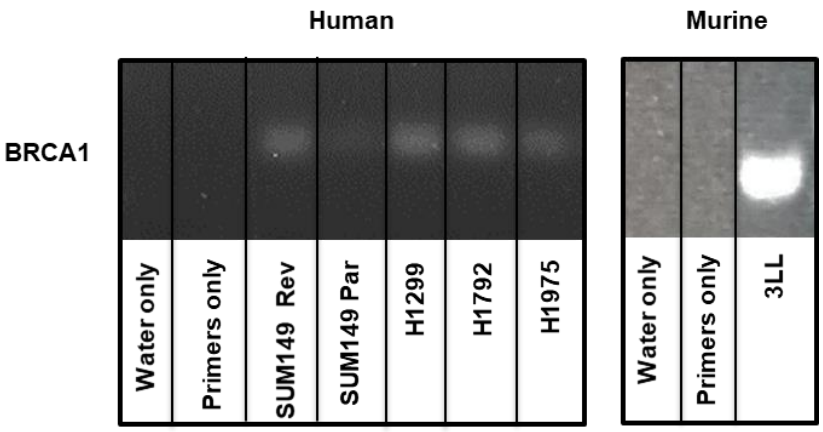
Human
Murine
BRCA1
Water only
Primers only
SUM149 Rev
SUM149 Par
H1299
H1792
H1975
Water only
Primers only
3LL

Figure 29: Functional BRCA1 protein and DNA detected in H1792, H1299, H1975 and 3LL lung cancer cell lines.

(A) Western blot analysis of BRCA1 protein in human (H1437, H1573, H1792, H1299 and H1975) and murine (3LL) NSCLC cell lines. SUM 149 Revertant and Parental cells (TNBC cell lines) were utilised as positive and negative controls respectively. (B) Densitometric presentation of western blots. (C) PCR of BRCA1 DNA in human (H1792, H1299 and H1975) and murine (3LL) NSCLC cell lines. SUM 149 Revertant and Parental cells were utilised as positive and negative controls respectively.

6.4.2 BRCA1 deficiency and radiosensitivity

Having established the BRCA1 status of the panel of human and murine NSCLC cell lines used within this thesis, we set out to demonstrate whether disrupting BRCA1 expression in BRCA1 wild-type cells would lead to radiosensitivity. As described previously, there is a wealth of data supporting this hypothesis in pre-clinical cellular and animal models (see section 6.4 introduction). Figure 30A confirms that SUM149 Revertant cells, which possess a secondary mutation that rescues functional BRCA1 expression, are more radioresistant than their Parental counterparts that are BRCA1 mutated, as shown using Cell Titre-Glo® viability assay; it can be seen that, although there were no differences in cell viability between the two cell lines in untreated and after 2Gy RT, treatment with higher doses of RT resulted in more cell death in SUM149 Parental cells compared with SUM149 Revertant cells. For SUM149 Parental cells the mean cell viability after 8 days from treatment were 100%, 111%, 96%, 85%, 58% and 46% after 0, 2, 4, 6, 8 and 10Gy RT, respectively. This was in comparison to the mean cell viability in SUM149 Revertant cells, which were 100%, 123%, 127%, 130%, 105% and 80% after 0Gy-, 2Gy-, 4Gy-, 6Gy-, 8Gy- and 10Gy RT, respectively.

A similar result was seen after BRCA1 knock down in the H1299 lung cancer cell line using siRNA; Figure 30B shows successful silencing of the *BRCA1* gene and the absence of BRCA1 protein 72 hrs after siBRCA1 transfection, compared with mock transfection, in H1299 cells. These siBRCA1 transfected H1299 cells were more radiosensitive compared to mock transfected H1299 counterparts as shown in Figure 30C; mean cell viability for mock transfected H1299 cells were 100%, 92% and 64% after 0, 4 and 8Gy RT, respectively. This is compared to mean cell viability in siBRCA1 transfected H1299 cells of 100%, 64% and 41% after 0, 4 and 8 Gy RT, respectively.

These results are consistent with previous publications that show BRCA1-deficient cells are more radiosensitive than BRCA1-profient counterparts. Furthermore, it confirms the proof of concept that by silencing BRCA1 expression in BRCA1 wild-type NSCLC cells, it would lead to increased radiation-induced cytotoxicity.

(A)

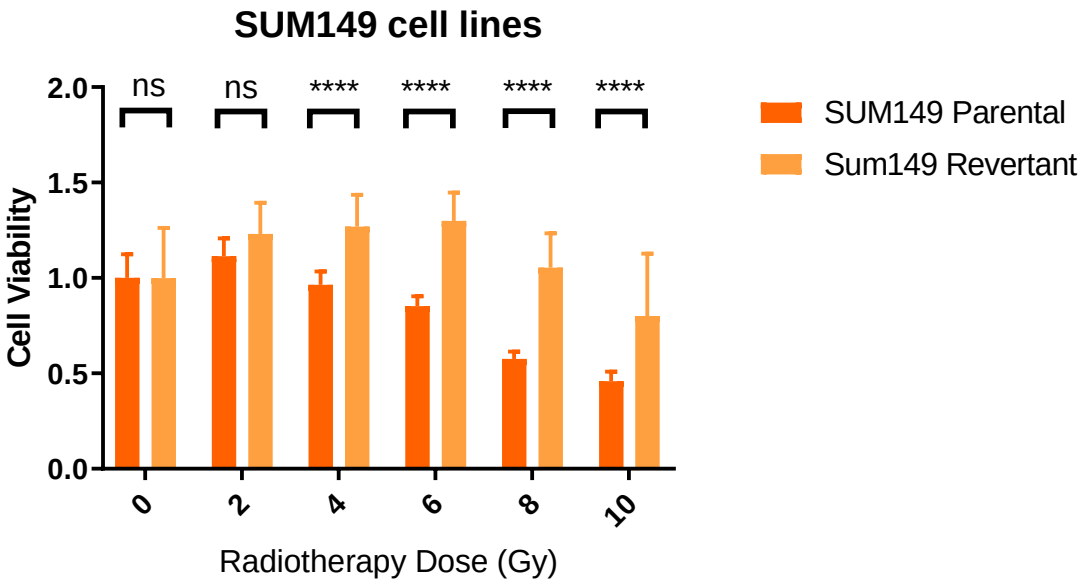
SUM149 cell lines
ns
ns
****
****
****
****
2.0
1.5
1.0
0.5
0.0
Cell Viability
0
2
4
6
8
10
Radiotherapy Dose (Gy)
SUM149 Parental
Sum149 Revertant

(B)

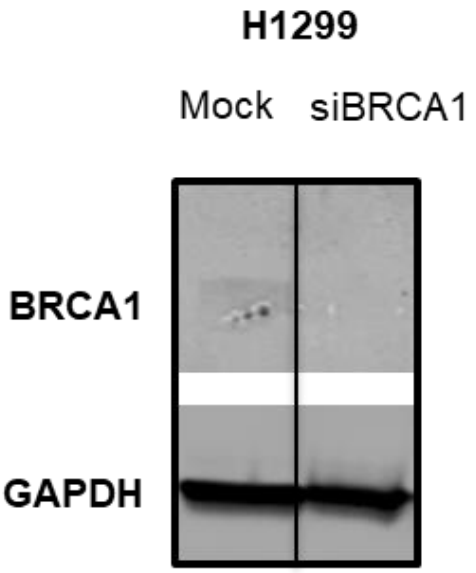
H1299
Mock
siBRCA1
BRCA1
GAPDH

(C)

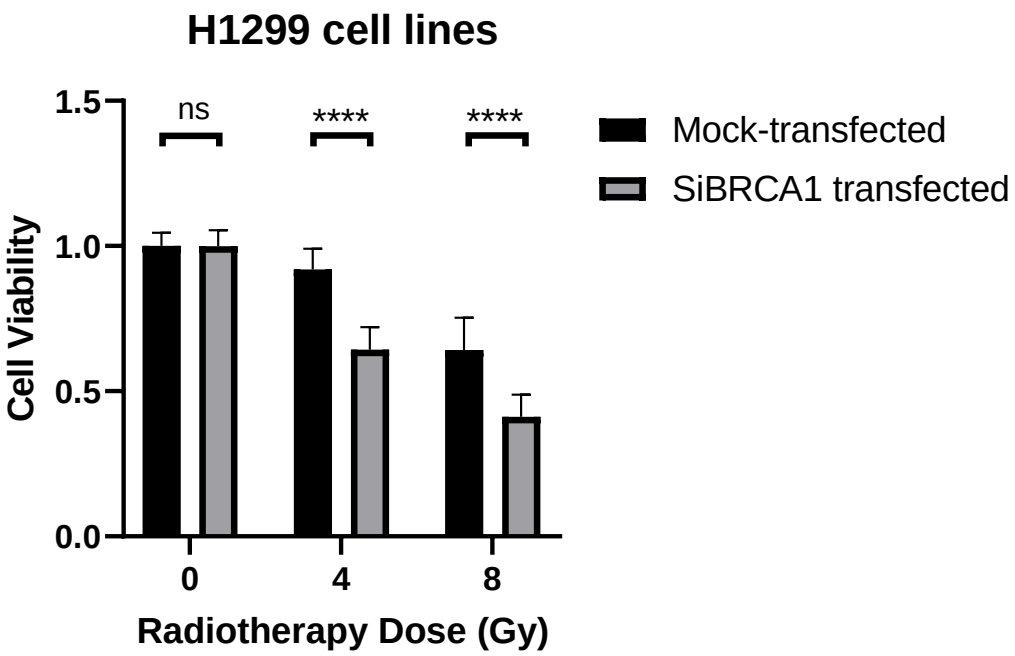

Figure 30: BRCA1-deficient cells are more radiosensitive than BRCA1-proficent counterparts.

*(A) Cell Titre Glo® viability assay for SUM149 Parental and Revertant cell lines 8 days after treatment with 2, 4, 6, 8, 10 Gy RT and non-irradiated cells. Graphs show the mean +SD of three independent experiments (ns p>0.1234 and ****p<0.0001; Two-way ANOVA statistical analysis corrected for multi-comparison using Sidak test). (B) Western blot analysis for BRCA1 protein in H1299 cells 72 hrs after mock transfection or siBRCA1 transfection. (C) Cell Titre Glo® viability assay for mock- and siBRCA1-transfected cell lines 5 days after treatment with 4, 8Gy RT and non-irradiated cells. Graphs show the mean +SD of three independent experiments (ns p>0.1234 and ****p<0.0001; Two-way ANOVA statistical analysis corrected for multi-comparison using Sidak test).*

6.4.3 MG1-shBRCA1 and Radiotherapy in NSCLC

Having shown that siRNA knockdown of BRCA1 can lead to radiosensitivity in human H1299 lung cancer cell line *in vitro*, we were therefore interested in whether disrupting BRCA1 protein expression *in vivo* would lead to beneficial survival advantage in combination with RT. Thus, MG1 vector expressing shRNA against human and murine BRCA1 was generated and knockdown of BRCA1 in H1792, H1299 and 3LL cells after 0.1 MOI MG1-shBRCA1 was investigated (Figure 31A). From the preliminary western blots, it is uncertain as to whether the generated MG1-shBRCA1 at the dose tested resulted in successful BRCA1 knockdown as for H1792; although the band for BRCA1 is absent, it was also absent after infection with a MG1-expressing a non-targeting control (NTC) shRNA (MG1-shNTC). As for H1299 cells there was a lighter BRCA1 band after MG-shBRCA1 infection compared to uninfected or MG1-shNTC virus infection. Whereas for 3LL, the results were inconclusive as there was artefact obscuring the band after MG1-shBRCA1 infection. Further repeats of these western blots are required for determining the success of the MG1-shBRCA1 virus.

Notwithstanding this inconclusive result the combination of MG-shBRCA1 with RT was tested in the 3LL murine syngeneic murine model. Figure 31B shows the Kaplan Meier survival curves for mice bearing 3LL tumours treated with MG-shNTC and MG-shBRCA-1 alone or in combination with 8 Gy RT. Treatment of mice bearing 3LL subcutaneous tumours with MG1-shBRCA1 and 8 Gy RT, did not lead to improved survival compared to single agents alone, PBS or MG1-shSLG +/-RT (Figure 31B and 31C). Consistent with previous experiments (Figure 15), intratumourally delivered virus alone did not lead to any significant survival advantage over PBS (mOS 24 vs 22.5 days compared to this experiments mOS 29 vs 29 days, PSB vs MG1). However, in contrast to the previous experiment, the anti-tumour effect of 8 Gy RT was abolished compared to Figure 28 (mOS 29.5 vs 42 compared to this experiment 29 vs 29, PBS vs 8 Gy). After reviewing the experiments, there appeared to be differences in the average 3LL tumour volumes at the start of RT treatment; although in both experiments the mice received RT at D11, the

average tumour volume in the 8 Gy RT monotherapy group was 41.63mm^3 in Figure 28's experiment, compared to 79.66mm^3 in this experiment. This may account for the difference in RT efficacy between the two experiments and is consistent with the knowledge that smaller tumours responds better to RT.

(A)

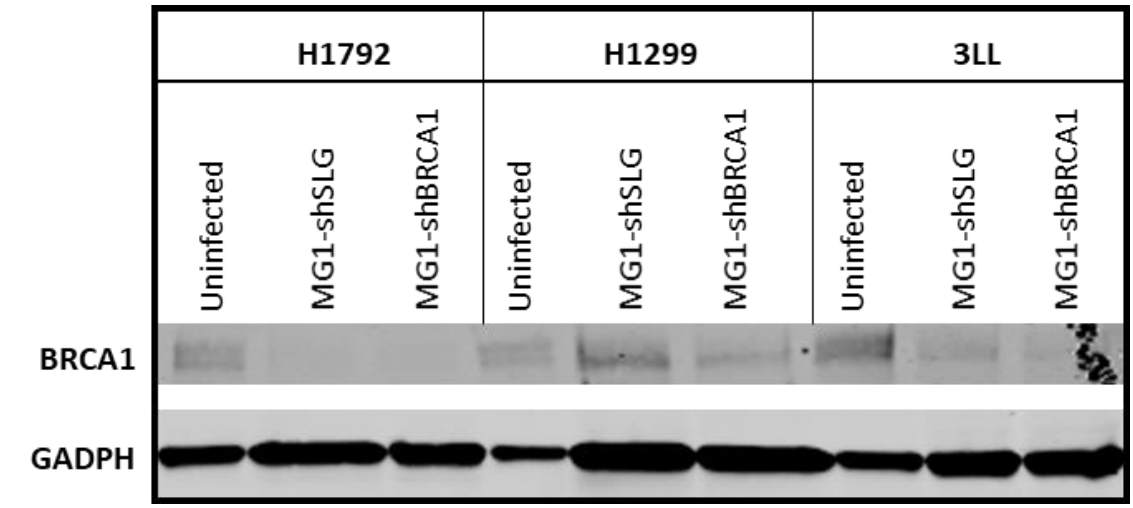
H1792
H1299
3LL
Uninfected
MG1-shSLG
MG1-shBRCA1
Uninfected
MG1-shSLG
MG1-shBRCA1
Uninfected
MG1-shSLG
MG1-shBRCA1
BRCA1
GADPH

(B)

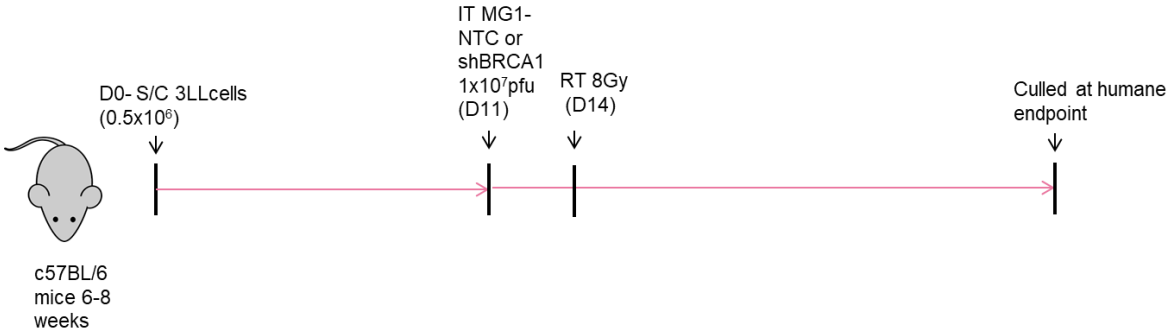
D0- S/C 3LLcells
(0.5x10⁶)
IT MG1-
NTC or
shBRCA1
1x10⁷pfu
(D11)
RT 8Gy
(D14)
Culled at humane
endpoint
c57BL/6
mice 6-8
weeks

(C)

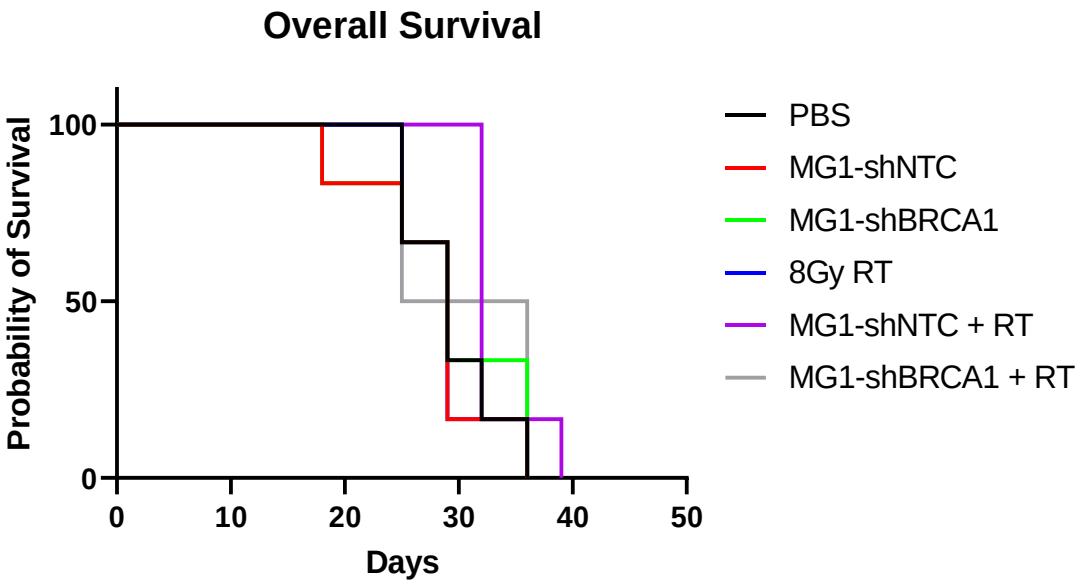

(D)

	PBS	MG1-shNTC	MG1-shBRCA	RT	MG1-shNTC+RT	MG1-shBRCA+RT
Median OS (days)	29	29	29	29	32	30.5
P-value: Log-rank (Mantel-Cox) [compared to PBS]	-	0.8108	0.7782	0.8912	0.0679	0.5389

Figure 31: MG1-shBRCA1 knockdown of BRCA1 protein expression inconclusive and did not improve MG1 therapy in combination with RT in 3LL murine lung cancer model

(A) *Western blot analysis of BRCA1 expressed in H1792, H1299 and 3LL cells 24 hrs after either exposure to PBS (untreated), 0.1 MOI MG1-shSLG or 0.1 MOI MG1-shBRCA1. (B) Schematic of in vivo experiment of combination modified MG1 virus and RT. (C) Kaplan-Meier survival of mice that harboured 3LL subcutaneous tumours and treated on day 11 with either IT PBS, IT MG1-shSLG or IT MG1-shBRCA1. Mice in the radiation alone and combination groups were also treated with 8Gy RT on day 14; n=6 mice per group. (C) Median overall survival (days) for each treatment group compared to IT PBS. Log-rank Mantel-Cox statistical analysis; ns P>0.1234*

6.5 Discussion

OVs are biological machines that can directly infect, self-amplify, kill cancer cells and mediate anti-tumour activity. MG1 virus has been shown in this thesis to possess these characteristics including the ability to promote ICD, which leads to release of DAMPs, thereby attracting and activating innate immune cells within the TME. Despite these properties, the therapeutic effect of MG1 as a single agent was limited in the 3LL murine lung cancer model tested (see section 4.3.4), Therefore in this chapter, the potential of combination treatments with MG1 in an attempt to enhance its beneficial anti-tumour effects was explored.

The strategy that arguably is the most likely to have immediate clinical relevance is to combine MG1 with current standard of care therapies such as immune checkpoint blockade and radiotherapy. Given that OVs can often convert a “cold” tumour immune environment “hot”, with increases in tumoural PD-L1 expression, they have proven to be a successful synergistic partner with immune checkpoint inhibitors in many pre-clinical models (172). Consistent with other OVs, MG1 infection also leads to increase in tumoural PD-L1 expression in a triple negative breast cancer murine model and successfully enhanced therapeutic response when given in the neoadjuvant setting followed by postoperative combination anti-CTLA-4 and anti-PD-1 immune checkpoint blockade (135). In addition, in section 5.4.1, we observed that both IT and IV delivery of MG1 resulted in an increasing trend in PD-1 expression on CD8+ T cells within the spleen in mice bearing 3LL subcutaneous tumours; therefore MG1 in combination with anti-PD1 became a rationale strategy to explore for enhanced therapy. However, disappointingly, we did not observe any increase in PD-L1 expression on 3LL murine lung cancer cells after MG1 infection *in vitro* and unsurprisingly this translated into no overall survival difference with combination MG1 and anti-PD1 therapy compared to single agents alone in mice harbouring subcutaneous 3LL tumours. Aside from the lack of induction of PD-L1 expression on tumoural cells, albeit this was not confirmed *in vivo*, 3LL Lewis lung carcinomas are also known to be weakly immunogenic, with the ability to

exclude T cells from the tumour immune microenvironment (224). Despite MG1 infection of 3LL tumours leading to innate immune activation, mainly NK cell tumour infiltration and activation, as shown in section 5.4.2, there was still a deficiency of CD8+ T cell recruitment observed within the tumour, which again likely contributes to the lack of combination therapy with anti-PD1 and MG1 virus.

Another attempt to enhance MG1 virotherapy in 3LL murine tumours was aimed at enhancing anti-tumour immune response by boosting type I IFN production with RT. As previously discussed (section 5.3), type I IFNs play a crucial role in the crosstalk between tumour cells and the immune system and result in the recruitment of NK and CD8+ T cells to the tumour immune microenvironment. MG1 infection has not only demonstrated the ability to induce ICD in NSCLC cells, but it also stimulates IFN-β production (section 5.2 and 5.3). In this chapter we have shown that, although the addition of RT to virus can increase IFN-β release in 3LL cells *in vitro*, this did not translate in *ex vivo* 3LL tumours harvested from mice treated after combination therapy at 72 hrs. Furthermore, MG1-RT treatment failed to stimulate any adaptive anti-tumour immune response detectable at 10 days post-administration, and thus there was no overall survival advantage seen in mice treated with dual therapy compared to single agents alone. An explanation for this somewhat disappointing finding may be due to the highly lytic nature of MG1 as shown *in vitro* whereby all NSCLC cell lines tested in this thesis were sensitive to viral cytotoxicity even at low doses of 0.01 MOI and, furthermore, 3LL cells were killed at even lower doses of 0.0001 MOI. Highly lytic viruses may be more immunogenic against the virus, and prime antiviral adaptive immune responses, which leads to rapid clearance of virus from the host before the anti-tumour adaptive response has time to mature; we showed that anti-viral NAbs began to develop after 72 hrs from systemic MG1 administration in the murine 3LL model (section 4.3.2). This may explain why there was a lack of IFN-β secretion detected in *ex vivo* 3LL tumours after MG1 virus monotherapy (Figure 26B) and also why there was an absence of adaptive anti-tumour immune response seen after MG1 virotherapy alone, as seen in section 5.4.3. Another possibility for the lack of anti-tumour immunity is due to the 3LL model

being poorly immunogenic; Lechner *et al*. investigated the immune-related gene expressions in Lewis Lung carcinoma (LLC) specimens, measured by qRT-PCR and, in the final immune profile, found that LLCs had generalised down-regulation of pan-leukocyte (CD45), T-cell (CD3, CD4) and myeloid cell (CD11c, CD11b) genes. Additionally, LLCs had decreased expression of T-cell activation genes (CD25, CD62L) and DC activation and co-stimulatory genes (CD80, CD86, OX40L, GITRL, CD40, CD137L). Murine LLC cells *in vivo* also showed lack of MHC class I molecule H2-D expression with IHC staining. Furthermore, the authors showed that the success of two immunotherapy regimens (CCL16 with low dose chemotherapy with or without a DC tumour vaccine) correlated directly with tumour immunogenicity, with LLC responding poorly to immunotherapy treatment (225). A study by Yaacov *et al*. has looked at using a sub-clone of 3LL, 3LL-D122 with a NDV, where they demonstrate some efficacy, although no long term cures (226). To date, there have been no other publications demonstrating long term cures with OVs in this model. The addition of RT then had limited enhancement of this immune response, as RT alone often fails effectively to initiate adaptive immunity as highlighted in the rarity of abscopal events seen clinically. The timing and/or dosage of OV and RT in this combination treatment are also crucial for total eradication of tumours as shown by Simbawa *et al*. in their spatiotemporal dynamic mathematical modelling of radiovirotherapy for cancer treatments (227). Therefore, the optimal dose and timing for MG1 and RT may not have been found yet from our experiments.

In a final attempt to enhance MG1 therapy, we also explored modified MG1 expressing shBRCA1 to use in combination with RT to sensitise NSCLC cells to irradiation. There is a wealth of pre-clinical data that shows BRCA1 deficient cells are more radiosensitive (as discussed in section 6.4) and we were also able to demonstrate that SUM149 parental cells (which are BRCA1 mutated), as well as siBRCA1-transfected H1299 cells, were more sensitive to RT than SUM149 revertant and mock transfected H1299 cells, respectively. However, the clinical data to support this theory is inconclusive and often conflicting. For example in a study of a small number of patients, there was a lower rate of subsequent ipsilateral breast tumours in BRCA1/2 carriers who were treated

by lumpectomy and breast RT compared with noncarriers treated in a similar fashion at a median follow-up time of 63 months (228). However, in another matched retrospective case-control study from the Institut Curie, which studied ipsilateral tumour recurrence, contralateral tumour development and overall survival in breast cancer patients that had undergone breast conserving surgery and RT, they demonstrated that there was no difference in ipsilateral breast tumour recurrence or OS between BRCA1/2 mutation carriers versus sporadic controls at a median follow-up of 161 months (229). Although results are somewhat mixed, this could be due to the higher inherent risk of tumour relapse in the ipsilateral breast in BRCA1/2 mutated patients despite adjuvant RT being more effective than in their BRCA wild-type paired counterparts. Therefore, there was still a good rationale to explore MG1-shBRCA1 which would selectively target and silence BRCA1 protein expression in NSCLC cells, thereby sensitising them to combination radiotherapy. However, we did not detect any overall survival in mice bearing 3LL subcutaneous tumours, with combination MG1-shBRA1 and RT compared to single treatments alone. A possible explanation for this result could be that MG1 is again highly lytic and, as a result, kills tumour cells before shBRCA1 had time to act for RT sensitisation. Therefore, further western blots to illicit whether MG1-shBRCA1 does indeed silence BRCA1 expression in 3LL tumours *in vivo* at the time point tested in our experiments are still required to demonstrate the virus is capable of achieving what it was designed to do. There was, however, difficulty in demonstrating MG1-shBRCA1 silencing BRCA1 protein expression in NSCLC cell lines *in vitro* via western blots (section 6.4.3 (A)). Future work will look to address this problem by cloning shBRCA-1 into a replication deficient Rhabdovirus backbone.

In summary, we were unable to find an effective combination partner to enhance the therapeutic effect of MG1 virotherapy. The failure of these strategies may be down to the particular nature of the model chosen, and also the timing and dosing of each combination component is likely to be crucial for the effectiveness in anti-tumour control.

Chapter 7:
Discussion

7. Chapter 7: Discussion

7.1 Conclusions

The results presented within this study demonstrate that MG1 virus can selectively infect, replicate and kill NSCLC cell lines while sparing normal cells like HFF. One of the major limitations for adopting OVs clinically has been the difficulty to administer effective viral doses to tumour sites not readily accessible by intratumoural injections. MG1, however, has the ability to maintain tumour tropism *in vivo* after systemic delivery and can reach 3LL tumours whether they are situated subcutaneously or at the orthotopic site. Crucially, there was also no significant difference in the maximum viral dose detected in the tumour at 24, 48 and 72 hrs after virus administration between systemic and intratumoural delivery, which makes MG1 a good potential OV for treating patients with metastatic disease.

MG1 has not only been shown to possess powerful oncolytic activity, lysing NSCLC cells at low viral concentrations, it can also induce ICD, which has not been previously described for this virus. This immune-promoting characteristic, together with the ability to stimulate type I IFN production, led to innate immune changes (mainly NK cell recruitment and activation) within the tumours and spleens of mice bearing 3LL subcutaneous malignancies, after IT or IV administration of MG1. Furthermore, systemic delivery of MG1 resulted in greater splenic, and possibly tumoural, NK cell activation compared to intratumoural administration. This could explain why tumour growth retardation was observed after IV MG1 virus, but not IT MG1 virus, in the 3LL murine model; however a further NK cell depletion experiment would be required in order to definitively prove this theory. The innate immune stimulating properties after MG1 virus infection was again demonstrated in human NK cell degranulation assays with NSCLC cell line targets; exposing PBMCs, obtained from healthy donors, to MG1 significantly enhanced NK cell degranulation against NSCLC targets, compared to virally-unexposed PBMCs.

Despite the beneficial innate immune stimulating characteristics of MG1, it failed to engage the adaptive CD8+ T cell response against 3LL tumours, which may have contributed to the lack of overall survival advantage seen in the 3LL murine model after virus treatment compared to PBS controls. A possible explanation for this is the highly lytic nature of MG1, which results in rapid anti-viral immune responses that clear the virus prior to the maturation of the adaptive anti-tumoural immune response. In this study we showed that neutralising antibodies to MG1 were detected in mice harbouring 3LL tumours as early as 72hrs after virus administration. However, we also noted MG1 doses of greater than $1x10^5$ pfu in *ex vivo* harvested 3LL tumours whether the virus was delivered intravenously or intratumourally despite the presence of Nabs. Therefore, the more likely reason for the lack of anti-tumour adaptive immunogenicity is the poorly immunogenic nature of the 3LL model. Lewis lung carcinoma has been shown to be infiltrated with mainly immunosuppressive MDSCs and tumour-associated macrophages (TAMs), with very few CD8+ or CD4+ T cells. As explained previously, Lechner *et al*. have also shown LLCs have reduced expression of pan-leukocyte and T cell co-stimulatory genes resulting in poor responses to immunotherapy (225). Therefore, it may be unsurprising that MG1 virotherapy was insufficient to cause engagement of anti-tumour adaptive immunity. Future work would look at MG1 therapy in tumours with higher immunogenicity.

Finally, in an attempt to enhance the therapeutic effect of MG1 virus, combination therapy was explored with anti-PD1 and RT, as well as modifying MG1 to express shBRCA1 in order to infect and sensitize NSCLC cells to irradiation. Although MG1 infection has been shown to increase PD-L1 expression in a TNBC model and subsequently improve the therapeutic outcome in mice receiving MG1 neoadjuvantly followed by combination anti-CTLA-4 and anti-PD1 therapy post-surgery (135), compared to either monotherapy alone, this effect seemed to be tumour model specific as there was no increase in PD-L1 expression in 3LL cells *in vitro*, nor did the combination virus and anti-PD1 therapy lead to any improved survival in the 3LL murine lung cancer model *in vivo*, compared to other treatment arms. If this combination treatment was explored in another lung cancer model with a

“hotter” immune TME, it may have led to a more positive outcome, as within our lab we also noted that MG1 increased PD-L1 expression in 4434 melanoma cells which also led to synergistic therapeutic benefits with anti-PD1 therapy in mice harbouring subcutaneous 4434 tumours.

Combination RT and MG1 did lead to increased IFN-β production *in vitro* as hypothesised, but unfortunately this did not translate when tested *in vivo*, which may explain the failure in stimulating the adaptive immune system against the tumour better than single treatments alone, when explored in the 3LL murine lung cancer model. This dual therapy subsequently did not result in any survival advantage in the mice bearing 3LL tumours compared to monotherapies alone. It was observed from *ex vivo* 3LL tumours that MG1 therapy did not lead to significantly greater amounts of IFN-β production compared to PBS controls, which was contrary to what was seen *in vitro,* again raising the possibility that the virus could have been cleared by anti-viral immunity before stimulating the type I IFN pathway. Another possibility could be due to timing of *ex vivo* IFN- β analysis, as with *in vitro* data IFN- β was shown to be present even at 24 hours; therefore the tumours being examined at 72hrs might have been too late to accurately detect combination effect on the type I IFN pathway. Therefore, future work to repeat this experiment at an early time point would be warranted.

Finally, modified MG1 expressing shBRCA1 was investigated in combination with RT as BRCA mutated cell lines have been shown in our study and others to be more radiosensitive. Furthermore, siBRCA1 knockdown of H1299 human cell line did increase radiation-induced cytotoxicity. However, we were unable to confidently determine whether our modified MG1-shBRCA did indeed knockdown BRCA1 protein expression in a panel of human and murine NSCLC cell lines *in vitro,* as there were mixed results on western blot with H1792 and 3LL cells, failing to demonstrate conclusive BRCA1 knockdown, unlike for the H1299 cell line after infection with 0.1 MOI MG1-shBRCA1. A plausible explanation for this could be that H1792 and 3LL were more sensitive to MG1 cytotoxicity, as shown in Figure 8, compared to H1299, hence these cells could have been killed before BRCA1 could be knocked down. Unsurprisingly therefore, MG1-shBRCA1 in combination with RT did not result

in better overall survival than single treatments alone in the 3LL murine model. However, further western blot analysis of *ex vivo* 3LL tumours would be required to determine whether MG1-shBRCA1 does indeed lead to knock down BRCA1 expression *in vivo*. If this is not the case, then the design of MG1-shBRCA1 may need to be reviewed or the modified MG1-shBRCA1 could be tested in other more resistant BRCA1-wild type cell lines.

In summary, MG1 does appear to be a powerful multifunctional tool that can be delivered systemically in the treatment of NSCLC with the ability to directly lyse tumour cells and stimulate an innate immune response *in vivo* via ICD and type I IFN production. However, although MG1 virotherapy has been shown to improve survival in mice bearing other tumour types such as S180 sarcoma (133) and CT26 colorectal adenocarcinoma (131), we did not detect any survival benefit in the 3LL lung cancer murine model. The true potential to enhance MG1's therapeutic ability likely lies in effective combination therapy, and although this did not materialise with the addition of anti-PD1 or RT in the lung cancer model we tested, there are other treatment partners that have good scientific rationale for exploration.

7.2 Improving experimental studies

In vivo studies, especially when analysing the change in immune landscape after MG1 therapy, could be improved by repeating the experiments with increased timepoints' number of mice per group (8-10), in order to enhance the confidence of not only the survival results, but the immunological readouts via flow cytometry. Moreover, panels that looked at DC phenotype would be informative, especially when compared to models with known efficacy. Increased numbers of *ex vivo* tumours harvested in a repeat experiment to determine the differences in IFN-β production after RT, MG1 or combination treatments would also potentially lead to tighter standard deviations and increased confidence in the results.

The radiotherapy administered to mice in these experiments was technically basic, where the whole mouse was essentially placed underneath a radiotherapy source, using lead shielding to isolate the subcutaneous tumours

for treatment while protecting the rest of the animal and using a dosimeter to measure the dose of RT given. Despite careful positioning of lead shielding in each experiment, some normal tissue including tumour-draining lymph nodes would inevitably end up in the RT field. Marciscano *et al*. illustrated in a MC38 colon cancer murine model that RT to the tumour significantly increased tumour infiltration of CD8+ effector T cells (Teffs) and Tregs, while RT to the tumour and elective draining lymph node irradiation (ENI), resulted in a smaller increase in Teffs but not Tregs (230). There was also difference in survival outcome between the mice who only had tumour irradiation compared to those who in addition had ENI, highlighting the importance of conformal RT to avoid inconsistent results. Therefore repeated *in vivo* experiments with the small animal radiation research platform (SARRP) would achieve more conformal RT administration and avoid lymph node irradiation, which would enhance the confidence of the conclusions made regarding survival and immune changes in mice harbouring 3LL tumours after RT or combination MG1-RT treatments.

7.3 Future studies

As mentioned previously, in order to definitively conclude that the innate immune changes seen in the spleen and tumour after systemic MG1 administration are contributing to the tumour growth retardation seen in mice bearing 3LL subcutaneous tumours, a repeat experiment with NK cell depletion would be required to see if this therapeutic benefit is ablated.

It would be interesting to test MG1 in combination with anti-PD1 in a more immunogenic lung cancer model, as it has been shown in other more immunogenic tumours such as 4T1 (TNBC) (135) and 4434 (melanoma) (unpublished data from our lab), that MG1 infection can sensitise these tumours to anti-PD1 therapy. One such model could be the 3LL clone, 3LL C75, which is a more highly immunogenic variant of the parent 3LL.

As mentioned previously, our modified MG1-shBRCA1 would need to be explored in other BRCA-WT cell lines that are more resistant to MG1 cytotoxicity or using a replication deficient MG1 (MG1Gless) to conclude whether a virus with less direct cytotoxicity is able to knock down BRCA1

expression. *Ex vivo* 3LL tumours could also be analysed after MG1-shBRCA1 infection to determine via western blot or IHC whether the expression of BRCA1 is reduced compared to MG1-shNTC. If not, then the design of MG1-shBRCA1 would need to be reviewed, especially if the virus fails to knock down BRCA1 expression in other more resistant BRCA1-WT cell lines. However, if the virus is deemed to be successful, then further combination therapy with PARPi and MG1-shBRCA1 could be tested in the 3LL murine model, as the clinical data for synergistic benefit of RT and BRCA mutated tumours are often inconclusive and conflicting, as discussed in section 6.5.

Finally, another potential combination partner for MG1 virus to treat NSCLC is with other immune checkpoint inhibitors, especially anti-TIGIT antibody. The immune checkpoint TIGIT has been often shown to be highly expressed on NK cells (231) for negative regulation of the innate immune response. From our data and other studies (116, 137), it has been shown that MG1 stimulates a strong anti-tumour innate response, in particular with NK cell recruitment and activation, and in Figure 19C we also show that there was increased TIGIT expression on splenic NK cells after MG1 infection. Therefore, combination anti-TIGIT antibody with MG1 virotherapy may lead to increase NK cell activation and improved survival in the 3LL murine lung cancer model compared to monotherapies.

Chapter 8:
Appendix

8. Chapter 8: Appendix

8.1 IASLC TMN staging for NSCLC

Table 6: T, N, and M descriptors for the 8th edition IASLC lung cancer staging.

T: Primary tumour	
Tx	Primary tumour cannot be assessed, or tumour proven by presence of malignant cells in sputum or bronchial washings but not visualized by imaging or bronchoscopy
T0	No evidence of primary tumour
Tis	Carcinoma in situ
T1	Tumour ≤3cm in greatest dimension surrounded by lung or visceral pleura without bronchoscopic evidence of invasion more proximal than the lobar bronchus (ie. Not in the main bronchus)*
T1a(mi)	Minimally invasive adenocarcinoma¶
T1a	Tumour ≤1cm in greatest dimension*
T1b	Tumour >1cm but ≤2cm in greatest dimension*
T1c	Tumour >2cm but ≤2cm in greatest dimension*
T2	Tumour >3 cm but ≤5 cm or tumour with any of the following features' ▪ Involves main bronchus regardless of distance from the carina but without involvement of the carina ▪ Invades visceral pleura ▪ Associated with atelectasis or obstructive pneumonitis that extends to the hilar region, involving part or all of the lung
T2a	Tumour >3cm but ≤4cm in greatest dimension
T2b	Tumour >4cm but ≤5cm in greatest dimension
T3	Tumour >5cm but ≤7cm in greatest dimension or associated with

	separate nodule(s) in the same lobe as the primary tumour or directly invades any of the following structures: chest wall (including the parietal pleura and superior sulcus tumours), phrenic nerve, parietal pericardium
T4	Tumour >7cm in greatest dimension or associated with separate tumour nodule(s) in a different ipsilateral lobe than that of the primary tumour or invades any of the following structures: diaphragm, mediastinum, heart, great vessels, trachea, recurrent laryngeal nerve, oesophagus, vertebral body and carina
N: Regional lymph node involvement	
Nx	Regional lymph node cannot be assessed
N0	No regional lymph node metastasis
N1	Metastasis in ipsilateral peribronchial and/or ipsilateral hilar lymph nodes and intrapulmonary nodes, including involvement by direct extension
N2	Metastasis in ipsilateral mediastinal and/or subcarinal node(s)
N3	Metastasis in contralateral mediastinal, contralateral hilar, ipsilateral, or contralateral scalene or supraclavicular lymph node(s)
M: Distant metastasis	
M0	No distant metastasis
M1	Distant metastasis present
M1a	Separate tumour nodule(s) in a contralateral lobe; tumour with pleural or pericardial nodule(s) or malignant pleural or pericardial effusion◊
M1b	Single extrathoracic metastases §
M1c	Multiple extrathoracic metastases in one or more organs

TNM: tumour, node, metastasis; Tis: carcinoma in situ; T1a(mi): minimally invasive adenocarcinoma.
* The uncommon superficial spreading tumour of any size with its invasive component limited to the bronchial wall, which may extend proximal to the main bronchus, is also classified as T1a.
¶ Solitary adenocarcinoma, ≤3 cm with a predominately lepidic pattern and ≤5 mm invasion in any one focus.
Δ T2 tumours with these features are classified as T2a if ≤4 cm in greatest dimension or if size cannot be determined, and T2b if >4 cm but ≤5 cm in greatest dimension.
◊ Most pleural (pericardial) effusions with lung cancer are due to tumour. In a few patients, however, multiple microscopic examinations of pleural (pericardial) fluid are negative for tumour and the fluid is nonbloody and not an

exudate. When these elements and clinical judgment dictate that the effusion is not related to the tumour, the effusion should be excluded as a staging descriptor.
§ This includes involvement of a single distant (nonregional) lymph node.

Table 7: IASLC 8th edition lung cancer stage groupings.

Stage groupings			
Occult carcinoma	TX	N0	M0
Stage IA1	T1a(mi)	N0	M0
	T1a	N0	M0
Stage IA2	T1b	N0	M0
Stage IA3	T1c	N0	M0
Stage IB	T2a	N0	M0
Stage IIA	T2b	N0	M0
Stage IIB	T1a to c	N1	M0
	T2a	N1	M0
	T2b	N1	M0
	T3	N0	M0
Stage IIIA	T1a to c	N2	M0
	T2a to b	N2	M0
	T3	N1	M0
	T4	N0	M0
	T4	N1	M0
Stage IIIB	T1a to c	N3	M0
	T2a to b	N3	M0
	T3	N2	M0
	T4	N2	M0
Stage IIIC	T3	N3	M0
	T4	N3	M0
Stage IVA	Any T	Any N	M1a
	Any T	Any N	M1b
Stage IVB	Any T	Any N	M1c

Chapter 9:
References

9. Chapter 9: References

1. [World Health Organization]. [Available from: https://www.who.int/news-room/fact-sheets/detail/cancer.

2. Molina JR, Yang P, Cassivi SD, Schild SE, Adjei AA. Non-small cell lung cancer: epidemiology, risk factors, treatment, and survivorship. Mayo Clin Proc. 2008;83(5):584-94.

3. Sun S, Schiller JH, Gazdar AF. Lung cancer in never smokers--a different disease. Nat Rev Cancer. 2007;7(10):778-90.

4. Hackshaw AK, Law MR, Wald NJ. The accumulated evidence on lung cancer and environmental tobacco smoke. Bmj. 1997;315(7114):980-8.

5. Mao Y, Yang D, He J, Krasna MJ. Epidemiology of Lung Cancer. Surg Oncol Clin N Am. 2016;25(3):439-45.

6. Shah R, Sabanathan S, Richardson J, Mearns AJ, Goulden C. Results of surgical treatment of stage I and II lung cancer. J Cardiovasc Surg (Torino). 1996;37(2):169-72.

7. Nesbitt JC, Putnam JB, Jr., Walsh GL, Roth JA, Mountain CF. Survival in early-stage non-small cell lung cancer. Ann Thorac Surg. 1995;60(2):466-72.

8. Blandin Knight S, Crosbie PA, Balata H, Chudziak J, Hussell T, Dive C. Progress and prospects of early detection in lung cancer. Open Biol. 2017;7(9).

9. de Koning HJ, van der Aalst CM, de Jong PA, Scholten ET, Nackaerts K, Heuvelmans MA, et al. Reduced Lung-Cancer Mortality with Volume CT Screening in a Randomized Trial. New England Journal of Medicine. 2020;382(6):503-13.

10. Reduced Lung-Cancer Mortality with Low-Dose Computed Tomographic Screening. New England Journal of Medicine. 2011;365(5):395-409.

11. Jones GS, Baldwin DR. Recent advances in the management of lung cancer. Clin Med (Lond). 2018;18(Suppl 2):s41-s6.

12. Feng SH, Yang ST. The new 8th TNM staging system of lung cancer and its potential imaging interpretation pitfalls and limitations with CT image demonstrations. Diagn Interv Radiol. 2019;25(4):270-9.

13. Kandoth C, McLellan MD, Vandin F, Ye K, Niu B, Lu C, et al. Mutational landscape and significance across 12 major cancer types. Nature. 2013;502(7471):333-9.

14. Govindan R, Ding L, Griffith M, Subramanian J, Dees ND, Kanchi KL, et al. Genomic landscape of non-small cell lung cancer in smokers and never-smokers. Cell. 2012;150(6):1121-34.

15. Comprehensive molecular profiling of lung adenocarcinoma. Nature. 2014;511(7511):543-50.

16. Comprehensive genomic characterization of squamous cell lung cancers. Nature. 2012;489(7417):519-25.

17. George J, Lim JS, Jang SJ, Cun Y, Ozretić L, Kong G, et al. Comprehensive genomic profiles of small cell lung cancer. Nature. 2015;524(7563):47-53.

18. Ding L, Getz G, Wheeler DA, Mardis ER, McLellan MD, Cibulskis K, et al. Somatic mutations affect key pathways in lung adenocarcinoma. Nature. 2008;455(7216):1069-75.

19. Pao W, Wang TY, Riely GJ, Miller VA, Pan Q, Ladanyi M, et al. KRAS mutations and primary resistance of lung adenocarcinomas to gefitinib or erlotinib. PLoS Med. 2005;2(1):e17.

20. Ahrendt SA, Hu Y, Buta M, McDermott MP, Benoit N, Yang SC, et al. p53 mutations and survival in stage I non-small-cell lung cancer: results of a prospective study. J Natl Cancer Inst. 2003;95(13):961-70.

21. Reck M, Rabe KF. Precision Diagnosis and Treatment for Advanced Non-Small-Cell Lung Cancer. N Engl J Med. 2017;377(9):849-61.

22. Swanton C. Intratumor Heterogeneity: Evolution through Space and Time. Cancer Research. 2012;72(19):4875-82.

23. Zhang J, Fujimoto J, Zhang J, Wedge DC, Song X, Zhang J, et al. Intratumor heterogeneity in localized lung adenocarcinomas delineated by multiregion sequencing. Science. 2014;346(6206):256-9.

24. Hanahan D, Coussens LM. Accessories to the crime: functions of cells recruited to the tumor microenvironment. Cancer Cell. 2012;21(3):309-22.

25. Hanahan D, Weinberg RA. The hallmarks of cancer. Cell. 2000;100(1):57-70.

26. Stankovic B, Bjørhovde HAK, Skarshaug R, Aamodt H, Frafjord A, Müller E, et al. Immune Cell Composition in Human Non-small Cell Lung Cancer. Frontiers in immunology. 2018;9:3101.

27. Koyama S, Akbay EA, Li YY, Aref AR, Skoulidis F, Herter-Sprie GS, et al. STK11/LKB1 Deficiency Promotes Neutrophil Recruitment and

Proinflammatory Cytokine Production to Suppress T-cell Activity in the Lung Tumor Microenvironment. Cancer Res. 2016;76(5):999-1008.

28. McGranahan N, Furness AJ, Rosenthal R, Ramskov S, Lyngaa R, Saini SK, et al. Clonal neoantigens elicit T cell immunoreactivity and sensitivity to immune checkpoint blockade. Science. 2016;351(6280):1463-9.

29. Scagliotti GV, Parikh P, von Pawel J, Biesma B, Vansteenkiste J, Manegold C, et al. Phase III study comparing cisplatin plus gemcitabine with cisplatin plus pemetrexed in chemotherapy-naive patients with advanced-stage non-small-cell lung cancer. J Clin Oncol. 2008;26(21):3543-51.

30. Paz-Ares L, de Marinis F, Dediu M, Thomas M, Pujol JL, Bidoli P, et al. Maintenance therapy with pemetrexed plus best supportive care versus placebo plus best supportive care after induction therapy with pemetrexed plus cisplatin for advanced non-squamous non-small-cell lung cancer (PARAMOUNT): a double-blind, phase 3, randomised controlled trial. Lancet Oncol. 2012;13(3):247-55.

31. Paz-Ares LG, Marinis Fd, Dediu M, Thomas M, Pujol J-L, Bidoli P, et al. PARAMOUNT: Final Overall Survival Results of the Phase III Study of Maintenance Pemetrexed Versus Placebo Immediately After Induction Treatment With Pemetrexed Plus Cisplatin for Advanced Nonsquamous Non–Small-Cell Lung Cancer. Journal of Clinical Oncology. 2013;31(23):2895-902.

32. Delbaldo C, Michiels S, Syz N, Soria JC, Le Chevalier T, Pignon JP. Benefits of adding a drug to a single-agent or a 2-agent chemotherapy regimen in advanced non-small-cell lung cancer: a meta-analysis. Jama. 2004;292(4):470-84.

33. Paccagnella A, Oniga F, Bearz A, Favaretto A, Clerici M, Barbieri F, et al. Adding gemcitabine to paclitaxel/carboplatin combination increases survival in advanced non-small-cell lung cancer: results of a phase II-III study. J Clin Oncol. 2006;24(4):681-7.

34. Comella P, Filippelli G, De Cataldis G, Massidda B, Frasci G, Maiorino L, et al. Efficacy of the combination of cisplatin with either gemcitabine and vinorelbine or gemcitabine and paclitaxel in the treatment of locally advanced or metastatic non-small-cell lung cancer: a phase III randomised trial of the Southern Italy Cooperative Oncology Group (SICOG 0101). Ann Oncol. 2007;18(2):324-30.

35. Perol M, Ciuleanu T-E, Arrieta O, Prabhash K, Syrigos KN, Göksel T, et al. REVEL: A randomized, double-blind, phase III study of docetaxel (DOC) and ramucirumab (RAM; IMC-1121B) versus DOC and placebo (PL) in the second-line treatment of stage IV non-small cell lung cancer (NSCLC) following disease progression after one prior platinum-based therapy. Journal of Clinical Oncology. 2014;32(18_suppl):LBA8006-LBA.

36. Wheeler DL, Dunn EF, Harari PM. Understanding resistance to EGFR inhibitors-impact on future treatment strategies. Nat Rev Clin Oncol. 2010;7(9):493-507.

37. Mok TS, Wu YL, Thongprasert S, Yang CH, Chu DT, Saijo N, et al. Gefitinib or carboplatin-paclitaxel in pulmonary adenocarcinoma. N Engl J Med. 2009;361(10):947-57.

38. Fukuoka M, Wu YL, Thongprasert S, Sunpaweravong P, Leong SS, Sriuranpong V, et al. Biomarker analyses and final overall survival results from a phase III, randomized, open-label, first-line study of gefitinib versus carboplatin/paclitaxel in clinically selected patients with advanced non-small-cell lung cancer in Asia (IPASS). J Clin Oncol. 2011;29(21):2866-74.

39. Maemondo M, Inoue A, Kobayashi K, Sugawara S, Oizumi S, Isobe H, et al. Gefitinib or chemotherapy for non-small-cell lung cancer with mutated EGFR. N Engl J Med. 2010;362(25):2380-8.

40. Zhou C, Wu YL, Chen G, Feng J, Liu XQ, Wang C, et al. Final overall survival results from a randomised, phase III study of erlotinib versus chemotherapy as first-line treatment of EGFR mutation-positive advanced non-small-cell lung cancer (OPTIMAL, CTONG-0802). Ann Oncol. 2015;26(9):1877-83.

41. Rosell R, Carcereny E, Gervais R, Vergnenegre A, Massuti B, Felip E, et al. Erlotinib versus standard chemotherapy as first-line treatment for European patients with advanced EGFR mutation-positive non-small-cell lung cancer (EURTAC): a multicentre, open-label, randomised phase 3 trial. Lancet Oncol. 2012;13(3):239-46.

42. Wu YL, Zhou C, Liam CK, Wu G, Liu X, Zhong Z, et al. First-line erlotinib versus gemcitabine/cisplatin in patients with advanced EGFR mutation-positive non-small-cell lung cancer: analyses from the phase III, randomized, open-label, ENSURE study. Ann Oncol. 2015;26(9):1883-9.

43. Park K, Tan EH, O'Byrne K, Zhang L, Boyer M, Mok T, et al. Afatinib versus gefitinib as first-line treatment of patients with EGFR mutation-positive non-small-cell lung cancer (LUX-Lung 7): a phase 2B, open-label, randomised controlled trial. Lancet Oncol. 2016;17(5):577-89.

44. Wu YL, Cheng Y, Zhou X, Lee KH, Nakagawa K, Niho S, et al. Dacomitinib versus gefitinib as first-line treatment for patients with EGFR-mutation-positive non-small-cell lung cancer (ARCHER 1050): a randomised, open-label, phase 3 trial. Lancet Oncol. 2017;18(11):1454-66.

45. Mok TS, Cheng Y, Zhou X, Lee KH, Nakagawa K, Niho S, et al. Improvement in Overall Survival in a Randomized Study That Compared Dacomitinib With Gefitinib in Patients With Advanced Non-Small-Cell Lung Cancer and EGFR-Activating Mutations. J Clin Oncol. 2018;36(22):2244-50.

46. Yu HA, Arcila ME, Hellmann MD, Kris MG, Ladanyi M, Riely GJ. Poor response to erlotinib in patients with tumors containing baseline EGFR T790M mutations found by routine clinical molecular testing. Ann Oncol. 2014;25(2):423-8.

47. Bean J, Brennan C, Shih JY, Riely G, Viale A, Wang L, et al. MET amplification occurs with or without T790M mutations in EGFR mutant lung tumors with acquired resistance to gefitinib or erlotinib. Proc Natl Acad Sci U S A. 2007;104(52):20932-7.

48. Engelman JA, Zejnullahu K, Mitsudomi T, Song Y, Hyland C, Park JO, et al. MET amplification leads to gefitinib resistance in lung cancer by activating ERBB3 signaling. Science. 2007;316(5827):1039-43.

49. Jänne PA, Yang JC, Kim DW, Planchard D, Ohe Y, Ramalingam SS, et al. AZD9291 in EGFR inhibitor-resistant non-small-cell lung cancer. N Engl J Med. 2015;372(18):1689-99.

50. Mok TS, Wu YL, Ahn MJ, Garassino MC, Kim HR, Ramalingam SS, et al. Osimertinib or Platinum-Pemetrexed in EGFR T790M-Positive Lung Cancer. N Engl J Med. 2017;376(7):629-40.

51. Ramalingam SS, Vansteenkiste J, Planchard D, Cho BC, Gray JE, Ohe Y, et al. Overall Survival with Osimertinib in Untreated, EGFR-Mutated Advanced NSCLC. New England Journal of Medicine. 2019;382(1):41-50.

52. Pikor LA, Ramnarine VR, Lam S, Lam WL. Genetic alterations defining NSCLC subtypes and their therapeutic implications. Lung Cancer. 2013;82(2):179-89.

53. Shaw AT, Solomon B. Targeting anaplastic lymphoma kinase in lung cancer. Clin Cancer Res. 2011;17(8):2081-6.

54. Solomon BJ, Mok T, Kim DW, Wu YL, Nakagawa K, Mekhail T, et al. First-line crizotinib versus chemotherapy in ALK-positive lung cancer. N Engl J Med. 2014;371(23):2167-77.

55. Soria JC, Tan DSW, Chiari R, Wu YL, Paz-Ares L, Wolf J, et al. First-line ceritinib versus platinum-based chemotherapy in advanced ALK-rearranged non-small-cell lung cancer (ASCEND-4): a randomised, open-label, phase 3 study. Lancet. 2017;389(10072):917-29.

56. Camidge DR, Dziadziuszko R, Peters S, Mok T, Noe J, Nowicka M, et al. Updated Efficacy and Safety Data and Impact of the EML4-ALK Fusion Variant on the Efficacy of Alectinib in Untreated ALK-Positive Advanced Non-Small Cell Lung Cancer in the Global Phase III ALEX Study. J Thorac Oncol. 2019;14(7):1233-43.

57. Peters S, Camidge DR, Shaw AT, Gadgeel S, Ahn JS, Kim DW, et al. Alectinib versus Crizotinib in Untreated ALK-Positive Non-Small-Cell Lung Cancer. N Engl J Med. 2017;377(9):829-38.

58. Zhou C, Kim SW, Reungwetwattana T, Zhou J, Zhang Y, He J, et al. Alectinib versus crizotinib in untreated Asian patients with anaplastic lymphoma kinase-positive non-small-cell lung cancer (ALESIA): a randomised phase 3 study. Lancet Respir Med. 2019;7(5):437-46.

59. Camidge DR, Kim HR, Ahn MJ, Yang JC, Han JY, Lee JS, et al. Brigatinib versus Crizotinib in ALK-Positive Non-Small-Cell Lung Cancer. N Engl J Med. 2018;379(21):2027-39.

60. Rothenstein JM, Chooback N. ALK inhibitors, resistance development, clinical trials. Curr Oncol. 2018;25(Suppl 1):S59-s67.

61. Shaw AT, Felip E, Bauer TM, Besse B, Navarro A, Postel-Vinay S, et al. Lorlatinib in non-small-cell lung cancer with ALK or ROS1 rearrangement: an international, multicentre, open-label, single-arm first-in-man phase 1 trial. Lancet Oncol. 2017;18(12):1590-9.

62. Davies KD, Le AT, Theodoro MF, Skokan MC, Aisner DL, Berge EM, et al. Identifying and targeting ROS1 gene fusions in non-small cell lung cancer. Clin Cancer Res. 2012;18(17):4570-9.

63. Cho BC, Drilon AE, Doebele RC, Kim D-W, Lin JJ, Lee J, et al. Safety and preliminary clinical activity of repotrectinib in patients with advanced ROS1 fusion-positive non-small cell lung cancer (TRIDENT-1 study). Journal of Clinical Oncology. 2019;37(15_suppl):9011-.

64. Drilon A, Siena S, Dziadziuszko R, Barlesi F, Krebs MG, Shaw AT, et al. Entrectinib in ROS1 fusion-positive non-small-cell lung cancer: integrated analysis of three phase 1-2 trials. Lancet Oncol. 2020;21(2):261-70.

65. Lim SM, Kim HR, Lee JS, Lee KH, Lee YG, Min YJ, et al. Open-Label, Multicenter, Phase II Study of Ceritinib in Patients With Non-Small-Cell Lung Cancer Harboring ROS1 Rearrangement. J Clin Oncol. 2017;35(23):2613-8.

66. Shaw AT, Ou SH, Bang YJ, Camidge DR, Solomon BJ, Salgia R, et al. Crizotinib in ROS1-rearranged non-small-cell lung cancer. N Engl J Med. 2014;371(21):1963-71.

67. Gainor JF, Tseng D, Yoda S, Dagogo-Jack I, Friboulet L, Lin JJ, et al. Patterns of Metastatic Spread and Mechanisms of Resistance to Crizotinib in ROS1-Positive Non-Small-Cell Lung Cancer. JCO Precis Oncol. 2017;2017.

68. Awad MM, Katayama R, McTigue M, Liu W, Deng YL, Brooun A, et al. Acquired resistance to crizotinib from a mutation in CD74-ROS1. N Engl J Med. 2013;368(25):2395-401.

69. Hirsch FR, Scagliotti GV, Mulshine JL, Kwon R, Curran WJ, Wu Y-L, et al. Lung cancer: current therapies and new targeted treatments. The Lancet. 2017;389(10066):299-311.

70. Forde PM, Kelly RJ, Brahmer JR. New strategies in lung cancer: translating immunotherapy into clinical practice. Clin Cancer Res. 2014;20(5):1067-73.

71. Burnet M. Cancer: a biological approach. III. Viruses associated with neoplastic conditions. IV. Practical applications. Br Med J. 1957;1(5023):841-7.

72. Thomas L. Delayed hypersensitivity in health and disease. In: Lawrence HS, editor Cellular and Humoral Aspects of the Hypersensitive States Hoeber-Harper; New York. 1959:529-32.

73. Old LJ, Boyse EA. IMMUNOLOGY OF EXPERIMENTAL TUMORS. Annu Rev Med. 1964;15:167-86.

74. Klein G. Tumor antigens. Annu Rev Microbiol. 1966;20:223-52.

75. Rygaard J, Povlsen CO. The mouse mutant nude does not develop spontaneous tumours. An argument against immunological surveillance. Acta Pathol Microbiol Scand B Microbiol Immunol. 1974;82(1):99-106.

76. Stutman O. Tumor development after 3-methylcholanthrene in immunologically deficient athymic-nude mice. Science. 1974;183(4124):534-6.

77. Dunn GP, Bruce AT, Ikeda H, Old LJ, Schreiber RD. Cancer immunoediting: from immunosurveillance to tumor escape. Nature Immunology. 2002;3(11):991-8.

78. Vesely MD, Kershaw MH, Schreiber RD, Smyth MJ. Natural innate and adaptive immunity to cancer. Annu Rev Immunol. 2011;29:235-71.

79. Liu Y, Zeng G. Cancer and innate immune system interactions: translational potentials for cancer immunotherapy. J Immunother. 2012;35(4):299-308.

80. Mortellaro A, Ricciardi-Castagnoli P. From vaccine practice to vaccine science: the contribution of human immunology to the prevention of infectious disease. Immunol Cell Biol. 2011;89(3):332-9.

81. Dunn GP, Old LJ, Schreiber RD. The three Es of cancer immunoediting. Annu Rev Immunol. 2004;22:329-60.

82. Olson BM, McNeel DG. Antigen loss and tumor-mediated immunosuppression facilitate tumor recurrence. Expert Rev Vaccines. 2012;11(11):1315-7.

83. Marincola FM, Jaffee EM, Hicklin DJ, Ferrone S. Escape of human solid tumors from T-cell recognition: molecular mechanisms and functional significance. Adv Immunol. 2000;74:181-273.

84. Groh V, Wu J, Yee C, Spies T. Tumour-derived soluble MIC ligands impair expression of NKG2D and T-cell activation. Nature. 2002;419(6908):734-8.

85. Kaplan DH, Shankaran V, Dighe AS, Stockert E, Aguet M, Old LJ, et al. Demonstration of an interferon gamma-dependent tumor surveillance system in immunocompetent mice. Proc Natl Acad Sci U S A. 1998;95(13):7556-61.

86. Kunimasa K, Goto T. Immunosurveillance and Immunoediting of Lung Cancer: Current Perspectives and Challenges. Int J Mol Sci. 2020;21(2).

87. Woo EY, Yeh H, Chu CS, Schlienger K, Carroll RG, Riley JL, et al. Cutting edge: Regulatory T cells from lung cancer patients directly inhibit autologous T cell proliferation. J Immunol. 2002;168(9):4272-6.

88. Konishi J, Yamazaki K, Azuma M, Kinoshita I, Dosaka-Akita H, Nishimura M. B7-H1 expression on non-small cell lung cancer cells and its relationship with tumor-infiltrating lymphocytes and their PD-1 expression. Clin Cancer Res. 2004;10(15):5094-100.

89. Zhang Y, Huang S, Gong D, Qin Y, Shen Q. Programmed death-1 upregulation is correlated with dysfunction of tumor-infiltrating CD8+ T lymphocytes in human non-small cell lung cancer. Cell Mol Immunol. 2010;7(5):389-95.

90. Chen YB, Mu CY, Huang JA. Clinical significance of programmed death-1 ligand-1 expression in patients with non-small cell lung cancer: a 5-year-follow-up study. Tumori. 2012;98(6):751-5.

91. Korkolopoulou P, Kaklamanis L, Pezzella F, Harris AL, Gatter KC. Loss of antigen-presenting molecules (MHC class I and TAP-1) in lung cancer. Br J Cancer. 1996;73(2):148-53.

92. Domagala-Kulawik J, Osinska I, Hoser G. Mechanisms of immune response regulation in lung cancer. Transl Lung Cancer Res. 2014;3(1):15-22.

93. Brahmer J, Reckamp KL, Baas P, Crinò L, Eberhardt WEE, Poddubskaya E, et al. Nivolumab versus Docetaxel in Advanced Squamous-Cell Non–Small-Cell Lung Cancer. New England Journal of Medicine. 2015;373(2):123-35.

94. Borghaei H, Paz-Ares L, Horn L, Spigel DR, Steins M, Ready NE, et al. Nivolumab versus Docetaxel in Advanced Nonsquamous Non–Small-Cell Lung Cancer. New England Journal of Medicine. 2015;373(17):1627-39.

95. Herbst RS, Baas P, Kim DW, Felip E, Pérez-Gracia JL, Han JY, et al. Pembrolizumab versus docetaxel for previously treated, PD-L1-positive, advanced non-small-cell lung cancer (KEYNOTE-010): a randomised controlled trial. Lancet. 2016;387(10027):1540-50.

96. Rittmeyer A, Barlesi F, Waterkamp D, Park K, Ciardiello F, von Pawel J, et al. Atezolizumab versus docetaxel in patients with previously treated non-small-cell lung cancer (OAK): a phase 3, open-label, multicentre randomised controlled trial. Lancet. 2017;389(10066):255-65.

97. Paz-Ares L, Luft A, Vicente D, Tafreshi A, Gümüş M, Mazières J, et al. Pembrolizumab plus Chemotherapy for Squamous Non-Small-Cell Lung Cancer. N Engl J Med. 2018;379(21):2040-51.

98. Gandhi L, Rodríguez-Abreu D, Gadgeel S, Esteban E, Felip E, De Angelis F, et al. Pembrolizumab plus Chemotherapy in Metastatic Non–Small-Cell Lung Cancer. New England Journal of Medicine. 2018;378(22):2078-92.

99. Kepp O, Senovilla L, Vitale I, Vacchelli E, Adjemian S, Agostinis P, et al. Consensus guidelines for the detection of immunogenic cell death. Oncoimmunology. 2014;3(9):e955691.

100. Maroun J, Muñoz-Alía M, Ammayappan A, Schulze A, Peng KW, Russell S. Designing and building oncolytic viruses. Future Virol. 2017;12(4):193-213.

101. Au GG, Lindberg AM, Barry RD, Shafren DR. Oncolysis of vascular malignant human melanoma tumors by Coxsackievirus A21. Int J Oncol. 2005;26(6):1471-6.

102. Shafren DR, Sylvester D, Johansson ES, Campbell IG, Barry RD. Oncolysis of human ovarian cancers by echovirus type 1. Int J Cancer. 2005;115(2):320-8.

103. Ochiai H, Campbell SA, Archer GE, Chewning TA, Dragunsky E, Ivanov A, et al. Targeted therapy for glioblastoma multiforme neoplastic meningitis with intrathecal delivery of an oncolytic recombinant poliovirus. Clin Cancer Res. 2006;12(4):1349-54.

104. Kohlhapp FJ, Kaufman HL. Molecular Pathways: Mechanism of Action for Talimogene Laherparepvec, a New Oncolytic Virus Immunotherapy. Clin Cancer Res. 2016;22(5):1048-54.

105. Balachandran S, Barber GN. Defective translational control facilitates vesicular stomatitis virus oncolysis. Cancer Cell. 2004;5(1):51-65.

106. Stojdl DF, Lichty BD, tenOever BR, Paterson JM, Power AT, Knowles S, et al. VSV strains with defects in their ability to shutdown innate immunity are potent systemic anti-cancer agents. Cancer Cell. 2003;4(4):263-75.

107. Dobbelstein M. Replicating adenoviruses in cancer therapy. Curr Top Microbiol Immunol. 2004;273:291-334.

108. Guo ZS, Thorne SH, Bartlett DL. Oncolytic virotherapy: molecular targets in tumor-selective replication and carrier cell-mediated delivery of oncolytic viruses. Biochim Biophys Acta. 2008;1785(2):217-31.

109. Ko D, Hawkins L, Yu DC. Development of transcriptionally regulated oncolytic adenoviruses. Oncogene. 2005;24(52):7763-74.

110. Marchini A, Daeffler L, Pozdeev VI, Angelova A, Rommelaere J. Immune Conversion of Tumor Microenvironment by Oncolytic Viruses: The Protoparvovirus H-1PV Case Study. Frontiers in immunology. 2019;10:1848.

111. Gujar S, Pol JG, Kim Y, Lee PW, Kroemer G. Antitumor Benefits of Antiviral Immunity: An Underappreciated Aspect of Oncolytic Virotherapies. Trends Immunol. 2018;39(3):209-21.

112. Harrington K, Freeman DJ, Kelly B, Harper J, Soria JC. Optimizing oncolytic virotherapy in cancer treatment. Nat Rev Drug Discov. 2019;18(9):689-706.

113. Pearl TM, Markert JM, Cassady KA, Ghonime MG. Oncolytic Virus-Based Cytokine Expression to Improve Immune Activity in Brain and Solid Tumors. Mol Ther Oncolytics. 2019;13:14-21.

114. Toda M, Rabkin SD, Kojima H, Martuza RL. Herpes simplex virus as an in situ cancer vaccine for the induction of specific anti-tumor immunity. Hum Gene Ther. 1999;10(3):385-93.

115. Diaz RM, Galivo F, Kottke T, Wongthida P, Qiao J, Thompson J, et al. Oncolytic Immunovirotherapy for Melanoma Using Vesicular Stomatitis Virus. Cancer Research. 2007;67(6):2840.

116. Zhang J, Tai LH, Ilkow CS, Alkayyal AA, Ananth AA, de Souza CT, et al. Maraba MG1 virus enhances natural killer cell function via conventional dendritic cells to reduce postoperative metastatic disease. Mol Ther. 2014;22(7):1320-32.

117. Burke S, Shergold A, Elder MJ, Whitworth J, Cheng X, Jin H, et al. Oncolytic Newcastle disease virus activation of the innate immune response and priming of antitumor adaptive responses in vitro. Cancer immunology, immunotherapy : CII. 2020;69(6):1015-27.

118. Errington F, Steele L, Prestwich R, Harrington KJ, Pandha HS, Vidal L, et al. Reovirus Activates Human Dendritic Cells to Promote Innate Antitumor Immunity. The Journal of Immunology. 2008;180(9):6018.

119. López CB, Yount JS, Hermesh T, Moran TM. Sendai virus infection induces efficient adaptive immunity independently of type I interferons. Journal of virology. 2006;80(9):4538-45.

120. Ribas A, Dummer R, Puzanov I, VanderWalde A, Andtbacka RHI, Michielin O, et al. Oncolytic Virotherapy Promotes Intratumoral T Cell Infiltration and Improves Anti-PD-1 Immunotherapy. Cell. 2017;170(6):1109-19 e10.

121. Noonan AM, Farren MR, Geyer SM, Huang Y, Tahiri S, Ahn D, et al. Randomized Phase 2 Trial of the Oncolytic Virus Pelareorep (Reolysin) in

Upfront Treatment of Metastatic Pancreatic Adenocarcinoma. Molecular therapy : the journal of the American Society of Gene Therapy. 2016;24(6):1150-8.

122. Pesonen S, Diaconu I, Kangasniemi L, Ranki T, Kanerva A, Pesonen SK, et al. Oncolytic immunotherapy of advanced solid tumors with a CD40L-expressing replicating adenovirus: assessment of safety and immunologic responses in patients. Cancer Res. 2012;72(7):1621-31.

123. Russell L, Peng K-W. The emerging role of oncolytic virus therapy against cancer. Chin Clin Oncol. 2018;7(2):16-.

124. Liu BL, Robinson M, Han ZQ, Branston RH, English C, Reay P, et al. ICP34.5 deleted herpes simplex virus with enhanced oncolytic, immune stimulating, and anti-tumour properties. Gene Ther. 2003;10(4):292-303.

125. Andtbacka RHI, Collichio FA, Amatruda T, Senzer NN, Chesney J, Delman KA, et al. OPTiM: A randomized phase III trial of talimogene laherparepvec (T-VEC) versus subcutaneous (SC) granulocyte-macrophage colony-stimulating factor (GM-CSF) for the treatment (tx) of unresected stage IIIB/C and IV melanoma. Journal of Clinical Oncology. 2013;31(18_suppl):LBA9008-LBA.

126. Andtbacka RHI, Collichio F, Harrington KJ, Middleton MR, Downey G, hrling K, et al. Final analyses of OPTiM: a randomized phase III trial of talimogene laherparepvec versus granulocyte-macrophage colony-stimulating factor in unresectable stage III-IV melanoma. J Immunother Cancer. 2019;7(1):145.

127. Kaufman HL, Kim DW, DeRaffele G, Mitcham J, Coffin RS, Kim-Schulze S. Local and distant immunity induced by intralesional vaccination with an oncolytic herpes virus encoding GM-CSF in patients with stage IIIc and IV melanoma. Ann Surg Oncol. 2010;17(3):718-30.

128. Lang FF, Conrad C, Gomez-Manzano C, Yung WKA, Sawaya R, Weinberg JS, et al. Phase I Study of DNX-2401 (Delta-24-RGD) Oncolytic Adenovirus: Replication and Immunotherapeutic Effects in Recurrent Malignant Glioma. Journal of Clinical Oncology. 2018;36(14):1419-27.

129. Xia ZJ, Chang JH, Zhang L, Jiang WQ, Guan ZZ, Liu JW, et al. [Phase III randomized clinical trial of intratumoral injection of E1B gene-deleted adenovirus (H101) combined with cisplatin-based chemotherapy in treating squamous cell cancer of head and neck or esophagus]. Ai Zheng. 2004;23(12):1666-70.

130. Travassos da Rosa AP, Tesh RB, Travassos da Rosa JF, Herve JP, Main AJ, Jr. Carajas and Maraba viruses, two new vesiculoviruses isolated from phlebotomine sand flies in Brazil. Am J Trop Med Hyg. 1984;33(5):999-1006.

131. Brun J, McManus D, Lefebvre C, Hu K, Falls T, Atkins H, et al. Identification of genetically modified Maraba virus as an oncolytic rhabdovirus. Mol Ther. 2010;18(8):1440-9.

132. Tong JG, Valdes YR, Barrett JW, Bell JC, Stojdl D, McFadden G, et al. Evidence for differential viral oncolytic efficacy in an in vitro model of epithelial ovarian cancer metastasis. Mol Ther Oncolytics. 2015;2:15013.

133. Le Boeuf F, Selman M, Son HH, Bergeron A, Chen A, Tsang J, et al. Oncolytic Maraba Virus MG1 as a Treatment for Sarcoma. Int J Cancer. 2017;141(6):1257-64.

134. Bourgeois-Daigneault MC, St-Germain LE, Roy DG, Pelin A, Aitken AS, Arulanandam R, et al. Combination of Paclitaxel and MG1 oncolytic virus as a successful strategy for breast cancer treatment. Breast Cancer Res. 2016;18(1):83.

135. Bourgeois-Daigneault MC, Roy DG, Aitken AS, El Sayes N, Martin NT, Varette O, et al. Neoadjuvant oncolytic virotherapy before surgery sensitizes triple-negative breast cancer to immune checkpoint therapy. Sci Transl Med. 2018;10(422).

136. Mahoney DJ, Lefebvre C, Allan K, Brun J, Sanaei CA, Baird S, et al. Virus-tumor interactome screen reveals ER stress response can reprogram resistant cancers for oncolytic virus-triggered caspase-2 cell death. Cancer Cell. 2011;20(4):443-56.

137. Alkayyal AA, Tai LH, Kennedy MA, de Souza CT, Zhang J, Lefebvre C, et al. NK-Cell Recruitment Is Necessary for Eradication of Peritoneal Carcinomatosis with an IL12-Expressing Maraba Virus Cellular Vaccine. Cancer Immunol Res. 2017;5(3):211-21.

138. Conrad DP, Tsang J, Maclean M, Diallo JS, Le Boeuf F, Lemay CG, et al. Leukemia cell-rhabdovirus vaccine: personalized immunotherapy for acute lymphoblastic leukemia. Clin Cancer Res. 2013;19(14):3832-43.

139. Tong JG, Valdes YR, Sivapragasam M, Barrett JW, Bell JC, Stojdl D, et al. Spatial and temporal epithelial ovarian cancer cell heterogeneity impacts Maraba virus oncolytic potential. BMC Cancer. 2017;17(1):594.

140. Atherton MJ, Stephenson KB, Tzelepis F, Bakhshinyan D, Nikota JK, Son HH, et al. Transforming the prostatic tumor microenvironment with oncolytic virotherapy. Oncoimmunology. 2018;7(7):e1445459.

141. Hassanzadeh G, Naing T, Graber T, Jafarnejad SM, Stojdl DF, Alain T, et al. Characterizing Cellular Responses During Oncolytic Maraba Virus Infection. Int J Mol Sci. 2019;20(3).

142. Atherton MJ, Stephenson KB, Nikota JK, Hu QN, Nguyen A, Wan Y, et al. Preclinical development of peptide vaccination combined with oncolytic MG1-E6E7 for HPV-associated cancer. Vaccine. 2018;36(16):2181-92.

143. Martin NT, Roy DG, Workenhe ST, van den Wollenberg DJM, Hoeben RC, Mossman KL, et al. Pre-surgical neoadjuvant oncolytic virotherapy confers protection against rechallenge in a murine model of breast cancer. Sci Rep. 2019;9(1):1865.

144. McGray AJR, Huang RY, Battaglia S, Eppolito C, Miliotto A, Stephenson KB, et al. Oncolytic Maraba virus armed with tumor antigen boosts vaccine priming and reveals diverse therapeutic response patterns when combined with checkpoint blockade in ovarian cancer. J Immunother Cancer. 2019;7(1):189.

145. Pol JG, Zhang L, Bridle BW, Stephenson KB, Resseguier J, Hanson S, et al. Maraba virus as a potent oncolytic vaccine vector. Mol Ther. 2014;22(2):420-9.

146. Kim R. Effects of surgery and anesthetic choice on immunosuppression and cancer recurrence. J Transl Med. 2018;16(1):8.

147. Hummel J, Bienzle D, Morrison A, Cieplak M, Stephenson K, DeLay J, et al. Maraba virus-vectored cancer vaccines represent a safe and novel therapeutic option for cats. Sci Rep. 2017;7(1):15738.

148. Pol JG, Acuna SA, Yadollahi B, Tang N, Stephenson KB, Atherton MJ, et al. Preclinical evaluation of a MAGE-A3 vaccination utilizing the oncolytic Maraba virus currently in first-in-human trials. Oncoimmunology. 2019;8(1):e1512329.

149. Jonker DJ, Hotte SJ, Abdul Razak AR, Renouf DJ, Lichty B, Bell JC, et al. Phase I study of oncolytic virus (OV) MG1 maraba/MAGE-A3 (MG1MA3), with and without transgenic MAGE-A3 adenovirus vaccine (AdMA3) in incurable advanced/metastatic MAGE-A3-expressing solid tumours: CCTG IND.214. Journal of Clinical Oncology. 2017;35(15_suppl):e14637-e.

150. Martin NT, Bell JC. Oncolytic Virus Combination Therapy: Killing One Bird with Two Stones. Mol Ther. 2018;26(6):1414-22.

151. O'Cathail SM, Pokrovska TD, Maughan TS, Fisher KD, Seymour LW, Hawkins MA. Combining Oncolytic Adenovirus with Radiation-A Paradigm for the Future of Radiosensitization. Front Oncol. 2017;7:153.

152. Forrester NA, Sedgwick GG, Thomas A, Blackford AN, Speiseder T, Dobner T, et al. Serotype-specific inactivation of the cellular DNA damage response during adenovirus infection. J Virol. 2011;85(5):2201-11.

153. Dilley J, Reddy S, Ko D, Nguyen N, Rojas G, Working P, et al. Oncolytic adenovirus CG7870 in combination with radiation demonstrates synergistic enhancements of antitumor efficacy without loss of specificity. Cancer gene therapy. 2005;12:715-22.

154. Toth K, Tarakanova V, Doronin K, Ward P, Kuppuswamy M, Locke JE, et al. Radiation increases the activity of oncolytic adenovirus cancer

gene therapy vectors that overexpress the ADP (E3-11.6K) protein. Cancer Gene Ther. 2003;10(3):193-200.

155. Emdad L, Sarkar D, Lebedeva IV, Su Z-Z, Gupta P, Mahasreshti PJ, et al. Ionizing radiation enhances adenoviral vector expressing mda-7/IL-24-mediated apoptosis in human ovarian cancer. J Cell Physiol. 2006;208(2):298-306.

156. Geoerger B, Grill J, Opolon P, Morizet J, Aubert G, Lecluse Y, et al. Potentiation of radiation therapy by the oncolytic adenovirus dl1520 (ONYX-015) in human malignant glioma xenografts. Br J Cancer. 2003;89(3):577-84.

157. McEntee G, Kyula JN, Mansfield D, Smith H, Wilkinson M, Gregory C, et al. Enhanced cytotoxicity of reovirus and radiotherapy in melanoma cells is mediated through increased viral replication and mitochondrial apoptotic signalling. Oncotarget. 2016;7(30):48517-32.

158. Adusumilli PS, Stiles BM, Chan MK, Chou TC, Wong RJ, Rusch VW, et al. Radiation therapy potentiates effective oncolytic viral therapy in the treatment of lung cancer. Ann Thorac Surg. 2005;80(2):409-16; discussion 16-7.

159. Adusumilli PS, Chan MK, Hezel M, Yu Z, Stiles BM, Chou TC, et al. Radiation-induced cellular DNA damage repair response enhances viral gene therapy efficacy in the treatment of malignant pleural mesothelioma. Ann Surg Oncol. 2007;14(1):258-69.

160. Chou J, Roizman B. Herpes simplex virus 1 gamma(1)34.5 gene function, which blocks the host response to infection, maps in the homologous domain of the genes expressed during growth arrest and DNA damage. Proc Natl Acad Sci U S A. 1994;91(12):5247-51.

161. Wilkinson MJ, Smith HG, McEntee G, Kyula-Currie J, Pencavel TD, Mansfield DC, et al. Oncolytic vaccinia virus combined with radiotherapy induces apoptotic cell death in sarcoma cells by down-regulating the inhibitors of apoptosis. Oncotarget. 2016;7(49):81208-22.

162. Fueyo J, Gomez-Manzano C, Alemany R, Lee PS, McDonnell TJ, Mitlianga P, et al. A mutant oncolytic adenovirus targeting the Rb pathway produces anti-glioma effect in vivo. Oncogene. 2000;19(1):2-12.

163. Badie B, Kramar MH, Lau R, Boothman DA, Economou JS, Black KL. Adenovirus-mediated p53 gene delivery potentiates the radiation-induced growth inhibition of experimental brain tumors. J Neurooncol. 1998;37(3):217-22.

164. Idema S, Lamfers ML, van Beusechem VW, Noske DP, Heukelom S, Moeniralm S, et al. AdDelta24 and the p53-expressing variant AdDelta24-p53 achieve potent anti-tumor activity in glioma when combined with radiotherapy. J Gene Med. 2007;9(12):1046-56.

165. Freytag SO, Stricker H, Lu M, Elshaikh M, Aref I, Pradhan D, et al. Prospective randomized phase 2 trial of intensity modulated radiation therapy with or without oncolytic adenovirus-mediated cytotoxic gene therapy in intermediate-risk prostate cancer. Int J Radiat Oncol Biol Phys. 2014;89(2):268-76.

166. Harrington KJ, Hingorani M, Tanay MA, Hickey J, Bhide SA, Clarke PM, et al. Phase I/II study of oncolytic HSV GM-CSF in combination with radiotherapy and cisplatin in untreated stage III/IV squamous cell cancer of the head and neck. Clin Cancer Res. 2010;16(15):4005-15.

167. Hodi FS, O'Day SJ, McDermott DF, Weber RW, Sosman JA, Haanen JB, et al. Improved Survival with Ipilimumab in Patients with Metastatic Melanoma. New England Journal of Medicine. 2010;363(8):711-23.

168. Reck M, Rodríguez-Abreu D, Robinson AG, Hui R, Csőszi T, Fülöp A, et al. Pembrolizumab versus Chemotherapy for PD-L1–Positive Non–Small-Cell Lung Cancer. New England Journal of Medicine. 2016;375(19):1823-33.

169. Bellmunt J, de Wit R, Vaughn DJ, Fradet Y, Lee J-L, Fong L, et al. Pembrolizumab as Second-Line Therapy for Advanced Urothelial Carcinoma. New England Journal of Medicine. 2017;376(11):1015-26.

170. Cohen EEW, Soulières D, Le Tourneau C, Dinis J, Licitra L, Ahn M-J, et al. Pembrolizumab versus methotrexate, docetaxel, or cetuximab for recurrent or metastatic head-and-neck squamous cell carcinoma (KEYNOTE-040): a randomised, open-label, phase 3 study. The Lancet. 2019;393(10167):156-67.

171. Trujillo JA, Sweis RF, Bao R, Luke JJ. T Cell–Inflamed versus Non-T Cell–Inflamed Tumors: A Conceptual Framework for Cancer Immunotherapy Drug Development and Combination Therapy Selection. Cancer Immunology Research. 2018;6(9):990-1000.

172. Chiu M, Armstrong EJL, Jennings V, Foo S, Crespo-Rodriguez E, Bozhanova G, et al. Combination therapy with oncolytic viruses and immune checkpoint inhibitors. Expert Opinion on Biological Therapy. 2020;20(6):635-52.

173. Chen CY, Hutzen B, Wedekind MF, Cripe TP. Oncolytic virus and PD-1/PD-L1 blockade combination therapy. Oncolytic Virother. 2018;7:65-77.

174. Smith HG, Mansfield D, Roulstone V, Kyula-Currie JN, McLaughlin M, Patel RR, et al. PD-1 Blockade Following Isolated Limb Perfusion with Vaccinia Virus Prevents Local and Distant Relapse of Soft-tissue Sarcoma. Clin Cancer Res. 2019;25(11):3443-54.

175. Mostafa AA, Meyers DE, Thirukkumaran CM, Liu PJ, Gratton K, Spurrell J, et al. Oncolytic Reovirus and Immune Checkpoint Inhibition as a Novel Immunotherapeutic Strategy for Breast Cancer. Cancers (Basel). 2018;10(6).

176. Shekarian T, Sivado E, Jallas AC, Depil S, Kielbassa J, Janoueix-Lerosey I, et al. Repurposing rotavirus vaccines for intratumoral immunotherapy can overcome resistance to immune checkpoint blockade. Sci Transl Med. 2019;11(515).

177. Zamarin D, Holmgaard RB, Subudhi SK, Park JS, Mansour M, Palese P, et al. Localized oncolytic virotherapy overcomes systemic tumor resistance to immune checkpoint blockade immunotherapy. Sci Transl Med. 2014;6(226):226ra32.

178. Kleinpeter P, Fend L, Thioudellet C, Geist M, Sfrontato N, Koerper V, et al. Vectorization in an oncolytic vaccinia virus of an antibody, a Fab and a scFv against programmed cell death -1 (PD-1) allows their intratumoral delivery and an improved tumor-growth inhibition. Oncoimmunology. 2016;5(10):e1220467.

179. Engeland CE, Grossardt C, Veinalde R, Bossow S, Lutz D, Kaufmann JK, et al. CTLA-4 and PD-L1 checkpoint blockade enhances oncolytic measles virus therapy. Mol Ther. 2014;22(11):1949-59.

180. Puzanov I, Milhem MM, Minor D, Hamid O, Li A, Chen L, et al. Talimogene Laherparepvec in Combination With Ipilimumab in Previously Untreated, Unresectable Stage IIIB-IV Melanoma. J Clin Oncol. 2016;34(22):2619-26.

181. Chesney J, Puzanov I, Collichio F, Singh P, Milhem MM, Glaspy J, et al. Randomized, Open-Label Phase II Study Evaluating the Efficacy and Safety of Talimogene Laherparepvec in Combination With Ipilimumab Versus Ipilimumab Alone in Patients With Advanced, Unresectable Melanoma. J Clin Oncol. 2018;36(17):1658-67.

182. Ilkow CS, Marguerie M, Batenchuk C, Mayer J, Ben Neriah D, Cousineau S, et al. Reciprocal cellular cross-talk within the tumor microenvironment promotes oncolytic virus activity. Nat Med. 2015;21(5):530-6.

183. Atherton MJ, Stephenson KB, Pol J, Wang F, Lefebvre C, Stojdl DF, et al. Customized Viral Immunotherapy for HPV-Associated Cancer. Cancer Immunol Res. 2017;5(10):847-59.

184. Pol JG, Atherton MJ, Bridle BW, Stephenson KB, Le Boeuf F, Hummel JL, et al. Development and applications of oncolytic Maraba virus vaccines. Oncolytic Virother. 2018;7:117-28.

185. Vile RG, Hart IR. Use of Tissue-specific Expression of the Herpes Simplex Virus Thymidine Kinase Gene to Inhibit Growth of Established Murine Melanomas following Direct Intratumoral Injection of DNA. Cancer Research. 1993;53(17):3860-4.

186. Trosko JE, Goodman JI. Intercellular communication may facilitate apoptosis: implications for tumor promotion. Mol Carcinog. 1994;11(1):8-12.

187. Jayawardena N, Poirier JT, Burga LN, Bostina M. Virus-Receptor Interactions and Virus Neutralization: Insights for Oncolytic Virus Development. Oncolytic Virother. 2020;9:1-15.

188. Ferguson MS, Lemoine NR, Wang Y. Systemic Delivery of Oncolytic Viruses: Hopes and Hurdles. Advances in Virology. 2012;2012:805629.

189. Berkeley RA, Steele LP, Mulder AA, van den Wollenberg DJM, Kottke TJ, Thompson J, et al. Antibody-Neutralized Reovirus Is Effective in Oncolytic Virotherapy. Cancer Immunology Research. 2018;6(10):1161-73.

190. Garcia-Carbonero R, Salazar R, Duran I, Osman-Garcia I, Paz-Ares L, Bozada JM, et al. Phase 1 study of intravenous administration of the chimeric adenovirus enadenotucirev in patients undergoing primary tumor resection. Journal for immunotherapy of cancer. 2017;5(1):71-.

191. Garg AD, Galluzzi L, Apetoh L, Baert T, Birge RB, Bravo-San Pedro JM, et al. Molecular and Translational Classifications of DAMPs in Immunogenic Cell Death. Frontiers in immunology. 2015;6:588-.

192. Kroemer G, Galluzzi L, Kepp O, Zitvogel L. Immunogenic cell death in cancer therapy. Annu Rev Immunol. 2013;31:51-72.

193. Serrano-Del Valle A, Anel A, Naval J, Marzo I. Immunogenic Cell Death and Immunotherapy of Multiple Myeloma. Front Cell Dev Biol. 2019;7:50.

194. Russell L, Peng KW, Russell SJ, Diaz RM. Oncolytic Viruses: Priming Time for Cancer Immunotherapy. BioDrugs. 2019;33(5):485-501.

195. Achard C, Surendran A, Wedge ME, Ungerechts G, Bell J, Ilkow CS. Lighting a Fire in the Tumor Microenvironment Using Oncolytic Immunotherapy. EBioMedicine. 2018;31:17-24.

196. Denton NL, Chen CY, Scott TR, Cripe TP. Tumor-Associated Macrophages in Oncolytic Virotherapy: Friend or Foe? Biomedicines. 2016;4(3).

197. Elankumaran S, Chavan V, Qiao D, Shobana R, Moorkanat G, Biswas M, et al. Type I Interferon-Sensitive Recombinant Newcastle Disease Virus for Oncolytic Virotherapy. Journal of Virology. 2010;84(8):3835-44.

198. Kawai T, Takahashi K, Sato S, Coban C, Kumar H, Kato H, et al. IPS-1, an adaptor triggering RIG-I- and Mda5-mediated type I interferon induction. Nat Immunol. 2005;6(10):981-8.

199. Tai LH, de Souza CT, Bélanger S, Ly L, Alkayyal AA, Zhang J, et al. Preventing postoperative metastatic disease by inhibiting surgery-induced dysfunction in natural killer cells. Cancer Res. 2013;73(1):97-107.

200. El-Sherbiny YM, Holmes TD, Wetherill LF, Black EV, Wilson EB, Phillips SL, et al. Controlled infection with a therapeutic virus defines the

activation kinetics of human natural killer cells in vivo. Clin Exp Immunol. 2015;180(1):98-107.

201. Jennings VA, Scott GB, Rose AMS, Scott KJ, Migneco G, Keller B, et al. Potentiating Oncolytic Virus-Induced Immune-Mediated Tumor Cell Killing Using Histone Deacetylase Inhibition. Mol Ther. 2019;27(6):1139-52.

202. Ma J, Ramachandran M, Jin C, Quijano-Rubio C, Martikainen M, Yu D, et al. Characterization of virus-mediated immunogenic cancer cell death and the consequences for oncolytic virus-based immunotherapy of cancer. Cell Death & Disease. 2020;11(1):48.

203. Miyamoto S, Inoue H, Nakamura T, Yamada M, Sakamoto C, Urata Y, et al. Coxsackievirus B3 is an oncolytic virus with immunostimulatory properties that is active against lung adenocarcinoma. Cancer Res. 2012;72(10):2609-21.

204. Nicolas Boisgerault CA. Induction of Immunogenic Tumor Cell Death by Attenuated Oncolytic Measles Virus. Journal of Clinical & Cellular Immunology. 2015;06(01).

205. Zitvogel L, Galluzzi L, Kepp O, Smyth MJ, Kroemer G. Type I interferons in anticancer immunity. Nat Rev Immunol. 2015;15(7):405-14.

206. Furr SR, Moerdyk-Schauwecker M, Grdzelishvili VZ, Marriott I. RIG-I mediates nonsegmented negative-sense RNA virus-induced inflammatory immune responses of primary human astrocytes. Glia. 2010;58(13):1620-9.

207. Kato H, Takeuchi O, Sato S, Yoneyama M, Yamamoto M, Matsui K, et al. Differential roles of MDA5 and RIG-I helicases in the recognition of RNA viruses. Nature. 2006;441(7089):101-5.

208. Parrish C, Scott GB, Migneco G, Scott KJ, Steele LP, Ilett E, et al. Oncolytic reovirus enhances rituximab-mediated antibody-dependent cellular cytotoxicity against chronic lymphocytic leukaemia. Leukemia. 2015;29(9):1799-810.

209. Fukuhara H, Ino Y, Todo T. Oncolytic virus therapy: A new era of cancer treatment at dawn. Cancer Sci. 2016;107(10):1373-9.

210. Haslam A, Prasad V. Estimation of the Percentage of US Patients With Cancer Who Are Eligible for and Respond to Checkpoint Inhibitor Immunotherapy Drugs. JAMA Network Open. 2019;2(5):e192535-e.

211. Baskar R, Lee KA, Yeo R, Yeoh KW. Cancer and radiation therapy: current advances and future directions. Int J Med Sci. 2012;9(3):193-9.

212. Burnette BC, Liang H, Lee Y, Chlewicki L, Khodarev NN, Weichselbaum RR, et al. The efficacy of radiotherapy relies upon induction of type i interferon-dependent innate and adaptive immunity. Cancer Res. 2011;71(7):2488-96.

213. Zhang F, Manna S, Pop LM, Chen ZJ, Fu YX, Hannan R. Type I Interferon Response in Radiation-Induced Anti-Tumor Immunity. Semin Radiat Oncol. 2020;30(2):129-38.

214. Li H, Peng KW, Dingli D, Kratzke RA, Russell SJ. Oncolytic measles viruses encoding interferon beta and the thyroidal sodium iodide symporter gene for mesothelioma virotherapy. Cancer Gene Ther. 2010;17(8):550-8.

215. Willmon CL, Saloura V, Fridlender ZG, Wongthida P, Diaz RM, Thompson J, et al. Expression of IFN-beta enhances both efficacy and safety of oncolytic vesicular stomatitis virus for therapy of mesothelioma. Cancer Res. 2009;69(19):7713-20.

216. Patel MR, Jacobson BA, Ji Y, Drees J, Tang S, Xiong K, et al. Vesicular stomatitis virus expressing interferon-β is oncolytic and promotes antitumor immune responses in a syngeneic murine model of non-small cell lung cancer. Oncotarget. 2015;6(32):33165-77.

217. Nandi S, Ulasov IV, Tyler MA, Sugihara AQ, Molinero L, Han Y, et al. Low-dose radiation enhances survivin-mediated virotherapy against malignant glioma stem cells. Cancer research. 2008;68(14):5778-84.

218. Hall AR, Dix BR, O'Carroll SJ, Braithwaite AW. p53-dependent cell death/apoptosis is required for a productive adenovirus infection. Nat Med. 1998;4(9):1068-72.

219. Shen SX, Weaver Z, Xu X, Li C, Weinstein M, Chen L, et al. A targeted disruption of the murine Brca1 gene causes gamma-irradiation hypersensitivity and genetic instability. Oncogene. 1998;17(24):3115-24.

220. Foray N, Randrianarison V, Marot D, Perricaudet M, Lenoir G, Feunteun J. Gamma-rays-induced death of human cells carrying mutations of BRCA1 or BRCA2. Oncogene. 1999;18(51):7334-42.

221. Scully R, Ganesan S, Vlasakova K, Chen J, Socolovsky M, Livingston DM. Genetic analysis of BRCA1 function in a defined tumor cell line. Mol Cell. 1999;4(6):1093-9.

222. Karanam NK, Srinivasan K, Ding L, Sishc B, Saha D, Story MD. Tumor-treating fields elicit a conditional vulnerability to ionizing radiation via the downregulation of BRCA1 signaling and reduced DNA double-strand break repair capacity in non-small cell lung cancer cell lines. Cell death & disease. 2017;8(3):e2711-e.

223. Dréan A, Williamson CT, Brough R, Brandsma I, Menon M, Konde A, et al. Modeling Therapy Resistance in BRCA1/2-Mutant Cancers. Molecular cancer therapeutics. 2017;16(9):2022-34.

224. Li M, Huang X, Zhu Z, Wong M, Watkins S, Zhao Q, et al. Immune response against 3LL Lewis lung carcinoma potentiates the therapeutic efficacy of endostatin. J Immunother. 2001;24(6):472-81.

225. Lechner MG, Karimi SS, Barry-Holson K, Angell TE, Murphy KA, Church CH, et al. Immunogenicity of murine solid tumor models as a defining feature of in vivo behavior and response to immunotherapy. Journal of immunotherapy (Hagerstown, Md : 1997). 2013;36(9):477-89.

226. Yaacov B, Eliahoo E, Lazar I, Ben-Shlomo M, Greenbaum I, Panet A, et al. Selective oncolytic effect of an attenuated Newcastle disease virus (NDV-HUJ) in lung tumors. Cancer Gene Therapy. 2008;1531:795-807.

227. Simbawa E, Al-Johani N, Al-Tuwairqi S. Modeling the Spatiotemporal Dynamics of Oncolytic Viruses and Radiotherapy as a Treatment for Cancer. Comput Math Methods Med. 2020;2020:3642654.

228. Robson M, Gilewski T, Haas B, Levin D, Borgen P, Rajan P, et al. BRCA-associated breast cancer in young women. J Clin Oncol. 1998;16(5):1642-9.

229. Kirova YM, Savignoni A, Sigal-Zafrani B, de La Rochefordiere A, Salmon RJ, This P, et al. Is the breast-conserving treatment with radiotherapy appropriate in BRCA1/2 mutation carriers? Long-term results and review of the literature. Breast Cancer Res Treat. 2010;120(1):119-26.

230. Marciscano AE, Ghasemzadeh A, Nirschl TR, Theodros D, Kochel CM, Francica BJ, et al. Elective Nodal Irradiation Attenuates the Combinatorial Efficacy of Stereotactic Radiation Therapy and Immunotherapy. Clin Cancer Res. 2018;24(20):5058-71.

231. Chauvin J-M, Zarour HM. TIGIT in cancer immunotherapy. Journal for ImmunoTherapy of Cancer. 2020;8(2):e000957.